NATIONAL AERONAUTICS AND SPACE ADMINISTRATION

Technical Report No. 32-915

Ranger Block III Attitude Control System: Manufacturing, Testing, and Performance

Teófilo A. Almaguer, Jr.
Theodore G. Baxter
Patrick J. Hand
Gerald S. Perkins
Robert H. Summers

JET PROPULSION LABORATORY
CALIFORNIA INSTITUTE OF TECHNOLOGY
PASADENA, CALIFORNIA

September 15, 1966

NATIONAL AERONAUTICS AND SPACE ADMINISTRATION

Technical Report No. 32-915

Ranger Block III Attitude Control System: Manufacturing, Testing, and Performance

Teófilo A. Almaguer, Jr.
Theodore G. Baxter
Patrick J. Hand
Gerald S. Perkins
Robert H. Summers

G. E. Sweetnam

G. E. Sweetnam, Manager
Spacecraft Control Section

JET PROPULSION LABORATORY
CALIFORNIA INSTITUTE OF TECHNOLOGY
PASADENA, CALIFORNIA

September 15, 1966

CONTENTS (Cont'd)

CONTENTS (Cont'd)

TABLES

TABLES (Cont'd)

FIGURES

FIGURES (Cont'd)

FIGURES (Cont'd)

FIGURES (Cont'd)

PREFACE

This report, in conjunction with Ref. 1, forms a comprehensive documentation of the Block III (*Rangers VI–IX*) attitude control system. As necessary, information is included from the attitude control systems of Block I (*Rangers I* and *II*) and Block II (*Rangers III–V*) which is pertinent to the evolution of the Block III system.

ABSTRACT

This report, in conjunction with JPL Technical Report No. 32-663, forms a comprehensive documentation of the Block III attitude control system. Descriptions, requirements, test plans, and results of the attitude control system and the various subsystems that comprise it are included.

I. DESCRIPTION

The basic attitude control system is a nonlinear, three-axis control system mechanized as shown in Figs. 1 and 2. The switching amplifier establishes an electrical deadband, which is translated into an angular position deadband by the celestial sensors and a rate deadband by the gyroscopes. The controlling torques about each axis are supplied by a cold-gas expulsion system, which is actuated by the switching amplifier. An articulated hinge servosystem is utilized to point the spacecraft transmitter high-gain antenna at the Earth.

A. Mission Requirements

The primary requirements of the attitude control system are to:

(1) Provide three-axis orientation and stabilization of the spacecraft with respect to the Sun (primary reference) and the Earth (secondary reference).

(2) Deploy the spacecraft transmitter high-gain antenna to some predetermined angle prior to Earth acquisition and, after Earth acquisition, to track the Earth so that the high-gain antenna remains pointed at Earth.

(3) Orient the thrust vector of the midcourse motor in a predetermined direction in space and maintain the orientation during powered flight.

(4) Provide a measure of spacecraft velocity during the motor burn period in order to control the magnitude of the midcourse velocity vector.

(5) Orient and maintain the spacecraft axes so that the spacecraft television camera optical axis is aligned in a predetermined direction, and to continue to point the spacecraft high-gain antenna at the Earth during the maneuver.

B. Operational Configurations

1. Acquisition

With the exception of the gyros and their respective electronics, the attitude control system is turned off during the launch and separation phases. At Sun acquisition, the power to the attitude control system is turned on, and the system configuration is:

(1) Excitation to primary and secondary Sun sensors is turned on, thus establishing a 4π-sterad field of view.

(2) The system is on gyro-rate control (nonderived rate).

(3) The Earth sensor remains off so that the only input for the roll switching amplifier is the roll gyro.

(4) The antenna servosystem is turned on; the antenna actuator drives the antenna from its nested position to the first preset angle.

Upon the application of power, the spacecraft will accelerate or decelerate to the acquisition rates until the Sun sensors indicate that the Sun is within the angular position deadband. At this point, the roll-axis rates are reduced to the roll-rate deadband limit. Once the position and rate error signals are reduced to their normal deadband limits, a limit cycle mode of operation is established about the pitch and yaw axes.

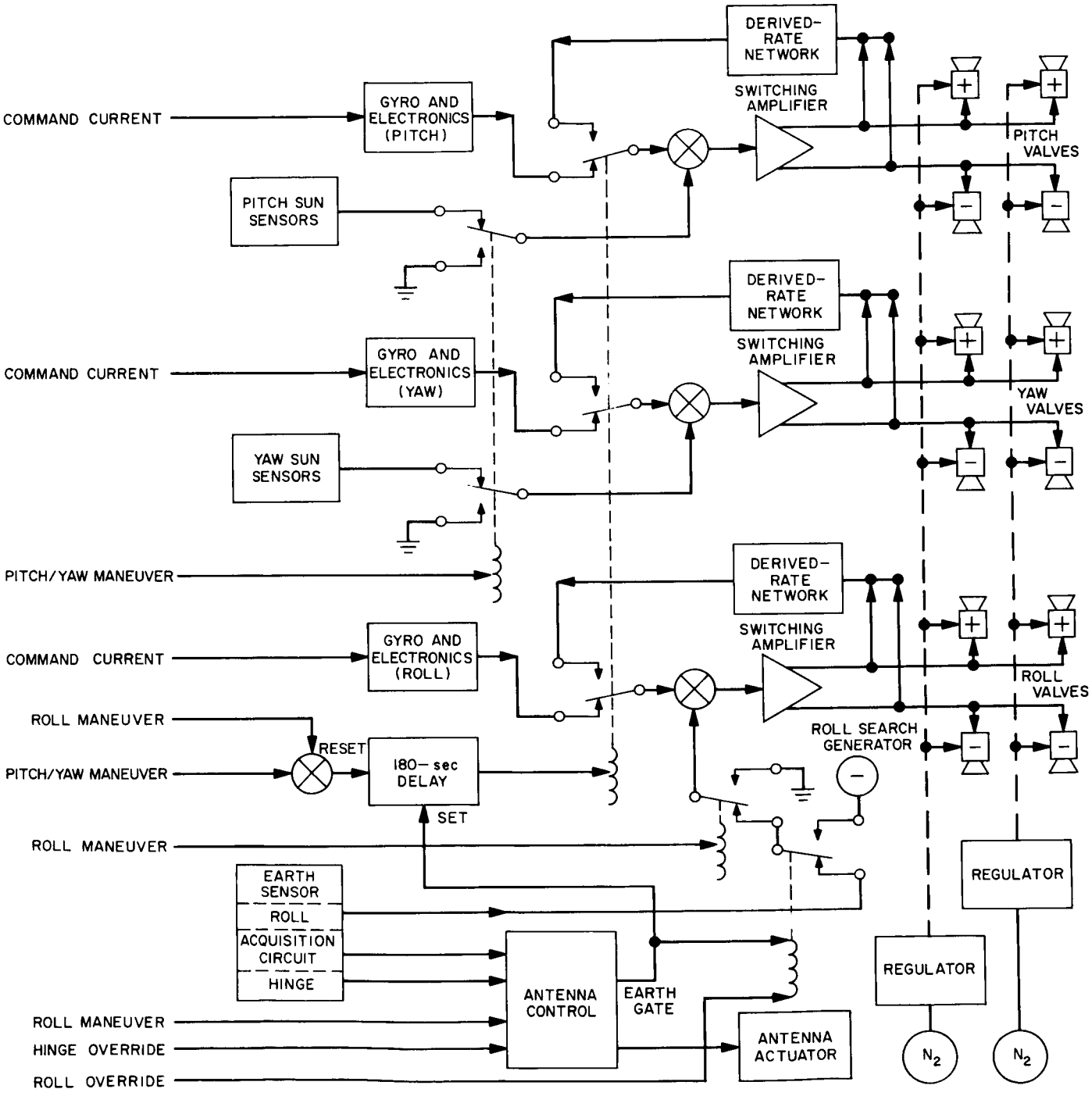

Fig. 1. Mechanization of attitude control system

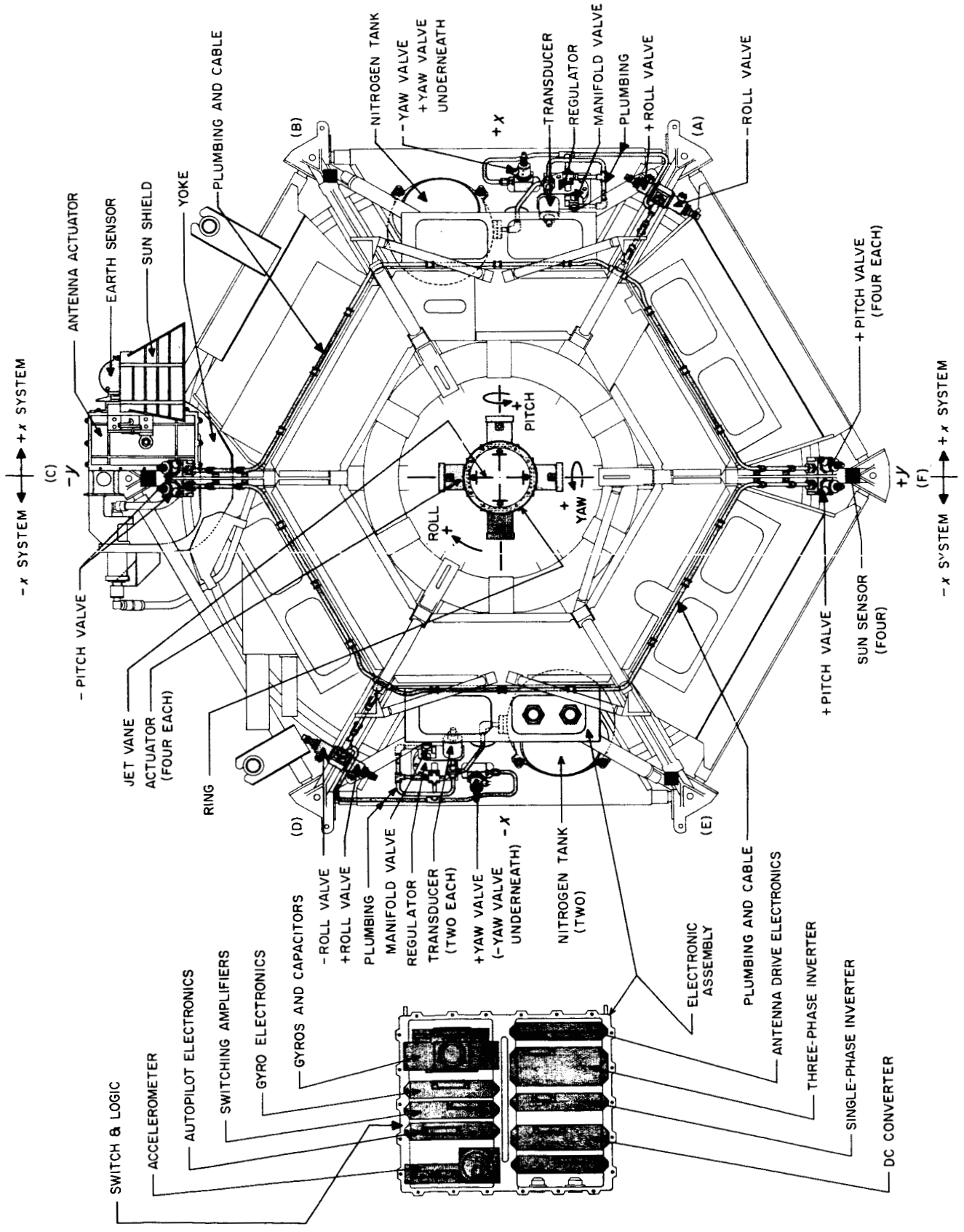

Fig. 2. *Ranger* attitude control configuration

At approximately 3½ hr after launch, the power to the Earth sensor is switched from the Earth sensor heater to the Earth sensor power supply. The input to the roll switching amplifier is then connected to the roll-search generator, resulting in a negative roll search. When the Earth sensor detects light in excess of a specified level, the following functions occur:

(1) The roll switching amplifier input is switched from the roll-search generator to the roll error signal from the Earth sensor.

(2) The hinge amplifier input is switched from the preset angle circuit to the hinge error signal from the Earth sensor.

(3) A 180-sec timer is started in the switching amplifier to transfer the switching-amplifier-rate feedback signal from the gyros to the derived-rate networks at timer expiration.

(4) The secondary Sun sensors are turned off, so that the field of view is reduced from 4π sterad to approximately 40 deg off of the negative roll axis of the spacecraft.

These functions allow the attitude control system to reduce the roll rate and position signals to within their deadband limits before the system is switched to derived-rate control.

2. Cruise

The cruise mode of operation is one in which the system is in derived-rate control and in limit-cycle operation. The hinge servosystem tracks the Earth within its deadband limits.

3. Maneuvers

During the normal sequence of events, two maneuvers are planned for the spacecraft: midcourse and terminal. The two maneuvers differ in that the midcourse maneuver is accomplished with a roll and pitch turn; the terminal maneuver is accomplished with a pitch, yaw, and second pitch turn. The terminal maneuver has the added requirement that Earth lock be maintained through the maneuver to impact.

a. Midcourse. This manuver orients the spacecraft to some predetermined direction prior to the midcourse motor burn period. The following events occur when the midcourse motor has been started by the roll turn:

(1) The derived-rate networks are disconnected from the switching amplifier inputs; the gyro-rate signals are reconnected.

(2) The roll error signal from the Earth sensor is switched out, and the position input to the switching amplifier is grounded.

(3) Capacitors are inserted in the roll gyro output, so that the gyro-rate signals are integrated and give a rate-plus-position error signal to the switching amplifier.

(4) The Earth sensor is turned off.

(5) The high-gain antenna is driven to the exit position so that the antenna is removed from beneath the midcourse motor; it then rotates the Earth sensor beneath the Sun shield, where it is protected from possible exposure to direct sunlight.

The turn itself is initiated and controlled by the central computer and sequencer (CC&S) and is accomplished by timing the application of a command current generator to the roll gyro, and selecting the polarity of the generator.

The pitch turn occurs in a similar manner to the roll turn, with the Sun sensor position error signals replaced by the rate-plus-position signals from the gyros.

b. Terminal. This maneuver orients the TV optical axis to some predetermined direction. It is initiated by the start of the first pitch turn; the following events occur:

(1) The derived-rate feedback signals are replaced with the gyro-rate signals.

(2) The pitch and yaw gyros have their integrating capacitors inserted so that their output is a rate-plus-position signal.

These turns are once more initiated and controlled by the CC&S in a manner identical to that for the midcourse maneuver.

4. Powered Flight

The midcourse autopilot system is used to control the attitude of the spacecraft during the midcourse motor burn period. The autopilot is mechanized as shown in Fig. 3. The system utilizes the rate-plus-position signals from the gyros and feedback signals from the jet vanes to adjust the jet vane angular positions. Since these vanes are mounted downstream of the midcourse motor exhaust, non-zero angles of the jet vanes result in controlling torques about the spacecraft principal axes.

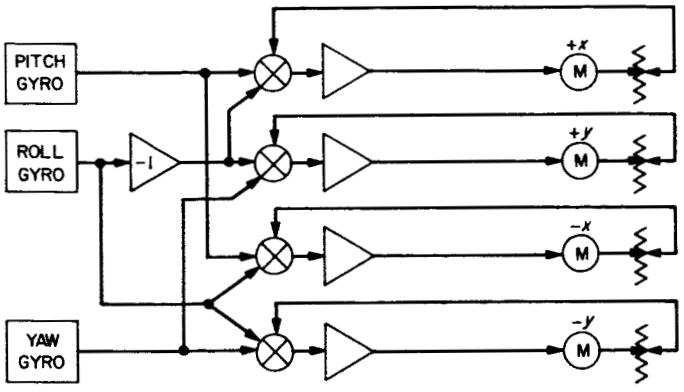

Fig. 3. Midcourse autopilot

A digital accelerometer is used to give a measure of the spacecraft velocity, allowing the CC&S to determine the midcourse velocity increment magnitude.

C. *Interfaces*

1. Mechanical

The spacecraft coordinate system is as shown in Fig. 4, and is used to define various alignments and locations of attitude control assemblies. In general, the spacecraft coordinate system is defined on the basis of two reference planes. The primary reference plane is defined by three of the six spacecraft mounting feet: A, C, and E (Fig. 4). The secondary reference plane is the mounting plane of the attitude control assembly.

The spacecraft coordinate system consists of three mutually perpendicular reference lines: pitch (x), yaw (y), and roll (z); these lines form a conventional Cartesian coordinate system. The roll reference line is defined normal to the primary reference plane with $+z$ aft, and it passes through the center of the basic bolt circle. The yaw reference line is defined parallel to the reference plane with $+y$ opposite the directional antenna. The pitch reference line is then defined such as to form a right-hand system. The reference lines intersect at the origin, which is located so that the primary reference plane becomes $z = 500$. These definitions are shown in Fig. 4.

Positive pitch, yaw, and roll angles and moments are defined as clockwise when looking from the origin along the positive reference lines. This is a conventional right-hand coordinate system in all respects (Fig. 5).

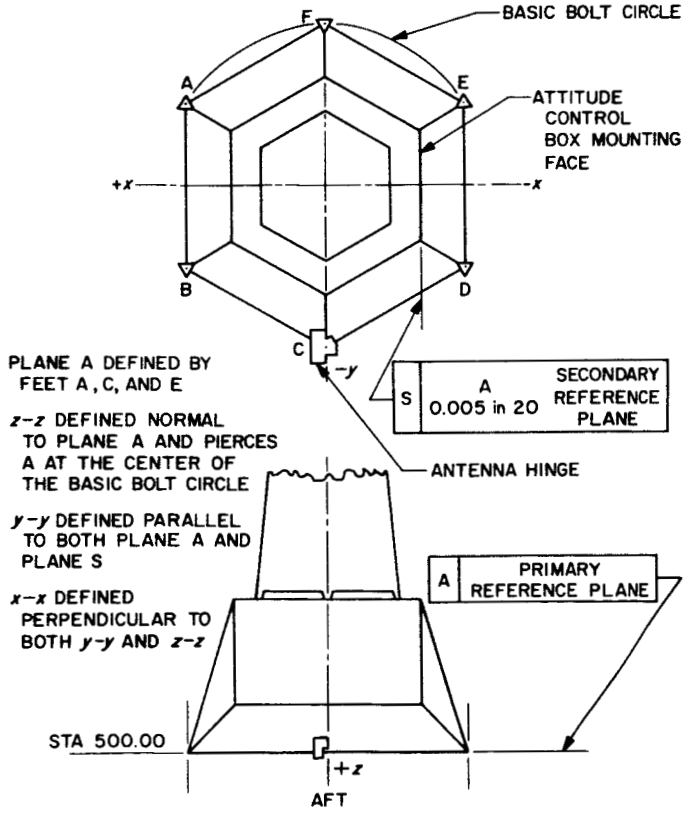

Fig. 4. Spacecraft reference planes and coordinates

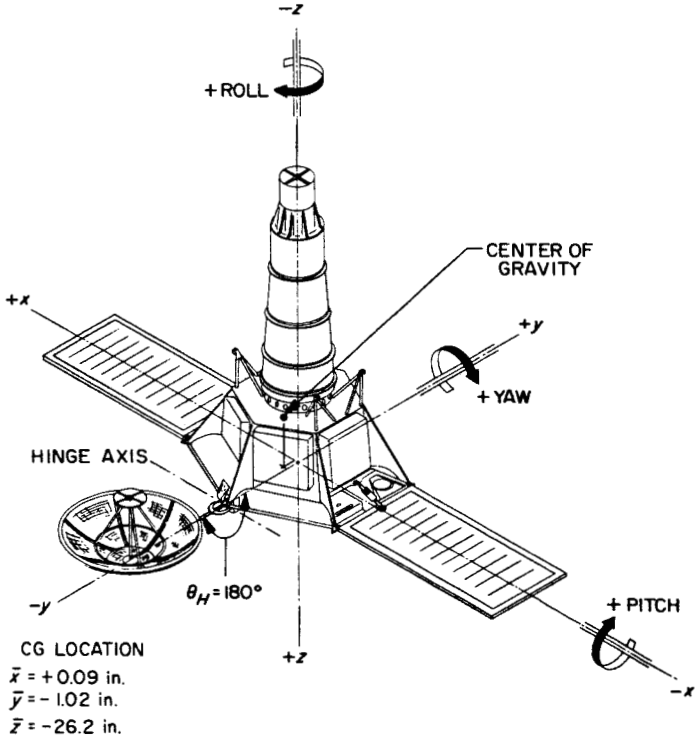

Fig. 5. Coordinate axis system (a standard right-hand coordinate system)

The jet vane angle definitions are shown in Fig. 6. Required alignment tolerances are:

(1) *Attitude control mounting surface.* The secondary reference plane (Fig. 4) is the mounting plane of the attitude control system. This plane surface is machined perpendicular to the primary reference plane within 0.005 in. in 20 in. (0.25 mrad).

(2) *Location of the center of gravity.* The center of gravity of the spacecraft must be located within 1.0 in. in the x-direction and 1.5 in. in the y-direction relative to the roll (z) reference line. The center of gravity must be 23^{+5}_{-1} in. from the center of lift of the jet vanes. The midcourse motor must be mounted so that the undeflected thrust vector passes within 0.1 in. of the actual spacecraft center of gravity in the midcourse configuration.

(3) *Antenna hinge axis.* The antenna hinge axis must be parallel to the base reference plane to within 0.88 mrad and perpendicular to the secondary reference plane to 0.88 mrad.

(4) *Earth sensor mounting.* The Earth sensor mounting surface shall be perpendicular to the antenna hinge axis to within 0.58 mrad.

(5) *Sun sensor mounting.* The pitch and yaw primary Sun-sensor mounting surfaces shall be perpendicular to the primary reference plane within 0.8 mrad.

(6) *Jet vane actuator alignment.* The axes of the jet vanes must be aligned parallel to the pitch and yaw reference lines within 20 mrad.

(7) *Gas jet valve mounting.* The mounting surfaces of the gas subsystem jet valves are aligned so that the cross-coupling torques due to misalignment are less than 20%.

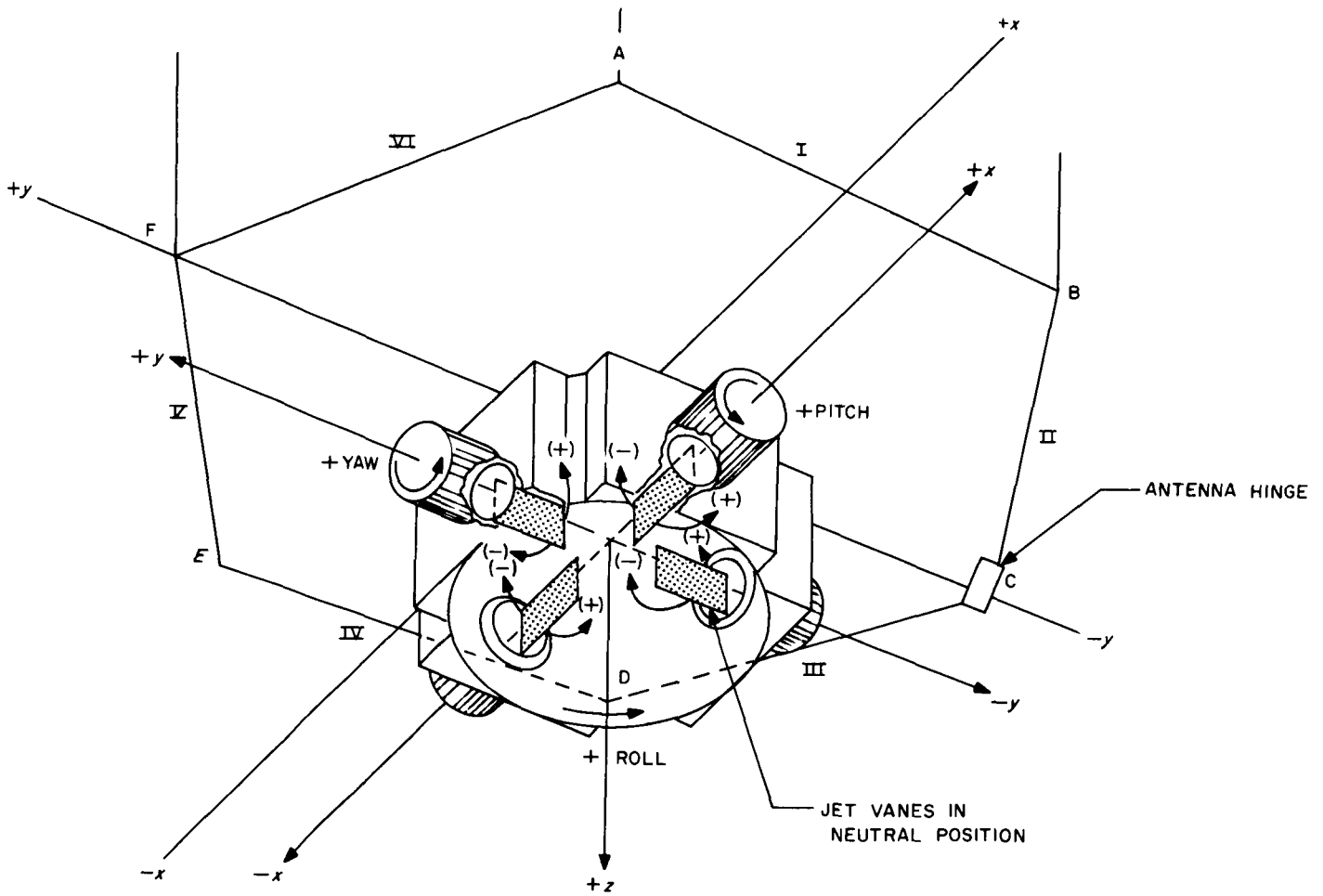

Fig. 6. Jet vane deflections: angle definitions

2. Command

The attitude control system accepts and acts upon commands received from the command and CC&S subassemblies. These commands are:

(1) Ground commands received by the spacecraft and transmitted to the attitude control system for the initiation of immediate action [designated as real-time commands (RTC)].

(2) Ground commands received by the spacecraft and stored in the CC&S for future attitude control use [designated stored commands (SC)].

(3) Commands generated by the CC&S in the normal sequence of events.

a. Real-time commands. The following real-time commands are used during standard and nonstandard sequences of events:

(1) *RTC 1: roll override/Earth sensor power on.* Prior to Earth acquisition, this command is used to turn on the Earth sensor and place the spacecraft in an Earth-search configuration. After Earth acquisition, in the event that a celestial body other than the Earth is acquired, this command is used (Fig. 1) to break optical lock in the roll channel and switch in the roll-search generator so that the spacecraft is returned to a roll-search mode. In the event that the celestial body had caused the hinge servo to track off of the preset angle, the roll override command would return the antenna to the first preset angle.

(2) *RTC 2: antenna hinge angle override.* There are eight preset hinge angles that can be selected by sending this command. The hinge preset circuit functions as follows (Fig. 7):

(a) The hinge ratchet advances one position for every command.

(b) The ratchet is continuous, so that the eighth command returns it to its starting point.

(c) With power application, the hinge ratchet returns to its first angle, thereby neglecting all commands previously sent.

(d) During Earth-acquired periods, the hinge ratchet is disconnected from the hinge servo, so that the preset angle may be changed without disturbing the system.

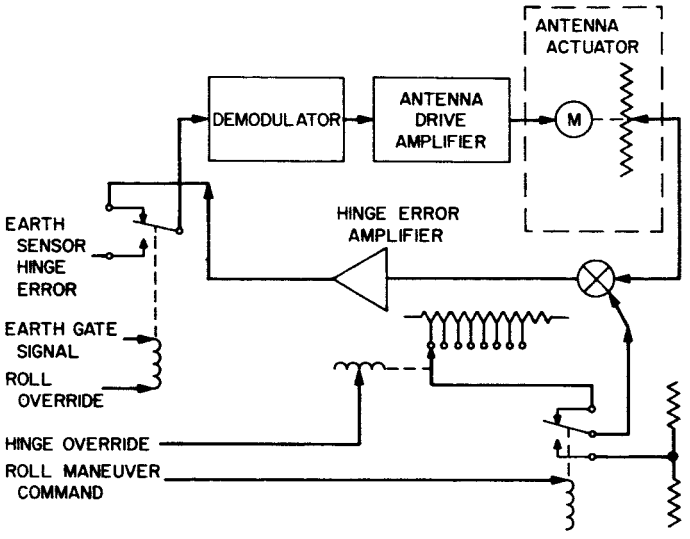

Fig. 7. Hinge servo loop

(3) *RTC 8: maneuver override.* This command is used to terminate a maneuver (either midcourse or terminal) sequence either prior to or during the maneuver, and to return the spacecraft to a Sun-acquire sequence. The command (Fig. 8) removes the excitation from the CC&S relays so that the maneuver sequence is brought to an immediate end. In the event that a terminal maneuver is not desired, but backup functions (such as TV power on, etc.) initiated by the terminal maneuver commands are required, then the maneuver is preceded by an RTC 8, which allows the CC&S to proceed with the maneuver sequence without affecting the attitude control system.

In the event that this command is sent during a nonstandard maneuver, and a second attempt at a maneuver is desirable, then the excitation for

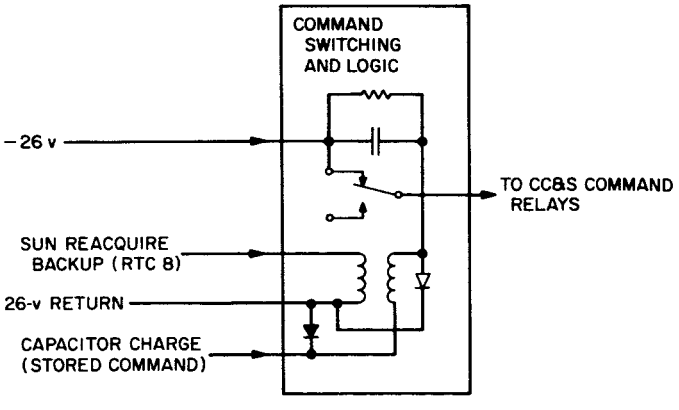

Fig. 8. Sun-reacquire backup details

the CC&S relays can be restored by repeating the midcourse sequence (capacitor charge).

b. CC&S commands. The following are the stored commands and the normal sequence of events generated by the CC&S. All commands utilize magnetic latching relays in the CC&S which switch −26 v from the attitude control DC converter on the specified signals. The commands are grouped by lowercase letters representing specific relays; the first transfer of contacts is listed as (1) and the return transfer of contacts is listed as (2).

(a)
- (1) Sun acquisition.

(b)
- (1) Earth acquisition.
- (2) Break Earth lock.
- (1) Reacquire Earth.

(c)
- (1) Connect roll capacitor and exit antenna.
- (2) Switch out roll capacitor and reposition antenna.

(d)
- (1) Turn on autopilot, accelerometer, and jet vane actuators.
- (2) Turn off autopilot, accelerometer, and jet vane actuators.

(e)
- (1) Positive polarity command.
- (2) Negative polarity command.

(f)
- (1) Start roll turn.
- (2) Stop roll turn.

(g)
- (1) Switch out Sun sensors and connect pitch and yaw capacitors.
- (2) Switch in Sun sensors and disconnect pitch and yaw capacitors.

(h)
- (1) Start pitch turn.
- (2) Stop pitch turn.

(i)
- (1) Start yaw turn.
- (2) Stop yaw turn.

Two additional functions performed by the CC&S, but which do not use relays, are:

(1) Capacitor cycling pulse to the gyros, which comes from an isolated transistor switch in the CC&S.

(2) Acceleration information supplied to the CC&S by the attitude control system in the form of a driven transistor switch.

Table 1. Attitude control system power input requirements

Voltage (RMS), v	Voltage tolerance, %	Frequency, cps	Spikes peak-to-peak, mv	Ripple peak-to-peak, mv	Frequency tolerance, %	Harmonic distortion, w	Load maximum, w	Remarks
Direct current								
±26	10		300	50			15.5	Attitude control power
±26	10		300	60			20.0	Autopilot power
±35	10						11.5	Gyro electronics
+20	+10 −5		200	20			0.5	Command current generator
Alternating current								
26	+18 −12	400			±0.01	≤10	18.5	Three-phase sine wave power for gyros
26	10	400			±0.01	≤30	7	Single-phase sine wave power for antenna actuator modulators and demodulators, accelerometer electronics

c. Hydraulic backup timer. As a backup command to the CC&S-initiated Sun acquisition, an hydraulic timer is used which is initiated at spacecraft separation. The timer is set so that the redundant Sun-acquire command is issued at spacecraft separation plus 60 min (±2 min).

3. Power

The attitude control system power requirements are given in Table 1.

4. Temperature Control

Temperature control for the subsystems of the attitude control system is achieved through the use of a passive temperature control system. By controlling the spacecraft internal heat-transfer capabilities and by the correct selection of surface finishes, the temperature control system maintains the temperature limits given in Table 2. (The Earth sensor, which uses a 5-w heater prior to turn-on, is the exception.)

Table 2. Temperature limits for subsystems

Unit	Operating temperature range, °C
Case IV electronics	+13 to +46
Earth sensor	−10 to +38
Sun sensors	
Primary	+13 to +46
Secondary	−75 to +75
Antenna actuator	−24 to +125
Gas	
Active elements	+5 to +70
Gas supply	+5 to +35

II. PERFORMANCE CHARACTERISTICS

The performance characteristics of the attitude control system are discussed in three parts: (1) spacecraft mission requirements as needed by the spacecraft in order to perform the Block III missions, (2) functional design requirements as necessary to ensure mission requirements, and (3) system design performance requirements as necessary to accomplish detail hardware design.

A. Spacecraft Mission Requirements

The spacecraft attitude control requirements, as defined in the design characteristics and restraints for Block III, are:

(1) *Separation rates.* The method of separating the spacecraft from the *Agena* adapter should not impart an angular rate greater than 3 deg/sec about each of the three principal spacecraft axes.

(2) *Solar panel orientation.* The solar panels should be oriented normal to the incident solar radiation within ±2.0 deg.

(3) *Midcourse maneuver accuracy.* The spacecraft should be capable of taking up and maintaining a commanded direction in space within 138 mrad.

(4) *Midcourse velocity increment accuracy.* The velocity increment errors due to the resolution accuracy of the accelerometer should be within the range of ±0.6 ft/sec.

(5) *Terminal maneuver pointing accuracy.* The spacecraft should be capable of taking up a commanded orientation in space within 90 mrad (5.15 deg).

(6) *Terminal maneuver orientation hold.* From the completion of the orientation maneuver in the terminal phase, the attitude control system should be capable of holding the initial orientation within 45 mrad over a 26-min period.

B. Functional Design

In order to accomplish the mission requirements, the following functional requirements were established:

(1) Pointing error of the roll reference line in cruise: 8.7 mrad (3 sigma).

(2) Pointing error of the antenna axis in cruise: 5 deg (3 sigma).

(3) Pointing error of the thrust vector in midcourse maneuver: 35 mrad (3 sigma).

(4) Pointing error of the roll reference line in the terminal maneuver: 35 mrad (3 sigma).

C. Design Performance Requirements

As seen from Figs. 1 and 2, simplicity was given a high priority in order to maximize the likelihood of mission success. In order to achieve simplicity, the following restraints were established:

(1) No premaneuver mode. Limit cycle size changes were made for pitch and roll control during the commanded turn mode only.

(2) No signal switching between the autopilot and the cruise attitude control mechanism.

(3) No turnoff of cruise attitude control during autopilot operation.

(4) No extra switching to provide rapid Sun acquisition or modified dynamic characteristics for the command turn or autopilot modes. The required dynamic changes were provided by the same switching function that removes the optical position signal and inserts the gyro position control, and by multiple taps on a single rate-plus-position network in each gyro loop.

Redundancy in the gas subsystem and in the primary commands (Sun acquisition, Earth acquisition, control over maneuvers) was accomplished. The gas subsystem was mechanized using two identical half gas systems, with each half system having its own gas reservoir and regulator. The system was mechanized so that controlling torques about each axis were established by actuating a valve from each half system. In the yaw and roll axes, the valves operated as a couple; in the pitch axis, they operated as a pair.

This mechanization also had the advantage that a failure of any valve in the open position did not abort the mission. As seen in Figs. 1 and 2, any open valve would result in the two opposing valves being actuated, so that a total of three valves would be expelling gas. Therefore, all of the gas in the malfunctioning half gas system could be expelled and attitude control maintained by depleting one-third of the gas supply of the remaining half system. The gas subsystem reservoirs were sized with this type of failure in mind.

Redundancies in the Earth and Sun acquisitions and the capability of terminating any maneuver by ground command were also incorporated.

An additional increase in the overall reliability of the system and an increase in the margin of the stored gas were accomplished on *Rangers VIII* and *IX* by the use of the derived-rate system. Because the derived-rate system did not require the gyros, gyro electronics, or the three-phase inverter to operate, the overall reliability was increased. (This is a significant factor because normal operation of the three-phase inverter requires that it obtain a three-phase synchronizing signal from the power system synchronizer. All other inverters and converters have the capability of free-running without their respective synchronizing signals.) The margin for the stored-gas system was increased as a result of a lower velocity increment of the derived-rate system.

The derived-rate system also enhances spacecraft reliability, since a probability exists of not performing a terminal maneuver after a successful midcourse maneuver. On lunar impact trajectories, the ability to salvage basic mission requirements with existing spacecraft malfunctions was enhanced.

III. COMPONENT SELECTION AND CONTROLS

A. Selection

The selection of the components of the attitude control system and their operating margins was accomplished through the use of the JPL Preferred Parts List. In instances where special components were required and did not appear on the Preferred Parts List, specifications for the components were written with the approval of the Component Evaluation Group. All non-Hi-Rel components were burned-in and screened by either the component manufacturer or by JPL. When component performance varied beyond specification limits, the test data was reviewed by the Component Evaluation Group and the parts dispositioned.

Components which affected the flight hardware in general and which required replacement were:

(1) *Daleohm resistors.* The "G" series resistor resistance element was opening when operated at low power levels and when exposed to humidity. Since the failure mode was catastrophic for all circuit applications, these resistors were replaced with another type (Allen Bradley).

(2) *Fairchild diode quads.* The FSP 126 diode quads had questionable bonds between the diode chips. These bonds were screened by submitting the diode quads to a 20,000-*g* centrifuge test.

(3) *Sprague 350D (Hi-Rel) capacitors.* All capacitors that had been screened to an early specification required replacement. The early specification required a temperature shock which may have been detrimental to the capacitor.

(4) *Triad transformers (SP 21, SP 22).* A manufacturing defect in the technique of welding the fine transformer wire to the lead material required transformer replacement of early lots.

(5) *Continental Devices diodes.* An internal gold flaking problem required replacement of all Continental Devices diodes.

1. Requirements

All of the following component performance requirements are relative to spacecraft coordinates and apply under all environmental conditions.

a. Earth sensor specification. The Earth sensor characteristics are shown in Table 3.

b. Sun sensor specification. The Sun sensor subsystem must have a pointing accuracy of 3.5 mrad and have a field of view over the complete sphere about the spacecraft. The Sun sensors, consisting of primary and secondary pairs, are interconnected to produce these correct error characteristics, which must lie within the limitations shown in Table 4.

To explain items in the following specifications, the two-axis Sun sensor orientation is shown. The Sun sensor location on the axes is as follows: primary pairs located on the bus, and two pairs of sensor elements in each secondary sensor located on the solar panels.

c. Attitude control gyro and gryo loop specification. The pitch and yaw gyro loops are shown in detail in Fig. 9; the characteristics are given in Table 5.

d. Hinge servo specification. The hinge servo (Fig. 7) should have a Sun–probe hinge angle-tracking capability of 22 mrad maximum. The servo should position the antenna to the preset angles within an accuracy of ± 3 deg. Characteristics and tolerances are given in Table 6.

e. Switching amplifier specifications. Two different switching amplifiers were flown in *Ranger* Block III. An hysteresis system (characteristics shown in Table 7) was used on *Rangers VI* and *VII*; a derived-rate system was used on *Rangers VIII* and *IX*. Aside from the derived-rate feedback within the amplifier, the derived-rate system differed from the hysteresis system in that it is a minimum on-time amplifier, which has a lower design value for the velocity increment. For *Rangers VI* and *VII*, the velocity increment was 60 ± 30 μrad/sec; for *Rangers VII* and *IX* the velocity increment was 20 ± 2 μrad/sec. The position and rate deadbands remained the same.

f. Nominal performance characteristics. A summary of nominal performance characteristics and scale factors follows:

(1) *Scale factors.*

Position:

Pitch, 18 v/deg.

Yaw, 18 v/deg.

Roll, 4.5 v/deg (midcourse).

Hinge, 2.0 v/deg.

Table 3. Earth sensor characteristics

Quantity	Nominal value	Tolerance
Roll null offset		
Electrical	0	8.0 mrad (0.458 deg), 3 sigma
Mechanical misalignment perpendicular to hinge axis	0	1.73 mrad (±0.099 deg), 3 sigma
Hinge null offset	0	±17.5 mrad (±1 deg), 3 sigma
Linearity		
Roll	Monotonic in ±22.5-mrad (1.29-deg) range	
Hinge	Monotonic in −2.5- to +2.5-deg range	
Null drift rate		
Roll	0	2 μrad/sec, 3 sigma
Hinge	0	2 μrad/sec, 3 sigma
Noise		
Roll	0	0.2 mrad peak-to-peak (max)
Hinge	0	1 mrad peak-to-peak (max)
Noise slope		
Roll	1 μrad/sec (max) or such that multiple switching at end of limit cycle does not increase design limit cycle velocity	
Rise time to step input (5 to 95% of final response)		
Roll	0.2 sec (max)	
Hinge	0.2 sec (max)	
Hinge-axis saturation for up to ±2-mrad (±0.115 deg) roll error	28 mrad (min) (1.605 deg)	
Scale		
Roll	8 v/deg ±8%	
Hinge	2 v/deg ±15%	

Table 4. Sun sensor characteristics

Quantity	Nominal value	Tolerance
At midcourse and terminal maneuver		
Mechanical misalignment	0	±0.126 deg, 3 sigma
Front null electrical offset	0	±0.16 deg, 3 sigma
Front null electrical offset at other times	0	±1.145 deg[a]
Rear null electrical offset	0	±20 deg (max)
Linearity	Monotonic in the −0.86- to +0.86-deg range	±10% change in slope to ±0.115 deg from front null
Null drift rate	0	2 μrad/sec, 3 sigma
Noise	0	0.2 mrad peak-to-peak (max)
Noise slope	1 μrad/sec (max) or such that multiple switching at end of limit cycle does not increase design limit cycle velocity	
Rise time to a step input (5 to 95% of final response)	0.2 sec (max)	
Primary and secondary Sun sensor field of view	4π sterad	0 (absolute requirement)
Primary Sun sensor field of view		
In plane of control (pair)	±45 deg	±5 deg (max)
In plane perpendicular to control plane	±30 deg	±5 deg (max)
Misalignment of null planes to vehicle reference planes	0	±40 mrad[a]

[a]Specifications are not critical and changes are possible.

Table 5. Pitch and yaw gyro characteristics

Quantity	Nominal value	Tolerance
Fixed torque drift after compensation	0	4.8 μrad/sec, 3 sigma
Steady-state response of spacecraft to turn command	3.5 mrad/sec	±5%
Deviation from calibrated turn response including variations of all components	0	±0.3%, 3 sigma
Gyro linearity deviation		
Monotonic over range ±10 mrad/sec		
0 to 0.5 mrad/sec	0	±4.85 μrad/sec (max)
0.5 to 7.0 mrad/sec	0	±48.5 μrad/sec (max)
Calibrated point, ±0.1 mrad/sec	0	±1.5 μrad/sec (max)
Gyro-loop angle storage capacitor random leakage	0	5.0 mrad, 3 sigma, for any turn up to 3150 mrad
Saturation turning rate	10 mrad/sec (min)	
Torquing amplifier voltage saturation	53 mrad (min)	
Damping ratio (gyro loop)	0.4 (min)	
$\tau_{GA} \cdot K_g$ product		
Acquisition and cruise mode, pitch and yaw axes	3.2 sec	±20%
Acquisition and cruise mode, roll axis	5.45 sec	±20%
Command turn, all axes	5.45 sec	±20%
Ground command	3.82 sec	±20%
Null drift rate	0	2 μrad/sec (or $2/\tau_{GA}$ μrad/sec^2), 3 sigma
Noise	0	0.2 mrad (or $0.2/\tau_{GA}$ mrad/sec) peak-to-peak (max)
Noise slope	1 μrad/sec (max) or such that multiple switching at end of limit cycle does not increase design limit cycle velocity	
Rise time (from application until 95% of steady-state gyro loop output)	100 msec (max)	
Pitch gyro misalignment in yaw from all sources	0	1.53 mrad, 3 sigma
Pitch gyro misalignment in roll from all sources	0	1.53 mrad, 3 sigma
Yaw gyro misalignment in roll from all sources	0	1.53 mrad, 3 sigma
Yaw gyro misalignment in pitch from all sources	0	1.53 mrad, 3 sigma
Roll gyro misalignment in pitch from all sources	0	1.53 mrad, 3 sigma
Roll gyro misalignment in yaw from all sources	0	1.53 mrad, 3 sigma

Rate:
Pitch, 2.6 v/mrad/sec.
Yaw, 2.6 v/mrad/sec.
Roll, 2.6 v/mrad/sec.

(2) *Deadbands.*

Position:
Pitch, ±2.9 mrad.
Yaw, ±2.9 mrad.
Roll, ±5.0 mrad (midcourse).
Hinge, ±20 mrad.

Rate:
All axes, 1 mrad/sec.

(3) *Commanded turns:* 3.5 mrad/sec.

(4) *Roll-search rate:* −3.5 mrad/sec.

(5) *Acceleration constant:* 0.72 mrad/sec^2.

(6) *Velocity increment:* 20×10^{-3} mrad/sec.

(7) *Switching amplifier on-time:* 20 msec.

(8) *Time allowed to eliminate tumbling rates:* 15 min (maximum).

(9) *Time allowed to turn spacecraft to face Sun:* 22 min (maximum).

Table 6. Hinge servo characteristics

Quantity	Nominal value	Tolerance
Pointing of preset angles	±3 deg (max)	
Preset angle	46	±3
	135	±3
	123	±3
	110	±3
	97	±3
	84	±3
	71	±3
	58	±3
Exit angle	180	±3
Misalignment of hinge axis in yaw	0	2.6 mrad, 3 sigma
Misalignment of hinge axis in roll	0	2.6 mrad, 3 sigma
Switch-on angle	±20 mrad	±2 mrad
Switch-off angle	±10 mrad	±2 mrad
Turning rate	5 mrad/sec	+50% −0
Turning rate rise time (from receipt of electrical signal to 90% of full turning rate)	10 sec (max)[a]	
Drive backlash: must cause less than 0.1-mrad spacecraft reaction angle		
Switching amplifier noise (referred to input)	0	1 mrad peak-to-peak (max)
Potentiometer linearity	±35 mrad	

[a]Specifications are not critical.

Table 7. Switching amplifier characteristics

Quantity	Nominal value	Tolerance
Roll dead zone in acquisition, cruise, and command turn	5.0 ±0.5 mrad, 3 sigma	
Pitch and yaw dead zone in acquisition and cruise	2.9 ±0.29 mrad	
Pitch and yaw dead zone in command turn	5.0 ±0.5 mrad, 3 sigma	
Hysteresis (*Rangers VI* and *VII*)		
Pitch and yaw axes	70 μrad	±50%
Roll axis	160 μrad	±50%
Rate deadband, all axes	1	±20%
Null offset	0	±1 mrad[a], 3 sigma
Null drift rate	0	2 μrad/sec, 3 sigma
Noise	0	0.2 mrad peak-to-peak (max)
Noise slope	1 μrad/sec (max)	
Rise time (from rapid crossing of switching line to 95% output)	200 mrad/sec (max)	
Fall time (from rapid crossing of switching line to 5% output)	50 mrad/sec (max)	

[a]Specifications are not critical.

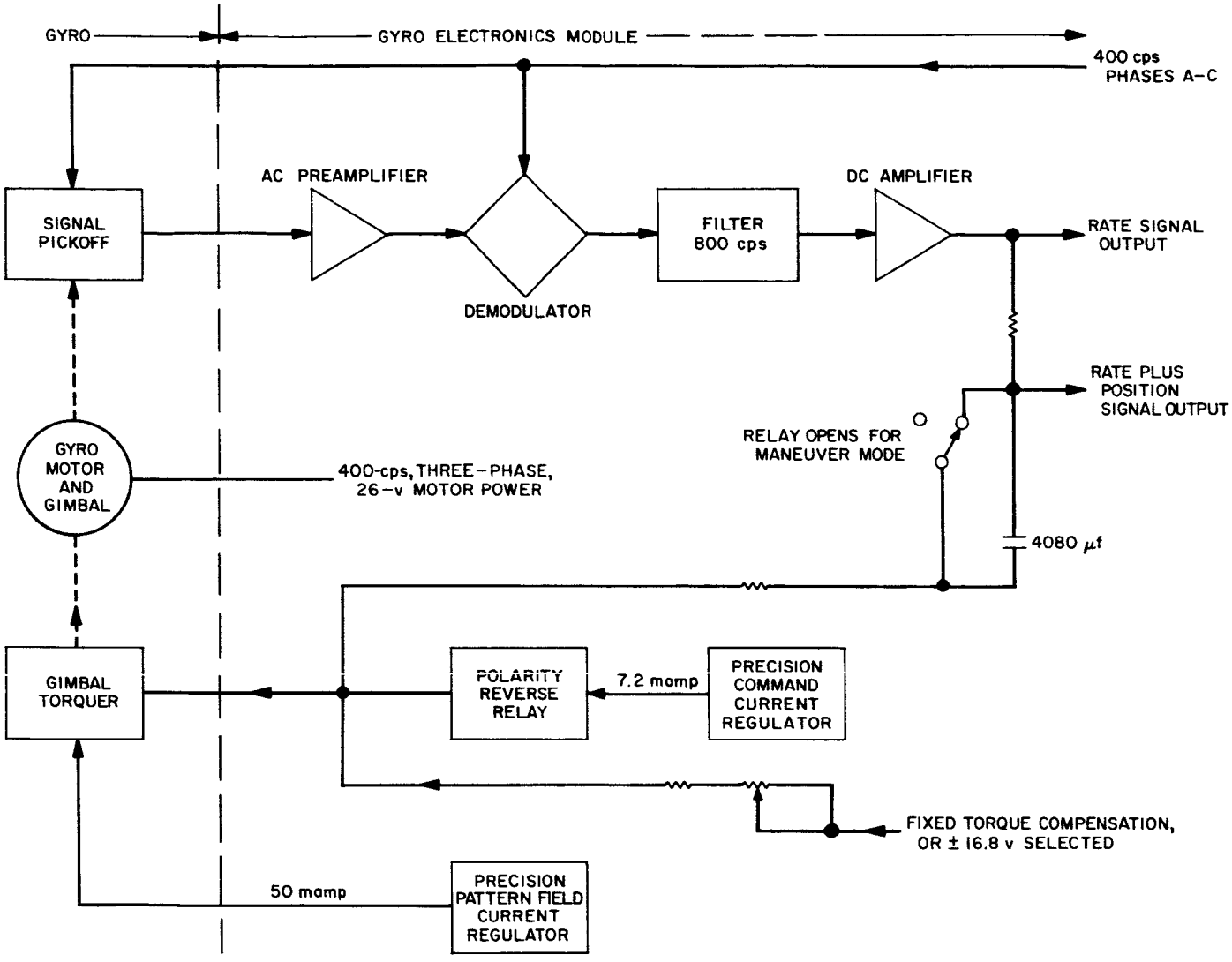

Fig. 9. *Ranger* gyro loops

B. Quality Control

A quality control organization was used by the manufacturer and included technicians and engineers in inspection and testing phases.

1. Process Bulletins

All applicable JPL specifications were reviewed by the manufacturer and were rewritten according to the individual format. Such documents were called Process Bulletins, and were used as working procedures for the manufacturing personnel. All Process Bulletins were approved for compliance with the original JPL specifications.

2. Test Work Orders

Detailed testing procedures for the flight hardware were written by the manufacturer and approved by JPL.

3. Flow Diagrams

Assembly sequence and schedule flow diagrams were generated, which allowed coordination of JPL surveillance and support during the assembly schedule. Typical flow diagrams may be seen in Figs. 10 through 13.

4. Inspections

As can be seen from Figs. 10 through 13, each JPL inspection was preceded by a vendor inspection. Complete JPL inspection was required at the manufacturer and at all subcontractor levels.

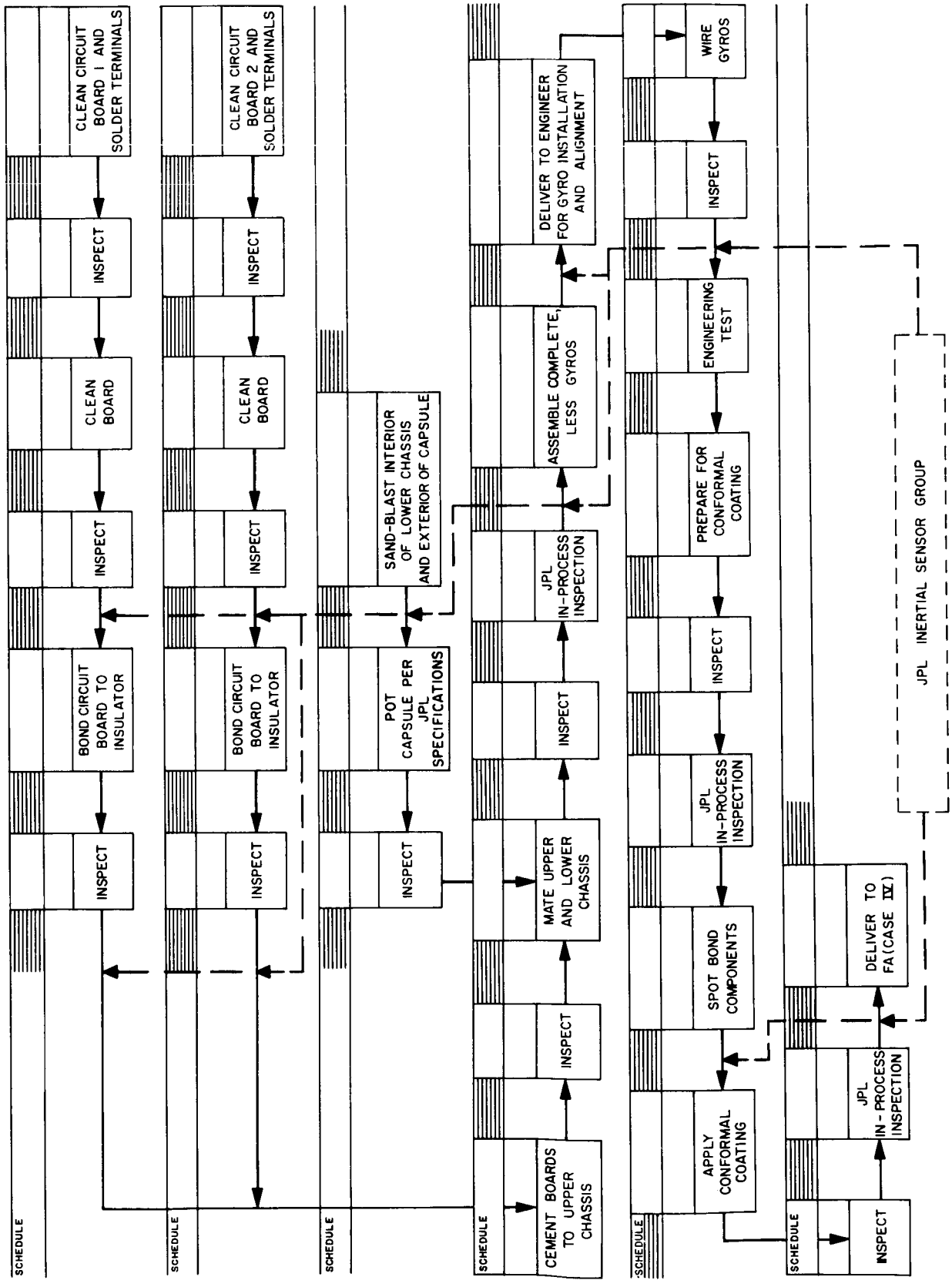

Fig. 10. Typical assembly sequence and schedule: gyro and capacitor module

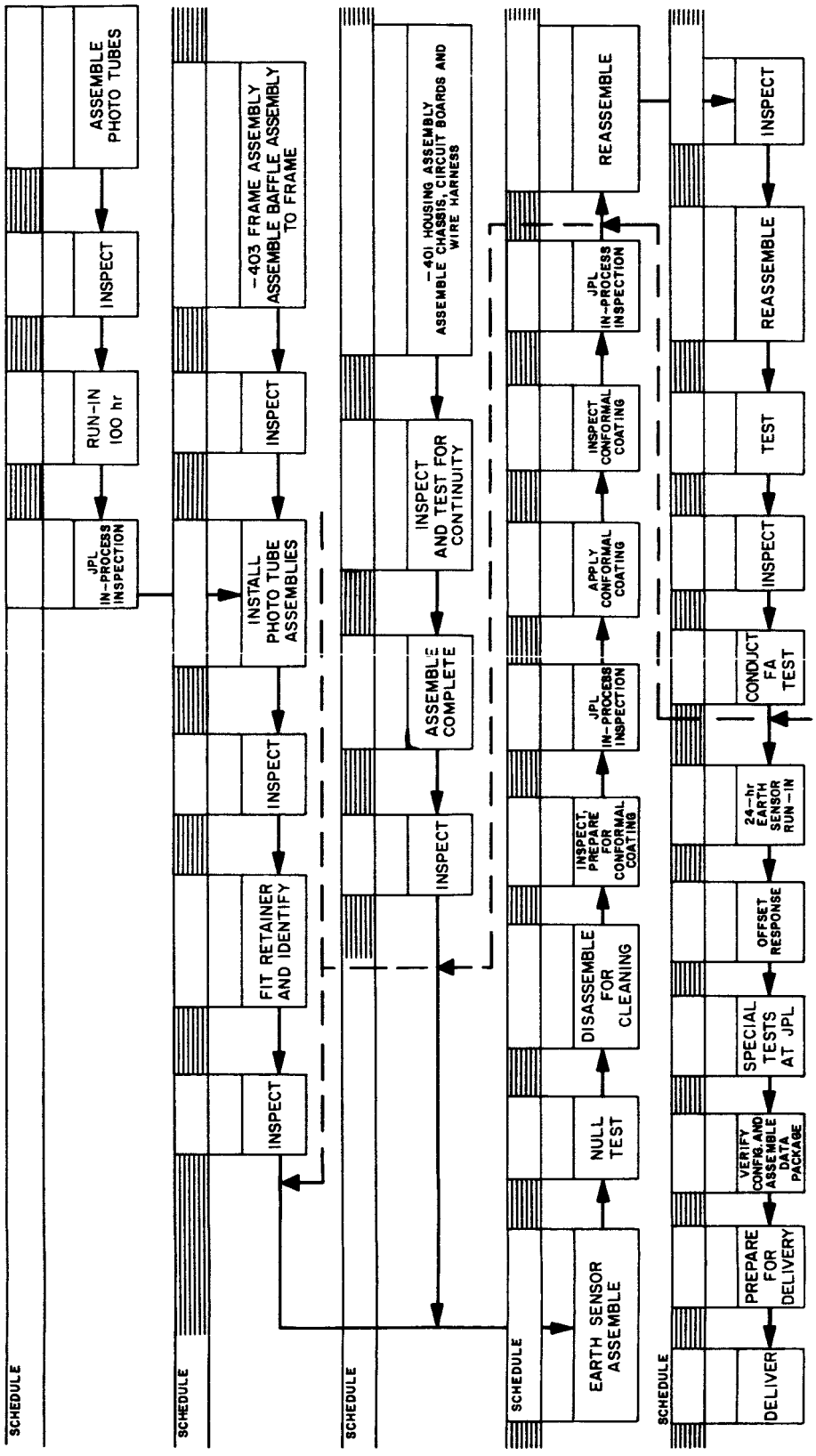

Fig. 11. Typical assembly sequence and schedule: short-range Earth sensor

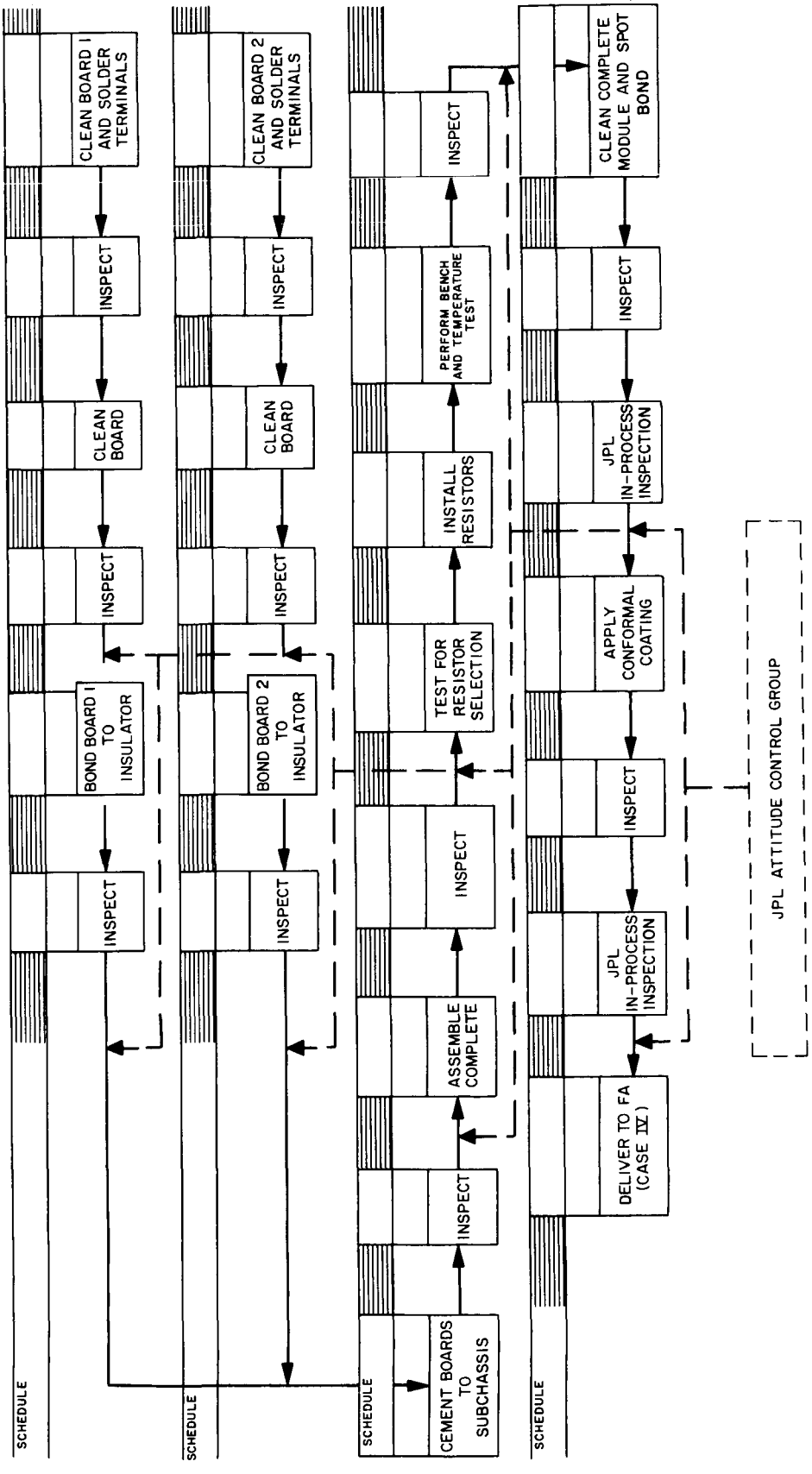

Fig. 12. Typical assembly sequence and schedule: switching amplifier

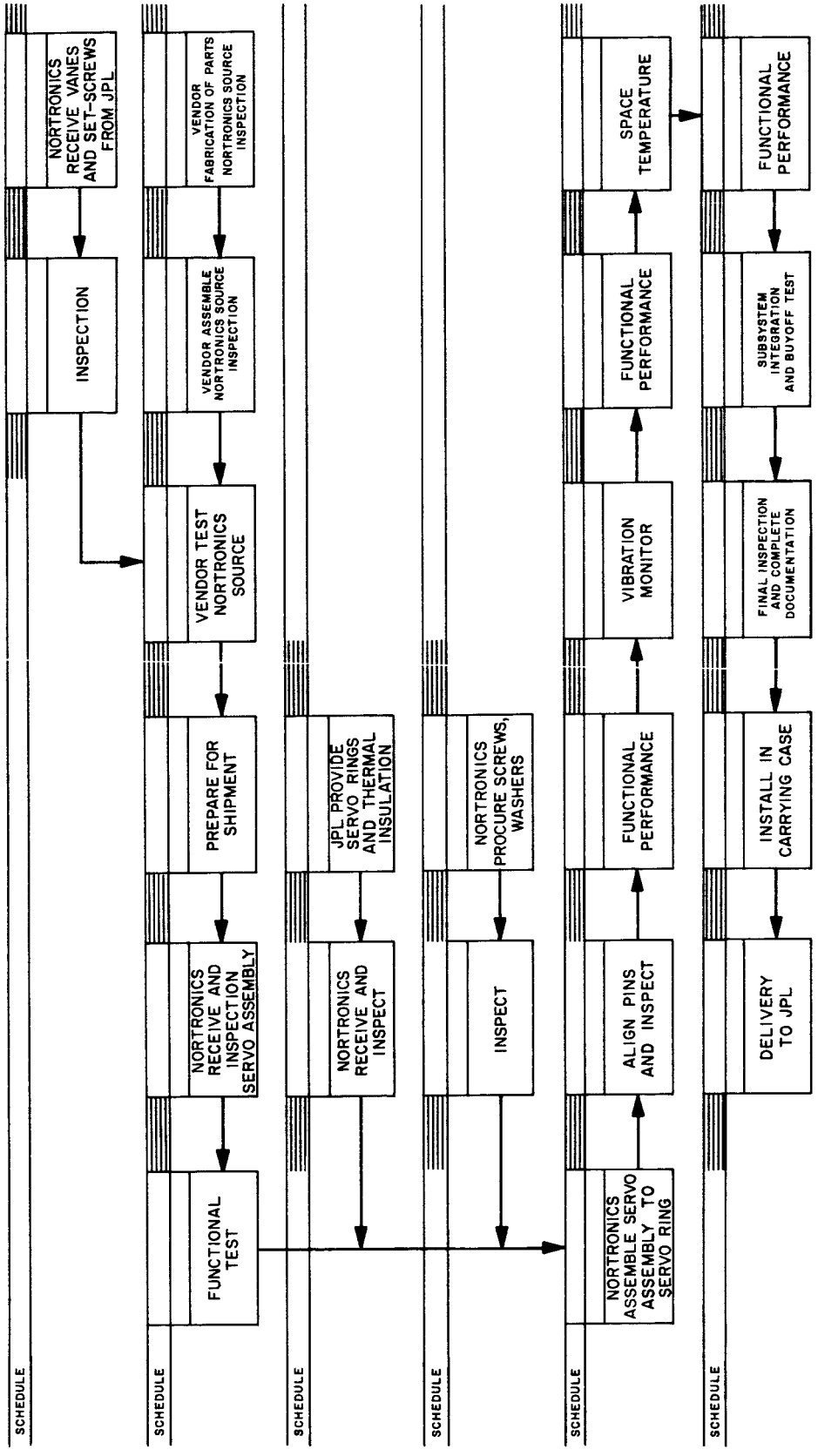

Fig. 13. Typical assembly sequence and schedule: jet vane actuator

5. Failure Reports

Failure reports were required of all malfunctions, at all levels and for all causes. These failures were reported by the manufacturer on his own form. JPL failure reporting forms were used by JPL inspectors and the manufacturing field teams which performed all systems and flight acceptance tests; these JPL forms were, in turn, used for on-Laboratory distribution. Failure analysis was performed by the manufacturer's engineering staff and the JPL cognizant engineer. Disposition and retest of flight hardware were defined by the JPL cognizant engineer.

6. AIR Books

All subassemblies had AIR (assembly, inspection, and record) books, which were compiled and maintained with the flight hardware. The AIR books listed in detail the following items:

(1) *Configuration record.* Logging of the drawings and drawing revisions used during manufacture.

(2) *Inspection sheet.* Signed and dated summary of all inspections required according to the flow diagrams.

(3) *Assembly operation sheet.* Chronological listing of operations performed during manufacture and place of performance.

(4) *Inspection pickup.* Listing of all inspection discrepancies and their subsequent rework and acceptance.

(5) *Assembly/part travel history.* Logging of the travel history (chronological).

(6) *Failure records.* Section containing all failure reports and subsequent failure analyses.

(7) *Inspection records.* Section containing copies of all vendor and JPL inspection reports.

(8) *Hi-Rel component serial number record.* Logging of the serial numbers of all components used during manufacturing.

(9) *Test data record.* Section containing a copy of all the test data. This section also contained a record of the operating time of the unit.

IV. SUBSYSTEMS

A. Earth Sensor

The Earth and Sun sensors are used for angular attitude reference on the *Ranger* spacecraft. Sun sensors are energized at approximately 1 hr after launch in order to provide two-axis error signals (pitch and yaw) to the attitude-control switching logic and gas jets, which then act to null the Sun-sensor error signals. The third or roll axis position of the spacecraft is controlled by error signals from the Earth sensor, which is energized approximately 3.5 hr after launch. The directional, or high-gain, radio antenna is then servoed toward Earth by a combination of spacecraft roll positioning and a fourth (redundant pitch) axis called hinge.

1. Description

The Earth-sensor optical mechanism uses a variable-aperture shadowing technique. The detectors are three 0.75-in.-diameter Dumont end-on photomultiplier tubes arranged so that their outputs can be resolved into two-axis error signals. The expected variation of Earth light intensity is in the range of from 0.06 to 40 ft-cd.

Figure 14 shows how the apertures in front of the three photomultiplier tubes inside an Earth sensor are shaded in an electrical null configuration. Under an electrical null condition, one-half of the C photomultiplier tube aperture is shaded; one-quarter of each of the A and B photomultiplier tube apertures is illuminated with light. A positive roll error signal results when more than one-half of aperture C is illuminated; a positive hinge error voltage occurs when more of aperture B is illuminated than aperture A. All three apertures have the same dimensions: 0.0685 by 0.137 in. The *Ranger* Block I and II Earth sensors have a total field of view of 60 deg in hinge by 40 deg in roll; the Block III Earth sensors have a total field of view of 20 deg in hinge and 10 deg in roll.

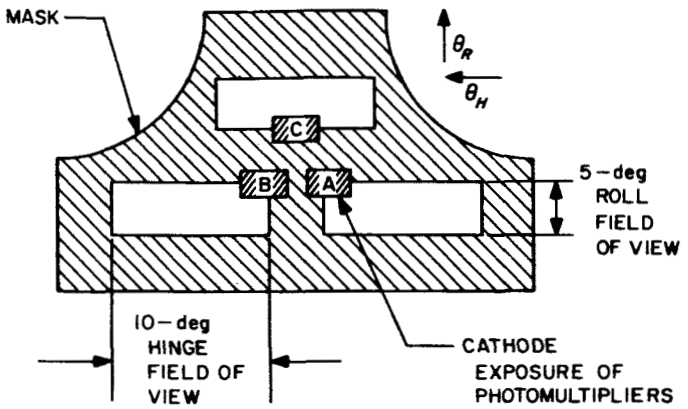

Fig. 14. Earth sensor shadow box

The initial *Ranger I* Earth sensor electronic design used three photomultiplier tubes excited with a 150-v ripple on 1200 v DC; six flight Earth sensors using this design were built and operated satisfactorily. However, it was decided to modify this design to improve photomultiplier gain stability on the *Ranger I* flight Earth sensors. The photomultiplier tubes in the new design are excited with DC instead of the DC and AC ripple that had been used previously. With the improved photomultiplier gain stability, the DC model has improved null stability and threshold characteristics. The excitation to the tube is filtered DC, giving DC outputs. These outputs are then mixed and modulated to give the hinge $(A - B)$, roll $(A + B - C)$, and control $(A + B + C)$ outputs. The control output is used to control the tube excitation so that the three tubes give a total output of 1-μamp current. Figure 15 is a block diagram of the Block I Earth sensor.

An electrostatic shield (which extends the life of the photomultiplier) was added around the cathode portion of the tube (Fig. 16) during the development period; this modification significantly improved the life characteristics of Earth sensor photomultiplier tubes in both versions $(A - C$ and $D - C)$.

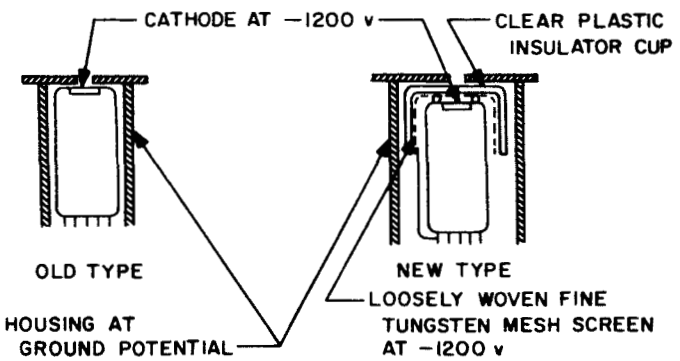

Fig. 16. PMT electrostatic shield

The Block II spacecraft configuration permitted a larger size Earth sensor; consequently, electronic design improvements were made to increase its reliability and performance characteristics. However, the input and output voltages of the Earth sensor remained unchanged. The input voltages to the Earth sensor are + and −26

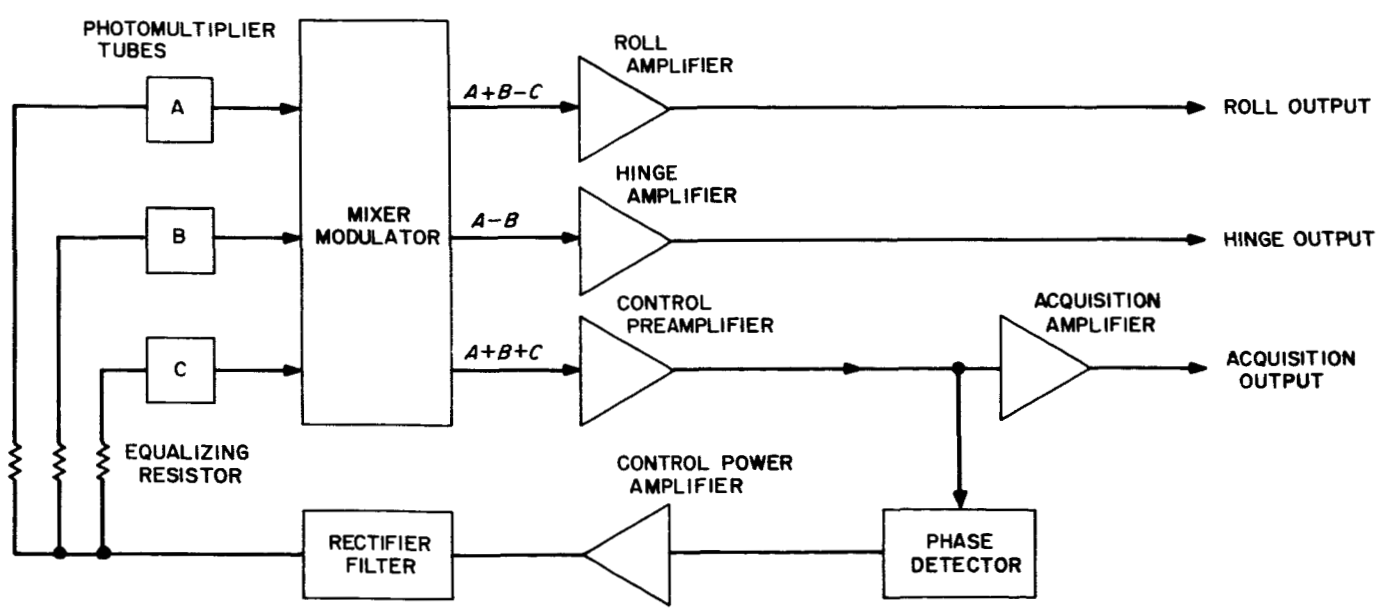

Fig. 15. *Ranger* Block I Earth sensor

v DC and a 400-cps, single-phase, 26-v-RMS signal. The output voltages from the Earth sensor are an acquisition signal, roll error, hinge error, Earth light-intensity signal, and temperature transducer readout. Although design improvements were made to the Block II Earth sensor, its basic mode of operation was similar to that of Block I.

A light hood was attached to the Block II Earth sensor so that it could track the Earth at Earth–probe–Sun angles of 73 deg or greater during terminal maneuver when the Earth sensor's optics might not be shaded by the Earth sensor Sun shield. (Without a light hood, the Earth–probe–Sun angle during terminal maneuver would have to be greater than 93 deg.) The light hood was made out of silastic rubber with embedded piano wire springs with thin Teflon film strips bonded onto the three areas that would touch the *Agena B* adapter before adapter–spacecraft separation. Separation tests were performed; it was found that the tip-off rate of the spacecraft, due to the light hood making contact with the adapter during adapter–spacecraft separation, was negligible. A light hood was type-approval tested and each flight light hood was flight-acceptance tested. In addition to these tests, special temperature tests were performed because of the wide range of temperatures to which the light hood would be exposed. The following temperatures were estimated during a *Ranger* flight: 0°F at the time of *Agena B* adapter–spacecraft separation; a minimum temperature of −200 to −300°F during cruise; and a maximum temperature of 140°F while in sunlight. The light hoods were sterilized at 326°F for 2 hr and passed all of the mentioned tests without any failures experienced.

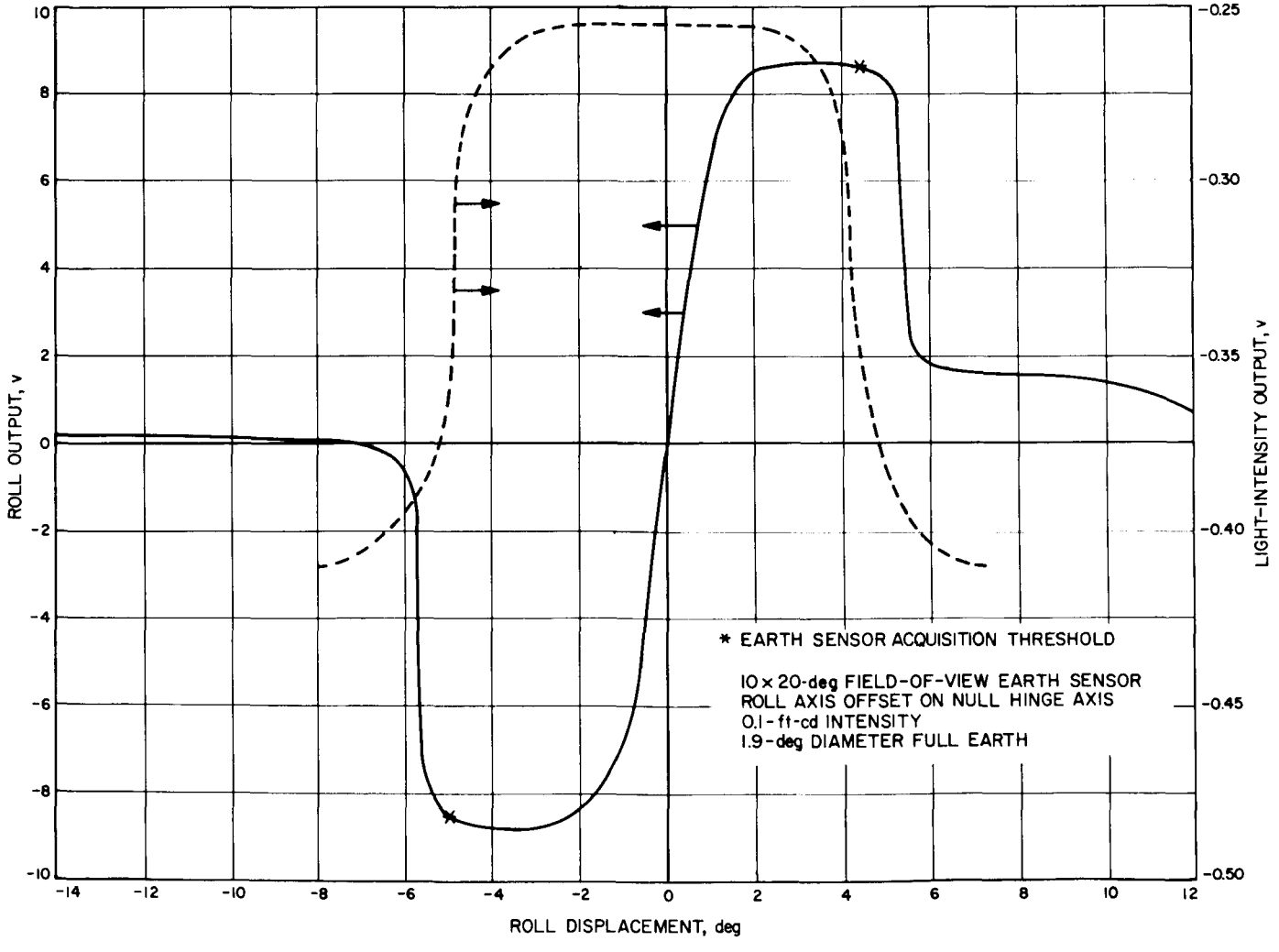

Fig. 17. Error signal and light intensity versus roll angle

Although further design improvements were made on the Block III Earth sensors, the initial improvements to the Block II Earth sensors were:

(1) New shadow cover assembly with a reduced field of view.

(2) Solithane conformal coating.

(3) No heat sterilization.

(4) Miscellaneous hardware changes.

So that changes in acquisition preset hinge angle would not be necessary during any launch period, a large field of view was used in the Block I and II Earth sensors; however, it presented many constraints to the *Ranger* terminal maneuver and picture-taking mission. In order to circumvent these constraints, the field of view was reduced to ±5 deg in roll and to ±10 deg in hinge for *Ranger VI* and all subsequent missions (*Rangers VII* through *IX*). An eight-position antenna preset-hinge-angle update system was incorporated to make the small field of view possible. With the smaller field of view, the light hood of the Earth sensor did not touch the *Agena* adapter.

A series of evaluation tests was performed on the redesigned Earth sensor in order to verify this modification. These tests consisted of a dynamic offset response curve, null-axis response data at light intensities which correspond to Earth sensor first turn-on, midcourse and terminal maneuvers, Earth–probe–near limb light Moon angle measurements, light reflection tests from the spacecraft into the Earth sensor, and type-approval environmental tests.

Figure 17 shows the effect of roll-axis angular offsets at a null hinge angle; it includes roll error voltages, Earth sensor light-intensity voltage outputs, and acquisition threshold points of the reduced field-of-view Earth sensor. The redesigned Earth sensor can operate safely within tolerance at Earth–probe–Sun angles of 47 deg or larger during terminal maneuvers; previously, modification on the Earth–probe–Sun angle constraints during terminal maneuver was 73 deg or larger. The reflection measurements indicate that the maximum antenna angle during Earth search is 140 deg; previously, it had been 126 deg.

The effects of light reflection (which is intense enough to produce an acquisition signal in the Earth sensors) into the 40- by 60-deg field-of-view design and into the reduced field-of-view Earth sensors are shown in Fig. 18. The Block III Earth sensor is shown in Figs. 19 and 20.

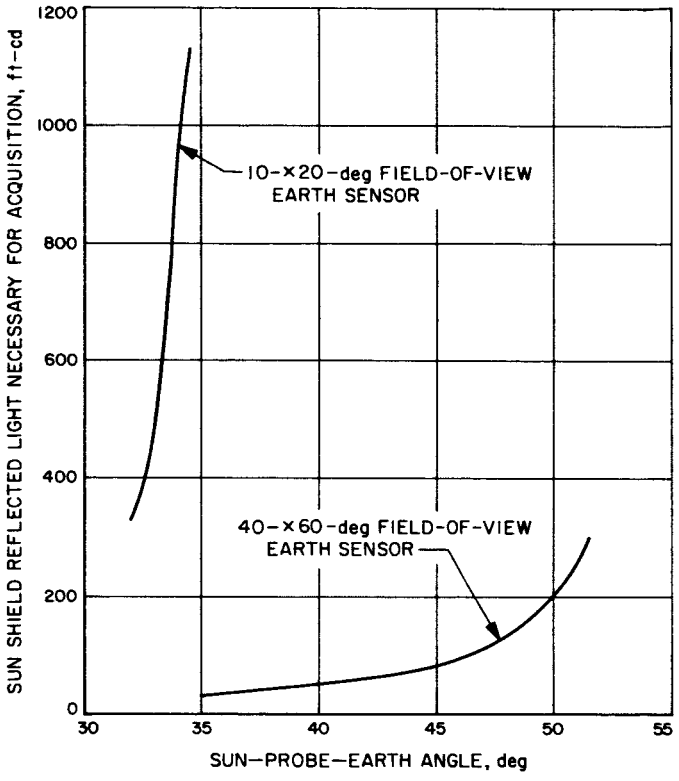

Fig. 18. Light reflection effects

The Earth sensor is mounted on the left half of the yoke on the antenna drive assembly, which is near leg C of the spacecraft structure just to the left of the antenna gear box, and shades the "optics" of the Earth sensor when the spacecraft is oriented toward the Sun. The internal heater of the Earth sensor is powered by the 400-cps, single-phase, 26-v input to the Earth sensor when the spacecraft is launched. At approximately 1 hr after launch, when the Sun sensors are first energized, the + and − 26-v DC is applied to the Earth sensor. At this time, the high-gain antenna is also rotated to its preset hinge angle so that the Earth will lie within the correct cone angle when the Earth sensor is first completely energized. At 3.5 hr after launch, the 26-v, 400-cps, single-phase voltage input to the Earth sensor is switched (Fig. 21) from the heater to the electronics of the Earth sensor; this completely energizes the Earth sensor, and the spacecraft rolls about its roll axis until the Earth sensor indicates Earth acquisition. The Earth sensor provides a two-axis error signal (roll and hinge) to the attitude control switching logic and gas jets, which then act to null the error signals of the Earth sensor. Once the Earth has been acquired, the spacecraft is stabilized

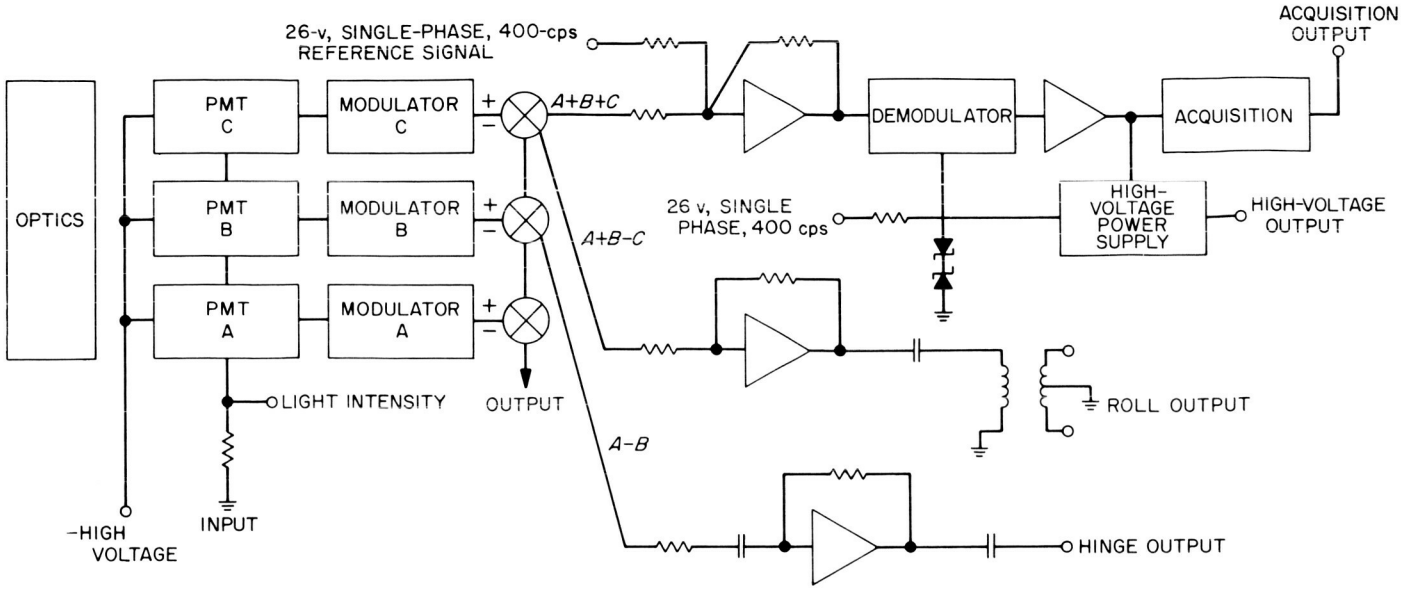

Fig. 19. *Ranger* Block III Earth sensor

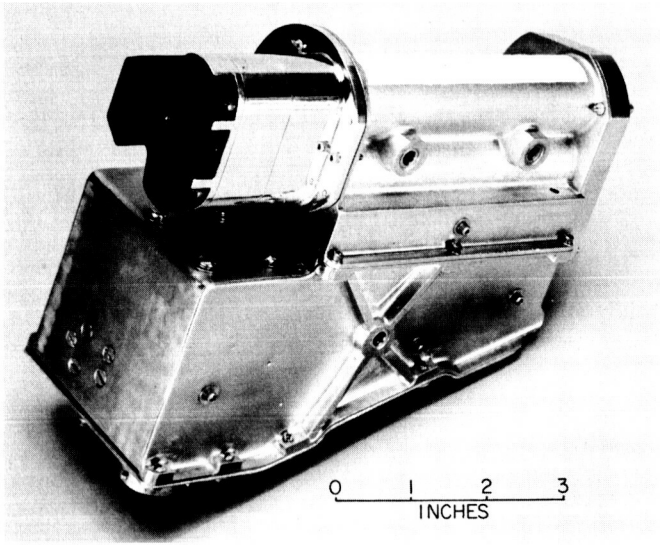

Fig. 20. Block III Earth sensor

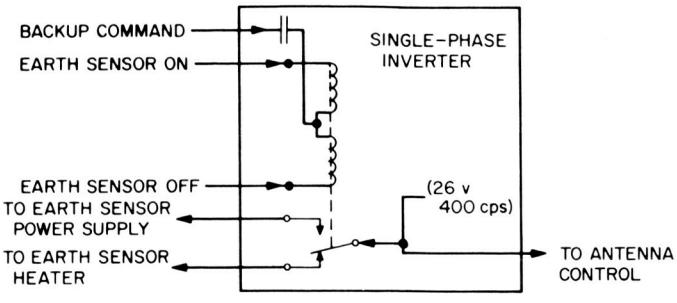

Fig. 21. Earth sensor power switching

in its roll axis, and the high-gain antenna is pointed toward Earth. The Earth light-intensity telemetry output from the Earth sensor helps to verify that the Earth sensor has acquired the Earth. A normal midcourse maneuver occurs at approximately 16 hr after launch. At that time, the 400-cps input signal to the electronics of the Earth sensor is switched to the internal heater of the Earth sensor. With the Earth sensor de-energized and the Sun sensor signals switched out of the attitude control electronics, the high-gain antenna is rotated to an antenna angle of 180 deg, and the midcourse correction is made. After that, the Sun and Earth are reacquired. During terminal maneuver, the Sun sensors are switched out of the attitude control electronics, and the spacecraft performs a pitch–yaw–pitch maneuver to align the TV cameras on the spacecraft to the velocity vector of the spacecraft. During this time, the Earth sensor continues to track the Earth until the spacecraft impacts the Moon. Table 8 is the expected power dissipation of the Earth sensor under various power inputs to the Earth sensor during the different stages of flight. The following are approximate nominal Earth angular diameters during various phases of the flight; 12 deg at first Earth acquisition, 4.4 deg at midcourse maneuver, and 1.9 deg at terminal manuever.

All flight *Ranger* Earth sensors must remain within operating tolerances during all performance tests and flight-acceptance environmental tests. A two-dimensional plot of the Earth sensor's output is shown in Fig. 22.

Table 8. Power dissipation

Time from launch (A), hr	Function	Event	Power dissipation, w		
			Voltage input, %		
			Nominal	−10	+10
A = 0	Heater on	Launch	1.4	1.1	1.6
A + 1	Heater on; DC on	Start of Sun acquisition	3.2	2.6	3.9
A + 3.5	Heater off; DC on; AC on;	Start of Earth acquisition			
		No light	3.4	2.9	4.6
		First acquisition	2.7	2.3	3.2
A + 16		Midcourse	3.8	2.4	3.3
		At acquisition threshold	3.2	2.8	3.7

2. Fabrication

The Earth sensor housing consists basically of a frame housing which contains the photomultiplier tubes, the electronics housing, and the shadow cover assembly containing the optics.

The electronics housing is heat-treated and machined. After machining, the housing is liquid-honed and gold-plated. The cover assembly consists of the following parts in the order that they extend outward from the frame housing surface where the faces of the photomultiplier are located: the aperture plate, cover base containing lower and upper baffles and shadow bar plate, and light hood. The aperture plate is made out of a conetic shield; the rest of the cover assembly, except for some stainless steel dowel pins and screw caps, consists of machined 6061-T6 aluminum alloy. The front and inside of the cover assembly are dull black anodized except for the aperture plate which is chemically blackened; the external sides are polished for temperature control reasons.

a. Photomultiplier tube. The photomultiplier tube (PMT), used in all *Ranger* Earth sensors and in the *Mariner* Venus long-range Earth sensor, is basically the Dumont type industrial photomultiplier tube without the potted base and with certain special mechanical and electrical requirements. It is a ten-stage tube employing silver magnesium dynodes. It has a flat end-window type photocathode, which has an S-11 response with a peak output at a wavelength of 4400 Å and cuts off at 3000 and 6750 Å.

This PMT has undergone a continual upgrading with the cooperation of Dumont during its use in the *Ranger* Earth sensor. Essentially, the changes represented better quality control measures in the fabrication of the tubes and tighter, more specific, electrical requirements.

Electrical output characteristics. After 24 to 72 hr of aging under input conditions, the tube had the following characteristics:

(1) 95% of the total tube drift occurred within the first 30 min when operated at 0.5 to 1.5 μamp (Fig. 23).

(2) Dark current did not exceed 0.05 μamp at 1260-v excitation (105 v/stage).

(3) Output had a minimum of 60 μamp at input conditions of 0.1 ft-cd of 6000°K illumination through an aperture at the tube cathode of 0.06 cm^2 and centered on the first dynode grid, and a total tube excitation of 1100 v (Fig. 23).

There were 12 Westinghouse PMT's tested in order to compare their performance with the Dumont tube used in the short-range Earth sensor. The two tubes were comparable in size, gain, and spectral response.

The tube matching data revealed a fairly linear cathode response over the 0.1- to 4-ft-cd interval over which the tubes were tested. Therefore, the voltage necessary to produce 1 μamp of output current is an inverse function of the dynode gain of the multiplier. Under high-level conditions, the Dumont tubes required 10% more voltage to produce the same output; thus, Westinghouse tubes have higher dynode gain than the Dumont tubes, but show a greater variation in dynode gain necessary to produce a given output, with 4 ft-cd of incident light, than the Dumont tubes.

Conclusions.

(1) Dark current of Dumont and Westinghouse PMT's was within acceptable tolerances.

(2) Sensitivity of Westinghouse tubes averaged 20% higher than Dumont tubes.

(3) Dumont and Westinghouse tubes changed radically in sensitivity after 100-hr run-in period; however, direction of change was random.

(4) Fatigue of Dumont tubes was lower than Westinghouse tubes by a factor of two.

(5) Stability of Westinghouse tubes improved after 100-hr run-in; fatigue of Dumont tubes increased.

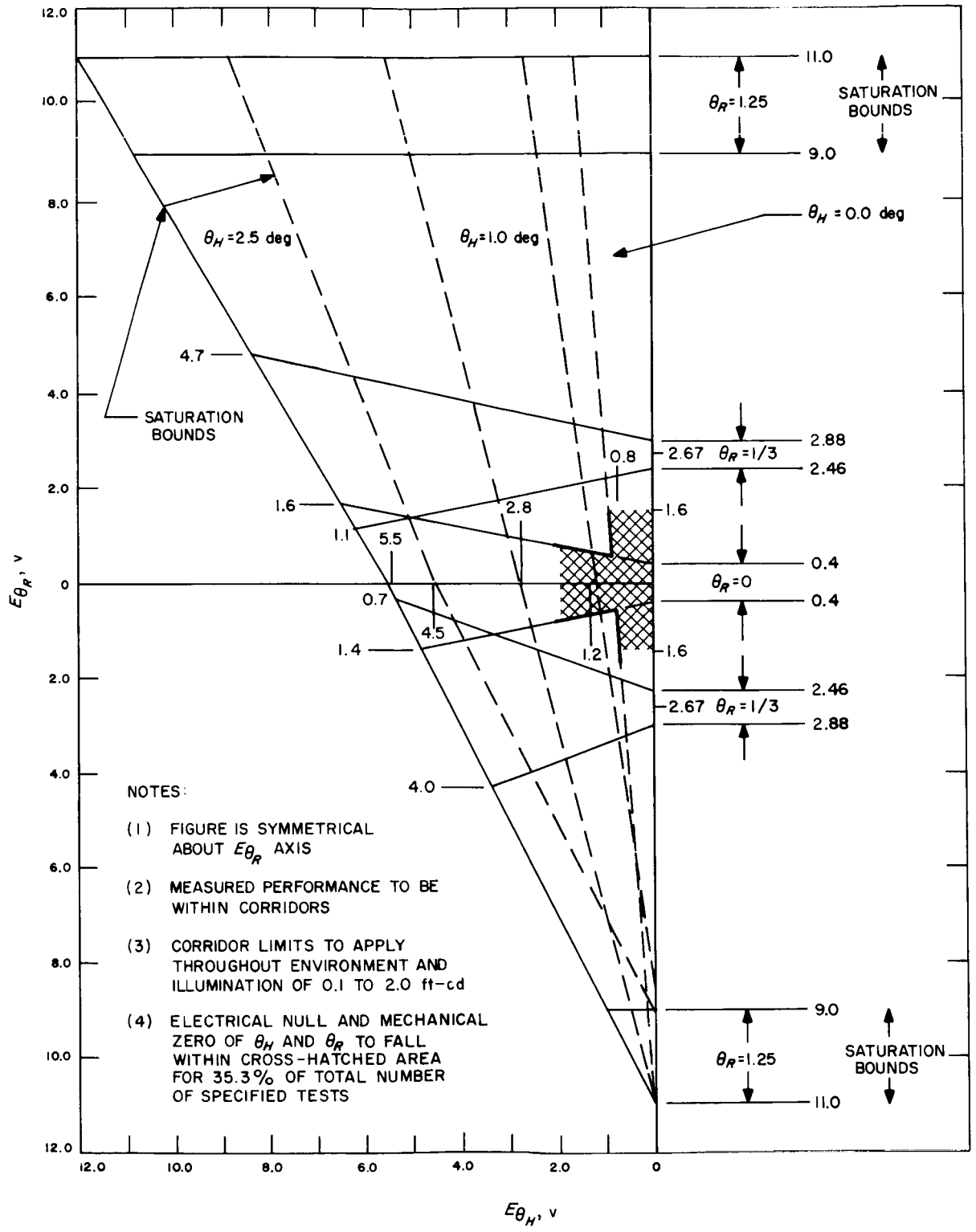

Fig. 22. Two-dimensional plot of Earth sensor's output

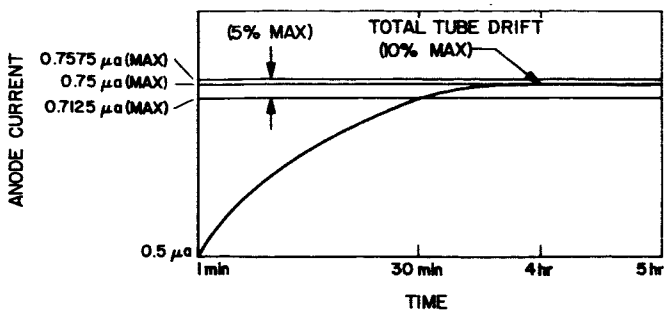

Fig. 23. Positive fatigue criteria

(6) Dynode gain of Westinghouse tubes was higher than Dumont tubes; Dumont tubes had smaller variation in dynode gain for sample lot.

(7) Dumont tube yield of tubes suitable for use in an Earth sensor was two times higher than Westinghouse sample.

A comparison was made of two RCA, Dumont, and Westinghouse PMT's after *Ranger* type-approval vibration and shock tests (Table 9). The percent change in tube microampere output under the same test conditions was made comparing after type-approval vibration to before any environmental testing and after the type-approval shock test to after the type-approval vibration test. These two environmental tests are considered to be the most severe environmental tests for the tubes; however, more tests must be performed before any real comparison can be made.

Table 9. PMT type-approval test comparisons

Tube tested	Change of microampere output after type-approval vibration, %	Change of microampere output after type-approval shock, %
Westinghouse		
Tube 1	−3	0
Tube 2	−21	11
RCA		
Tube 1	−41	−5
Tube 2	−16	0
Dumont		
Tube 1	4	−22
Tube 2	1	−22

Figure 24 shows a Dumont PMT in flight configuration; its dynode resistors and electrostatic shielding are installed on the tube inside a Teflon spool which fits against a Teflon cap attached to the back of the PMT. Teflon insulation is used on the wires to guard against any potential cold flow conditions that might exist during assembly of the dynode resistors into the spool.

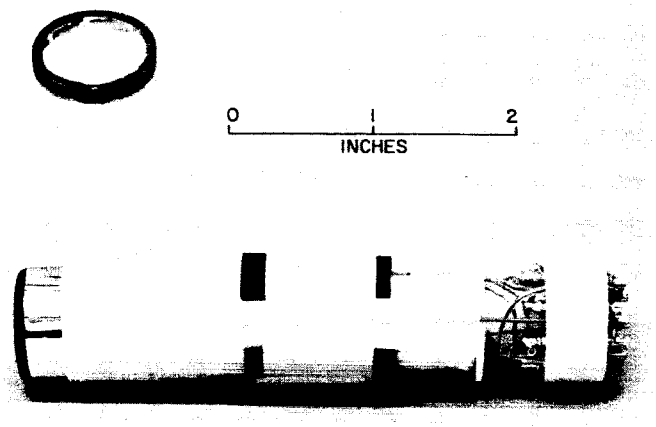

Fig. 24. Dumont PMT in flight configuration

3. Testing and Calibrations

These preliminary tests are functional checks and calibrations of the Earth sensor and adjust the following parameters: hinge amplifier gain setting, roll amplifier gain setting, acquisition threshold setting, PMT current level setting, balance of PMT's, and high-voltage telemetering output setting.

An Earth simulator, which is a constant brightness collimated light source, simulates the Earth at its color temperature, various sizes, and light intensities at midcourse and terminal maneuvers. The Earth sensor, mounted on top of a mechanical alignment fixture and a T-2 theodolite, can be rotated to any desired angle with respect to the Earth by means of the theodolite; the mechanical null position of the Earth sensor with respect to the Earth can be determined with the mechanical alignment fixture. The small telescope on the mechanical alignment fixture is adjusted parallel to the mounting reference surfaces on the Earth sensor using autocollimation techniques. Figure 25 shows the Earth sensor on top of a T-2 theodolite looking at an Earth simulator; Fig. 26 shows the test facility for the Earth sensor using an Earth simulator.

After an Earth sensor has been calibrated and functionally checked, the following tests are performed: short-term stability, light-intensity variations, voltage variations, acquisition threshold, a long time operating drift test, hinge and roll characteristic curves, light-intensity telemetry, offset response curve, power dissipation measurements, temperature transducer and heater

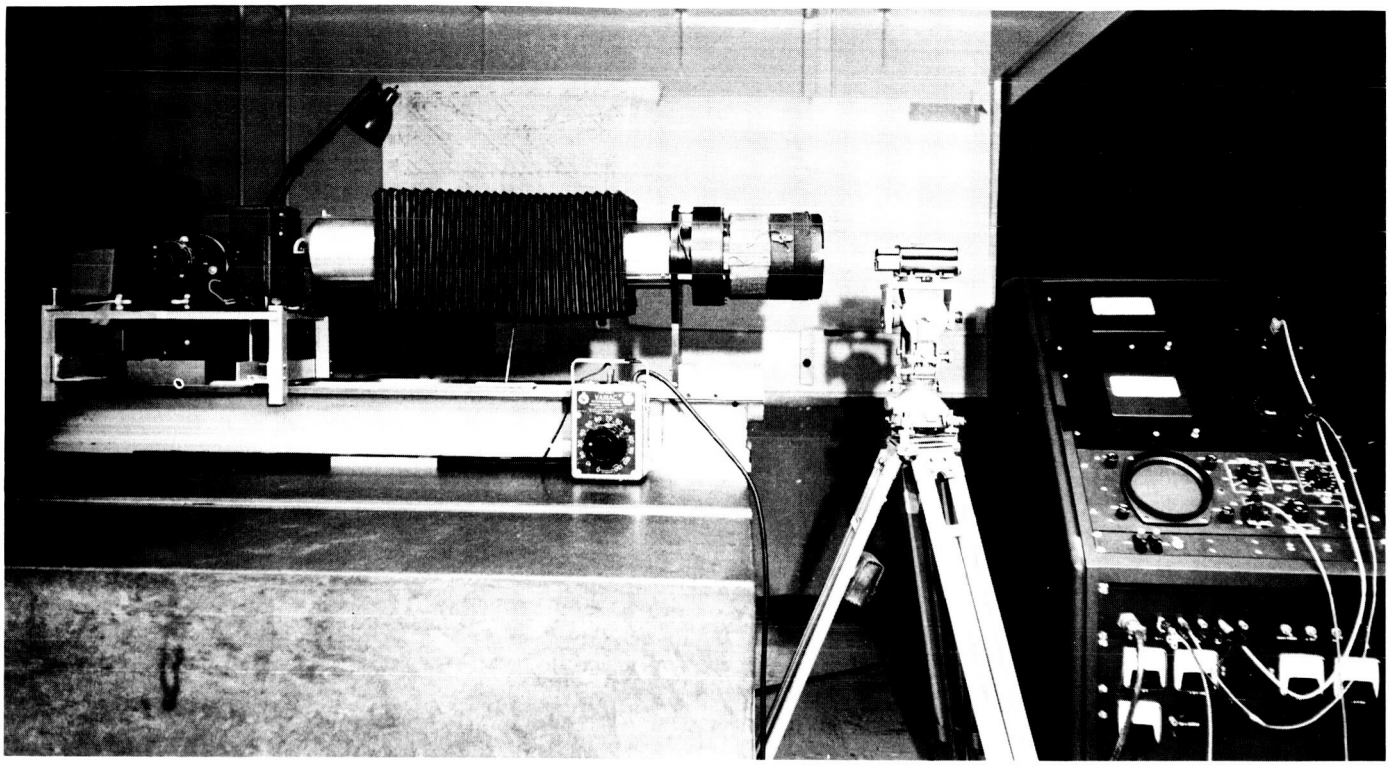

Fig. 25. Earth sensor mounted on T-2 theodolite

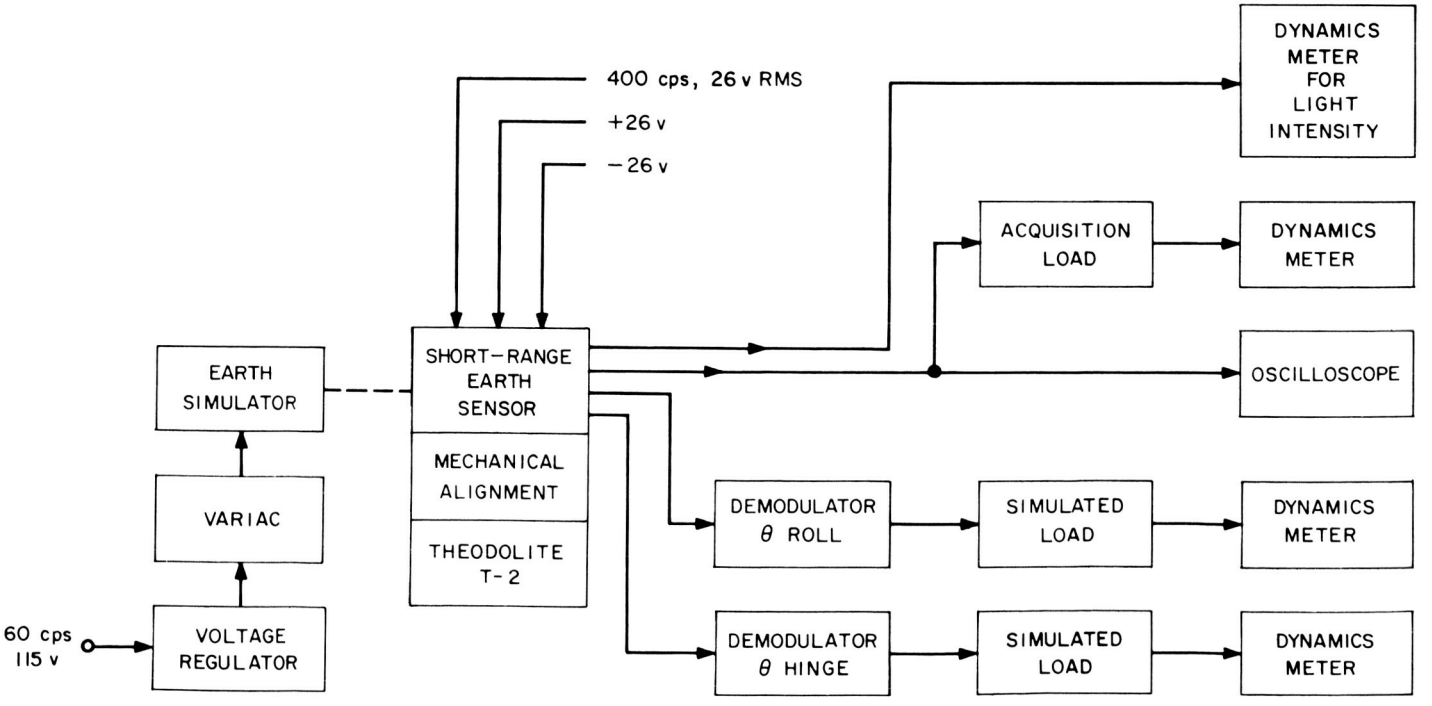

Fig. 26. Test facility for Earth sensor using an Earth simulator

checks, 24-hr burn-in, Earth–probe–Sun angle measurement, and Earth–probe–near limb light Moon angle measurements.

a. Test tolerances. The short-term stability test is run under the following tolerances:

(1) Roll scale factor: 8 v/deg ±8%.

(2) Hinge scale factor: 2 v/deg ±15%.

(3) Roll saturation: + and − 10 v ±2 v at + and − 3 deg, respectively.

(4) Hinge saturation: + and − 5 v ±1 v at + and − 5 deg, respectively.

(5) Read and record hinge and roll null offset at a given light intensity. Hinge null: 0 ±0.4 deg; roll null: 0 ±0.2 deg.

(6) Record room temperature and resistance of temperature transducer.

b. Test conditions. The short-term stability test is run under the following conditions:

(1) Ambient conditions of temperature and pressure.

(2) Nominal power inputs.

(3) Light intensity of 0.1 ft-cd at color temperature between 5000 to 6000°K.

(4) Light source angular diameter between 1.5 and 2 deg at full phase.

For the light-intensity variation test, short-term stability tests are performed at the following light intensities in the indicated order:

(1) 10 ft-cd after 0.5-hr warmup at 10 ft-cd.

(2) 2-ft-cd test after Earth sensor has been exposed to 2-ft-cd light intensity for 1 hr.

(3) 0.1-ft-cd test after Earth sensor has been exposed to 0.1-ft-cd light intensity for 1 hr.

At 2- and 0.1-ft-cd light intensities, the Earth sensor has the tolerances stated in the description of the short-term stability test. At 10 ft-cd, the Earth sensor has the tolerances given in Table 3.

The voltage variation test consists of short-term stability tests at 0.1, 2, and 10 ft-cd for ±23.4, ±26, and ±28.6-v input to the Earth sensor. The Earth sensor tolerance must be within the values indicated in Table 3.

The acquisition threshold level is measured at ±23.4, ±26, and ±28.6 v. At nominal power inputs, the acquisition threshold should be within 0.01 ±0.025 ft-cd.

For null hinge angle, a roll output voltage versus roll angle curve should be made to check the linear range through null, the saturation levels, and backside characteristics. A similar curve should be made for hinge outputs at a roll null. This test should be performed under ambient conditions, nominal power inputs, and 10-ft-cd light intensity.

Temperature transducer and heater resistor resistance measurements should be made and their values checked against calibration values.

Figure 27 is an offset response curve. Its value should lie within the tolerances noted in Fig. 22.

A light intensity versus Earth sensor telemetry voltage output curve should be made as a flight calibration curve (Fig. 28).

An Earth–probe–Sun angle measurement should be made of the Earth sensor. The light intensities of the simulated Earth and Sun should be at the correct ratio of values. Voltage inputs to the Earth sensor should be ±28.6 v; yaw angles of 0, ±90, and ±180 deg should be tested. The sensor must limit cycle within a safe margin, and its null offset value should not exceed the value given in Table 3. The smallest Earth–probe–near limb light Moon angle at which the Earth sensor can pass the mentioned conditions must be recorded.

Two curves should be made of the hinge and roll output voltage versus angular deflection throughout the linear range at simulated midcourse and terminal distant Earths.

A power dissipation measurement should be performed and recorded as shown in Table 8. An operating time estimate should be made on all units during each test, and a total operating time estimate made upon delivery to JPL.

All Earth sensors should be burned-in for 24 hr under ambient conditions and nominal power inputs to the sensor at a light intensity somewhere in the range of 0.1 to 4 ft-cd.

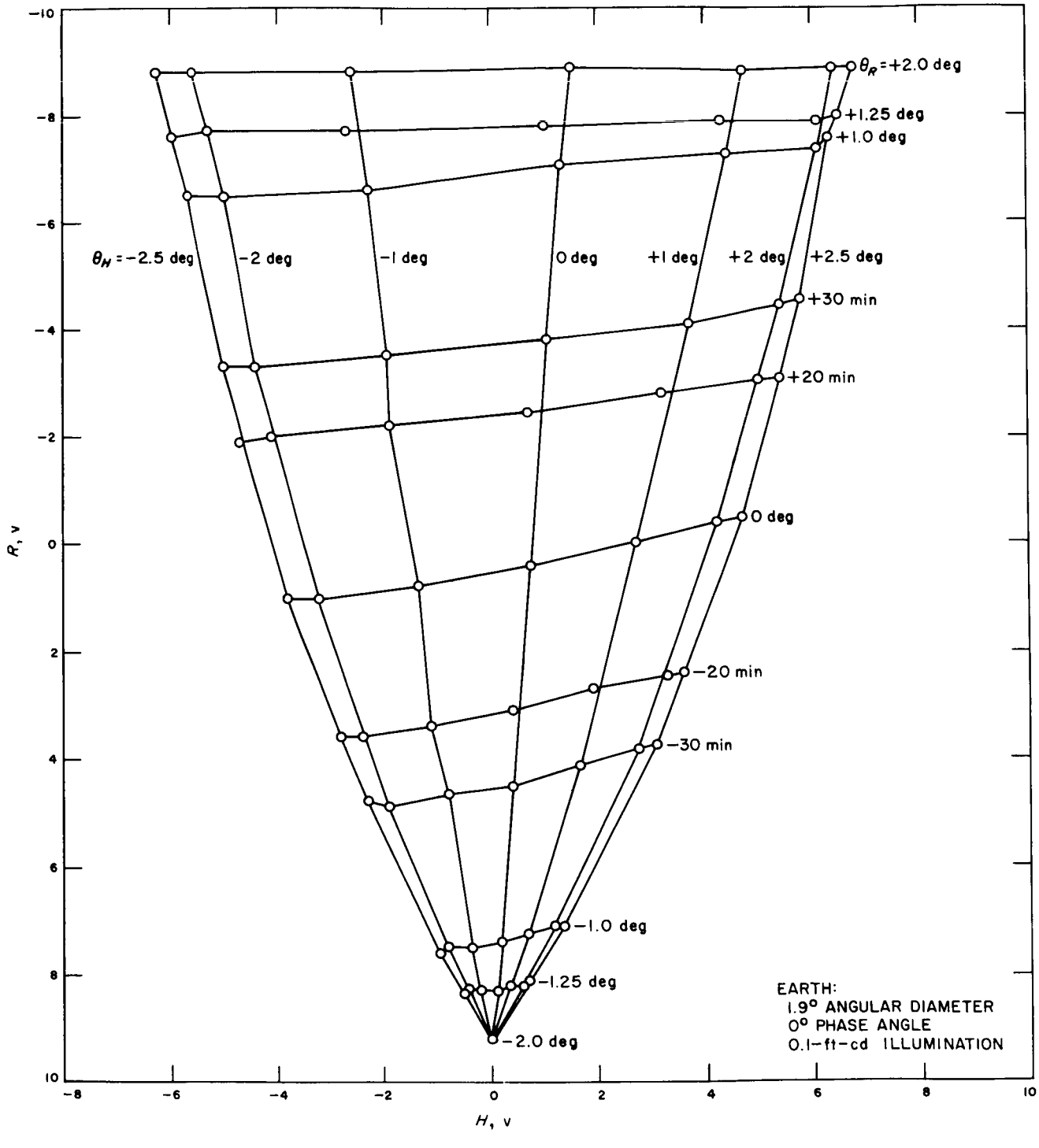

Fig. 27. Earth sensor offset response

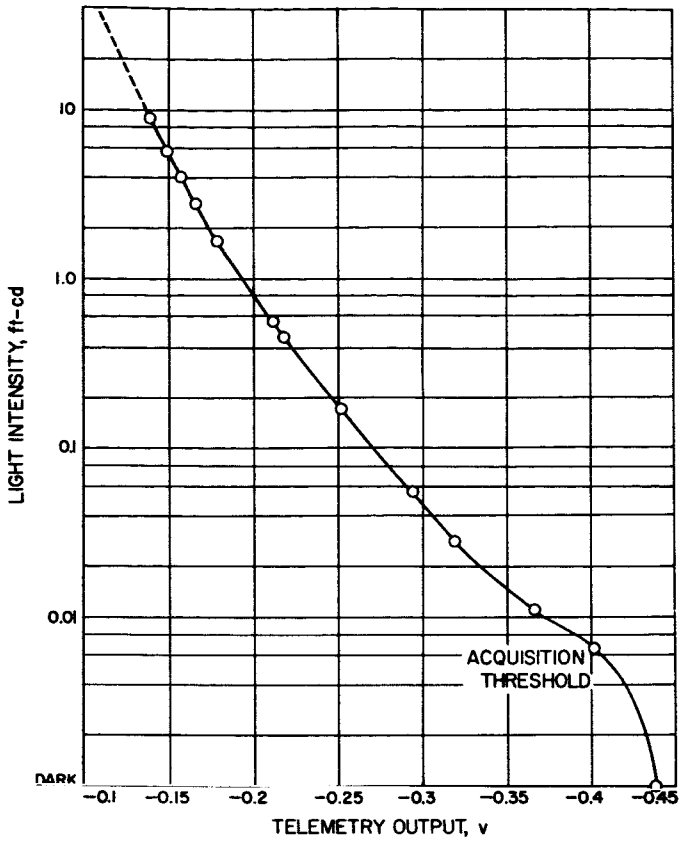

Fig. 28. Light intensity versus Earth sensor telemetry voltage output

4. Qualification for Flight

a. Flight-acceptance testing. All flight Earth sensors must perform within flight tolerances during and after subjection to all flight-acceptance (FA) tests.

A short-term stability test is performed before and after FA vibration and temperature tests. In order to pass these tests, the Earth sensor must perform within prescribed limits. There are four groups of readings during the temperature test:

(1) Under ambient conditions before the test.

(2) After soak at the minimum temperature.

(3) After soak at the maximum temperature.

(4) Under ambient conditions after the test.

The Earth sensor is energized only at atmospheric pressure or at a pressure less than 10^{-4} mm Hg; an energized flight Earth sensor must not be subjected to temperatures above 95°F.

Table 10 is a summary of flight *Ranger* Block III Earth sensor performance tests and FA tests. The table shows the average magnitude change, the average value change, and the RMS (1 sigma) dispersion from the average value change of null offset in degrees and of scale factor in volts per degree from one test condition to another test condition. All values of null offset and of scale factor for each test condition are within the short-term stability test tolerances.

b. Type-approval testing. All flight Earth sensors must perform and operate satisfactorily after subjection to all type-approval (TA) tests.

A short-term stability test is performed before and after each of the following TA environments: handling shock, transportation vibration, humidity, shock, static acceleration, low-frequency vibration, complex wave vibration, temperature test, and thermal shock. In order to pass these tests, the Earth sensor must operate within the Earth sensor limits given in Table 3.

The TA temperature test is performed in the same manner as described in the FA temperature test except at different temperature soak times and at different temperature levels.

A flight Block III Earth sensor and a flight Block II Earth sensor with a Block III shadow cover assembly unit were TA tested for *Ranger* Block III. Table 11 is a TA test summary for the two Earth sensors.

A reworked Block II Earth sensor (S/N 40) was TA tested because a Block III sensor was not available to start TA testing. It can readily be seen from a comparison between the reworked Block II Earth sensor and a Block III Earth sensor that the sensor of Block II would be less likely to pass the TA series of tests. Thus, from the results of the TA testing of the reworked Block II Earth sensor, it was confidently felt that the Block III Earth sensor could pass TA testing.

Test results showed that:

(1) The Earth sensor suffered a large scale factor change from transportation vibration.

(2) The PMT's in this Earth sensor were able to withstand TA flight vibration surprisingly well; however, from experience, this does not indicate that other PMT's could do as well.

Table 10. *Ranger* Block III Earth sensor performance and FA test summary

Condition	Null offset, deg			Scale factor, v/deg		
	Average magnitude change	Average value change	1-sigma change	Average magnitude change	Average value change	1-sigma change
From 0.1 to 10 ft-cd ±26 v DC	0.067/0.115	−0.0065/0.0782	0.0812/0.134	0.352/0.189	−0.345/0.0162	0.360/0.244
From 0.1 to 2 ft-cd ±26 v DC	0.0380/0.102	−0.0088/0.0206	0.0465/0.119	0.160/0.0900	−0.0200/0.0025	0.223/0.121
From 10 ft-cd ±26 v DC to 10 ft-cd ±28.6 v DC	0.0173/0.0306	0.0128/0.0071	0.0215/0.0451	0.269/0.141	0.166/−0.0012	0.306/0.216
From 10 ft-cd ±26 v DC to 10 ft-cd ±23.4 v DC	0.0100/0.0345	−0.0055/0.0185	0.0111/0.0510	0.335/0.186	−0.335/−0.186	0.246/0.213
From 2 ft-cd ±26 v DC to 2 ft-cd ±28.6 v DC	0.0077/0.248	0.0020/−0.0068	0.0102/0.0311	0.176/0.0624	−0.0362/0.575	0.211/0.0667
From 2 ft-cd ±26 v DC to 2 ft-cd ±23.4 v DC	0.0082/0.0298	−0.0078/0.0122	0.0079/0.0332	0.401/0.0850	−0.319/−0.0675	0.318/0.0618
From 0.1 ft-cd ±26 v DC to 0.1 ft-cd ±28.6 v DC	0.0095/0.0205	0.0040/0.0082	0.0106/0.0312	0.221/0.0625	0.0662/0.0525	0.277/0.0604
From 0.1 ft-cd ±26 v DC to 0.1 ft-cd ±23.4 v DC	0.0101/0.0276	−0.0081/0.0116	0.0121/0.0299	0.372/0.100	−0.372/−0.100	0.140/0.632
From before to after 24-hr run-in test	0.0651/0.144	−0.0103/−0.0107	0.0815/0.186	0.166/0.186	−0.0800/−0.0686	0.168/0.226
From before to after FA vibration test	0.0456/0.105	−0.0284/0.0408	0.0485/0.132	0.138/0.0762	−0.0550/0.0138	0.179/0.0942
From before to after FA space temperature test	0.103/0.208	−0.0284/−0.0168	0.117/0.296	0.215/0.149	−0.070/0.0612	0.268/0.153

NOTE:
(1) All tests were performed on an Earth simulator with a 1.9-deg-diameter Earth at full phase.
(2) The numerator represents roll values; the denominator represents hinge values.
(3) The run-in tests and the FA tests were performed on an Earth simulator with a 0.1-ft-cd Earth and a ±26-v-DC input to the Earth sensor.
(4) A ±26-v-RMS, single-phase, 400-cps input to the Earth sensor was used in all of these tests.

Table 11. *Ranger* Block III Earth sensor TA test summary

TA tests	Serial Number 301				Serial Number 40			
	Null offset, deg	Null offset (from preceding test), deg	Scale factor, v/deg	Scale factor (from preceding test), %	Null offset, deg	Null offset (from preceding test), deg	Scale factor, v/deg	Scale factor (from preceding test), %
Start	−0.114/−0.093		7.31/2.2		−0.176/0.106		7.5/2.25	
After bench handling	−0.125/−0.081	−0.01/0.01	7.55/1.89	3.3/−16.5	−0.2/−0.2	−0.02/−0.31	6.2/2	0/1
After transportation vibration					−3.42/0.072	0/0	6.8/2.54	−10/12.8
After humidity	−0.122/−0.149	0/−0.07	7.24/1.90	−4.5/0	−0.345/0.072	0/0	6.75/2.50	0.1/−1.6
After shock	−0.126/−0.163	0/−0.01	7.4/2.09	2.5/10	−0.347/0.111	0/0.03	6.69/2.56	2.3/2.4
After static acceleration	−0.107/−0.260	0.02/−0.10	7.32/1.92	−1.3/−9	−0.354/0.089	0/−0.02	6.55/2.58	−2.3/0.08
After vibration	−0.132/0.33	−0.03/−0.07	7.57/1.98	3.5/3	−0.405/0.104	−0.06/0.01	6.57/2.62	0.05/1.5
After thermal vacuum					−0.557/0.294	−0.16/0.39	5.75/2.42	−14/−8.3
After thermal shock	−0.268/−0.295	−0.14/−0.03	7.07/2.1	−7.0/6	−0.21/−0.18	0.35/0.11	6.2/1.98	7.8/−22

NOTE:
(1) The numerator represents roll values; the denominator represents hinge values.
(2) The TA tests are listed in the order in which they were performed.
(3) On S/N 40, the bench handling test was conducted after the thermal shock test.

(3) The Earth sensor could withstand the bench handling test; therefore, it would be performed in the proper sequence for the Block III Earth sensor TA test.

(4) Large null offsets were resulting from the PMT's; thus, it was decided to stop the thermal vacuum test at 109°F. The sensor recovered well at lower temperatures. This once again substantiates a maximum temperature of 95°F for flight units.

(5) The failure that occurred after the last TA flight vibration test was easily corrected by insulating the high-voltage wire at the questionable −26-v terminal. This failure could not occur on a Block III sensor because the corresponding wire was routed a little differently and contained a glass braid.

Table 12. Operating time of flight Earth sensors

Spacecraft	Laboratory test time, hr	System test time, hr	Total test time, hr
Ranger VI	267	234	501
Ranger VII	191	468	659
Ranger VIII	257	279	536
Ranger IX	144	234	378

NOTE: The lab test time does not include the 100-hr PMT burn-in time.

The Block III Earth sensor (S/N 301) successfully passed the *Ranger* Block III TA environmental tests. The values of the Earth sensor remained within the tolerances given in Table 3.

c. Life testing. Table 12 lists the operating times recorded on the Block III flight Earth sensors.

A total of 24 Dumont PMT's, housed in four groups (each with six PMT's), in *Ranger* flight configuration have

Table 13. Test parameters of PMT life test at last test

Channel	Tube	Color temperature, °K	Light intensity, ft-cd	Filter transmission	Aperture area, ft^2	Volts	Anode net current, $v \times 10^5$	Cathode net current, $v \times 10^9$
A	1	5400	10	0.0548	3.18×10^{-5}	−1100	9.4	0.28
	2	5400	10	0.1825	3.18×10^{-5}	−1100	1.8	4.19
	3	5400	10	0.1825	3.18×10^{-5}	−1100	3.3	1.86
	4	5400	10	0.0548	3.18×10^{-5}	−1100	6.8	2.35
	5	5400	10	0.1825	3.18×10^{-5}	−1100	3.2	4.97
	6	5400	10	0.1825	3.18×10^{-5}	−1100	5.3	6.2
B	1	5200	24	0.1334	1.59×10^{-5}	−1100	3.6	1.03
	2	5200	24	0.1365	1.59×10^{-5}	−1100	2.6	1.53
	3	5200	24	0.1365	1.59×10^{-5}	−1100	1.8	1.52
	4	5200	24	0.1334	1.59×10^{-5}	−1100	1.6	1.71
	5	5200	24	0.1365	1.59×10^{-5}	−1100	1.3	1.56
	6	5200	24	0.1365	1.59×10^{-5}	−1100	2.65	1.46
C	1	5400	30	1.0	6.37×10^{-5}	− 750	5.0	43.00
	2	5300	30	1.0	6.37×10^{-5}	− 750	5.7	25.00
	3	5200	30	1.0	6.37×10^{-5}	− 750	5.35	30.00
	4	5400	30	1.0	6.37×10^{-5}	− 750	5.05	46.00
	5	5300	30	1.0	6.37×10^{-5}	− 750	5.1	31.00
	6	5200	30	1.0	6.37×10^{-5}	− 750	7.2	29.00
D	1	5400	16.5	1.0	6.37×10^{-5}	− 750	4.4	26.00
	2	5400	17.8	1.0	6.37×10^{-5}	− 750	2.6	21.00
	3	5400	19	1.0	6.37×10^{-5}	− 750	4.6	21.00
	4	5400	16.5	1.0	6.37×10^{-5}	− 750	4.6	29.00
	5	5400	17.8	1.0	6.37×10^{-5}	− 750	3.5	17.00
	6	5400	19	1.0	6.37×10^{-5}	− 750	5.6	14.00

undergone a life test. The four PMT housing assemblies, located in a light tight compartment, face a single light source. Each tube has an aperture in front of it and a neutral density filter. Table 13 shows the test parameters at the last test. During burn-in, the light intensity at the tubes is approximately 0.4 ft-cd at 5900°K color temperature. While the tubes are being evaluated, the light intensity at the tubes is above 27 ft-cd at 5300°K. Table 14 shows the change of tube gain during a life test; Table 15 shows the variation of tube sensitivity during the test.

Table 14. PMT life test (gain)

Channel	Tube	Gain measurements: various life test operating times					
		At 0 hr	At 336 hr	At 768 hr	At 1705 hr	At 3750 hr	At 5256 hr
A	1	174300	222600	220300	277000	274500	333300
	2	7034	9229	6654	6400	5890	4296
	3	9846	14190	19520	15300	18900	17790
	4	33380	81250	35230	29550	27800	28940
	5	11400	18220	15940	10380	7970	6439
	6	8647	9073	8633	8900	8620	8550
B	1	25680	48570	27610	33800	34000	34920
	2	10390	12540	17200	15830	15900	16990
	3	7547	7909	11670	11300	11900	11860
	4	10490	11690	11130	9440	10000	9357
	5	11120	11350	10820	10320	8890	8333
	6	14360	19170	14750	22200	19950	18150
C	1	932	1027	1026	978	1090	1164
	2	1394	1605	1691	1855	2100	2259
	3	929	1032	1171	1443	1666	1784
	4	657	703	846	914	1103	1098
	5	975	967	1154	1218	1500	1621
	6	1682	1676	1863	2080	2270	2452
D	1	761	852	1027	1083	1561	1696
	2	316	389	542	705	978	1216
	3	992	1052	1212	1535	1926	2148
	4	1032	1068	1244	1365	1495	1608
	5	867	882	1075	1370	1765	2030
	6	1646	2054	2692	3550	3470	3916

Two Block II Earth sensors with Block III optics have been continuously operated for over a year without any malfunctions at ambient temperature and pressure. The Earth sensors are being energized at the same time interval as they would be in flight with a flight cycle of 67.9 hr. Table 16 gives the test parameters of the life test.

Results of short-term stability tests performed at various intervals during the life tests are given in Table 17. These tests were run after 1 hr of operation on a constant brightness collimated Earth simulator with a 0-deg phase angle, a 1.9-deg angular diameter, and a 0.2-ft-cd light intensity. Table 18 shows the test results of Earth sensors S/N 39 and S/N 42 (run, respectively, before the life test and after 1 yr of the life test). Finally, Fig. 29 shows the difference in sensitivity of Earth sensor S/N 39 from 346

Table 15. PMT life test (sensitivity)

Channel	Tube	Sensitivity measurements at various life test operating times, μamp/lumen					
		At 0 hr	At 336 hr	At 768 hr	At 1705 hr	At 3750 hr	At 5256 hr
A	1	12.5	9.87	11.7	10.2	11.2	16.2
	2	60.0	34.9	51.8	42.3	45.0	72.2
	3	33.0	20.2	16.7	20.9	18.8	32.0
	4	70.9	25.5	43.9	66.0	79.6	135.0
	5	52.8	30.2	35.5	46.3	54.0	85.7
	6	59.4	49.8	56.4	50.8	64.2	107.0
B	1	23.3	10.3	18.6	17.5	19.0	20.3
	2	39.2	28.4	33.8	25.4	27.5	29.3
	3	40.7	31.8	37.9	41.6	26.8	29.1
	4	41.7	28.8	30.6	36.0	33.7	33.7
	5	38.4	28.9	47.4	27.9	29.1	29.9
	6	30.0	20.9	43.1	39.8	26.8	28.0
C	1	25.6	27.6	26.3	30.1	32.9	22.9
	2	17.4	18.7	17.5	17.0	19.2	13.1
	3	21.2	25.3	22.58	19.8	22.4	15.2
	4	27.0	32.9	28.1	30.0	32.9	24.5
	5	20.3	24.5	21.2	20.3	23.2	16.3
	6	19.0	22.8	19.7	19.4	22.3	14.9
D	1	32.7	37.8	32.0	37.2	37.7	24.7
	2	33.5	38.4	31.7	31.4	33.8	18.9
	3	30.8	36.7	29.5	29.7	36.0	17.7
	4	32.5	38.9	32.7	40.4	44.0	27.2
	5	22.7	27.9	22.9	24.0	27.4	15.3
	6	19.8	23.3	19.4	18.3	24.8	11.8

Table 16. Earth sensor life test parameters

Event	Time from launch, hr	OSE lights	Inputs to Earth sensor		
			±26 v DC	26 v, single phase, 400 cps	Heater
Launch phase	0 to 1	Off	Off	Off	On
First Sun acquire	1 to 4	Off	On	Off	On
First Earth search	4 to 4.5	Off	On	On	Off
First cruise	4.5 to 16	On	On	On	Off
Midcourse maneuver	16 to 16.5	On	On	Off	On
Second cruise	16.5 to 67.9	On	On	On	Off

Table 17. Earth sensor life test

Date	Time (PST)	Number of missions (cycle: 67.9 hr)	Time, hr	Voltage output, v	Null offset, deg	Scale factor, v/deg	Saturation				Acquisition threshold, ft-cd
							+3° (Roll), v	−3° (Roll), v	+5° (Hinge), v	−5° (Hinge), v	
Serial Number 39											
April 24, 1964	15:00	0	0	−0.05/0.7	−0.006/0.376	7.87/1.86	8.8	7.7	4.5	3.8	0.009
May 14, 1964		5	346	−0.96/1.23	−0.121/0.542	7.92/2.27	8.8	7.7	5.1	4.0	0.01
June 3, 1964		13	937	−1.1/1.4	−0.139/0.636	7.89/2.2	8.9	8.0	5.3	4.1	
July 21, 1964		30	2070	−1.35/1.7	−0.173/0.757	7.8/2.25	8.9	8.0	5.3	4.2	0.012
October 8, 1964		58	3930	−1.82/1.48	−0.246/0.596	7.4/2.48	9.0	7.9	5.4	4.4	0.0088
October 28, 1964	10:54	65	4411	−2.25/1.31	−0.309/0.517	7.29/2.53	9.0	8.01	5.42	4.41	0.0082
November 25, 1964	17:40	75	5089	−2.2/1.19	−0.297/0.49	7.4/2.45	9.0	8.02	5.41	4.41	0.008
December 29, 1964	16:10	87	5903	−2.13/1.42	−0.296/0.584	7.21/2.43	8.4	7.57	5.55	4.45	0.01
March 16, 1965	17:00	114	7753	−2.16/2.0	−0.286/0.794	7.56/2.52	8.95	8.02	5.85	4.4	0.011
May 5, 1965	13:00	132	9026	−2.7/2.0	−0.419/0.762	6.45/2.63	8.8	8.0	6.0	4.43	0.01
Serial Number 42											
April 24, 1964		0	0	0.1/0.7	0.013/0.425	8.02/1.65	10.7	9.3	4.2	3.4	0.012
May 14, 1964		5	346	−0.22/1.62	−0.027/1.01	8.13/1.61	10.9	9.45	4.5	3.45	0.01
June 3, 1964		13	937	0.022/1.68	0.003/1.09	8.16/1.54	10.7	9.6	4.38	3.4	
July 21, 1964		30	2070	1.2/1.1	0.148/0.748	8.1/1.47	10.8	9.3	4.0	3.3	0.011
October 8, 1964		58	3930	1.69/0.405	0.2/0.274	8.44/1.48	10.8	9.41	3.78	3.4	0.01
October 28, 1964	10:54	65	4411	2.08/−0.232	0.256/−0.148	8.14/1.57	10.8	9.62	3.25	3.5	0.0097
November 25, 1964	17:40	75	5089	2.28/−0.074	0.279/−0.049	8.19/1.50	10.8	9.8	3.45	3.45	0.0092
December 29, 1964	16:10	87	5903	2.44/−0.53	0.316/−0.342	7.73/1.55	10.0	8.95	3.1	3.45	0.013
March 16, 1965	17:00	114	7753	2.9/−0.70	0.346/−0.486	8.16/1.44	11.0	9.6	3.2	3.5	0.013
May 8, 1965	13:00	132	9026	2.85/−1.38	0.342/−1.045	8.34/1.32	11.1	9.8	3.0	3.8	0.015

NOTE:
The numerator represents roll values; the denominator represents hinge values.

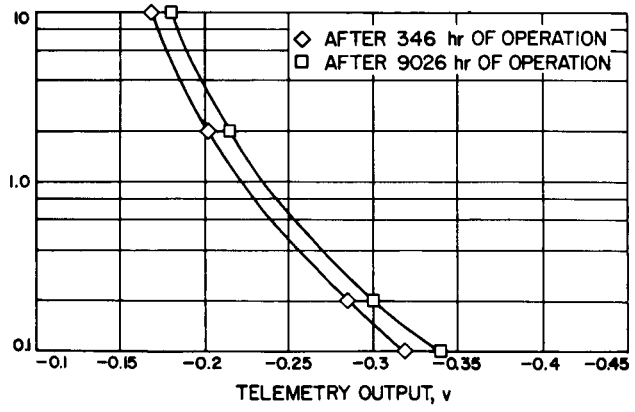

Fig. 29. Earth sensor life test results (S/N 39)

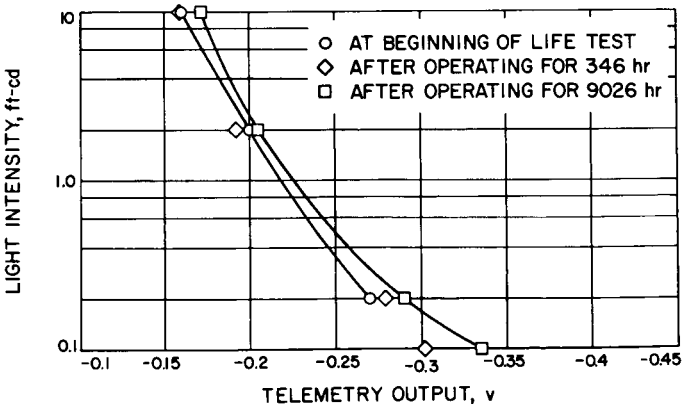

Fig. 30. Earth sensor life test results (S/N 42)

hr of continuous operation to after 9026 hr; Fig. 30 indicates the change in sensitivity of Earth sensor S/N 42 at the start of the test, after 346 hr, and after 9026 hr of continuous operation.

d. Special calibrations. Before the flight and flight spare Earth sensors are transported to AMR, they are tested at the Jet Propulsion Laboratory in Pasadena. Flight calibration curves are also run on these Earth sensors.

The flight Earth sensor calibration curves and data are contained for each flight in a memorandum, which contains information about an Earth light-intensity monitor

Table 18. Earth sensor life test: variation of Earth light intensity and DC

When performed	Voltage output (0°), v	Null offset, deg	Scale factor, v/deg	Saturation				Voltage input, v	Light source	
				+3° (roll), v	−3° (roll), v	+5° (hinge), v	−5° (hinge), v		Intensity, ft-cd	Color temperature, °k
Serial Number 39										
Before life test	1.15/1.08	0.137/0.597	8.4/1.81	9.3	8.1	4.6	3.5	±26	10	3000
After 1 yr	−1.55/1.5	−0.195/0.588	7.98/2.55	9.3	8.4	6.0	4.4	±26	10	3000
Before life test	1.0/1.2	0.124/0.612	8.1/1.96	9.6	8.4	5.0	3.8	±28.6	10	3000
After 1 yr	−1.6/1.4	−0.194/0.542	8.24/2.58	9.4	8.45	6.0	4.5	±28.6	10	3000
Before life test	1.0/1.1	0.128/0.662	7.8/1.66	8.6	7.5	4.2	3.1	±23.4	10	3000
After 1 yr	−1.58/1.47	−0.194/0.583	8.17/2.52	9.3	8.4	5.9	4.4	±23.4	10	3000
Before life test	1.07/1.04	0.128/0.56	8.4/1.86	9.1	7.95	4.6	3.6	±26	2	4300
After 1 yr	−1.8/1.8	−0.224/0.698	8.03/2.58	9.3	8.35	6.0	4.4	±26	2	4600
Before life test	0.95/1.05	0.109/0.535	8.7/1.96	9.6	8.4	5.05	3.9	±28.6	2	4300
After 1 yr	−1.8/1.8	−0.224/0.7	8.03/2.58	9.35	8.4	6.0	4.4	±28.6	2	4600
Before life test	0.9/1.02	0.115/0.561	7.87/1.82	8.55	7.45	4.2	3.2	±23.4	2	4300
After 1 yr	−1.7/1.8	−0.213/0.706	8.0/2.55	9.2	8.3	6.0	4.4	±23.4	2	4600
Before life test	0.04/0.78	0.005/0.4	8.05/1.95	8.8	7.6	4.6	3.8	±26	0.2	5100
After 1 yr	−2.7/2.0	−0.419/0.762	6.45/2.63	8.8	8.0	6.0	4.43	±26	0.2	5000
Before life test	0.07/0.76	0.008/0.36	8.7/2.11	9.5	8.3	5.2	4.3	±28.6	0.2	5100
After 1 yr	−2.75/2.05	−0.447/0.76	6.15/2.7	8.8	8.0	6.05	4.45	±28.6	0.2	5000
Before life test	0/0.78	0/0.424	7.54/1.84	8.3	7.2	4.25	3.4	±23.4	0.2	5100
After 1 yr	−2.65/2.08	0.387/0.808	6.84/2.57	8.7	7.9	6.0	4.4	±23.4	0.2	5100
Serial Number 42										
Before life test	−1.0/1.7	−0.126/0.945	7.95/1.8	11.0	9.7	4.65	3.7	±26	10	3000
After 1 yr	2.02/0.14	0.229/0.081	8.81/1.74	11.3	10.0	4.2	3.65	±26	10	3000
Before life test	−1.25/1.8	−0.156/0.922	8.02/1.95	11.2	10.0	5.2	4.1	±28.6	10	3000
After 1 yr	2.05/0.12	0.236/0.068	8.7/1.77	11.2	9.9	4.2	3.6	±28.6	10	3000
Before life test	−1.1/1.5	−0.148/1.0	7.42/1.5	10.0	9.2	4.2	3.4	±23.4	10	3000
After 1 yr	2.03/0.12	0.231/0.070	8.8/1.73	11.3	10.0	4.2	3.6	±23.4	10	3000
Before life test	0.65/1.5	−0.081/0.908	8.02/1.65	11.0	9.6	4.6	3.6	±26	2	4300
After 1 yr	2.73/−0.43	0.324/−0.271	8.43/1.59	11.3	10.0	3.65	3.6	±26	2	4600
Before life test	−0.65/1.6	−0.082/0.942	7.95/1.7	10.8	9.5	4.7	3.5	±28.6	2	4300
After 1 yr	2.75/−0.445	0.325/−0.272	8.48/1.64	11.3	9.8	3.7	3.6	±28.6	2	4600
Before life test	−0.66/1.45	−0.086/0.918	7.65/1.58	10.0	9.1	4.1	3.3	±23.4	2	4300
After 1 yr	2.75/−0.44	0.325/−0.277	8.48/1.59	11.2	9.9	3.62	3.6	±23.4	2	4600
Before life test	0.1/0.7	0.013/0.424	8.02/1.65	10.7	9.3	4.2	3.4	±26	0.2	5100
After 1 yr	2.85/−1.38	0.342/−1.05	8.34/1.32	11.1	9.8	3.0	3.8	±26	0.2	5000
Before life test	0.06/0.76	0.007/0.453	8.25/1.68	11.2	9.8	4.5	3.9	±28.6	0.2	5100
After 1 yr	2.9/−1.4	0.35/−1.07	8.28/1.31	11.0	9.7	3.0	3.75	±28.6	0.2	5000
Before life test	0.1/0.65	0.013/0.411	7.88/1.58	10.0	8.9	3.8	3.3	±23.4	0.2	5100
After 1 yr	2.95/−1.32	0.351/−1.0	8.4/1.32	11.1	9.6	3.0	3.75	±23.4	0.2	5000

NOTE:
The numerator represents roll values; the denominator represents hinge values.

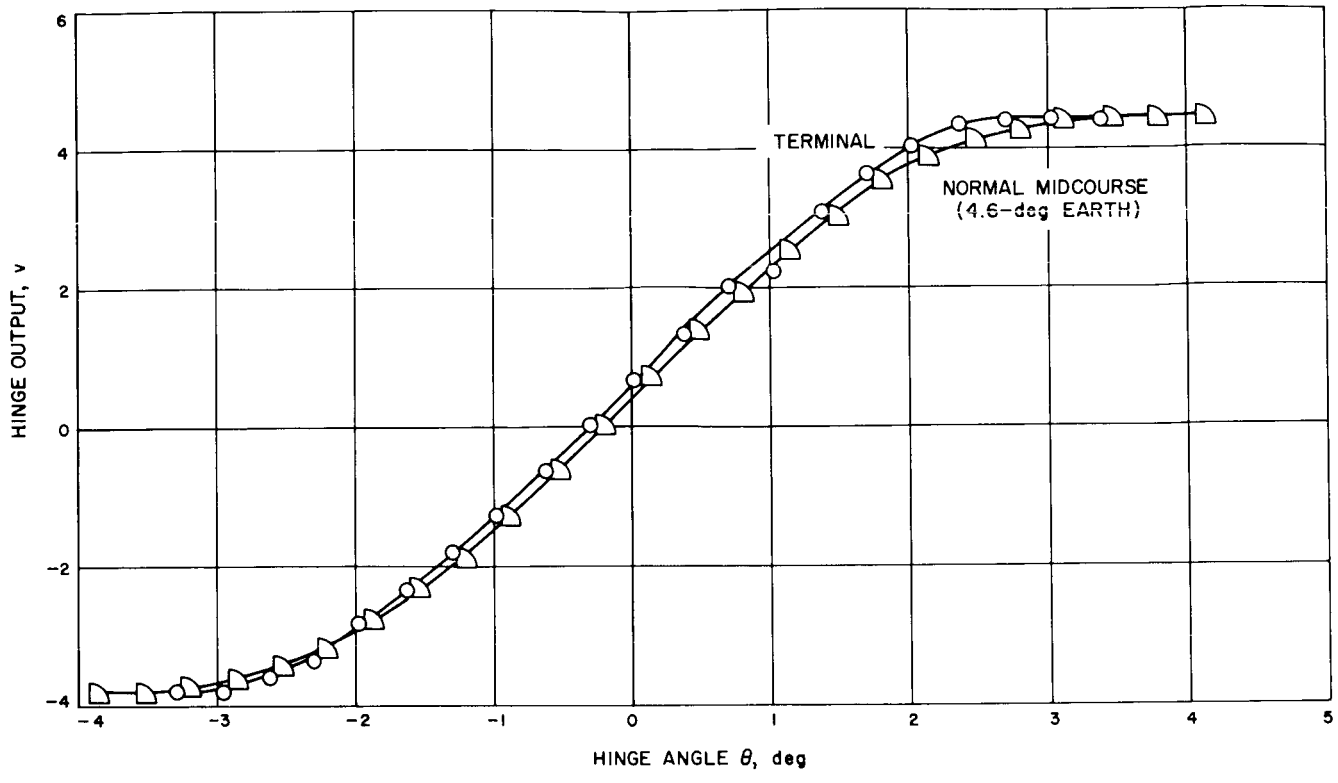

Fig. 31. Hinge output versus hinge angle

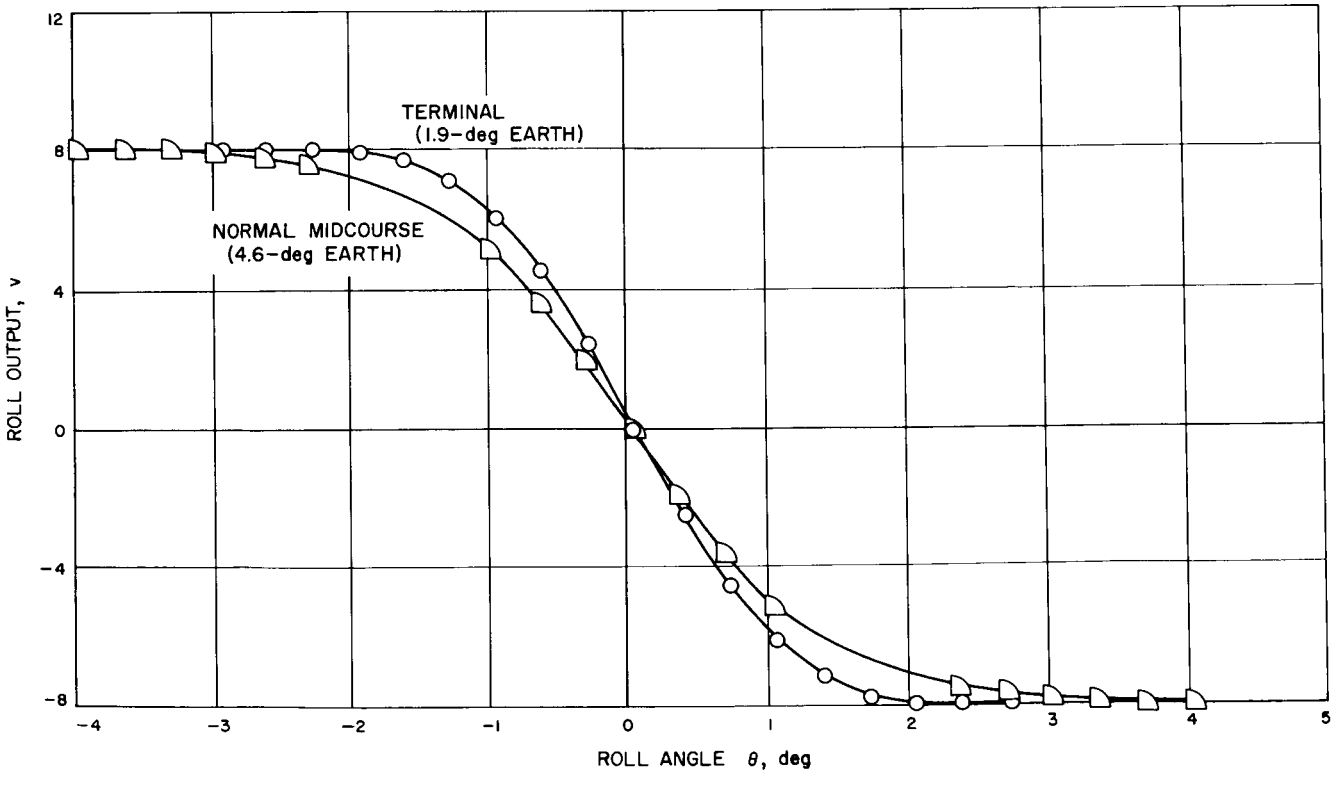

Fig. 32. Roll output versus roll angle

(Fig. 28), a hinge output versus hinge angle for a roll mechanical null angle (Fig. 31), a roll output versus roll angle for a hinge mechanical null angle showing saturation values (Fig. 32) and showing the limit cycle region for each launch day for a nominal midcourse maneuver (Fig. 33), an offset response curve for terminal maneuver (Fig. 27) and for midcourse maneuver (Fig. 34), a roll scale factor versus the apparent Earth diameter (Fig. 35), and a null offset peak-to-peak in percent of apparent Earth diameter versus the Earth phase angle (Fig. 36). In order to obtain greater accuracies during the midcourse maneuver, separate plots of the roll null axis error signals are plotted for each of the launch days. Another table contains the roll null offsets, hinge null offsets, hinge scale factor, and roll scale factors of the Earth sensor for normal midcourse maneuvers during each of the launch days and for the terminal maneuver. All of the Earth sensor calibration curves except for Figs. 27, 34, 35, and 36 used the TA attitude control system and the *Ranger* flight single-phase inverter. All the angles in the graphs are with respect to spacecraft coordinates. The roll mechanical null values of the Earth sensor are with respect to the center of light illumination from the Earth and have a roll null offset 3-sigma tolerance of ±0.3 deg about the roll null values given in the table. The roll 3-sigma null offset tolerance for this Earth sensor might be further reduced a few hours after the sensor has been fully energized in flight once the temperature of the unit and the Earth light intensity have been determined.

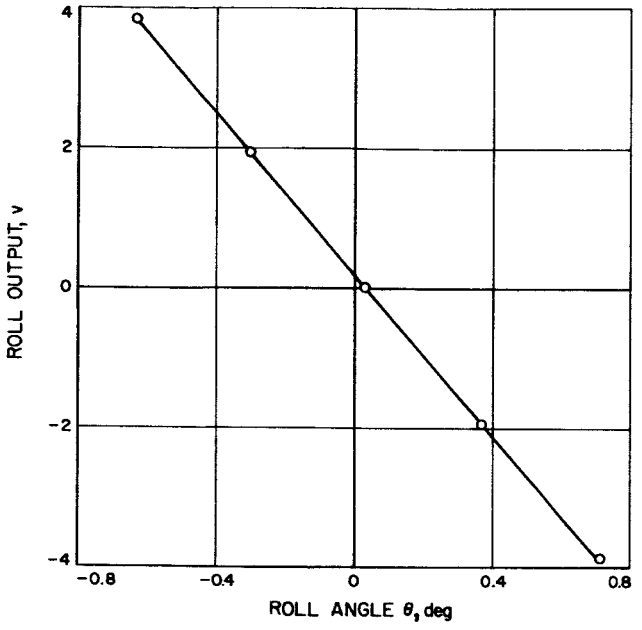

Fig. 33. Roll output versus roll angle

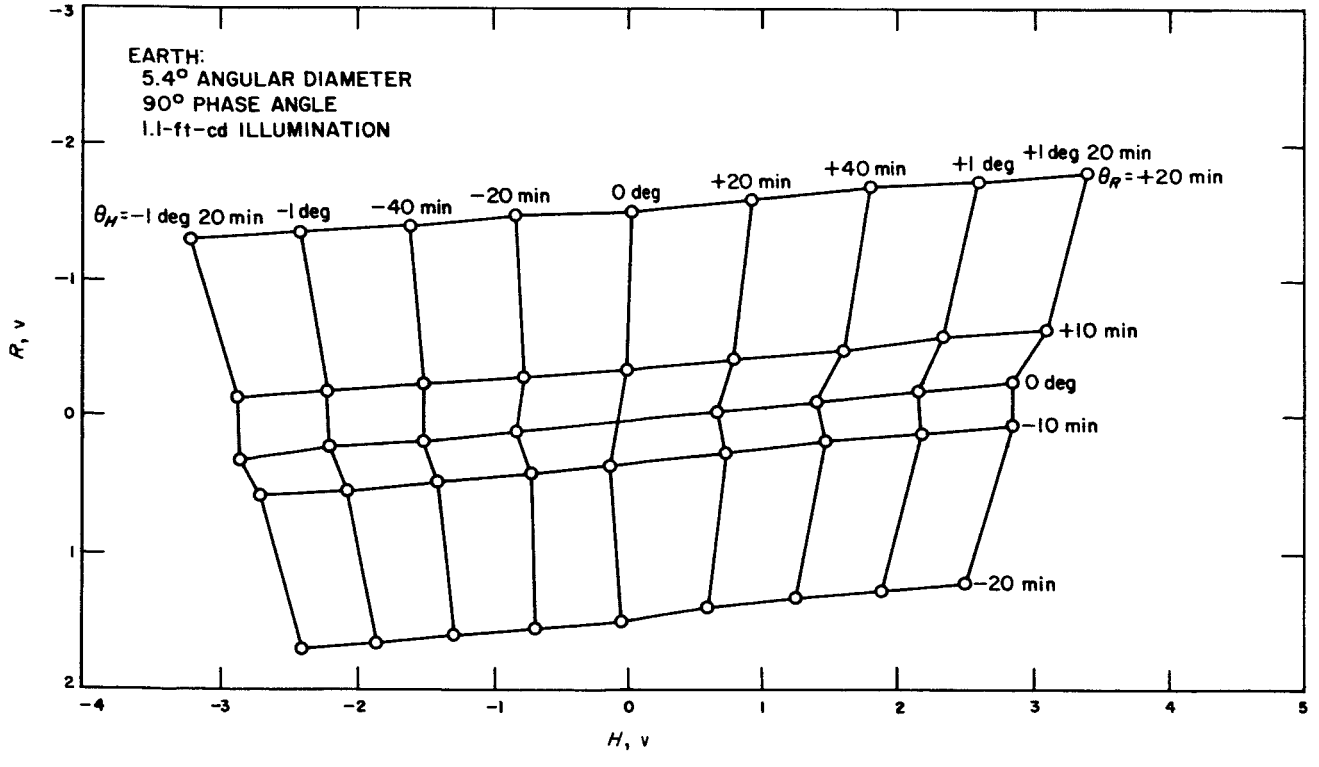

Fig. 34. Offset response for midcourse maneuver

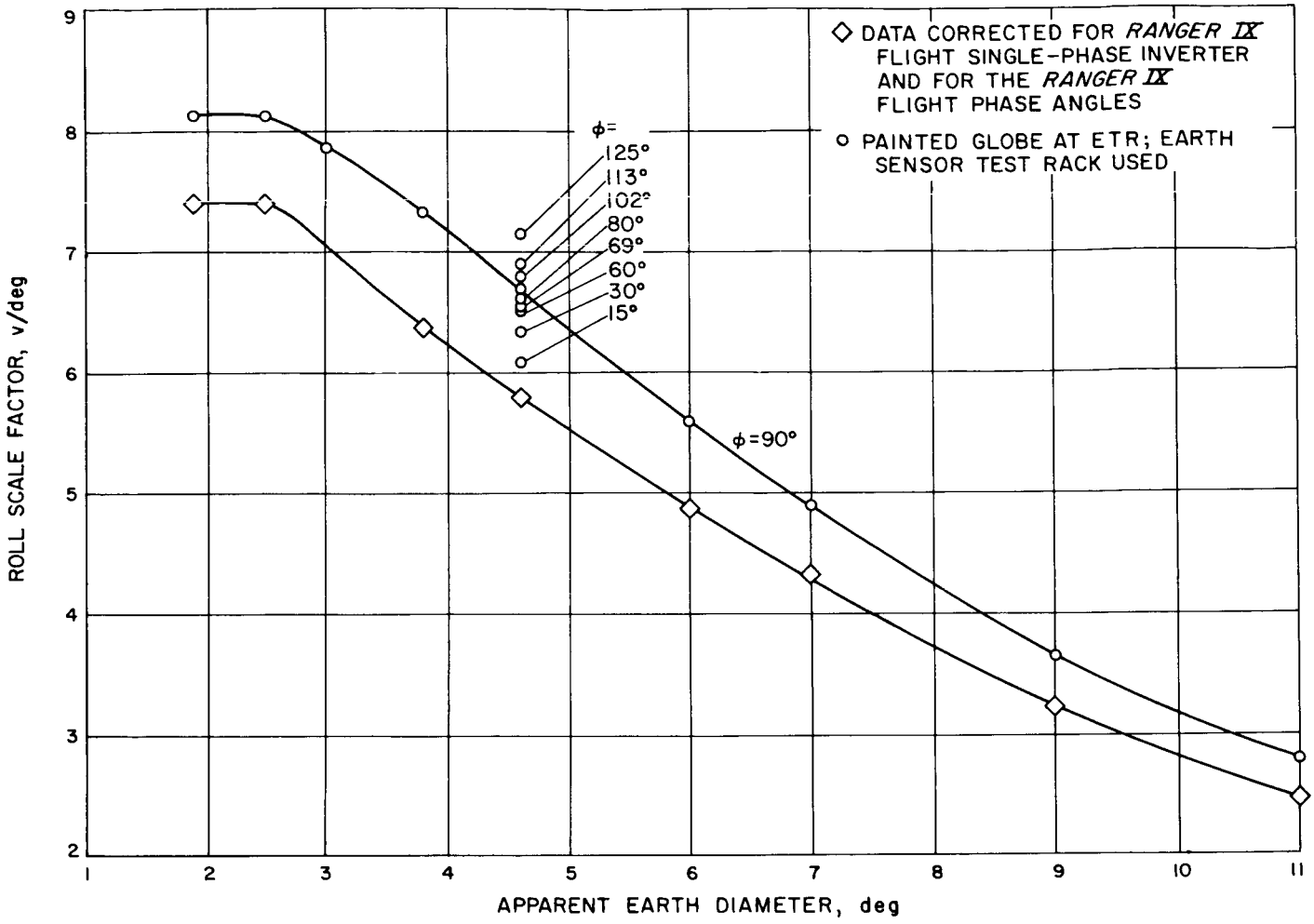

Fig. 35. Roll scale factor versus apparent Earth diameter

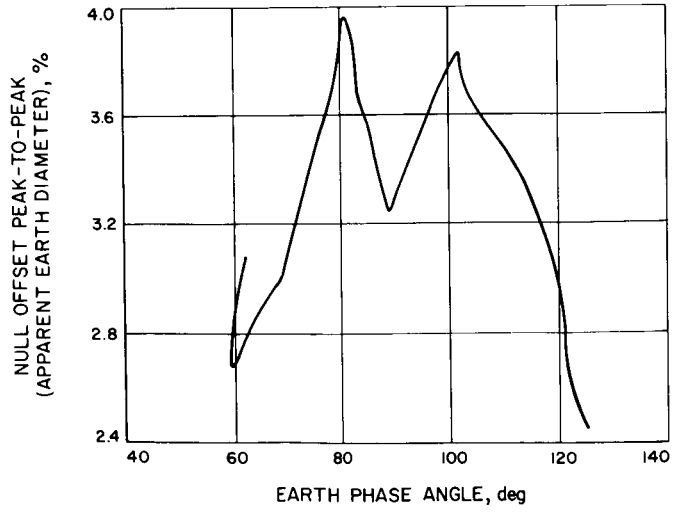

Fig. 36. Null offset peak-to-peak: apparent Earth diameter versus Earth phase angle

All mechanical nulls are with respect to the reference mounting legs of the Earth sensor, and do not include the Earth sensor mounting surfaces on the yoke.

The Earth sensor test rack was used in Figs. 27, 34, 35, and 36; thus, the results in these graphs should not be considered as flight calibration points. However, they can be used with the flight calibration curves to investigate hinge and roll cross-coupling during midcourse and terminal maneuvers to see how the roll scale factor will change as the apparent Earth diameter changes, and to see how the rotation of the painted globe simulator affected the null offset of the Earth sensor for various Earth phase angles at a midcourse size Earth.

The painted globe Earth simulator is a 12-in.-diameter globe painted in such a manner that the land masses

have a reflectance of 0.5 and the water areas have a reflectance of 0.3. The *Mariner II* flight to Venus indicated that the land masses on Earth had a larger albedo than the water areas, most likely because there was more cloud cover over the land. The painted globe was suspended by a thin wire from the ceiling and illuminated by a 3500°K temperature light source. An Earth sensor was mounted on a theodolite and looked at the illuminated globe (Fig. 37) at various distances and phase angles.

The *Ranger VIII* flight Earth sensor roll scale factor, as measured on the painted globe simulator and on the constant brightness source collimated simulators, is compared to the roll scale factor calculated from the *Ranger VIII* flight roll-rate gyro telemetry data in Fig. 38. The following formula was used to calculate the roll scale factor from the roll-rate gyro data:

$$SF_{roll} = \frac{E_2 - E_1}{\int \dot{\theta}_R \, dt \sin H + (Y_2 - Y_1) \cos H}$$

where

E = Earth sensor roll error voltage

Y = yaw angle

$\dot{\theta}$ = roll rate

H = hinge angle

t = time

Figure 38 shows good agreement of roll scale factor, as measured on the Earth sensor looking at the painted globe simulator, and the values calculated from the *Ranger VIII* flight data.

Figure 35 shows how the *Ranger IX* flight roll scale factor, as measured on the painted globe simulator, varies with apparent Earth diameter and phase angle. The change in hinge scale factor for the *Ranger IX* flight Earth sensor, as a function of apparent Earth diameter and phase angle, is shown in Fig. 39.

The painted globe was rotated and the peak-to-peak null offset change was noted for the *Ranger IX* light Earth sensor in Fig. 36. The maximum null offset change at nominal midcourse size Earth for the *Ranger IX* flight unit was 0.18 deg, and for the flight spare unit was 0.25 deg. The values can be compared to the midcourse maneuver 3-sigma roll sensor albedo asymmetry value of 0.55 deg.

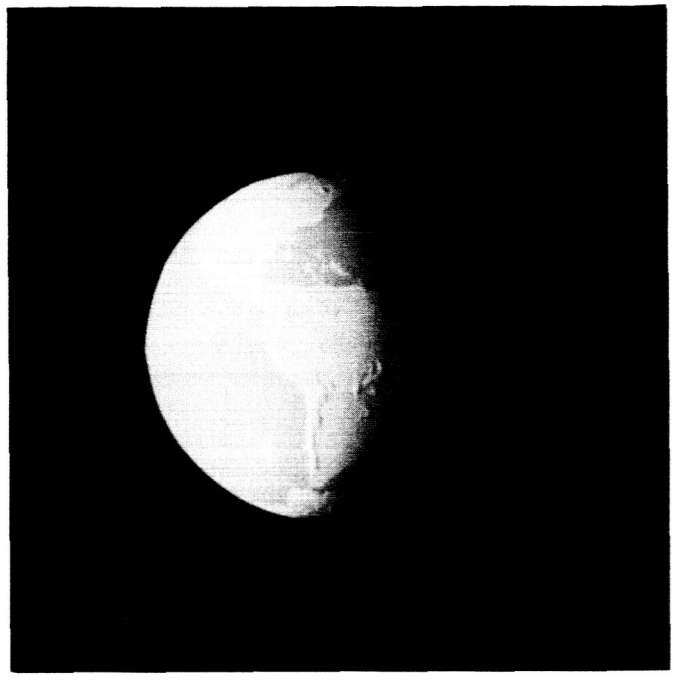

Fig. 37. Illuminated globe seen by Earth sensor

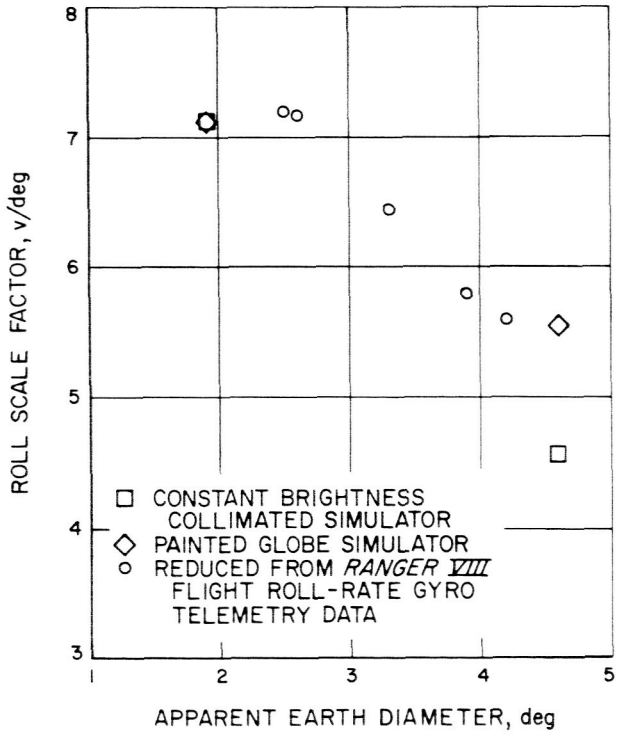

Fig. 38. Roll scale factor

The rounding of the curves in Figs. 31 and 32 near the saturation points is due to the finite size of the Earth. If the Earth were a point of source of light, the curves

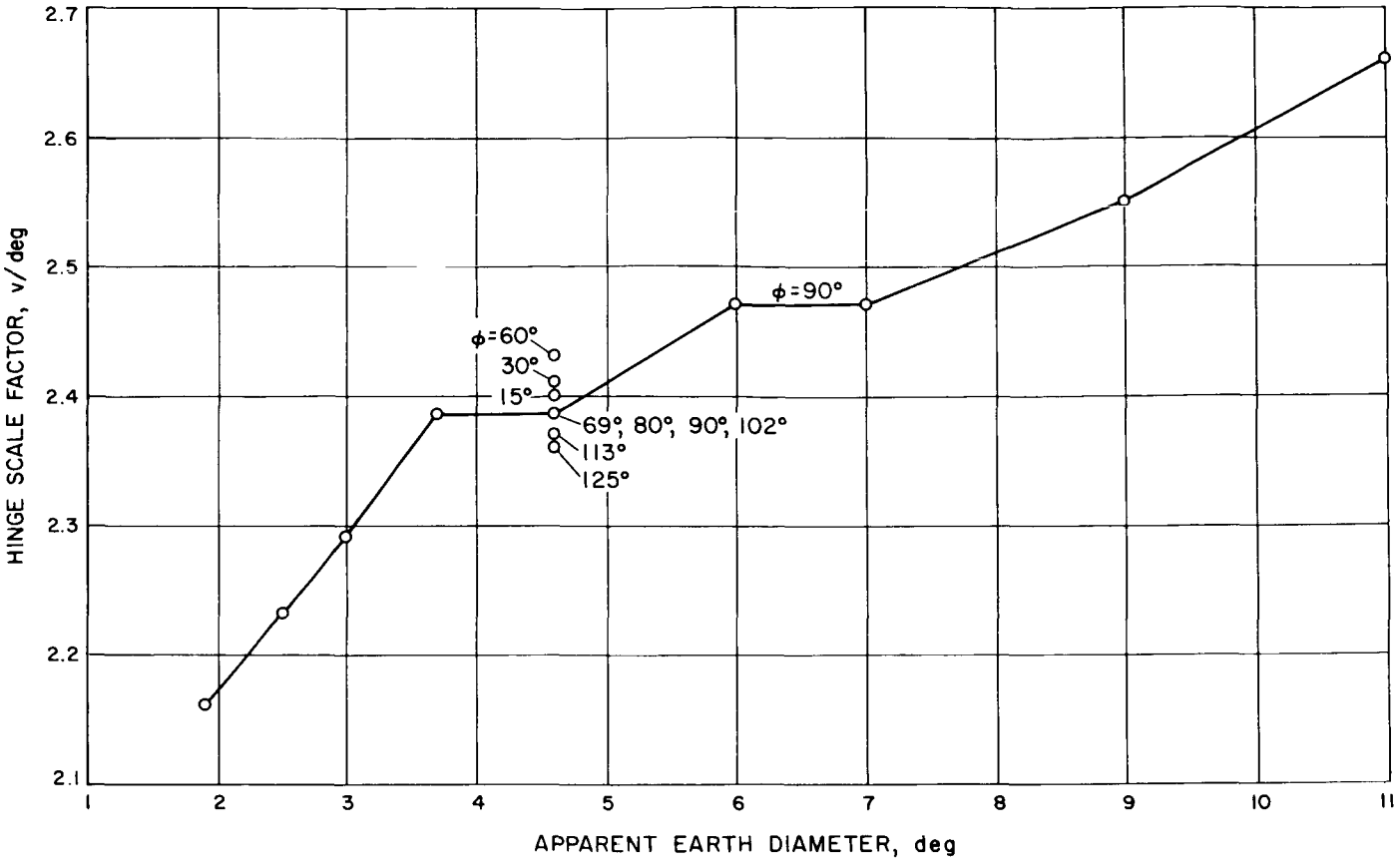

Fig. 39. Hinge scale factor

would be a straight line saturating at 1.25 deg for roll and 2.5 deg at hinge. The finite size of the Earth causes these intersecting lines to curve in a region of plus and minus the radius of the Earth from the saturation points of the point source. This is readily seen in Fig. 32. Because there is only a half-illuminated Earth in the hinge direction in Fig. 31, this effect is very much diminished. If the Earth moves away from null on a line not along either axis, the performance becomes truly two-dimensional. Note from Fig. 24 that, as the Earth moves in the positive θ roll direction, the hinge error signal weakens because there is less exposure of the cathode A and B PMT's. For motion in the hinge direction, however, the gain on the roll axis remains essentially constant. In reality, neither of these conditions will be precisely true because of variations in sensitivity over the PMT cathode surfaces. The actual experimental situation is illustrated in Fig. 27. The coordinate axes are roll and hinge DC error signals. The vertical lines are lines of constant hinge angle θ_H, and the horizontal ones are constant roll angle θ_R. The nonsymmetry of the actual two-axis output plot cannot be justified entirely by variations in cathode sensitivity, and thus remains unexplained at this time.

5. Hardware Limitations

a. Environment. Because of the high voltage in the Earth sensor (a 1300-v maximum under nominal power inputs), there was concern over the possibility of high-voltage arcing and the probable consequences.

Whenever there was a circuit change involving any portion of the high-voltage area, the Earth sensor was operated in a partial vacuum to see whether the high-voltage arcing could cause an Earth sensor failure. There have been no DC *Ranger* Earth sensor failures while operating in a partial vacuum.

A detailed test was performed on the *Ranger I* TA Earth sensor, which was operated at a maximum voltage in a bell jar. Arcing inside the Earth sensor occurred 1 min after the bell jar started pumping down at a pressure of 800 μ and continued until the bell jar was at a

pressure of 75 μ, 10.5 min later. The current in the plus and minus DC volt lines from the Earth sensor was monitored, and the current levels, because of the arcing, in the lines were not of sufficient magnitude to cause any trouble in the attitude control system. The Earth sensor continued to operate satisfactorily after the arcing had stopped.

The *Ranger I* TA Earth sensor did not have any holes in its housing for pad gas sterilization purposes. The Block II and III Earth sensors had three holes in the housing for pad gas sterilization reasons; thus, this further decreased the likelihood of a difference of pressure existing inside and outside of the Earth sensor. The most important point is that the Earth sensor is first energized in flight 3.5 hr after launch.

Even though it was felt that there was no chance of the high voltage in the Earth sensor arcing over in flight, testing in a partial vacuum was continued when any change had been made to the Earth sensor's electronics.

After the shroud has been ejected from the spacecraft and after *Agena*–spacecraft separation, sunlight could fall upon the *Ranger* Earth sensor PMT's as the spacecraft is tumbling in space before Sun acquisition. This could not occur during midcourse maneuver because the Earth sensor Sun shield shades the optics of the Earth sensor from direct sunlight. Therefore, tests were made on two Earth sensors to see whether there was exposure of sunlight on the PMT faces while the sensor was energized (which could occur before the first Sun acquisition of the spacecraft) and while the sensor was energized with DC voltage only (which would occur during midcourse maneuver). There appeared to be no significant degradation in the two Earth sensors after exposure to the maximum expected exposures of sunlight on the tubes.

The effect of temperature has been periodically tested on *Ranger* Earth sensors; this test is shown in Fig. 40. The Earth sensor was tested at a wide range of temperatures with a wide range of test results. One sensor operated satisfactorily from 130 to −4°F; another Earth sensor operated satisfactorily from 95 to −30°F; however, at 110°F, the hinge and roll scale factors decreased approximately 25%. This Earth sensor stayed at that low scale factor at 120°F, and returned to a satisfactory value at ambient temperature. Problems began on one Earth sensor at temperatures above 109°F during the TA thermal vacuum test. On the basis of these tests and other temperature tests, the maximum flight Earth sensor temperature was set at 95°F. The cesium photocathode of the tube starts to migrate at temperatures above 100°F.

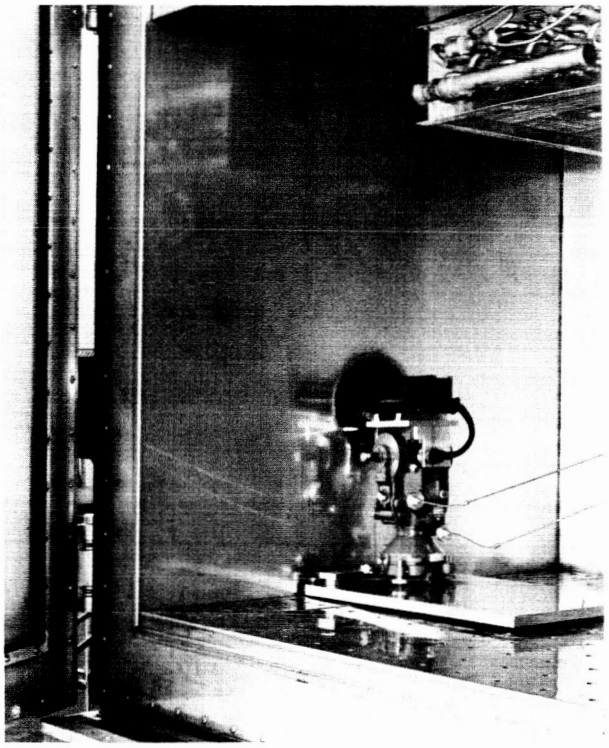

Fig. 40. Earth sensor during temperature test

b. Trajectory. The following is a summary of the present Block III Earth sensor trajectory constraints:

(1) The *Ranger* Earth sensor must not be turned on until Sun acquisition is complete. (Normally, this is ensured 1 hr after the acquire-Sun command is given and the spacecraft is in full sunlight.)

(2) The Earth sensor must be energized only at atmospheric pressure or pressures less than 10^{-4} mm Hg.

(3) During Earth search, the antenna angle should be less than or equal to 135 deg.

(4) The Earth–probe–Sun angle should be greater than 40 deg at the time of first Earth acquisition, and the calculated Earth flux at the spacecraft should be greater than 0.7 ft-cd.

(5) For high accuracy during periods of flight such as pre-midcourse and pre-terminal maneuvers, the antenna angle (during Earth lock) should be less than

150 deg − 10 deg − one-half apparent Earth diameter − 3.5 =

135.5 deg − one-half apparent Earth diameter

(The 3.5 deg is for Sun sensor null offset, Earth sensor limit cycling, Sun sensor limit cycling, hinge Earth sensor null offset.)

(6) In order to prevent the loss of Earth lock due to the Earth sensor Sun shield blocking the Earth sensor's view of the Earth, the antenna angle should be less than

150 deg − one-half apparent Earth diameter
−3.5 deg =

146.5 deg − one-half apparent Earth diameter

(7) The preset hinge angles on the spacecraft should provide overlap of the 20-deg field of view of the Earth sensor within the normal flight working range of the Earth sensor.

(8) The calculated Earth flux at the spacecraft should always be greater than 0.06 ft-cd and less than 40 ft-cd.

(9) When the spacecraft has lost Sun lock during terminal maneuver, the Earth–probe–Sun angle should be greater than 47 deg.

(10) During terminal maneuver, the Earth–probe–near limb (light side of Moon) angle should be greater than 15 deg. (There has been limited testing for this constraint; many Earth sensors should be tested before this constraint becomes firm.)

(11) During terminal maneuver, the antenna angle should be less than 137 deg.

c. Handling and shipping. The Earth sensor should always be hand-carried in its carrying case in order to protect it from transportation vibration, shocks, extreme storage temperatures, and stray light.

Because of the great difference in light intensities between the Earth sensor and the Sun, the Earth sensor is greatly susceptible to stray light reflections. Stray light tests were performed in which a high light-intensity light beam illuminated that portion of the Proof Test Model spacecraft in the vicinity of the Earth sensor (Fig. 41). The Earth sensor was energized and looking at an Earth; the ratio of the high-intensity light beam to the intensity of the artificial Earth was in the same ratio as the intensity of the Sun and the minimum allowable Earth intensity while in flight. The light reflections from various areas on the spacecraft were decreased, and the effects on the Earth sensor outputs were noted. These tests were also run without an Earth to simulate the Earth-search phase of the flight. From these tests certain areas on the spacecraft were either painted with a flat black paint or covered with an especially evaluated black cloth to reduce the intensity of reflections into the Earth sensor.

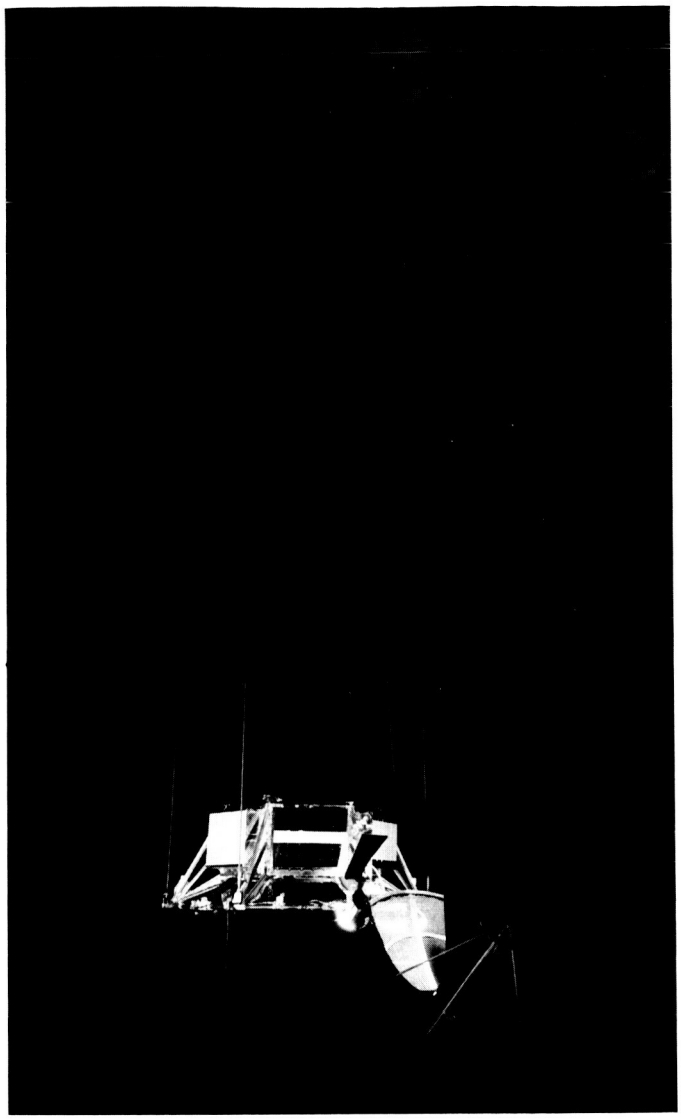

Fig. 41. Proof Test Model spacecraft illuminated by high light-intensity light beam during stray light tests

6. Operations Summary

a. Flight performance. The function of the Earth light-intensity telemetry signal from the *Ranger* Earth sensor is to verify that the Earth sensor is tracking the Earth and not the Moon. This requires that the Earth light-intensity telemetry signal be within an order of magnitude of the theoretically predicted Earth light intensity. This tolerance condition for the Earth light-intensity signal from the Earth sensor has been satisfied for all

Ranger flights in which the Earth sensor has been energized. It is, therefore, a mistake to consider it a failure or a problem if the Earth light-intensity signal from the flight Earth sensor does not agree exactly with the theoretical Earth light-intensity prediction for that flight, as long as the agreement is within an order of magnitude from the theoretical prediction.

There are many possible causes for disagreement between the theoretical prediction and the telemetered signal for Earth brightness: telemetry signal uncertainties, variations in Earth albedo, Earth simulator calibration, disagreements between theoretical predictions, and experimental observations made by other experimenters as a function of planet phase angles, and the disagreements between theoretical predictions.

Figures 42 and 43 show the Earth light intensity in foot-candles as a function of time from launch in hours, spacecraft distance from the center of the Earth in Earth radii, and Earth phase angle in degrees for the *Ranger VIII* and *IX* telemetry data from the Earth sensor and for the predictions from the attitude reference program and computer program 5501. A hand-calculated approximation would lie between the attitude reference prediction and the computer program 5501 prediction. All predictions assume the Earth to be a perfectly diffuse (lambert) reflector. The equation for the hand-calculated approximation is of the following form:

$$H \approx \frac{2aL}{3} \frac{R^2}{(R+h)^2} \frac{\sin\phi + (\pi - \phi)\cos\phi}{(11.43 \times 10^{-6})\,\pi}$$

(foot-candles)

where

a = Earth albedo

L = solar constant at 1 AU

ϕ = Earth phase angle

R = Earth radius

h = distance from the surface of the Earth to the spacecraft

The predictions from the attitude reference program and the hand-calculated approximation should be used only when the distance of the probe to the planet is much greater than the radius of the planet ($h > 10\ R$).

The angular diameter of the Earth was larger than the roll field of view of the Earth sensor until 5.5 hr after launch, so one would not expect that the telemetry data would be a true indication of Earth intensity for the first few hours after Earth sensor power turnon. It is believed that, after that time in flight, the Earth light intensities, telemetered back from the Earth sensor during the *Ranger* flights, were accurate (taking into consideration a possible 0.6 of a cycle uncertainty factor in the telemetry signal). The Earth light-intensity calibration curve for the Earth sensor had 1.77 to 1.81 correction factor included to compensate for the difference in spectral characteristics as seen by the Earth sensor of the light reflected from the Earth and the Earth simulator, which is used to calibrate the Earth sensor.

The *Ranger VIII* flight gives Earth light intensities for phase angles from 133 to 122 deg; the *Ranger IX* flight shows Earth light intensities for phase angles from 110 to 95 deg. This information could then be combined with Earth light intensities obtained from the *Mariner II* flight to Venus for Earth phase angles from about 10 to 45 deg.

Up to and including the *Ranger VI* flight, the Earth simulator and the Earth sensor test rack were used to calibrate the Earth light-intensity curve. For *Ranger VII*, the Earth sensor test rack and Star Planet Simulator 2 were used to calibrate Earth light intensity. This simulator had a recent spectral measurement made of its output. It was found that the wave distortion of the 400-cps, single-phase input to an Earth sensor made a difference of approximately 10% to the Earth light-intensity calibration curve using the Earth sensor test rack versus the Block III TA single-phase inverter. Therefore, for *Rangers VIII* and *IX*, the respective flight single-phase inverters were used with Star Planet Simulator 2. The following is a discussion of how the correction factor was obtained using the Earth simulator.

If an optical sensor such as an Earth sensor is to be accurately threshold calibrated and it is not possible or is inconvenient to calibrate on the actual planet, a simulator must be used. Ideally, the simulator should have the same absolute spectral "output" as the planet outside the Earth atmosphere. This is difficult, since present sources have spectral characteristics much different than a typical planet or star. This report indicates a practical approach of relating tracker response on one source to that on another source through an intermediate calibration (which would logically be the foot-candle or other convenient standard).

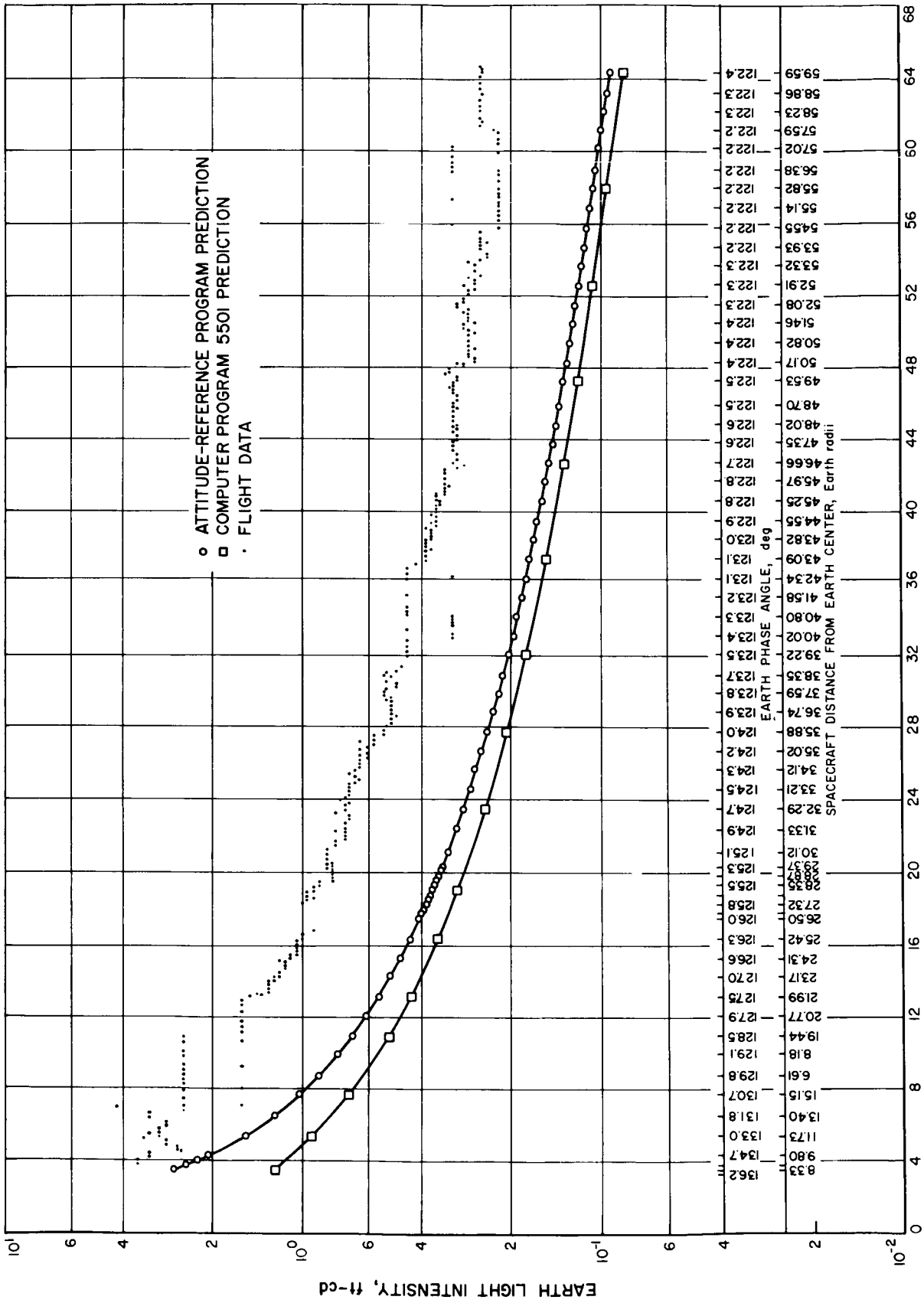

Fig. 42. Earth sensor light-intensity plot: *Ranger VIII*

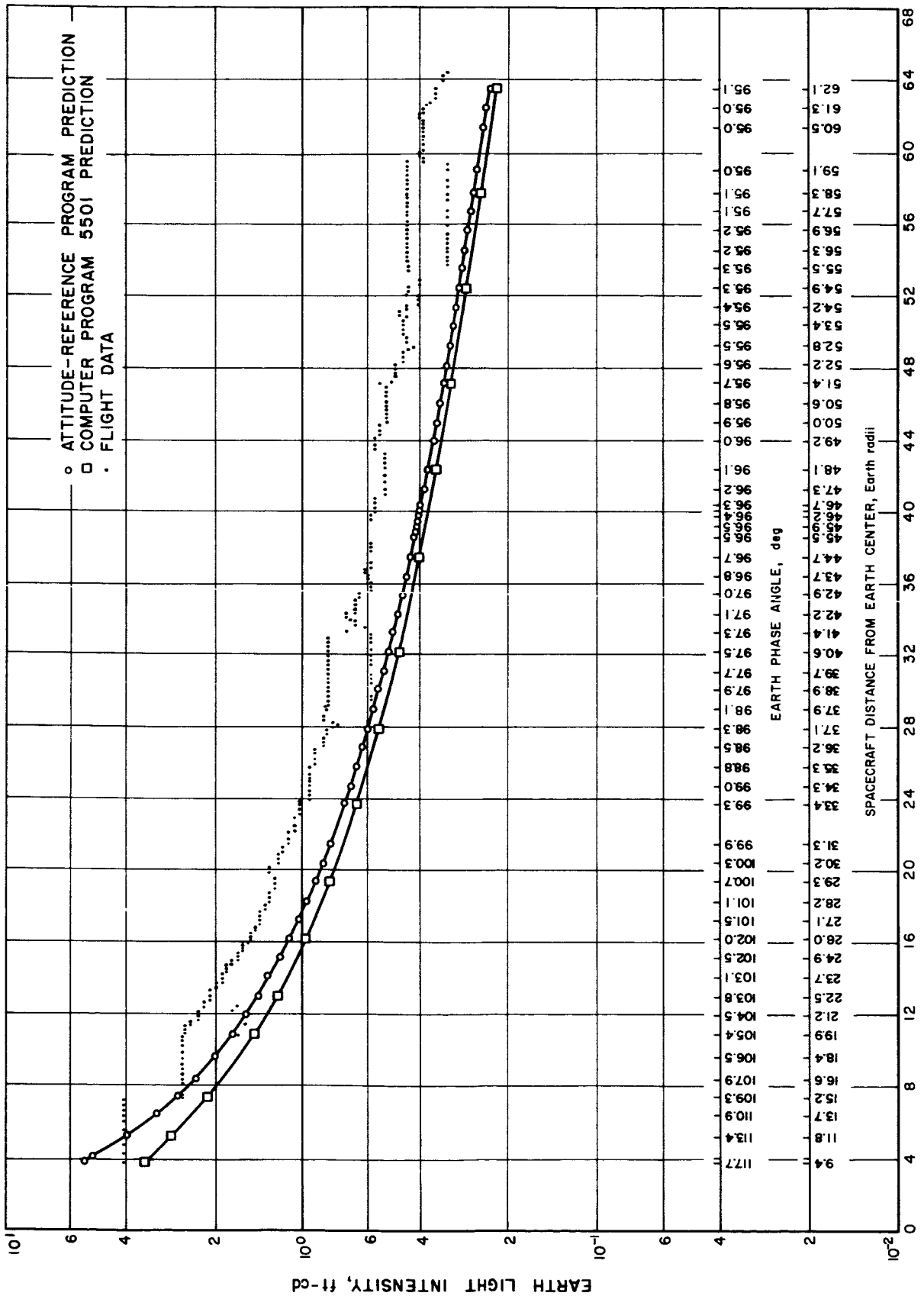

Fig. 43. Earth sensor light-intensity plot: *Ranger IX*

b. Assumptions. Star or celestial reference "output" at the tracker location

$$= K_2 f_2(\lambda) \text{ w/cm}^2 - \mu$$

where

$$f_2(\lambda) = \text{Sun } (\lambda) \cdot \text{Earth albedo } (\lambda)$$

Laboratory simulator output

$$= K_1 f_1(\lambda) \text{ w/cm}^2 - \mu$$

Tracker response versus wavelength

$$= K_3 f_3(\lambda) \text{ amp/w}$$

where $f_3(\lambda)$ is for an S-11 PMT response. Area of collecting optic

$$= A \text{ in square centimeters}$$

Star or celestial reference output in foot-candles at the tracker location

$$= [930]\ 685 K_2 \int_0^\infty f_2(\lambda)\, V(\lambda)\, d$$

Simulator output in foot-candles

$$= [930]\ 685\, K_1 \int_0^\infty f_1(\lambda)\, V(\lambda)\, d$$

Eye response normalized to 1 at peak

$$= V(\lambda)$$

c. Computations. If tracker output operated against simulator is to be equal to its output against the star, then:

$$AK_1K_3 \int_0^\infty f_1(\lambda)\, f_3(\lambda)\, d\lambda = AK_3K_2 \int_0^\infty f_2(\lambda)\, f_3 d\lambda \quad (1)$$

and if simulator foot-candle flux equal R times the star foot-candle, then:

$$[930]\ 685K_1 \int_0^\infty f_1(\lambda) V(\lambda)\, d\lambda =$$

$$[930]\ 685RK_2 \int_0^\infty f_2(\lambda)\, V(\lambda)\, d\lambda \quad (2)$$

which implies

$$K_1 = \frac{RK_2 \int_0^\infty f_2(\lambda)\, V(\lambda)\, d\lambda}{\int_0^\infty f_1(\lambda)\, V(\lambda)\, d\lambda} \quad (3)$$

substituting Eq. (3) into (1) yields

$$R = \frac{\int_0^\infty f_1(\lambda)\, V(\lambda)\, d\lambda \int_0^\infty f_2(\lambda)\, f_3(\lambda)\, d\lambda}{\int_0^\infty f_2(\lambda)\, V(\lambda)\, d\lambda \int_0^\infty f_1(\lambda)\, f_3(\lambda)\, d\lambda} \quad (4)$$

The simulator should, therefore, be set to a foot-candle level that is R times the star foot-candle level. When this is done, the sensor response to the simulator will be equal to its response on the star.

Conversion factor from watts per square centimeter to foot-candles. The assumptions of albedo invariant with wavelength and Sun spectrum equivalent to that of a 6000°K blackbody make it possible to calculate a standard conversion factor of watts per square centimeter to foot-candles for all the planets of our solar system. This is done by calculating the luminous efficiency of a 6000°K blackbody.

$$\text{Luminous } Eff = \frac{685 \int_0^\infty F(\lambda)\, V(\lambda)\, d\lambda}{\int_0^\infty F(\lambda)\, d\lambda}$$

$$= 94.2 \text{ lumen/w for } 6000°\text{K blackbody}$$

where

$F(\lambda)$ = emitted energy of a 6000°K blackbody, w/cm²-μ

$V(\lambda)$ = normalized human eye response

Since 1 ft-cd equals 1 lumen/ft², it is possible to further derive that

$$1 \text{ ft-cd} = 11.43 \times 10^{-6} \text{ w/cm}^2.$$

Equations used. The following equations have been used in this report:

Null offset = NO

$$= NO\,|_{\pm 20'} = \frac{[E_o|_{+20'} + E_o|_{-20'}]}{[(2)\, SF]} \text{ deg} \quad (1)$$

Scale factor = SF

$$= SF\,|_{\pm 20'} = \frac{[E_o|_{+20'} + E_o|_{-20'}]}{[2/3]} \text{ v/deg} \quad (2)$$

Average magnitude = *av mag*

$$= \sum_{j=1}^{N} \frac{|X_j|}{N} \quad (3)$$

Average value = *av value*

$$= \sum_{j=1}^{N} \frac{X_j}{N} \tag{4}$$

RMS deviation = 1 sigma = *RMS*

$$= \left[\sum_{j=1}^{N} \frac{(X_j - X_{av\ value})^2}{N-1} \right]^{1/2} \tag{5}$$

PMT sensitivity =

$$\frac{(\text{light cathode current}) - (\text{dark cathode current})}{(\text{foot-candles})(\text{filter transmission})(\text{aperture area})} \tag{6}$$

PMT gain =

$$\frac{(\text{light anode current}) - (\text{dark anode current})}{(\text{light cathode current}) - (\text{dark cathode current})} \tag{7}$$

Percent difference = $\%\Delta$

$$= \frac{(X - X_{ref})}{X_{ref}} (100) \tag{8}$$

Change = Δ

$$= (X_{final}) - (X_{initial}) \tag{9}$$

The Earth sensor functioned in *Rangers I–III* and *VI–IX*. On *Rangers IV* and *V*, the Earth sensors were never energized. *Rangers I* and *II* operated in a low Earth orbit; the Earth sensors indicated acquisition on lighted objects. (*Ranger I* gave more information.) The Earth sensor appeared to be operating correctly even though its temperature was close to the maximum allowable Earth sensor temperature, and the intensity of the Earth was ten times brighter than expected on normal *Ranger* trajectories.

Ranger III provided the first good in-flight evaluation of Earth sensor performance. This evaluation indicated that the sensor performed as intended during flight. A spurious pitch command at terminal (Moon distance) caused the spacecraft to pitch in the direction of Earth, eventually bringing the Sun shade between Earth sensor and Earth; this caused a loss of Earth acquisition. From this point on, the spacecraft performance became quite confused; further Earth sensor performance cannot be adequately stated.

On *Rangers VI–IX*, the Earth sensors operated within tolerance and once again provided good in-flight data.

7. Reliability

All *Ranger* Block III Earth sensor failures and problems have been recorded starting from the initial functional checks of a unit and extending through all of the spacecraft system tests.

8. Engineering Change Requirements

A brief description of the Block III Earth sensor change requirements that occurred after Block II are given below.

(1) Change of cadmium-plated items in the sensor to CRES material.

(2) Change from allocated-to-actual weights of the assembly.

(3) Application of black cloth and black paint to various areas on the spacecraft to reduce intensity of light reflections into Earth sensor.

(4) Replacement of all Continental Device diodes in Earth sensor.

(5) Use of two smaller standoff terminals in sensor to prevent a possible cold-flow condition on some wires.

(6) Insulation and sealing of the backside of the connector in Earth sensor.

(7) Modification of paint pattern on *Ranger IX* and Spare 1 Earth sensors so that the temperature of the sensor would be cooler in flight.

B. Sun Sensor

1. Description

The *Ranger* Sun sensors are optical devices using a shadowing technique on cadmium sulfide photoconductive detectors. There are two pairs of primary Sun sensors and two secondary Sun sensor assemblies on each *Ranger* spacecraft to provide a combined 4π-sterad field of view. Each primary Sun sensor contains a single detector cell; each secondary Sun sensor contains four detectors, used only while the spacecraft is searching for the Sun. Once the Sun has been acquired, only the primary Sun sensors are required to keep the spacecraft oriented toward the Sun.

The Sun sensors deliver position error signals in the pitch and yaw axes to the attitude control logic, and thus to the spacecraft control jets. This orients the z-axis of the spacecraft toward the Sun. A positive pitch or yaw angular deflection of the spacecraft from the direction of the Sun would give a negative error signal in that particular axis.

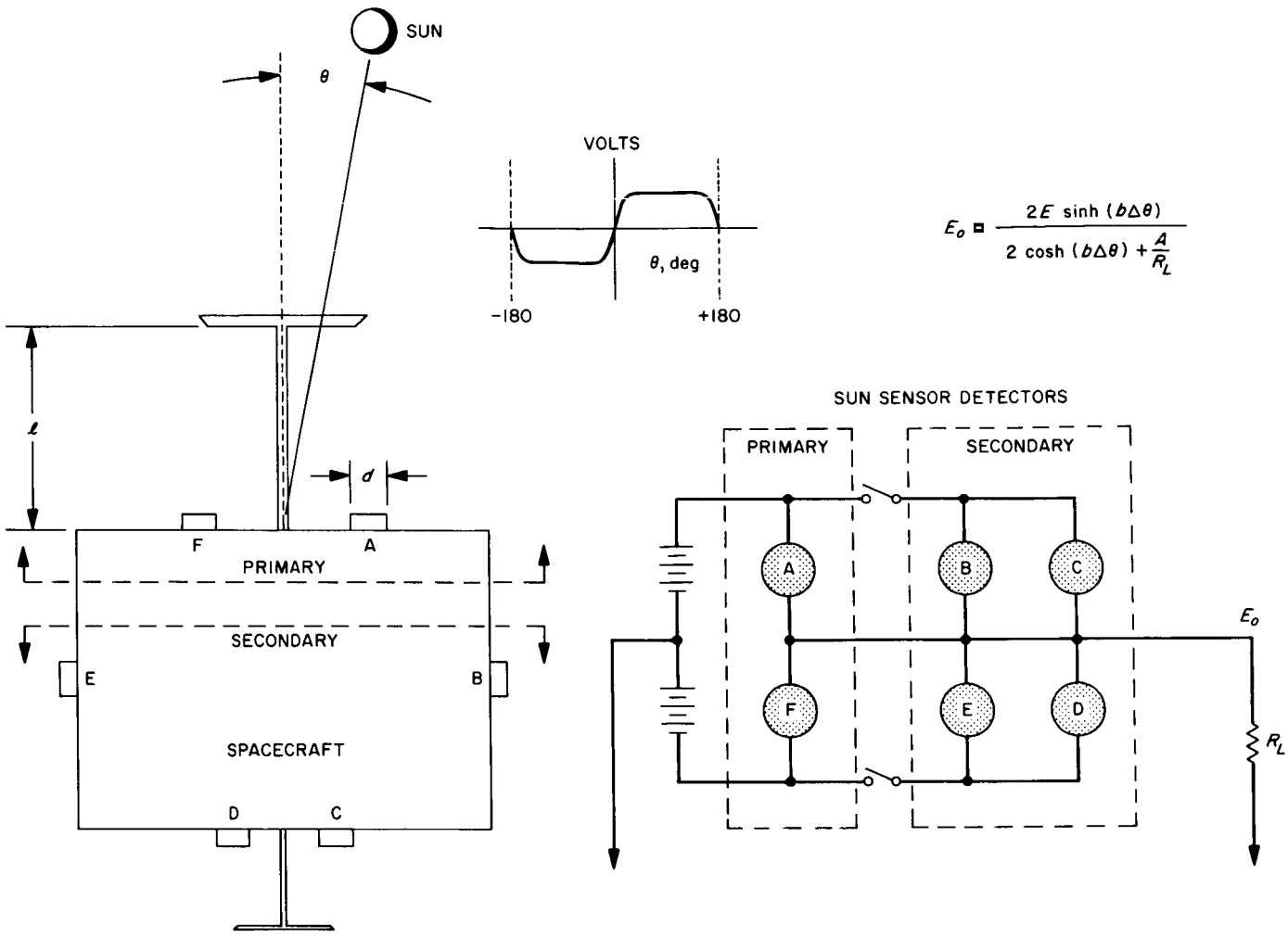

Fig. 44. Sun sensor schematic

Fig. 44 is a schematic of Sun sensor operation. The letters of the cells shown, which can be considered as variable resistors, are for Sun orientation of the yaw axis of the spacecraft. If the photoconductive strip on the cell is completely exposed to the Sun, its resistance would be about $10^2\Omega$; if it were half exposed to the Sun, its resistance would be about $6 \times 10^3\Omega$; and if it were dark, its resistance would be greater than $10^6\Omega$.

As seen in Fig. 44, the detectors are connected in a bridge circuit. The Sun sensor output signal is a voltage developed across a load resistor (R_L). In the spacecraft, this load will be the input resistance of a switching amplifier and telemetry impedance (which are both in parallel). For most laboratory tests (except for flight calibration) the load resistance is 50 kΩ. The spacecraft load resistance for *Rangers VI* and *VII* is 99 kΩ and for *Rangers VIII* and *IX* is ⅔ MΩ. The positive and negative voltage supplies to the Sun sensors are 16.8 v.

An analysis of the circuit (Fig. 44) leads to the following equation for the primary and secondary voltage outputs while the spacecraft is trying to orient itself with respect to the Sun:

$$E_o = \frac{ER_L\left[\left(\frac{1}{R_A} + \frac{1}{R_B} + \frac{1}{R_C}\right) - \left(\frac{1}{R_F} + \frac{1}{R_E} + \frac{1}{R_D}\right)\right]}{1 + R_L\left(\frac{1}{R_A} + \frac{1}{R_B} + \frac{1}{R_C} + \frac{1}{R_F} + \frac{1}{R_E} + \frac{1}{R_D}\right)}$$

After the spacecraft has acquired the Sun, the above equation reduces to:

$$E_o = \frac{E(R_F - R_A)}{R_A + R_F + \frac{R_A R_F}{R_L}}$$

Note that the above equations represent yaw Sun acquisition only, and that the equations would be the same for pitch Sun acquisition except for different letter subscripts.

Because of the shadowing method on the semiconductor, the resistances of the cell as a function of angle from null are very closely approximated by

$$R_{A,F} = Ae^{-b\Delta\theta}$$

where $\Delta\theta$ is the angular deviation of sensor from null in degrees.

The sign on the exponent is opposite for two opposed detectors. Although the constants A and b vary with the particular cell chosen, paired detectors with these constants approximately equal have been obtained through a matching process. The nominal values are $A = 6$ kΩ and $b = 0.962$ deg^{-1}. Using these forms for R_A and R_F, the voltage output as a function of angle from null becomes

$$E_o = \frac{2E \sinh(b\Delta\theta)}{2\cosh(b\Delta\theta) + \frac{A}{R_L}}$$

Figure 44 also shows the voltage output from either the pitch or yaw Sun sensors versus angular displacement from the Sun for primary and secondary configurations.

2. Fabrication

Figure 45 shows a complete set of four primary and two secondary Sun sensors, whose housing is machined out of 6061-T6 aluminum alloy; the parts of the housing are then black anodized and assembled. The cadmium sulfide detectors are the CL605 photocells from the Clairex Corporation.

The *Ranger* Block II primary Sun sensors were designed to improve the null stability by a factor of two over the Block I primary Sun sensors. The main change was an

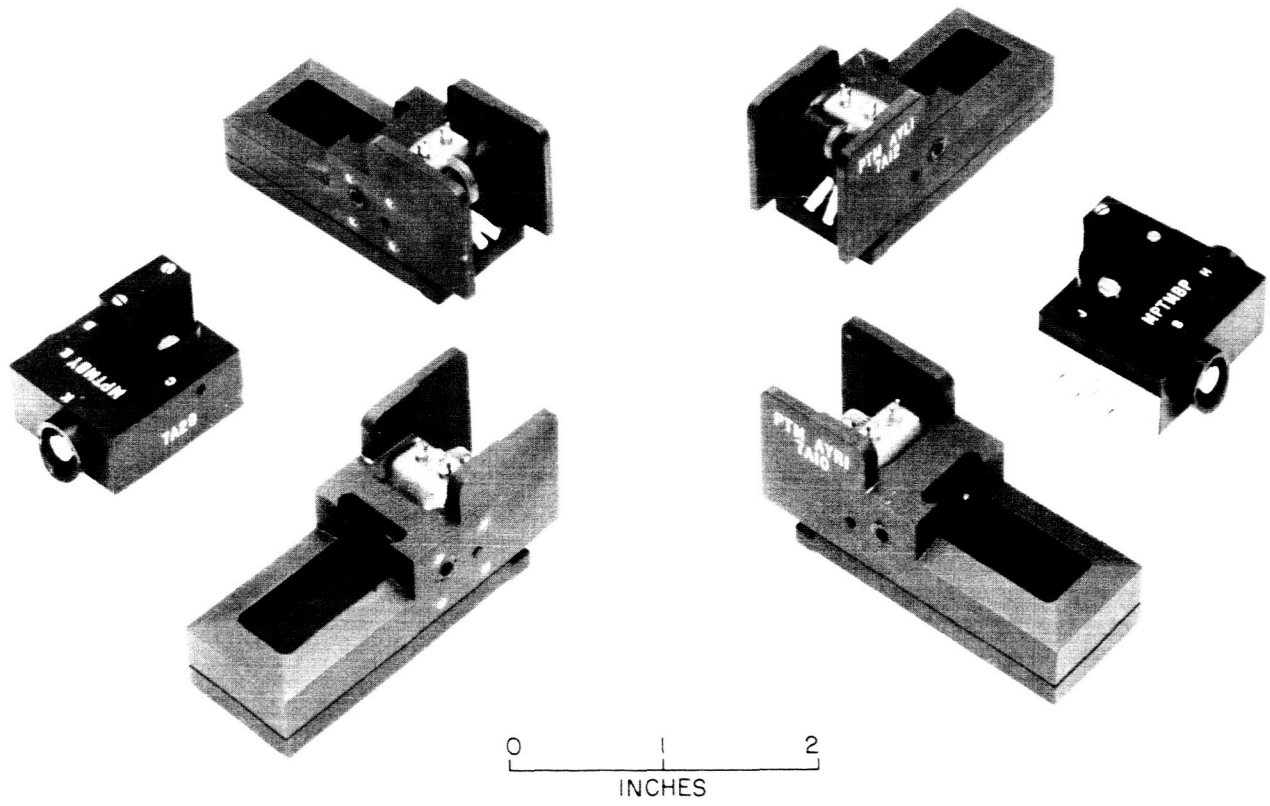

Fig. 45. Complete set of *Ranger* Sun sensors

approximate doubling of the distance between the detector cell and the shadow bar in the support housing of the sensor. The changes originally made for the Block III Sun sensors are:

(1) Nominal scale factor changed from 16 to 18 v/deg.

(2) Sun sensor excitation voltage changed from + and − 16 v to + and − 16.8 v.

(3) Miscellaneous hardware changes.

The following weight changes were made:

(1) Block II
  (a) Primary Sun sensors: 0.1 lb each.
  (b) Secondary Sun sensors: 0.07 lb each.

(2) Block III
  (a) Primary Sun sensors: 0.106 lb each.
  (b) Secondary Sun sensors: 0.077 (pitch); 0.082 (yaw).

One of the early design problems involved a rather large thermal shock received by the cells while in flight. The secondary Sun sensors, mounted on the back side of the solar panels, may undergo a significant temperature change between injection and Sun acquisition while the spacecraft is in the Earth's shadow after removal of the shroud. Unpotted detectors in their housings were subject to a thermal shock of 18°F/min from 250 to −100°F with no damage or change in characteristics; however, the glass detector cracked in the potted units.

The problem of mounting the Sun sensor detector was solved by the use of quad rings, which brought support to bear on the strongest section of the glass detector envelope rather than complete support as provided by the potting compound. By using the quad-ring mounting, a Sun sensor assembly can survive an extreme temperature range from −100 to +125°C without failure.

After close scrutiny under a 40-power microscope, 17 out of 100 Clairex cadmium sulfide cells were rejected because the solder joints connecting the cadmium sulfide element to two wires used for external electrical connection appeared questionable. Six of these 17 cells were then subjected to TA tests by JPL.

It was decided that the cells should be mounted in a flight manner using quad rings and standard primary cell housings. At the environmental facility, a fixture was made to hold the cell assemblies and to fit the standard mounting jigs, which would give accurate levels of shock and vibration to all the cells.

For this test, an excitation voltage was applied to the cells and a photo-flood lamp was used to illuminate them. (This is not a standard procedure for environmental testing, but in this case would permit the detection of any intermittent failures during the test.) The light used was sufficient to give a resistance of 1500 Ω for each cell, or 7500 Ω for each string of five cells in series. A 5-amp meter and a 10,000-Ω load were put in series with each string. A scope was used to measure the output across the 10,000-Ω loads to detect any intermittents because the response time of the meters was too slow.

The cells were first given two TA shocks in each of three planes; they were then subjected to three planes of TA vibration, after which they were shaken at double TA level (maximum capability of the shaker). There was no indication of failure, intermittent or permanent, at any time during these tests.

A visual inspection of these cells was given after completion of these tests; no change was found in their physical characteristics. It was concluded that the cells would have been satisfactory for flight.

3. Testing and Calibrations

A constant problem in testing primary Sun sensors is having an acceptable sky condition. There are many difficulties inherent in the problem of simulating an extremely bright, collimated light; therefore, most of the Sun sensor testing has been done with the Sun as the source. Because of the intensity requirements and the fact that there can be no clouds to interfere with tracking of the Sun, the test schedule must be thoroughly planned.

Two facilities have been provided for Sun sensor testing: One facility, at Palos Verdes, California, uses a two-mirror heliostat Sun tracking system to provide a collimated Sun bundle at a constant position. This facility tested all the Sun sensors prior to delivery of the Sun sensors to JPL for assignment to the various spacecraft. Once the Sun sensors were formally delivered to JPL, the primary Sun sensor testing was then performed at the JPL test site at Chilao, California. This facility uses a two-mirror coelostat system to provide a collimated Sun bundle at a constant position. This bundle is directed through a tube into a trailer to a Leitz optical dividing head which rests on a stable tripod. Both systems include a boresighting telescope and motors to drive the tracking mirrors. The overall accuracy of both pointing systems is better than 10 sec of arc. The sensors in both systems are tested by mounting them on a dividing head and positioning to known angles, while monitoring the outputs.

The following test equipment (other than the Sun tracking system and its associated test equipment) is used in Sun sensor testing: thermocouple indicator, an L and N resistance bridge, a dynamics voltmeter, two 16.8-v DC power supplies, temperature control box for optical test fixture, an optical test fixture assembly with an angle generator (at Palos Verdes) or with a Leitz optical dividing head (at Chilao), an operating test fixture, GSE light hoods, a photocell holding fixture with a thermal control apparatus and switching panel, a load resistor, and the various environmental holding fixtures.

4. Qualification for Flight

The photocell detectors are given a temperature matching test before they are assembled into a Sun sensor. The primary Sun sensor pair is calibrated to a master primary Sun sensor pair. The primary Sun sensors are then qualified for flight by the following tests:

Performance tests.

(1) Short-term stability tests.

(2) Photocell linearity tests.
   (a) Light-intensity tests.
   (b) Voltage excitation tests: symmetrical and asymmetrical.
   (c) Temperature tests.
   (d) Long-term stability tests.
   (e) Burn-in tests.

Environmental tests.

(1) Type-approval tests.

(2) Flight-acceptance tests.

Flight calibration tests. The secondary Sun sensors receive ambient, burn-in, TA, and FA tests.

a. Performance tests. All performance tests use the heliostat to track the Sun. Table 19 shows the testing schedule for primary Sun sensors and the percent of flight units subjected to the various tests.

A short-term stability test consists of a pair of primary Sun sensors mounted back-to-back on a dividing head and rotated 0, ± 0.01, and ± 5 deg with respect to the mechanical null position of the planes formed by the mounting pads of the primary Sun sensors and the Sun. At each angular position, the voltage output signal from the pair of primary Sun sensors is recorded across a 50K load resistor.

Table 19. Testing schedule for primary Sun sensors

Test	Flight units tested, %
Front null offset (null offset at ± 0.1 deg)	100
Front null offset (null offset at ± 0 deg)	100
Slope through null	100
Saturation	100
Light-intensity variation	25[a]
Excitation voltage (symmetrical)	10[a]
Excitation voltage (asymmetrical)	10[a]
Temperature (symmetrical)	100
Flight-acceptance environment	100
Type-approval environment	10[b]
Long term, null offset, null slope	2[a]
Resistance at null	100
Sun sensor burn-in	100

[a]All percentages are random sample unless otherwise specified.
[b]One complete spacecraft shipset for each design.

The purpose of the light-intensity variation test is to determine the performance of the Sun sensor under varying light conditions; thus, the amount of sunlight striking the Sun sensor is changed by filters which have 50 and 30% light attenuation. Five short-term stability tests must be performed for each filter setting.

The symmetrical voltage excitation test consists of a + and − 18.8-v excitation for Block III units and a + and − 18 v for Block II units. It also consists of a + and − 14.8-v excitation for Block III units and a + and − 14 v for Block II sensors. Five short-term stability tests are performed at each excitation voltage.

The temperature test consists of testing the Sun sensors at 40°F and then at 140°F (the high temperature used for Block II units) and at 160°F (the high temperature used for Block III units). Five short-term stability tests are made at each temperature for each temperature cycle. The test consists of three temperature cycles for a total of 15 short-term stability tests at each temperature.

All primary and secondary Sun sensors have a 100-hr burn-in under ambient conditions prior to environmental testing. Five short-term stability tests are performed before and after the burn-in test.

A Sun sensor must be capable of operating and performing satisfactorily after subjection to all specified TA tests.

Table 20. TA test summary for Block III primary Sun sensors

TA tests	Null offset, deg	Null offset change (from preceding test), deg	Null offset (RMS), deg	Scale factor, v/deg	Percentage change scale factor (from preceding test), deg	Scale factor (RMS), v/deg
Start	0.00733/0.00171		0.00074/0.00041	18.59/18.70		0.1208/0.1059
After bench handling	0.00596/0.00689	−0.00137/0.00518	0.00071/0.00080	18.84/18.90	1.346/1.070	0.1507/0.1784
After drop	0.00664/0.00689	0.00068/0.00000	0.00076/0.00065	18.52/18.65	−1.697/−1.325	0.0498/0.0928
After transportation vibration	0.00571/0.01124	−0.00093/0.00435	0.00100/0.00105	18.6/18.71	0.432/0.322	0.1303/0.1230
After humidity	0.00532/0.01136	−0.00039/0.00012	0.00161/0.00059	18.45/18.53	−0.807/−0.962	0.0579/0.1889
After shock	0.01833/0.00494	0.01301/−0.00642	0.00064/0.00051	18.58/18.63	0.706/0.54	0.1199/0.0276
After static acceleration	0.01052/0.00580	−0.00781/0.00086	0.00204/0.00067	18.70/18.77	0.646/0.752	0.1080/0.1308
After flight vibration	0.00221/−0.00234	−0.00831/−0.00814	0.00165/0.00049	18.66/18.69	−0.217/−0.427	0.05413/0.2487
After thermal vacuum and thermal shock	−0.00047/−0.00826	−0.00268/−0.00592	0.00143/0.00107	19.5/19.59	4.3/4.82	0.1067/0.1348

NOTE:
(1) The numerator represents the average value for primary Sun sensor S/N R04A; the denominator represents the average value for primary Sun sensor pair S/N R08A.
(2) TA tests are listed in the order of performance.

A *Ranger* Block III Sun sensor shipset, which contains four primary and two secondary Sun sensors, had successfully completed TA testing by November 1963 with only one deviation: The secondary Sun sensors would not stabilize below −91°F because of the inability of the units to radiate heat generated by the Sun sensor cells and the test lights. At that time, the primary Sun sensors reached a minimum temperature of −38°F. TA test results for the primary Sun sensors can be seen in Table 20.

All flight Sun sensors must operate and perform satisfactorily after subjection to the FA test specifications. Table 21 gives FA test results for the Block III Sun sensors.

Five short-term stability tests are performed for each condition with the exception of the temperature performance test, which is temperature cycled three times with five short-term stability test runs made at each temperature cycle. A RMS calculation is made for each series of five short-term stability tests. Tables 22 and 23 contain summaries of short-term stability tests performed on Blocks II and III. The average value and its 1-sigma dispersion value have been summarized for the various test conditions for null offset, RMS null offset, scale factor, percent difference from scale factor, and RMS scale factor. The percent difference change in scale factor for the performance tests and after the FA tests have been compared to the initial short-term stability tests. The percent difference from scale factor after the FA vibration test and after the FA space temperature test for the Block III sensors is with respect to the test's conditions immediately preceding those tests. All the tests except for the long-term tests, which were done at the Chilao test site, were performed at the Palos Verdes test facility. The percent difference from scale factor for the long-term tests is with respect to the last tests performed at the Palos Verdes site.

The same pairs of primary Sun sensors are not involved in post 2.3- and 3.5-yr tests. Those primary Sun sensors had been subjected to many different conditions during that time interval.

The test data in Tables 22 and 23 are well within the attitude control design requirements for the *Ranger* primary Sun sensors. The null offset tolerance for the primary Sun sensor during midcourse and terminal maneuvers is ±0.16 deg, 3 sigma, and the scale factor tolerance is ±10%. The flight Sun sensor excitation voltage tolerance is ±0.25 v.

Table 21. Test data summary for null offset (RMS), Block III primary Sun sensors

Column test conditions	Number of pairs tested	Number of short-term stability tests	Null offset, deg	Null offset (RMS), deg	Scale factor, v/deg	Scale factor change, %	RMS scale factor, v/deg
Initial short-term stability tests	14	125	−0.00114/0.00410	0.00124/0.00084	18.24/0.5201		0.1166/0.0688
40°F temperature short-term stability tests	14	210	0.00036/0.00354	0.00174/0.00192	18.54/0.5092	+1.744/2.263	0.1389/0.1467
160°F temperature short-term stability tests	14	210	−0.00315/0.00244	0.00135/0.00071	17.95/0.5151	−1.706/2.446	0.1341/0.0762
After 100-hr burn-in, short-term stability	13	65	−0.00345/0.00810	0.00085/0.00053	18.60/0.3292	+2.698/2.369	0.1229/0.0673
30% light attenuation short-term stability tests	4	20	−0.00372/0.00259	0.00130/0.00055	18.30/0.4130	+0.658/0.7294	0.0844/0.0274
50% light attenuation short-term stability tests	4	20	−0.00342/0.00391	0.00111/0.00033	18.29/0.3971	+0.7025/0.4952	0.1341/0.0283
±18.8-v excitation voltage short-term stability tests	2	10	−0.0002/0.00438	0.0008/0.00028	20.83/0.1061	+11.35/0.3536	0.0963/0.0215
±14.8-v excitation voltage short-term stability tests	2	10	0.0006/0.00368	0.0012/0.00028	16.39/0.0707	−12.4/0.424	0.1074/0.0139
±15.8-,−17.8-v excitation voltage short-term stability tests	2	10	0.0530/0.00438	0.00205/0.00134	18.50/0.1909	+1.125/0.163	0.1220/0.0924
After FA space temperature	12	60	−0.00007/0.0144	0.00091/0.00058	18.81/0.5227	+0.4875/1.975	0.0813/0.0440
After FA vibration short-term stability	12	60	0.00331/0.0143	0.00113/0.00125	18.76/0.4585	+0.247/0.580	0.0726/0.0332
After FA and perforation tests, short-term stability	12	60	0.0020/0.0185	0.00074/0.00043	18.84/0.5340	+3.632/3.229	0.0744/0.0347
After 1 yr short-term stability tests	8	40	−0.00321/0.01215		18.41/0.5471	+1.963/1.513	

NOTE:
The numerator represents the average value; the denominator represents the 1-sigma deviation from the average value.

Table 22. Test data summary for *Ranger* Block II and III primary Sun sensors

Column test conditions	Number of pairs tested	Number of short-term stability tests	Null offset, deg	RMS null offset, deg	Scale factor change, %	RMS scale factor, v/deg
All data summary except TA tests	38	1955	0.00139/0.01207			
Initial TA short-term stability tests	38	260	0.00014/0.00389	0.00130/0.00088		
40°F temperature short-term stability tests	35	525	0.00236/0.00462	0.00165/0.00133	+1.700/1.682	0.1494/0.1479
160°F temperature short-term stability tests	21	315	0.00216/0.00665	0.00166/0.00106	−4.332/4.519	0.1659/0.1638
±18- and ±18.8-v excitation voltage short-term stability tests	7	35	0.00067/0.00335	0.00114/0.00054	+11.47/0.7804	0.1156/0.0522
±14- and ±14.8-v excitation voltage short-term stability tests	7	35	0.00142/0.00363	0.00179/0.00143	−12.30/0.8930	0.0892/0.0330
−17, +15 and −17.8, +15.8-v excitation voltage	7	35	0.0574/0.00632	0.00165/0.00080	+0.4336/1.9016	0.1202/0.0538
30% light attenuation short-term stability test	10	50	0.00151/0.00278	0.00093/0.00046	+0.678/0.4789	0.0991/0.0536
50% light attenuation short-term stability tests	10	55	0.00005/0.00452	0.00093/0.00030	+0.7044/0.5745	0.1212/0.0404
After FA and perforation tests, short-term stability	35	180	−0.00014/0.0116	0.00086/0.00051	+1.343/2.526	0.1013/0.0575
After 1-yr short-term stability tests	14	70	−0.00170/0.01018		+1.400/1.894	

NOTE:
The numerator represents the average value; the denominator represents the 1-sigma deviation from the average value.

Table 23. Test data summary for Block II primary Sun sensors

Test conditions	Number of pairs tested	Number of short-term stability tests	Null offset, deg	RMS null offset, deg	Scale factor, v/deg	Scale factor change, %	Scale factor (RMS), v/deg
Initial short-term stability tests	24	135	0.00133/0.00333	0.00135/0.00093	16.53/0.7122		0.1260/0.0711
40°F temperature short-term stability tests	21	315	0.00369/0.00485	0.00159/0.00077	16.91/0.7087	+1.67/1.215	0.1564/0.1520
140°F temperature short-term stability tests	14	210	−0.0010/0.00695	0.00145/0.00055	16.08/0.5915	−3.301/0.5479	0.1296/0.0369
160°F temperature short-term stability tests	7	105	−0.00020/0.00345	0.00228/0.00141	15.00/0.4388	−9.584/2.615	0.2295/0.2642
30% light attenuation short-term stability tests	6	30	−0.00004/0.00184	0.00068/0.00012	16.26/0.4244	0.6923/0.3050	0.1088/0.0666
50% light attenuation short-term stability tests	7	35	0.00203/0.00371	0.00082/0.00026	16.47/0.6813	0.7050/0.6538	0.1138/0.0463
±18-v excitation voltage short-term stability tests	5	25	0.00102/0.00339	0.00127/0.00058	17.89/0.8546	+11.52/0.9338	0.1234/0.0610
±14-v excitation voltage short-term stability tests	5	25	0.00174/0.00399	0.00203/0.00168	14.03/0.7175	−12.26/1.070	0.0819/0.0368
−17- and +15-v excitation voltage short-term stability tests	5	25	0.05922/0.00643	0.00149/0.00062	16.08/0.8735	+0.1570/2.254	0.1195/0.0470
After FA perforation short-term stability tests	23	120	−0.00121/0.00626	0.00092/0.00054	16.66/0.7372	+0.1985/0.7884	0.1148/0.0624
After 1-yr short-term stability tests	6	30	0.00033/0.00735	0.00171/0.00091	16.38/0.5393	+0.6493/2.221	0.1153/0.0797
After 2⅓-yr short-term stability tests	4	20	−0.00725/0.0102	0.00098/0.00029	15.94/0.5315	−1.037/1.388	0.0968/0.0358
After 3½-/2-yr short-term stability tests	8	40	0.00054/0.0138	0.00123/0.00029	15.34/1.125	−7.33/4.824	0.0909/0.0602

NOTE:
The numerator represents the coverage value; the denominator represents the 1-sigma deviation from the average value.

The following formulas have been used:

$$\text{Average value} = \overline{X} = \sum_{j=1}^{N} \frac{X_j}{N}$$

$$\text{Root mean square deviation} = RMS = 1 \text{ sigma} = \left[\sum_{j=1}^{N} \frac{(X_j - \overline{X})^2}{N-1}\right]^{1/2}$$

$$\text{Percent difference} = \%\Delta = \frac{X - X\,ref}{X\,ref}(100)$$

$$\text{Null offset} = NO\,|_{\pm 0.1^\circ} \frac{[E_o\,|_{-0.1^\circ} + E_o\,|_{\pm 0.1^\circ}]}{[E_o\,|_{-0.1^\circ} - E_o\,|_{+0.1^\circ}]}(0.1)$$

$$\text{Scale factor} = SF\,|_{\pm 0.1^\circ} = \frac{E_o\,|_{-0.1^\circ} - E_o\,|_{+0.1^\circ}}{0.2}$$

Once the primary Sun sensors have been installed on the spacecraft and the secondary Sun sensors have been installed on the solar panels, the Sun sensors should be given the Sun sensor verification test. Essentially, the test consists of a resistance measurement on each detector cell when the cell is dark and when it is illuminated with the test light hood. The cell should be greater than 1 MΩ when it is dark and about 5 kΩ when it is illuminated with the test light hood.

Figures 46 and 47 are typical examples of pitch and yaw Sun sensor flight calibration curves, respectively. These particular calibration curves were used to support the *Ranger IX* flight. These data were taken at the Chilao test facility with a 680-kΩ load resistor, which simulates the resistance of the *Ranger IX* flight switching amplifier and telemetry load.

b. Life test. There have been a number of tests that could be termed life tests performed on the Clairex CL605. A DC potential of 24.5 v was placed across each of six cells tested so that during full solar illumination each cell dissipated approximately 100 mv of power. The *Ranger* Sun sensors never dissipate over 75 mv per cell. Only the electrical connections to a terminal board were protected from the weather. After 4 yr of continuous light–dark cycling, the cells showed no degradation in mechanical or electrical properties.

A 10.5-mo life test was conducted on the Mariner Mars 1964 TA primary Sun sensors. A Xenon arc lamp solar simulator, providing approximately a one-fifth solar constant with a 0.5-deg diameter was used as a Sun source. Because of the limited size of the simulator light bundle, only the yaw primary sensor was tested. An excitation

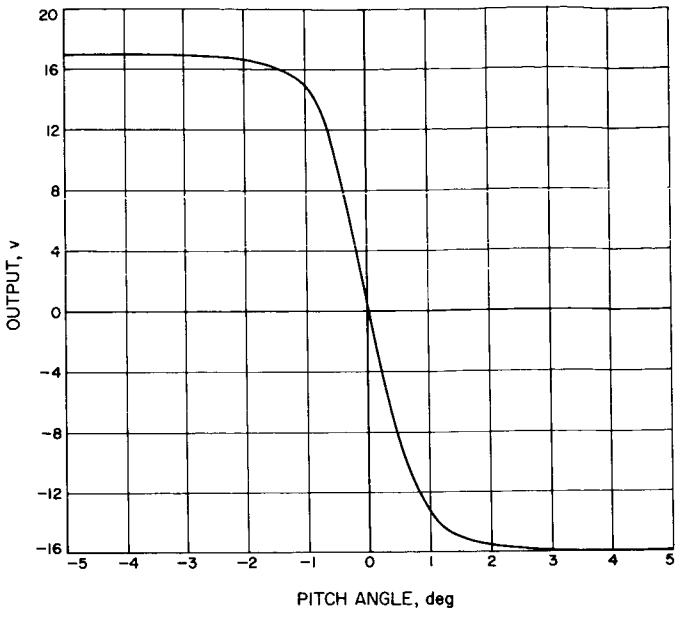

Fig. 46. Sun sensor flight calibration (pitch)

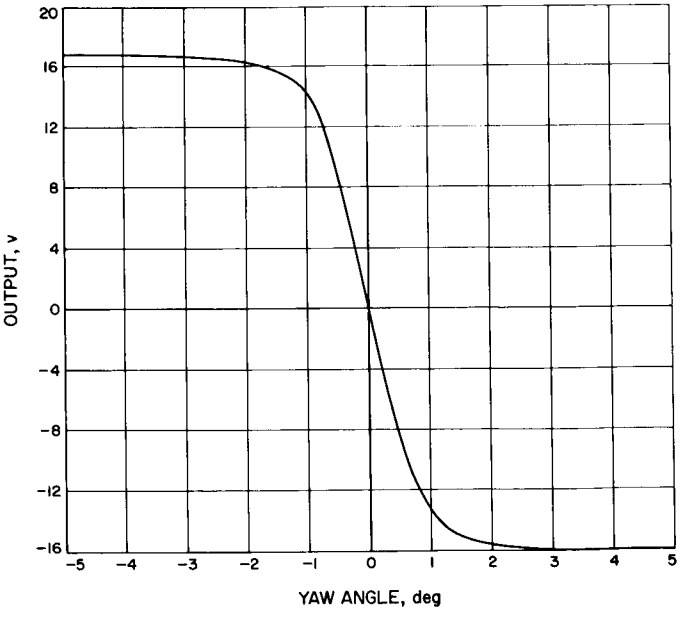

Fig. 47. Sun sensor flight calibration (yaw)

voltage of ±16 v DC and a load of 50 kΩ were used to simulate flight conditions. Total operating time was 7692 hr. Except for simulator power supply problems totaling 144 hr, the sensor was continuously illuminated throughout its total operating time. Throughout the test, sensor null stability was continuously monitored. Bi-weekly readings of sensor null output and scale factor were recorded. All sensor output changes were attributed

to simulator changes. No noticeable degradation of the CL605 cells was observed during or after the test.

The *Mariner* flight to Venus can also be considered a life test. Four primary Sun sensors and nine secondary Sun sensors were on the spacecraft with no cell failures after 130 days of continuous operation of the primary Sun sensors. The secondary Sun sensors were energized during only the search phases of the flight.

Mariner Mars can also be considered a life test for the CL605 cells. This spacecraft contains four primary Sun sensors and 12 secondary Sun sensors. No cell degradation has been observed.

The total time of these life tests on CL605 cells amounts to 256,508 hr of cell operating time without any cell failures, or an equivalent of one cell operating for over 29 yr without experiencing a failure.

5. Hardware Limitations

During midcourse and terminal maneuvers, the primary Sun sensor lower temperature is 40°F; the maximum temperature limit is 140°F. During the noncritical phases of flight, the lower temperature limit can be reduced to 14°F.

6. Operations Summary

Table 24 shows the operating time on the Block III flight Sun sensors at the time of launch.

Table 24. Operating time at time of launch

Mission	Operating time on each primary Sun sensor, hr	Operating time on each secondary Sun sensor, hr
Ranger VI	454	149
Ranger VII	738	152
Ranger VIII	504	149
Ranger IX	454	149

7. Reliability

The most vital problem was the shorting of the two detector cell leads on the Proof Test Model spacecraft; this would have been catastrophic for the spacecraft if it had occurred in flight. Failure reports have been written against the Block III Sun sensors as a result of FA testing.

8. Engineering Change Requirements

A brief description of Engineering Change Requirements made on the Block III Sun sensors is given below.

(1) Deletion of RTV fill in secondary Sun sensor wiring cavity.

(2) Change from allocated to actual weights of assemblies.

(3) Deletion of solithane conformal coating on C coil of primary Sun sensor.

(4) Application of solithane conformal coating between Teflon sleeving and cell as well as terminal.

(5) Extension of effectivity to include *Ranger VII* and Spare 1 secondary Sun sensors.

C. *Sun Shield*

1. Description

The Earth sensor Sun shield is a two positioned mechanical device whose function is to shade most of the Earth sensor housing from sunlight while the spacecraft is acquired on the Sun for cooler Earth sensor temperatures; to shield the Earth sensor's optics from direct sunlight while the spacecraft is oriented toward the Sun in order to permit the Earth sensor to search for and to track the Earth at smaller Earth–probe–Sun angles; and to shade the photocathode surfaces of the PMT's inside the Earth sensor from the Sun during the midcourse maneuver.

The Sun shield is mounted on top of the antenna gear box, and is cocked in position so as not to interfere with the spacecraft shroud. At approximately 1 hr after launch, after the shroud has been ejected from the spacecraft, the Sun shield is actuated when a cam, located on the antenna actuator, moves the lever arm on the Sun shield when the high-gain antenna first rotates out of its nested position; the shield remains in this actuated position for the rest of the flight.

To achieve more efficiency and reliability, the internal actuation mechanism of the Earth sensor Sun shield was redesigned for Block III (Fig. 48). There was also a slight weight change involved with the redesign: the Block I and II Sun shield weighed 1.2 lb compared with a weight of 1.28 lb for the Block III shield.

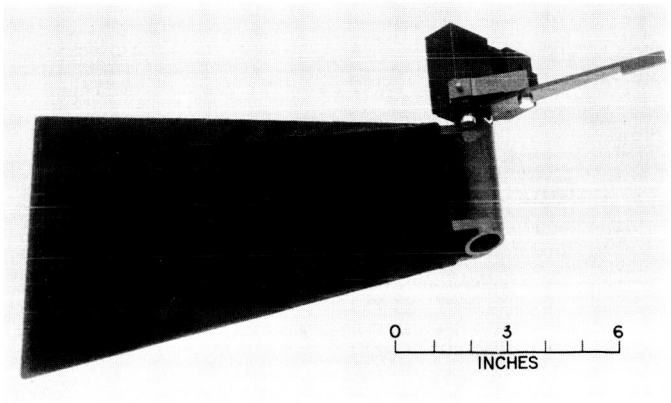

Fig. 48. Earth sensor Sun shield

2. Fabrication

For the most part, the Sun shield is machined from 5086-H112 aluminum alloy material. After the shield and the shaft of the shield weldment have been machined, they are welded together. After the machining and welding operation, the component parts are black anodized and certain areas are electrofilmed. The component parts are then assembled, and a specially tested and qualified low-light-reflecting black cloth is bonded onto the shield in its critical reflection area; it is then functionally and environmentally tested.

3. Testing and Calibrations

It is important that inspections are performed on the Sun shield during fabrication and at certain designated periods thereafter.

4. Qualification for Flight

After the Sun shield has been assembled, it is tested and qualified as a flight unit. These tests consist of functional checks, a run-in test, FA environmental tests, and periodical functional checks after the unit has been assigned to a given spacecraft. A separate Sun shield, the TA unit, must also pass more stringent tests in order to qualify the design of the shield for flight.

a. Type-approval testing. The Sun shield must operate and perform satisfactorily after having been subjected to all of the TA tests and must pass a functional test before and after each of the following TA tests: handling shock, transportation vibration, humidity, shock, static acceleration, low-frequency vibration, complex wave vibration, temperature test, and thermal shock. The Sun shield is required to actuate during the TA thermal vacuum test and during the TA thermal shock tests; it must pass the functional test at the minimum and the maximum temperature of the temperature test using the Sun shield actuation test fixture. This requires putting the Sun shield into its stowed position at atmospheric pressure after each actuation. The Sun shield also has to remain in its stowed position during shock, static acceleration, low-frequency vibration, and complex wave vibration in order to pass these tests.

b. Flight-acceptance testing. All flight Sun shields must pass the FA tests and a functional test before and after the FA vibration and temperature test. It must remain in its stowed position during the vibration test in order to pass the test, and must pass the functional test at the minimum and maximum temperature of the temperature test using the Sun shield actuation test fixture. This requires putting the Sun shield into its stowed position at atmospheric pressure after actuation at the minimum temperature.

c. Functional checks. The functional check on the spacecraft is ensuring that the Sun shield comes to rest in its actuated position against a 1-g field after being released from its stowed position. When the Sun shield is on the spacecraft, a functional check is also made to check the release of the pin latch in the shield. This is accomplished by rotating the actuation cam into its position when the high-gain antenna is nested while the shield is in its actuated position.

d. Run-in test. The run-in test, which is performed before the environmental tests, consists of 30 actuations for flight Sun shields and 100 actuations for the TA unit. A functional check is made before and after the run-in test.

Once a flight Earth sensor Sun shield has been assigned to a certain spacecraft, it is functionally checked many times on the spacecraft; it is also tested and given a visual examination just before the last system test in Pasadena, California, and just before the final system test at Cape Kennedy, Florida.

The test equipment used for Sun shield testing consists of a fixture to hold the shield for the ambient functional tests; the Sun shield actuation test fixture, which consists of a holding fixture, a DC drive motor, and a cam arrangement; and the various environmental mounting fixtures.

The *Ranger* Block III TA Sun shield successfully passed the *Ranger* Block III TA testing, although it experienced

one failure that was later corrected. The Sun shield failed TA vibration after having passed TA bench handling, TA drop test, 100-actuation run-in test, TA transportation vibration, TA humidity, TA shock, and the TA static acceleration test. After the second axis of the TA vibration, the Sun shield failed to actuate because a bushing came out of the Sun shield when actuated. Examination of the hole in the weldment in which the bushing was press-fitted showed that some material on the side walls of the hole had been removed when the bushing was installed initially. The bushing was then staked into the weldment; the Sun shield then successfully passed another 100-actuation run-in test, TA vibration, TA space temperature, and the TA thermal shock test.

A Sun shield of the same design built by JPL had successfully passed TA vibration testing some months before as part of a design verification test. Consequently, it seems as though the Sun shield failure after TA vibration was due to poor workmanship when the bushing was press-fitted into the weldment rather than to poor design. To avoid the possibility of a similar occurrence on another unit, all flight Sun shields have been reworked by staking the bushing.

5. Hardware Limitations

a. Handling and shipping. The Sun shield must not be kept in the stowed position when it is not in test or flight because fatigue could occur in the actuation spring.

b. Requirements. Each flight Earth sensor Sun shield receives approximately 50 actuations before it is assigned to a spacecraft; after assignment, it is actuated approximately 12 times. Each Sun shield in flight has had approximately 62 actuations performed on it, although in actual flight it actuates only once.

6. Reliability

There was a malfunction in the TA testing as a result of poor workmanship in installing the bushing that failed into the Sun shield weldment; there were no Nortronics malfunction reports on flight Sun shields. The only significant malfunction at JPL, other than having to change slightly the design of the cam, was the flight Sun shield that would not always actuate against a 1-*g* field. This was caused by a slight out-of tolerance condition in two machined parts of the Sun shield that caused a slight binding action after many actuations.

In summary, the Block III Earth sensor Sun shield's performance has proved to be extremely reliable and has operated satisfactorily on all *Ranger* flights.

7. Engineering Change Requirements

A brief description of the Engineering Change Requirements performed on the Block III Sun shield is given below.

(1) General redesign of actuation mechanism of Sun shield for Block III.

(2) Redesign of Sun shield cam to correct an interference condition between Earth sensor and Sun shield while on spacecraft.

(3) Change of allocated to actual weights of assembly.

(4) Stake bushing in shaft of Sun shield.

(5) Two changes on Sun shield installation drawing.

D. Jet Vane Actuator

1. Description

The actuator is a gearless DC torquer requiring 60 mamp of current at 12 v DC in order to generate 2 oz-in. of torque; it weighs 0.5 lb.

Four jet vane actuators are mounted in a ring (Fig. 49) around the exit plane of the vernier propulsion motor. Their function is to hold vanes in the exhaust stream of the 50-lb-thrust vernier propulsion motor and to deflect its gases to apply torques to the spacecraft for the autopilot function. The actuators are required to function during only the midcourse maneuver of the *Ranger* spacecraft.

A jet vane actuator itself is a limited angle torquer with an amplitude of ± 25 deg between limit stops. A dual infinite-resolution potentiometer is used for the feedback element as well as the telemetry readout for position angle. The actuator has a flat response in reference to sinusoidal input out to 10 cps.

2. Fabrication

No unusual problems or specialized test equipment were required to fabricate and test or calibrate this actuator.

3. Qualification for Flight

a. Type-approval testing. As a result of TA testing, there was a mechanical damage to the shaft and bearing

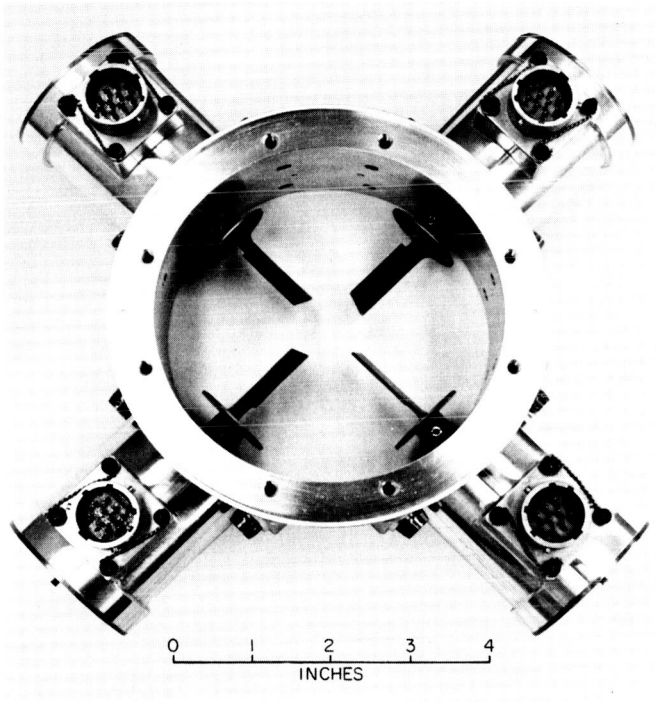

Fig. 49. Jet vane actuator ring assembly

of the actuator. This required a design change limiting the amplitude of the shaft at resonance. After this change was made, the actuator was again put through TA testing; no further problems were encountered.

b. Flight-acceptance testing. The actuators were mounted in clusters of four on their mount ring and put through FA testing; some actuators failed because the leak rates went out of tolerance. The seals were reworked, the FA testing repeated; in these cases, successful passing of the FA procedures was experienced.

c. Life testing. The possible limiting elements in the actuator were the potentiometer and the stop pin. An actuator was put through 40,000 cycles of impact against the stop pin with no resulting damage. Some noise did appear on the potentiometer; however, this was repaired by ensuring that the potentiometer was carefully lubricated at the time of assembly.

E. Antenna Actuator

1. Description

The actuator performs as the drive mechanism for a limiting type servo. Upon command, it runs until it reaches the updated limit at which time the power is cut. The actuator then holds that position until next commanded to move. A torque limiting clutch protects the actuator against damage due to accidental back driving and possible damage in ground handling test procedures. It has the following performance characteristics:

(1) *Power.* The actuator operates on 26-v, 400-cps power with less than 4-w input.

(2) *Clutch.* The clutch is set between breakaway limits of 19 and 24 ft-lb.

(3) *Feedback.* Feedback is an infinite resolution dual potentiometer. One side is used for servo control; the other side is used for telemetry readouts.

(4) *Output shaft speed.* The maximum slewing speed of the actuator should be 3 rev/hr.

a. Performance characteristics. The antenna actuator is used to carry the high-gain antenna on the *Ranger* spacecraft. Its function is to point the antenna toward the Earth as commanded by the control system. The actuator is a simple geared servomechanism completely housed in a sealed aluminum gear box, which is polished to a mirror finish in order to provide thermal control; it performs a spacecraft structural function in that its output shaft directly carries the boom that supports the high-gain antenna. The Earth sensor is also precisely aligned and mounted to the same antenna carrying boom (Fig. 50).

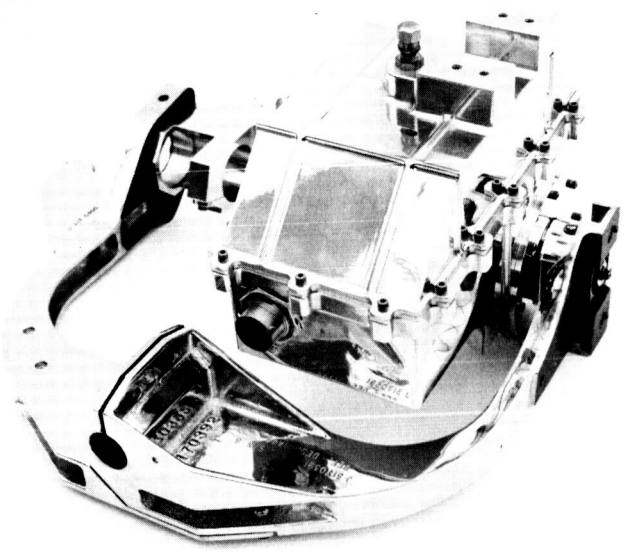

Fig. 50. Hinge actuator

2. Fabrication

The fabrication of the actuator presented no unusual problem, since it was an extremely conventional type of gear train and housing.

3. Testing and Calibrations

There were no particular problems involved in testing and calibrating the actuator. The potentiometer was zeroed in accordance with the zero setting of the boom. The actuator tested for conformance to its specified parameters using standard type test equipment.

4. Qualification for Flight

a. Type-approval testing. The actuator passed the *Ranger* TA test program with no problems, no rework, and no design changes required.

b. FA testing. Each actuator went successfully through flight acceptance with no restarts required for any of the actuators used on Block III.

c. Life testing. One actuator was run continuously under maximum torque load for 64 hr with no measurable degradation of any of its operating components.

F. Gas

1. Description

The function of this subsystem is to generate torques and hold the spacecraft at the proper attitude for various flight requirements. These requirements include reducing the separation tumbling rates to a value below 0.9 mrad/sec about each of three orthogonal axes relative to the spacecraft; turning the spacecraft through the Sun and Earth acquisition and reacquisition searches; stopping rotational motion during the cruise mode of flight at the prescribed limits of orientation as detected by Sun and Earth sensors; orienting the spacecraft for midcourse and terminal maneuvers in response to gyro turn commands; and holding stable orientation during the descent to the lunar surface.

Turning the spacecraft requires, in general, a change in angular velocity, i.e., an angular acceleration. Since torque is the product of an inertia and the angular acceleration experienced by that inertia, good design would provide pure torques as a means of generating the angular velocity change required. This can be accomplished only by two equal and opposite parallel forces separated by some distance. Two equal torques about an

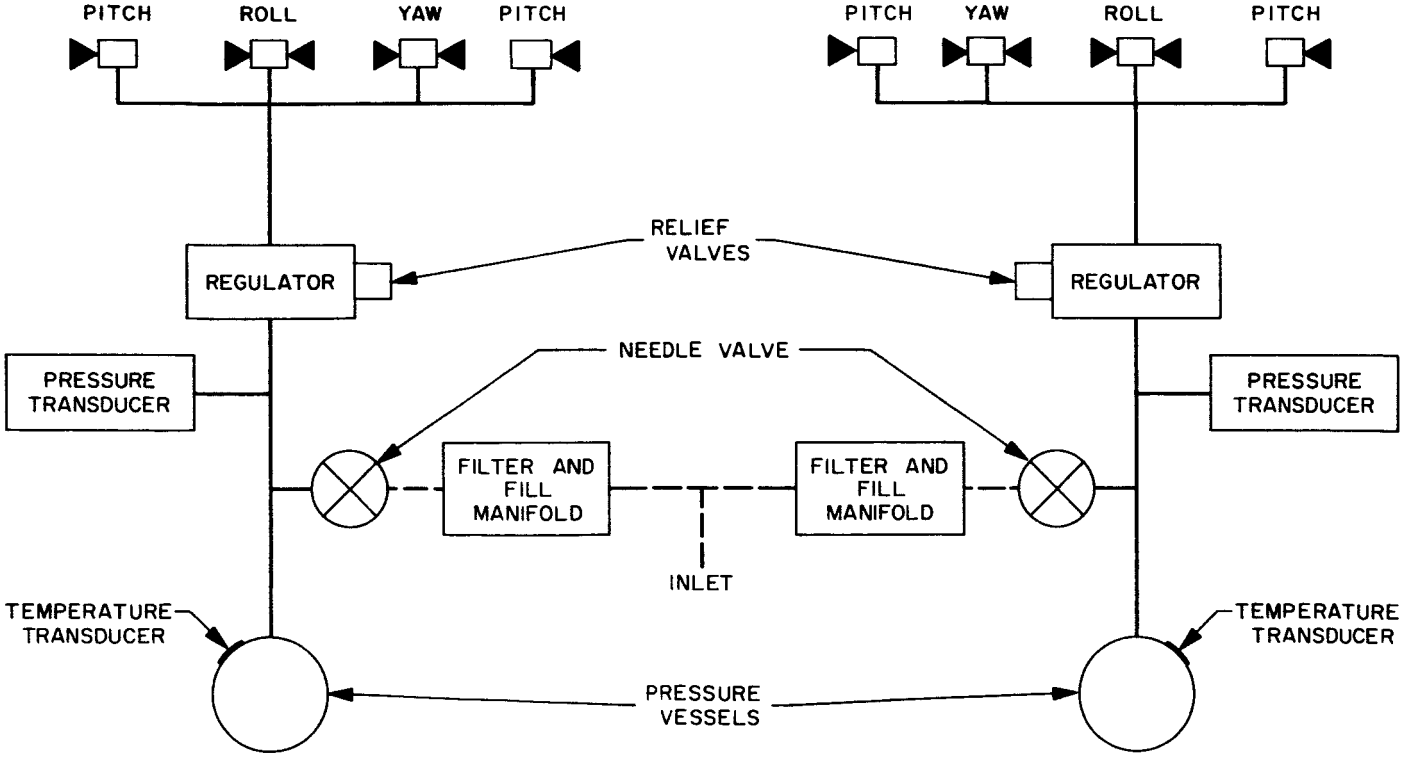

Fig. 51. Semi-redundant gas actuator subsystem

axis can be provided with unequal forces and corresponding moment arms, but the resultant is a couple plus a net force through the center of gravity. This tends to change the trajectory of the spacecraft and is, therefore, undesirable if large enough to be significant. Equal and opposite forces have been provided about the roll axis to give a pure couple. However, the structure of the spacecraft did not permit this arrangement about pitch and yaw axes. Yaw torques are provided by one small thrust at a long arm, about 28 in., and one larger thrust at a short arm, about 11 in. All pitch thrusters are oriented in the same general direction with no approach to a couple.

Thrust is generated by ejecting stored nitrogen gas through nozzles in response to solenoid actuated valves. By using 12 valves, two identical half systems provided complete redundancy in turning the spacecraft in both directions about all axes. The minimum acceleration capability of one half system was established at 0.24 mrad/sec^2 to permit the necessary commanded turns without gyro saturation.

Figure 51 shows the simplicity of the system and how it is divided into two halves; the hardware and plumbing are mounted on the spacecraft bus as shown in Fig. 52. The system's operation consists of storing nitrogen gas at high pressure (3650 psig maximum at 100°F) in a titanium alloy pressure vessel, reducing the pressure through a pneumatic regulator to 15.0 $\pm$1.2 psi above ambient for distribution to the solenoid valves, and actuating the solenoid valves by signals to provide a reaction thrust in the proper direction by expulsion of the low-pressure nitrogen through a nozzle.

The pressure vessel temperature and pressure are obtained by telemetry to monitor total gross performance of the system. Figures 52 and 53 show details of plumbing and the arrangement of the regulator and pressure transducer with a thermal shield removed.

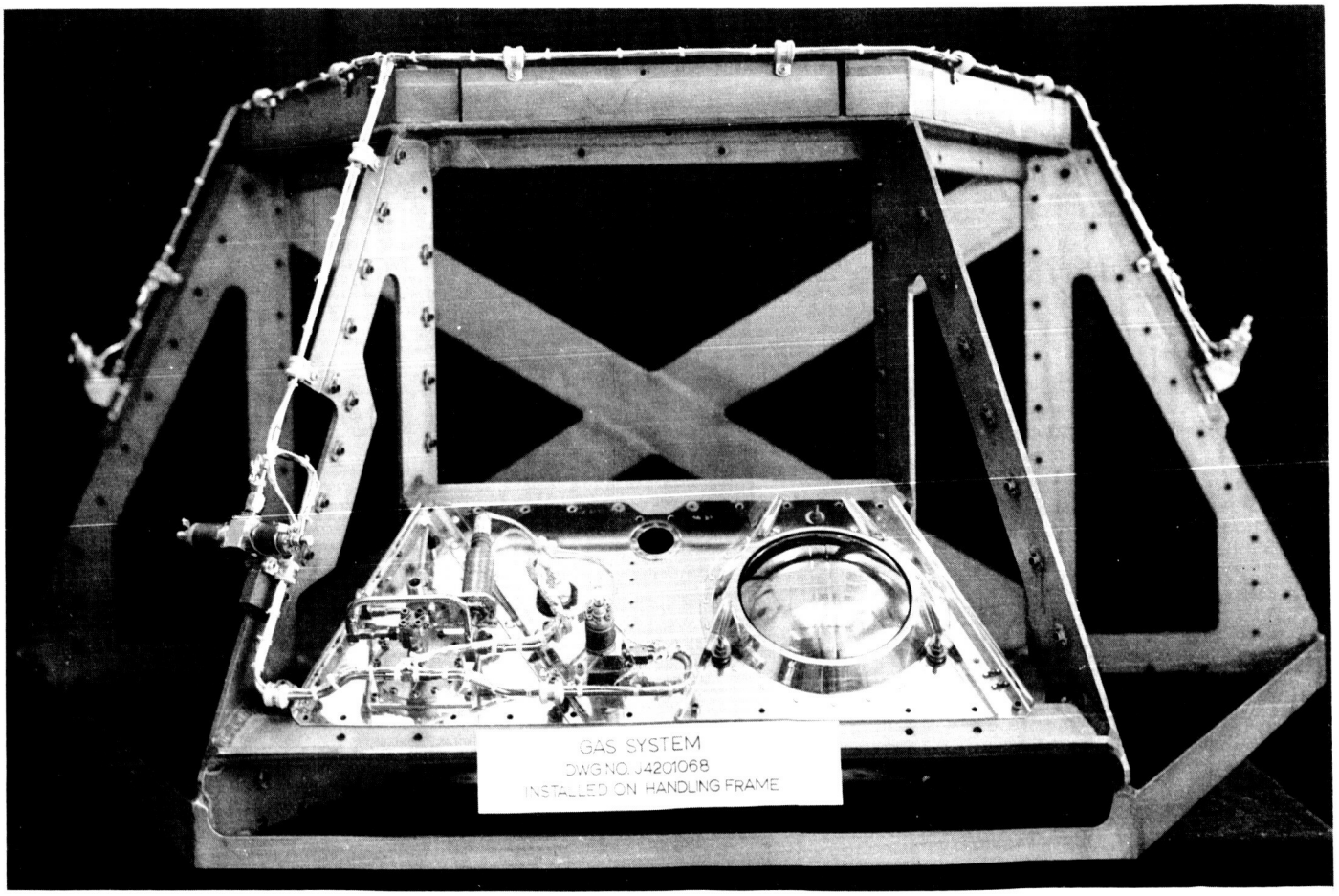

Fig. 52. Gas subsystem installed on handling frame

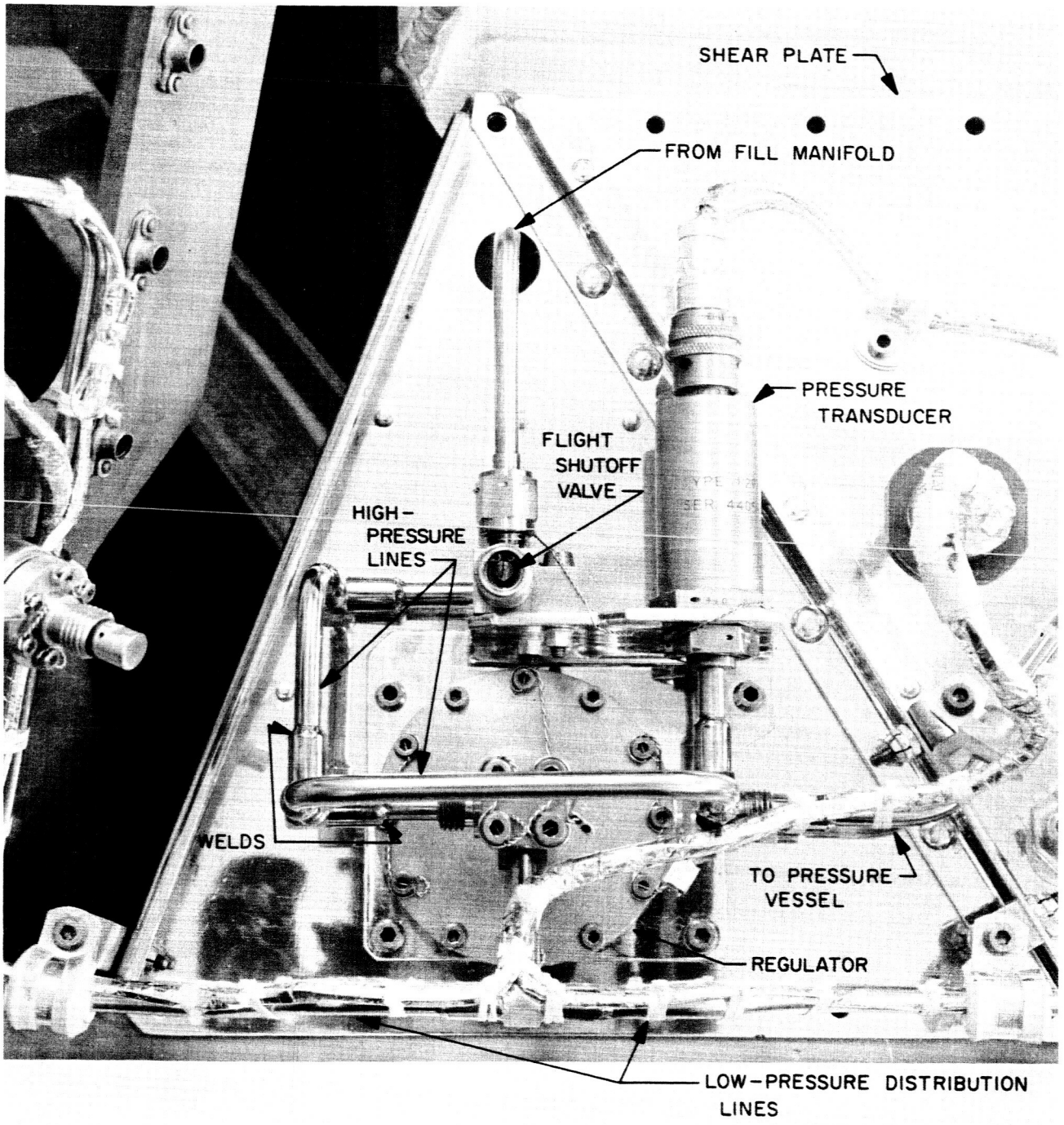

Fig. 53. Gas subsystem installed on handling frame

The only specification requirement of the subsystem was to provide angular velocity changes by accelerating the spacecraft about each axis as commanded for the nominal 66-hr mission. The required accelerations were 0.60 $\pm$0.06 mrad/sec^2 for *Rangers VI* and *VII* and 0.72 $\pm$0.18 mrad/sec^2 for *Rangers VIII* and *IX*. The change in this requirement between *Ranger VII* and *Ranger VIII* was due to an acceleration about the roll axis which was 20% low (established by careful analysis of *Ranger VII* data). No detrimental effect to flight characteristics was involved by the increased upper limit. A possible increase in gas usage was so small as to be negligible and was more than offset by a reduction in usage with the derived-rate mode in cruise. The low value did not compromise the actual performance of the *Ranger VI* and *VII* missions, but could have been serious if the loss of one half system had occurred.

A review of the basic spacecraft dimensions indicated that only a calculated mass moment of inertia I_{zz} about the roll axis was available. Subsequent measurement of the Proof Test Model showed that value to be 20% low, but was not available in time to use in *Ranger VIII* nozzle design calculations. The new sizes were based on an arbitrary thrust increase of 20% about the roll axis, plus a 20% increase in the acceleration requirement for all axes.

In this system with fixed thrust generators, compensation for the changes in spacecraft inertia because of

Table 25. Comparative data

Control axis	Nozzle throat diameter, in.	Thrust, lb	Moment arm, in.	Torque, in.-lb	Moment of inertia (measured or computed), slug-ft^2 and center-of-gravity location,[a] in.	Angular acceleration, rad/sec^2 $\times$ 10^{-3}		Measured angular acceleration, rad/sec^2 $\times$ 10^{-3}		
						Predicted	Specification limits	Midcourse commanded turn	Rate reductions and acquisitions	Terminal commanded turn
Ranger VI										
+Pitch	0.0256	0.0114	29.85	0.340	97.62	+0.582	0.54 to 0.66	+0.59[b]	Sun: +0.46	Not performed
	0.0256	0.0114	29.85	0.340	($\bar{x}$ = +0.13)			−0.57[b]	Sun: +0.55	
−Pitch	0.0263	0.0120	28.08	0.337	($\bar{y}$ = −0.98)	−0.574			Sun: −0.37	
	0.0263	0.0120	28.08	0.337	($\bar{z}$ = +473.36)				Sun: −0.60	
+Roll	0.0225	0.0089	26.39	0.235	67.68[a]	+0.579	0.54 to 0.66	+0.45[c]	No value	Not performed
	0.0225	0.0089	25.97	0.231	($\bar{x}$ = +0.13)					
−Roll	0.0225	0.0089	25.97	0.231	($\bar{y}$ = −0.98)	−0.570		−0.48[c]	Rate: −0.59?	
	0.0225	0.0089	26.39	0.235	($\bar{z}$ = +473.36)					
+Yaw	0.0268	0.0124	32.51	0.403	117.98	+0.570	0.54 to 0.66	Not performed	Rate: 0.40	Not performed
	0.0467	0.0358	11.21	0.402	($\bar{x}$ = +0.13)				Sun: 0.50 to 0.52	
−Yaw	0.0267	0.0124	32.30	0.401	($\bar{y}$ = −0.93)	−0.567				
	0.0458	0.0349	11.47	0.400	($\bar{z}$ = +473.46					
Ranger VII										
+Pitch	0.0256	0.0118	30.00	0.354	94.79[a]	+0.622	0.54 to 0.66	+0.59[b]	Rate: 0.47	Not performed
	0.0256	0.0118	30.00	0.354	($\bar{x}$ = +0.09)				Sun: +0.47	
−Pitch	0.0263	0.0125	28.16	0.352	($\bar{y}$ = −1.02)	−0.618		−0.56[b]	Sun: −0.43	
	0.0263	0.0125	28.16	0.352	($\bar{z}$ = +473.08)					
+Roll	0.0227	0.0094	25.75	0.241	66.73[a]	+0.609	0.54 to 0.66	+0.48[c]	Earth: 0.28?	Not performed
	0.0225	0.0092	26.60	0.246	($\bar{x}$ = +0.09)					
−Roll	0.0227	0.0094	25.75	0.241	($\bar{y}$ = −1.02)	−0.609		−0.48[c]		
	0.0225	0.0092	26.60	0.246	($\bar{z}$ = +473.08)					
+Yaw	0.0269	0.0132	32.52	0.428	117.80[a]	+0.603	0.54 to 0.66	Not performed	Rate: 0.44	Not performed
	0.0467	0.0379	11.16	0.423	($\bar{x}$ = +0.09)				Sun: 0.49	
−Yaw	0.0269	0.0132	32.67	0.430	($\bar{y}$ = −0.97)	−0.601				
	0.0460	0.0371	11.34	0.421	($\bar{z}$ = +473.17)					

? Questionable data

[a] Computed values.

[b] Correct values of angular acceleration leading to change of specified requirement.

[c] Incorrect values of angular acceleration leading to measurement of moment of inertia about roll axis on PTM spacecraft.

position changes and mass expulsion of control systems cannot be provided. For this reason, the nozzle design is based on thrust requirements for the commanded turns. Pitch and roll thrusts are based on spacecraft geometry prior to the midcourse motor burn; yaw thrust is based on the geometry of terminal conditions. Comparative data are tabulated in Table 25.

2. Fabrication

Many unique fabrication features are embodied in the construction of this subsystem. One significant aspect is the step toward eliminating leakage at joints by welding the fittings and tubing together into a permanent unitized assembly, which also reduces contamination. Subsequent disassembly and reassembly operations have also been virtually eliminated by the welded joints, and the unitized construction permits the unit to be pressurized at all times after assembly.

Another feature involved the use of all stainless steel tubing in a very thin walled size for the low-pressure section. It is not possible to bend the 0.25- by 0.016-in.-OD wall tubing by usual methods because of its tendency to collapse and wrinkle. This problem was overcome by filling each piece with pitch, making the bend on a precision tube bender, and then melting out the pitch before cleaning the tubes.

Each interchangeable half system was constructed on an assembly fixture, which duplicated the spacecraft

Table 25. Comparative data (Cont'd)

Control axis	Nozzle throat diameter, in.	Thrust, lb	Moment arm, in.	Torque, in.-lb	Moment of inertia (measured or computed), slug-ft² and center-of-gravity location,[a] in.	Angular acceleration, rad/sec² × 10⁻³		Measured angular acceleration, rad/sec² × 10⁻³		
						Predicted	Specification limits	Midcourse commanded turn	Rate reductions and acquisitions	Terminal commanded turn
Ranger VIII										
+Pitch	0.0293	0.0147	27.74	0.408	97.6	+0.746	0.54 to 0.90	Data	Sun: +0.848	Not
	0.0293	0.0147	27.74	0.408	($\bar{x}$ = +0.09)			not	Sun: −0.705	performed
−Pitch	0.0293	0.0147	29.74	0.436	($\bar{y}$ = −1.111)	−0.696		analyzed	Sun: −0.465	
	0.0293	0.0147	29.74	0.436	($\bar{z}$ = +473.82)				Sun: +0.560	
+Roll	0.0285	0.0140	26.62	0.373	65.5 (81.6)[a]	+0.932	0.54 to 0.90	+0.642	Earth: −0.778	Not
	0.0285	0.0140	25.68	0.360	($\bar{x}$ = +0.09)	(+0.748)		−0.646		performed
−Roll	0.0285	0.0140	25.68	0.360	($\bar{y}$ = −1.111)	−0.932				
	0.0285	0.0140	26.62	0.373	($\bar{z}$ = +473.82)	(−0.748)				
+Yaw	0.0305	0.0158	32.16	0.510	117.98	+0.720	0.54 to 0.90	Not	Sun: −0.506	Not
	0.0573	0.0445	11.42	0.508	($\bar{x}$ = +0.09)			performed	Sun: +0.657	performed
−Yaw	0.0305	0.0158	32.04	0.509	($\bar{y}$ = −1.05)	−0.725				
	0.0573	0.0445	11.58	0.515	($\bar{z}$ = +473.89)					
Ranger IX										
+Pitch	0.0293	0.0152	29.97	0.455	97.6	+0.778	0.54 to 0.90	+0.85	Sun: +0.593	First: +0.75
	0.0293	0.0152	29.97	0.455	($\bar{x}$ = +0.08)			−0.75	Sun: −0.513	−0.70
−Pitch	0.0293	0.0152	27.98	0.425	($\bar{y}$ = −1.096)	−0.726				Second: +0.84
	0.0293	0.0152	27.98	0.425	($\bar{z}$ = +473.35)					−0.70
+Roll	0.0285	0.0144	26.65	0.384	81.6	+0.770	0.54 to 0.90	+0.77	Earth: −0.91	Not
	0.0285	0.0144	25.70	0.370	($\bar{x}$ = +0.08)			−0.925		performed
−Roll	0.0285	0.0144	25.70	0.370	($\bar{y}$ = −1.096)	−0.770				
	0.0285	0.0144	26.65	0.384	($\bar{z}$ = +473.35)					
+Yaw	0.0305	0.0165	32.43	0.535	122.36	+0.719	0.54 to 0.90	Not		+0.58
	0.0573	0.0460	11.30	0.520	($\bar{x}$ = +0.08)			performed		−0.66
−Yaw	0.0305	0.0165	32.31	0.532	($\bar{y}$ = −0.84)	−0.720				
	0.0573	0.0460	11.45	0.526	($\bar{z}$ = +473.52)					

? Questionable data.

[a] Computed values.

[b] Correct values of angular acceleration leading to change of specified requirement.

[c] Incorrect values of angular acceleration leading to measurement of moment of inertia about roll axis on PTM spacecraft.

mounting surfaces and supported the light-weight gangling plumbing (Fig. 52). Assembly to the fixture and welding of the joints were performed in a carefully controlled cleanroom in an effort to limit particulate contamination to metallic particles of 5 μ or smaller and plastic particles of 25 μ and smaller. The fillet welds where the tubing emerges from the fitting socket are shown in Fig. 53. Assemblies were welded together after all parts were ultrasonically cleaned and checked for cleanliness by microscopically examining the residue from a rinse solution collected on a filter paper and the dried part itself. Purging with argon gas was continued until the dew point of the exit gas was less than $-100°$F and until less than 7 parts/million of free oxygen was present. Welding was accomplished in a sequence which always welded first the joint farthest upstream of the flow of purging argon. A very low argon flow rate was necessary during welding to eliminate aspiration of the outside atmosphere at the joints to be welded. This eliminated heat tinting of the tube ID, which was considered to be a potential source of contamination. Immediately upon completion of welding, the system was purged of argon and pressurized to 200 psig with dry nitrogen. Except during repair in a cleanroom equivalent to the fabrication facility, the system was maintained at this pressure at all times.

To minimize system weight, the plate upon which most of the components are mounted was made a shear plate as part of the spacecraft structure.

The electrical cabling was built into the assembly so that complete control of all functions was available at a single connector. (This was advantageous in the subsystem test phases of the program and whenever a problem arose on the spacecraft.) Disconnection from the spacecraft control was accomplished by unplugging a connector at each half system; all functions were then available to a test cable connector.

Prior to assembly of operating components, i.e., solenoid valve and regulators, a significant operating history was required. By the time completion of the FA testing of the subsystem was reached, 10 to 15% of the total life cycles of these units had been used. Experience indicated that this extensive testing eliminated infant mortality failures from flight hardware. It is possible that this experience was a function of the particular valve designs, which consisted of tungsten carbide ball poppets operating against hardened stainless steel seats with no lubrication of the sliding parts other than the nitrogen gas.

3. Testing and Calibrations

This discussion is limited to testing which occurs before the environmental FA testing of the subsystem assembly. All tests in this category are covered by specification requirements. Three types of tests are required as necessary:

(1) Safety tests for those items which store high-pressure gas in quantity.

(2) Performance tests to prove that the unit is a good operating item and meets the requirements set forth for its use.

(3) Cleanliness tests to show freedom from contamination.

a. Safety tests. Probably the most important tests are those that establish the safety of a pressure vessel and the limits of further proof testing. These are well covered by JPL specifications limiting the permissible materials and requiring the minimum burst pressure to be 2.2 times the working pressure of the vessel. The design of other high- and low-pressure components is based on a factor of safety of 4 although they are not necessarily subjected to burst tests. The regulator, pressure transducer, and fill manifold, as well as the pressure vessel, undergo proof tests to 1.5 times the working pressure or more; the welded subsystem is subjected to this same test for a minimum of three cycles immediately after completion. In this system, the proof pressure was 5475 psig.

b. Cleanliness tests. Since the internal cleanliness of the system has a great bearing on its performance, cleanliness checks to the 5- and 25-μ level are made at many points in the fabrication and test cycle. As component pieces of all assemblies are cleaned, a distilled water rinse is filtered; an estimate of the total number and size of particles on the grid-marked filter paper is made by counting a sample number of squares under a microscope. Cleaning is repeated until the count is within the requirement of no metallic particles over 5 μ in size and no plastic particles over 25 μ in size. At assembly time, each piece is examined microscopically for cleanliness. After assembly of operating units such as valves or regulators, nitrogen gas is run through the unit and through a downstream filter. Again, the count of particles collected on this filter must be within the stated limits. The absence of any significant hydrocarbons is verified by examining each piece for characteristic fluorescence under ultraviolet light before assembly. Once the assembly is made, the unit is protected from contamination by careful handling. This required maintenance of a minimum of

200-psig pressure in the vessel. Pressurization required a filter with 0.2-μ pores located in the fill manifold. This filter unit is in place at all times including FA testing and is removed only after final pressurization during launch preparation. All charging gas must pass through this filter and must also have a dew point of $-60°F$ or lower. The dew point at the end of the charging line is checked every time it is to be connected to the inlet port of the fill manifold.

c. Performance tests. Performance tests are repeated frequently as a means of exercising the hardware to keep it operational and to verify that degradation has not taken place. Such tests are specified for the operating subassemblies and are performed at the vendor's plant with JPL quality control coverage prior to shipment and again upon receipt of the hardware by the assembly facility.

Certain of these tests are repeated immediately after a subsystem has been fabricated and at intervals during and after FA testing. Some degradation is expected during these operations and is limited by careful selection of permissible leak rates of the units. Jet valves and regulators may have a leak rate up to 1.0 cm^3/hr when accepted at the assembly facility and may leak up to 3.0 cm^3/hr at completion of FA testing.

Performance tests are run on such subassemblies as jet valves and regulators to be sure that they are received from the vendor in good working order and to verify that consistent results of test instrumentation are obtained by both vendor and assembly testing facilities. These tests include a check of opening and closing times, pull-in and drop-out currents, and leakage of jet valves and pressure regulation at one valve and five valve flow rates through 0.020-in.-diameter orifices; and leakages, cracking, and reseat pressures of the relief valve of the regulator. The required values are:

Jet valve.

Opening time: 15 msec (maximum).

Closing time: 7 msec (maximum).

Pull-in current: 62 mamp.

Internal leakage: 3 cm^3/hr (maximum).

Regulator.

Regulated pressure: 15.0 $\pm$1.2 psig.

Internal leakage: 3 cm^3/hr (maximum).

Relief pressure: 22 psi (maximum).

Reseat pressure: 10 psi (minimum).

External leakage: none.

At this point, the only calibrations were those involving the pressure and temperature transducers. This calibration is repeated prior to spacecraft environmental tests at JPL and serves as the final calibration of these transducers for flight.

4. Qualification for Flight

Three major types of testing were conducted to qualify this actuator for flight. Each complete subsystem was subjected to a FA environmental test series composed of a vibration test simulating the launch phase, and a long time vacuum–temperature test simulating performance requirements in outer space. A TA test of one flight-type system subjected it to a series of environmental tests representative of all the environments that the actual hardware would face from the time of assembly to impact on the Moon and in the approximate sequence in which they would normally occur. These tests include transportation vibration and handling shock, humidity, static acceleration, vibration at a level 1.5 times the FA level, vacuum–temperature, and thermal shock tests for a longer duration and at greater extremes than the FA test requirements. The final test was a life test of the TA system to verify that the life requirements of the specifications were being met and that the mission would not be jeopardized by wearout failures.

a. Type-approval testing. The TA environmental tests were designed to evaluate the ability of the system to withstand the expected life usage and provide some margin of reserve to cover unknown levels of greater extremes.

For the gas actuator, certain tests were eliminated. A bench drop test was out of the question because, since the unit was not self-supporting, it could not help but be fatal. The explosive atmosphere test was not made because no switching contacts are used in the system. Sterilization was not a requirement. The unit and supporting vibration test fixture weighed over 450 lb, which was beyond the capacity of the shock test device. Another deviation of the testing was to perform the handling drop test last in order not to delay all the other tests if the fragility of the system were below this requirement. The 5-ft-radius of the centrifuge meant that, during the static acceleration along the yaw axis, a 1.5-g gradient occurred so that one pitch valve was subject to an acceleration of 0.75 g less than the 3 g specified and the other 0.75 g more.

Serial Number 57 was designated as TA specimen following malfunction in FA test vibration and subsequent replacement of a tube, damaged by a welding burnthrough which had not been reported, and replacement of three jet valves contaminated by particulate residue from the burnthrough.

Transportation vibration and handling shock. The transportation vibration test was conducted at the Norair Environmental Laboratory in Hawthorne, California; The Hawk shaker and the MSE shaker were used as test apparatus. Although the Hawk is a vertically driven shaker and the MSE is horizontally driven, both are driven hydraulically with electronic input.

The shipping container construction and padding were in accordance with JPL specifications. The gas subsystem was secured in the container in a normal shipping configuration and the container securely fastened to the vibration platform.

The vibration spectrum covered was a low-frequency sinusoidal waveform from 1.3 to 5.0 g and 2 to 500 cps. The elapsed time for each axis of vibration was 60 min. The gas subsystem was pressurized to 200 psi, the normal shipping pressure.

There was no performance test requirement during the transportation vibration.

After vibration in each axis, the shipping container was uncovered and the gas subsystem examined. There were no visible signs of damage.

The *before* transport vibration performance test was conducted with all functions performing normally. The *after* transport vibration/*before* humidity performance test revealed that there was no recorder response to pressure in the vessel. After making several checks, it was ascertained that the pressure transducer had an open in the resistance winding. The decision was made to attack a new pressure transducer in parallel to the malfunctioning one and to continue with the humidity phase of the TA environmental test while the chamber was available. After satisfactory completion of the humidity test, the new pressure transducer was permanently attached to the gas subsystem by cutting out the malfunctioning transducers and welding in the newly tested one. This necessitated repeating the transportation vibration test.

The transportation vibration retest of the gas subsystem was conducted as described. The same parameters applied to the retest. The *before* test was performed with all components functioning normally except yaw valve 5, which was leaking in excess of the specification. There was a considerable amount of resonance at 8 cps. After each axis of vibration, a visual examination was made of the shipping container and the gas subsystem. There was no evidence of damage to either.

The *after* test was performed with all components functioning normally except yaw valve 5, which was leaking in excess of the specification.

Humidity. The humidity test was conducted at the Norair Environmental Laboratory in Hawthorne, California. A 12-ft humidity chamber was used for the test.

No performance tests were required during the humidity test; however, it was required that the system be pressurized to nominal launch pressure, 3500 psia at 75°F. This was a deviation from the specification, which required that functional test be performed during the humidity test.

The *before* humidity test was performed with all functions normal. The pressure transducer mounted in parallel to the malfunctioning unit was in operation during this test. The required chamber conditions were stabilization at 70°F, then a humidity raise to 95%. After stabilization, the temperature was raised to 100°F and 95% humidity. This environment was maintained for 30 min.

The *after* humidity test was performed with all components functioning normally except yaw valve 5, which was leaking in excess of 3.00 cm^3/hr, the maximum allowable after FA testing, but not in excess of the 5.00 cm^3/hr allowable after TA testing. The gas subsystem was returned to the cleanroom for the replacement of the malfunctioned pressure transducer.

Static acceleration test. The static acceleration test was conducted in Hawthorne. The 5-ft centrifuge was used to perform this test.

The test requirements were 3-*g* acceleration in two orthogonal directions and 14-*g* acceleration in the direction of the launch. The time of test was 5 min in each axis.

There was no performance requirement during the static acceleration test; the gas subsystem was pres-

surized to full system pressure of 3650 psi. Examination of the test specimen between each axis revealed no evidence of damage or malfunction as a result of the static acceleration test.

During the *after* test, it was observed that the pressure regulation (flow characteristics) test at 3500 psig exceeded specified tolerances when five valves were actuated. The value recorded was 13.75 psi. The allowable per the specification is 15 psig $\pm$1.2 psi. Continued TA testing revealed a steady degradation of pressure regulation. A valve bubble check revealed that yaw valve 5 and pitch valve 6 exceeded the maximum allowable leakage of 3.00 cm^3/hr.

Vibration (1.5 times that of FA level). The vibration test was conducted in two areas: The low-frequency vibration was conducted on the MSE shaker; the high-frequency vibration was conducted on the Ling shaker. The vibration spectrum covered was a sinusoidal waveform at 1 to 15 cps at a maximum level of 3 *g*.

The gas subsystem was secured to the vibration fixture and subjected to three axes of vibration. It was not necessary to monitor any functions during the test; however, the testing was done with the system fully pressurized to 3650 psig. Each axis was vibrated for approximately 3 min. After each axis of vibration, the gas subsystem was examined for any damage. There was no visible evidence of damage as a result of vibration at the low frequency.

The high-frequency vibration spectrum was taken from the standard JPL tape for TA testing of systems weighing over 10 lb. The spectrum covered random noise from 2 to 14 *g*; the duration of the test for each axis was 636 sec (Fig. 54). Vibration in the roll axis was completed with

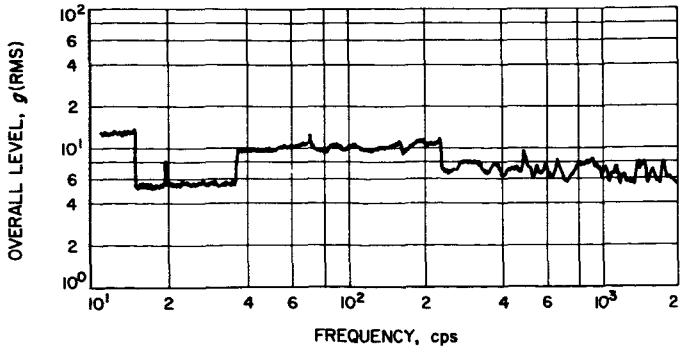

Fig. 54. Typical test level: y-axis (TA level)

no apparent damage to the system. Examination after the vibration in the pitch axis revealed a broken lead at pitch valve 6. The wire lead was repaired and the pitch axis vibration repeated. During the second vibration, one screw holding the pitch valve 6 manifold loosened; the second screw failed because of high-tensile loads on the screw. Pitch valve 1 manifold screws loosened and one of the leads to the valve revealed several broken strands. The broken screw was replaced and the loosened ones tightened. The wire lead to pitch valve 1, with the broken strands, was left as it was until it actually failed. Later, this specimen was modified to the new wire routing; however, to permit continued testing, a mockup of the pitch valve assembly, manifold, and tubing was made up and successfully tested to a level above the TA test level.

Vibration in the *y*-axis (yaw) revealed no further damage. High pressure, temperature, and regulated (low) pressure were monitored on strip chart recorders.

The *before* vibration performance data is the same as *after* static acceleration. The response time close was not available because of instrumentation difficulties.

The *after* vibration indicated that the response time close was functioning normally for all valves, confirming suspected instrumentation problems during the previous test. This test also revealed degradation of the pressure regulation at 3500 psig with valves 1 and 5 actuated. A bubble check revealed valve leakage in excess of the specification.

Vacuum–temperature and thermal shock. Requirements for these tests were as follows: specimen stabilization, $-10°C$; chamber pressure, 10^{-4} mm Hg (maintained for 4 hr); temperature stabilization, 75°C, chamber pressure, 10^{-4} mm Hg. The duration of the latter part of the temperature test was 116 hr.

The thermal shock was conducted as part of the temperature test. The requirement was that when the test specimen was stabilized at 75°C with the chamber walls at LN_2 temperature, all heat sources were turned off. This allowed all heat to radiate to the chamber walls. This was maintained for 2 hr. At the close of the 2-hr period, the heat lamps were turned to the same setting as before the thermal shock and held until the test specimen temperature had stabilized at 75°C again. Chamber vacuum of 10^{-4} mm Hg or better was maintained throughout the test.

It was required that functional responses be recorded during the entire period of the temperature test. Step A, initial functional testing, was done before the vacuum–temperature test was started; Step B, final functional testing, was done at the conclusion.

Steps 1 through 7, intermediate functional tests, were performed during the low- and high-temperature soak and during the transitional period from ambient to cold, then to hot. Flight pressure was maintained at 1500 psi negative to 75°F during Steps A, 1 through 7, and B.

Each valve (except P1) was cycled for a maximum of 1 sec once each hour during the test, except during the time required to perform Steps 1 through 7. P1 is excluded because the regulated pressure is monitored from P1.

It was necessary to interrupt the test after 41 hr at stable high temperature (75°C). The reason for the interruption was that the Tygon tube attached to P1 had become excessively hot and slipped off the nozzle. The repair was made and the test resumed. At the end of the 116 hr at 75°C, temperature and pressure were brought to ambient and Step B performed. The chamber pressure was again lowered to 10^{-4} mm Hg and Steps 1 through 4 repeated. This deviation was necessary because Step 3 was not done during the normal sequence of the test. When the temperature was stabilized at 75°C, after Step 4, the thermal shock test was conducted. The test of pressure regulation revealed an "out-of-specification" condition at 3500 psig with valves 1a and 5 actuated. This follows the degradation curve of the flow characteristic referred to previously. The *after* test revealed excessive valve leakage on R2 and Y5.

Handling shock. An overhead crane, a pneumatic breakaway jaw, and a suitable rope sling are used in accomplishing this test.

The test requirement was that the shipping container, with the gas subsystem secured inside, be dropped six times from a specified height. The container was subjected to six drops; the gas subsystem was removed from the shipping container and a performance test conducted.

The *after* handling shock test revealed "out-of-specification" conditions in the following tests:

(1) *Pressure regulation* (when the system is pressurized to 3500 psig at 75°F and valves 1 and 5 are actuated); regulated pressure drops below the allowable minimum of 13.80 psi.

(2) *Response time close* on R2: exceeds the maximum of 5.0 msec.

(3) *Leakage* on R2, R3, and Y5: in excess of 3.00 cm^3/hr.

It is concluded that the gas subsystem successfully demonstrated an ability to withstand the environments to which it was subjected.

A post-TA vibration test was requested. The post-test conditions established were:

(1) 200 psig in the pressure vessel.

(2) The fill manifold replaced by a fill manifold plug.

(3) All flight hardware on valves and equipment plate.

(4) Monitor pressure transducer and pressure transducer mounting bracket with a low-mass, three-axis accelerometer.

(5) Monitor P6 valve with a low-mass, three-axis accelerometer.

When these conditions were met, the specimen was subjected to a low-level sine sweep. It was evident that this low-level input was greatly amplified at the pressure transducer. It was decided to design and install a support bracket on the pressure transducer before further testing on the TA level.

The newly designed and fabricated bracket was attached to the pressure transducer and secured to the equipment plate. After vibration, with the bracket and without it, it was found that the bracket made no appreciable difference in damping the excessive amplification at the transducer. After analyzing this data, it was decided to continue with the post-TA test as previously planned. The gas subsystem was subjected to vibration in the roll (z) axis. All functions appeared normal. Examination of the specimen after vibration showed that the pressure vessel had twisted in its mount. The second axis subjected to vibration was the pitch (x) axis. The pressure vessel was observed to rotate as in the previous axis. Total excursion of the vessel was approximately 15 deg. At the end of the vibration, the vessel remained radially displaced by several degrees. A wire lead on pitch valve 6 broke during the test. The screws securing pitch valve 6 to the holding fixture had loosened, causing severe vibration of the valve.

The third axis vibrated was the yaw (y) axis. The pressure vessel was observed to rotate again, but not as much

Table 26. TA

Test	Date (1963)	Internal leakage of regulator, cm³/hr	Pressure regulation (flow characteristics), psig								Response time opening, msec						Respo	
			Inlet pressure at 3500		Inlet pressure at 2500		Inlet pressure at 1500		Inlet pressure at 500									
			1v	5v	1v	5v	1v	5v	1v	5v	P1	R2	R3	Y4	Y5	P6	P1	R2
Pre-TA	9/18	1.35	14.50	14.30	15.90	15.70	15.40	15.10	15.80	15.50	12.4	10.4	12.0	13.0	12.0	10.4	2.5	4.0
Humidity																		
Before	9/27	2.90	—	—	15.30	15.10	15.70	15.20	15.90	15.70	9.8	9.3	11.0	11.5	10.1	9.5	3.2	4.8
After	9/28	0.79	14.37	14.12	14.82	14.57	15.20	15.00	15.65	15.35	9.6	9.0	10.9	11.0	10.2	9.5	3.5	4.8
Transportation vibration																		
Before	10/9	1.34	14.10	13.87	14.50	14.30	14.95	14.75	15.82	15.20	11.0	10.5	11.5	12.5	12.0	10.0	3.0	4.5
After	10/10	1.79	14.03	13.83	14.52	14.28	14.90	14.70	15.50	15.10	10.4	10.6	10.5	12.4	12.2	10.4	3.3	4.7
Static acceleration																		
Before	10/10	1.79	14.03	13.83	14.52	14.28	14.90	14.70	15.50	15.10	10.4	10.6	10.5	12.4	12.2	10.4	3.3	4.7
After	10/11	0.67	13.93	13.75	14.38	14.18	15.00	14.60	15.90	15.03	10.2	9.8	11.0	11.8	11.0	9.6	—	—
Vibration (Procedure I)																		
Before	10/11	0.67	13.93	13.75	14.38	14.18	15.00	14.60	15.90	15.03	10.2	9.8	11.0	11.86	11.0	9.66	—	—
After	10/15	0.73	13.75	13.58	14.22	14.05	14.64	14.38	15.20	14.98	10.4	9.6	11.0	12.4	11.8	8.7	3.2	4.5
Temperature test and thermal shock																		
Before	10/15	0.73	13.75	13.58	14.22	14.05	14.64	14.38	15.20	14.98	10.4	9.6	11.0	12.4	11.8	8.7	3.2	4.5
After	10/25	0.72	13.58	13.43	14.08	13.93	14.68	14.48	15.08	14.48	10.0	8.8	10.0	11.2	10.1	9.2	3.6	3.5
Handling shock (drop test)																		
Before	10/28	3.23	13.78	13.58	13.48	13.28	14.08	14.83	15.13	14.73	10.4	8.9	10.0	10.0	9.9	9.4	4.0	5.3
After	10/30	1.28	13.61	13.42	14.02	13.81	14.44	14.26	15.51	14.71	10.35	8.4	10.05	10.4	9.8	9.4	4.0	5.3
Post-TA	11/29	3.00	14.15	13.97	14.63	14.42	15.05	14.85	15.55	15.24	11.0	9.5	10.5	12.2	11.0	9.8	3.0	4.1

performance test data

Jet valves																						Quantitative leak check of entire assembly, cm³/hr
...se time closing, msec				Pull in current, mamp						Drop-out current, mamp						Leakage, cm³/hr						
R3	Y4	Y5	P6	P1	R2	R3	Y4	Y5	P6	P1	R2	R3	Y4	Y5	P6	P1	R2	R3	Y4	Y5	P6	
2.6	1.8	3.4	2.4	46	41	47	48	47	40	9.0	6.0	9.0	12.0	6.0	10.0	1.25	1.35	2.44	0.50	2.88	2.88	
3.3	2.5	3.3	2.8	45	44	51	54	50	45	5.8	4.0	7.8	9.5	5.4	8.4	1.62	1.00	1.25	0.50	3.00	2.62	
3.2	2.5	4.5	3.4	46	44	50	52	50	45	6.0	3.8	7.5	9.8	5.0	7.3	1.75	1.62	1.87	0.38	3.87	2.50	
2.8	2.2	4.0	2.8	47.5	42	49	51	49	43	9.0	5.5	9.0	11.5	6.0	10.0	1.50	1.00	1.75	0.50	5.00	2.25	
3.2	3.0	4.1	2.7	48	46	57	54	53	46	7.2	5.0	7.0	7.6	5.0	8.6	1.38	1.12	1.75	0.50	4.25	2.50	
3.2	3.0	4.1	2.7	48	46	57	54	53	46	7.2	5.0	7.0	7.6	5.0	8.6	1.38	1.12	1.75	0.50	4.25	2.50	
—	—	—	—	49	45	52	54	50	46	6.2	4.8	7.4	8.0	5.4	8.4	1.12	1.00	1.75	0.50	3.87	3.12	
—	—	—	—	49	45	52	54	50	46	6.2	4.8	7.4	8.0	5.4	8.4	1.12	1.00	1.75	0.50	3.87	3.12	
2.8	2.1	4.1	2.7	48	41	49.5	50.5	48.5	43.5	8.0	5.5	9.0	7.5	6.5	11.0	1.50	6.25	4.75	0.25	4.75	3.50	
2.8	2.1	4.1	2.7	48	41	49.5	50.5	48.5	43.5	8.0	5.5	9.0	7.5	6.5	11.0	1.50	6.25	4.75	0.25	4.75	3.50	
3.0	2.9	3.8	3.0	45	41	50	51	49	44	7.3	4.8	8.0	9.8	5.1	8.7	2.13	8.50	2.25	0.25	3.12	1.25	
3.8	3.0	5.0	3.8	49	42	49	51	49	44	7.0	4.9	8.3	9.7	5.1	9.0	0.04	6.30	1.62	0.09	4.62	0.50	
3.7	3.0	4.9	3.8	48	40	48	50	48	43	6.8	4.5	7.4	9.4	5.0	8.3	2.38	7.50	3.75	0.88	3.75	1.50	
2.6	2.0	3.8	2.7	48	40	46	51	48	43	9.0	6.0	10.0	12.0	7.0	10.0	2.08	4.88	2.24	1.20	10.08	6.24	20.2

as in the previous test. The wire lead on pitch valve 1 had broken; this was the wire that had been noted previously as having several strands broken.

A tabulation of the results showed only relatively minor deviations from the specification limits at the conclusion of the tests. One valve was 0.3 msec over on response time close. This was not serious as the specification was relaxed 2.0 msec to accommodate a variation in manufacturing of some later valves. That same valve was over specification by 2.5 cm^3/hr on leakage; however, after some post-TA vibration tests, it was found to be back within specification limits. Also, the regulator was found to be 0.4 psi below the specification under maximum pressure and load. This five-valve load would never occur in flight. It was expected that the pressure would soon be reduced by usage which would bring operation back into required limits. The unit had been degraded by the tests such that it regulated at approximately 0.9 psi below the original valve at the same high-pressure conditions. Table 26 summarizes the test results.

b. Flight-acceptance testing. The purpose of the FA test is to ensure that a subsystem will operate as designed in a space-type atmosphere after sustaining severe vibration environment. It is not proposed to duplicate the environments of a mission, but to cover a broad range of vibration frequencies and vacuum–temperature combinations that will pinpoint any superficial weaknesses in the specific piece of hardware under test. The particular design is presumed to have already passed a TA test.

Transportation vibration and handling shock. Initially, the vibration fixture alone was equalized flat from 15 to 2000 cps using a 1.5-*g* sine sweep and broad-band random noise at an overall level of 3 or 4 *g* RMS. Instrumentation was connected to monitor the pressure and temperature of the pressure vessel and the regulated pressure and temperature of the gas in the low-pressure system on continuous recordings. A schematic of the specimen and the test setup instrumentation is shown in Fig. 55. Figure 56 shows the test fixture and a specimen in place on a slip plate oriented for vibration along the launch axis. Before vibration, the system is charged with dry nitrogen to the equivalent of 3650 and 100°F. The test input to the equalization system consists of one sweep up the frequency scale and down the scale for each of three mutually perpendicular axes at combinations of sine and random noise vibration at specified frequencies and *g* levels. This is recorded on a standard magnetic tape for playback to the driver for the test.

The fixture was so designed that it could be laid on its back for the launch axis vibration and turned to two positions at right angles to each other in the upright position for vibration along the other two orthogonal axes.

Vacuum–temperature. To ensure that proper operation will take place in a space environment, simulated conditions are provided in a vacuum chamber while operation of the system and checks of that operation take place. The unit is insulated from the weld handling fixture by Teflon shims, and the whole assembly is suspended from the chamber walls on three thin cables. With the pressure maintained at 10^{-4} torr or lower, deep space temperatures are simulated by operating the walls at liquid nitrogen temperature. Radiation heating is simulated by heat lamps. To give uniform heat distribution from the lamps over the localized chunks of the gas actuator, separate shrouds are fitted to the pitch and roll valve assemblies and to the equipment plate. During the test, with the exception of performance checks, five of the valves are operated in sequence; each one is operated once approximately every 20 min. The sixth valve is held open continuously so the regulated pressure in the system can be monitored, both by a gage in the chamber and a transducer to produce a permanent strip chart of the seven performance tests.

For more complete determination of the flightworthiness of a system, a quantitative leak measurement was run before and at some time after the vibration test. A change of 25% helium and 75% nitrogen was used, and the leakage measured on a helium mass spectrometer leak detector.

The program environmental test specification specifies only the particular environment that a unit must survive; it does not evaluate the operation or survival of the unit in that environment. This was done by running an extensive performance test of the gas subsystem immediately before and after each environment and by causing it to operate in a normal manner in those environments where it would normally be expected to operate. Any change in operating parameters from the specification was individually evaluated for acceptability, and only very small changes in parameters over that at acceptance valves and regulators were permitted.

The tests run were:

(1) Regulator internal leakage and pressure regulation for one-valve and five-valve loads at four inlet pressures.

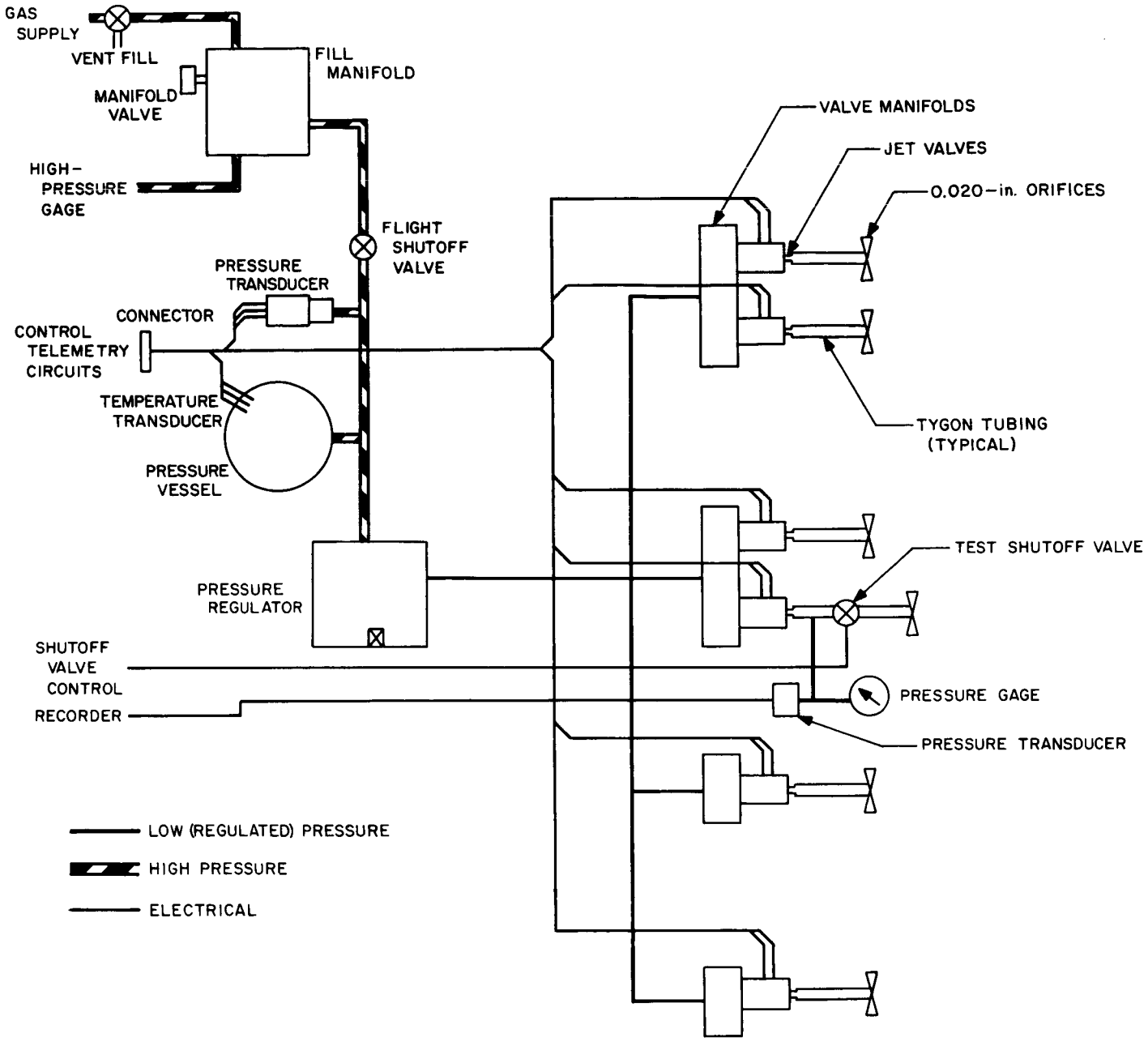

Fig. 55. Gas actuator assembly test setup

(2) Jet valve response time, open, close, and consistency, pull-in and drop-out currents, and leakage.

(3) A quantitative leak test.

Figure 57 shows the typical levels. Jet valve leakage was checked by bubbling the leak through isopropyl alcohol into a filled inverted graduated test tube.

The greatest problem was that of contamination in the systems. Two major sources were identified and eliminated: The first was too liberal use of "Snoop," a soap bubble type leak-detecting solution, at valve test nozzles, regulator vent openings, and other points where entry into the system was not over too long a path for a good wetting agent. A final conclusive test was run after conclusion of the flight program by purposely putting this solution in a valve and checking the results against the same treatment with water and against previous failures. The second major source was a wire mesh filter placed at the inlet to each of the four valve manifolds. When

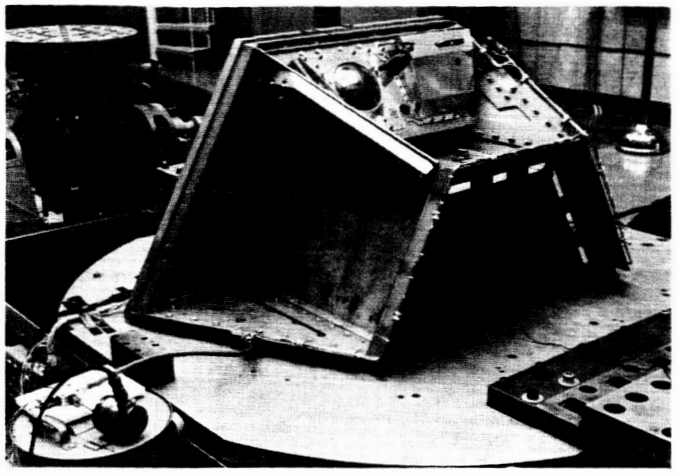

Fig. 56. Test fixture and specimen on slip plate

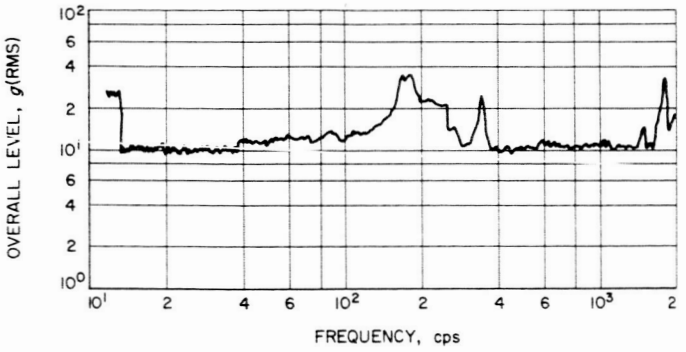

Fig. 57. Typical test level: x-axis (FA level)

several valves were lost due to excessive leakage after the vibration environment in each of several systems, an investigation disclosed that these filters were being rinsed only instead of ultrasonically cleaned. Even though *Ranger VII* was ready to ship, the gas actuators were removed and these filters cleaned in time for assembly in the normal schedule. It took many hours of ultrasonic agitation of these units in distilled water to bring the particulate residue down to an acceptable level. The vibration environment seemed most effective in showing up systems which contained contamination; the leak test of valves and regulator was the most effective method of detecting the location of that contamination.

Another source of trouble was the pressure transducer. Several instances of burned spots on the windings were discovered; however, no obvious errors were discovered in test circuits. Small improvements and protective resistors were added, but subsequent failures occurred. Only one leak was found in *Ranger* parts; it was masked by the test fittings, which were improved to eliminate that possibility. An identical unit, assigned to the *Mariner* Project, was found to have an internal leak which pressurized the case and created a hazard. All *Ranger* cases were vented, which changed the pressure readings from absolute to gage readings on Earth, but meant no change in outer space.

Many failures (as just described) occurred during or after the vibration testing. In this event, the failed item was removed from the system, a new item installed, and the vibration testing repeated. Later in the project, a number of valves were FA tested separately so that rapid backup of the flight operations could be maintained whenever the spare subsystem was required.

In some areas, excessively rigid requirements were maintained. This permitted evaluation of those components, namely jet valves and regulators, for missions where more rigid requirements would be in order. As an example of this, a jet valve was permitted a leakage of 3 cm^3/hr at launch time. Actually, if all other contingencies for gas usage were ignored, a leakage of approximately 90 cm^3/hr per valve was possible. This permitted use of items, which jumped out of specification during the test sequence when engineering judgment indicated that the jump in leakage was not one of continuous increase, but had stabilized at a new level. No excess use of gas was ever encountered in the last four *Ranger* missions.

c. Life testing. A life test was conducted on the TA unit after all the environmental testing was complete in order to be sure that the functional components would meet their respective life requirements and to determine, where feasible, what additional margin was available. In addition to testing the single half system, two additional jet valves were tested throughout 310 cycles of operation. No planned environmental variations were included as part of the tests.

The TA unit was set up in a rope net isolating barricade so that it could be charged periodically to full flight. A set of motor-driven cams was used to cycle the jet valves. Each valve was cycled once per second in sequence and the open time set approximately 70 msec in order to cause the regulator to operate for each valve actuation. The gas jetted through each valve, passed through a millipore filter, and then on to a pressure switch, which in turn operated individual counters to keep track of the operations. The filters were changed every 25,000 cycles and the particulate contamination

counted. At this same interval, a complete performance check of the system was made so any gradual change could be noted. Each pressurization of the unit would provide gas for approximately 9800 cycles of each valve. This also provided about 30 cycles of pressurization, causing a full swing of the pressure transducer wiper. Figure 58 shows the system with filters and pressure switches connected.

The regulator was operated in this manner with approximately 1,500,000 opening and closing cycles and completed the test with leak rates well within the specification limit of 500,000 cycles.

One of the jet valves exceeded the specification leak rate of 5 cm^3/hr somewhere between 150,000 and 175,000 cycles and was removed from the test. The other five valves continued operation to 300,000 cycles and were still operating in an acceptable fashion. A detailed analysis of the failed valve was not made; however, from the fact that the quantity of fine particulate contamination was very high throughout the test and that the opening time doubled, it was concluded that wear and galling of the plunger and poppet took place until failure occurred. This failure mode has been observed on other valves where a particle wedges between the plunger and its bore and starts wear of the plated surfaces. These wear particles then flow downstream and lodge between the tungsten carbide ball poppet and its closely fitting hardened stainless steel guides and cause galling of the guides, buildup on the ball, and sometimes sticking to the poppet, usually in the closed position. With leak rate beyond measure in this valve and the opening time doubled, it was suspected that the poppet was stuck partly open and the plunger restricted from free operation by the excessive contamination measured at the outlet.

A worst-case analysis of gas usage was reported in Ref. 1, p. 145. From a nominal total storage of 4.18 lb at launch time, only 0.23-lb reserve was estimated to remain at the mission end in this case. In actuality, no failures were found in analysis of the flight data, and the system

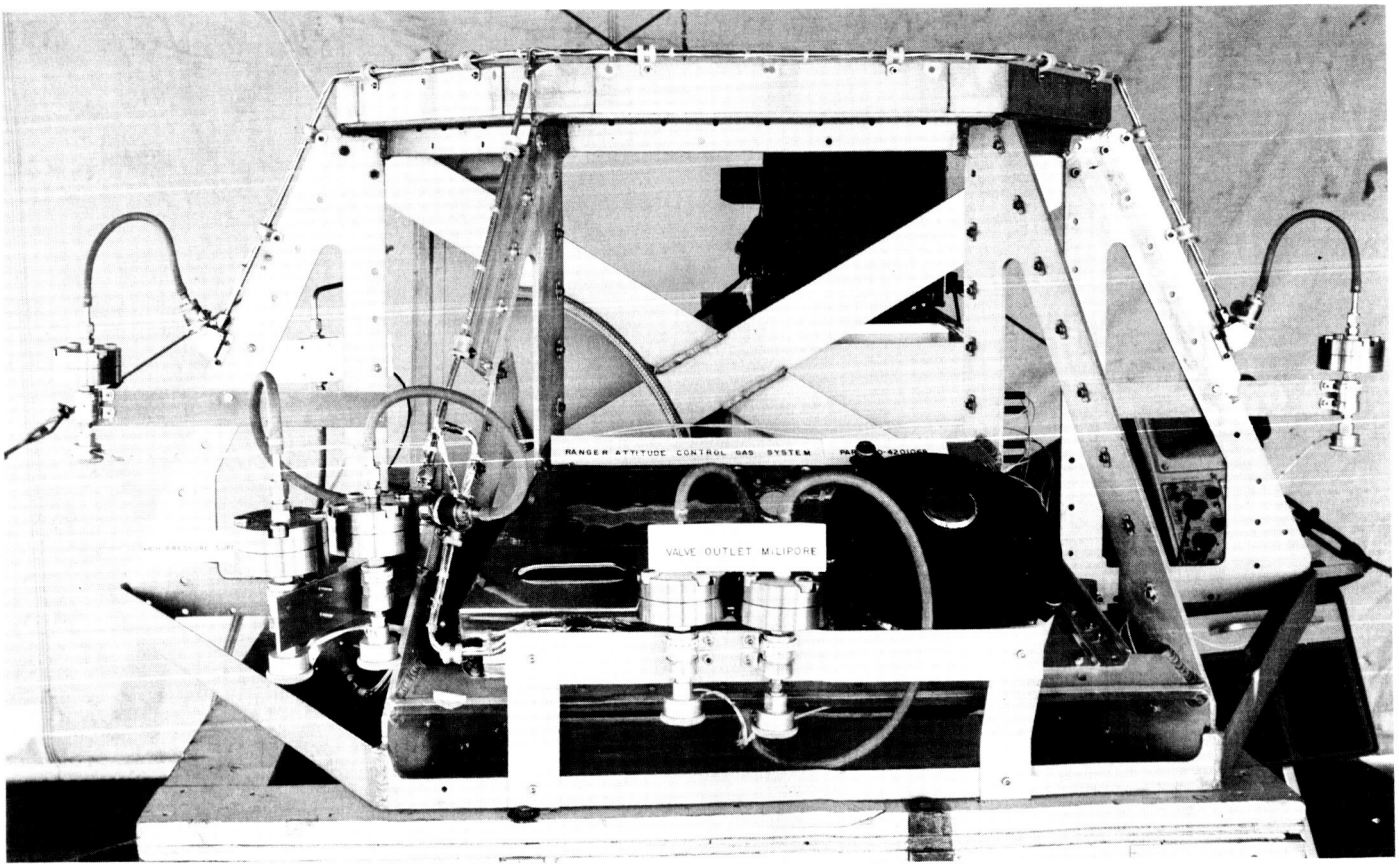

Fig. 58. Gas subsystem showing filters and pressure switches connected

performed significantly better than the nominal case with respect to gas usage. Telemetered data of temperature and pressure was not fine enough to show any usage. Calculated use is tabulated below along with the initial charge of nitrogen:

Spacecraft	Initial charge, lb	Calculated use, lb	Nominal use (estimated), lb
Ranger VII	4.24	0.16	
Ranger VIII	4.21	0.115	0.54
Ranger IX	4.20	0.133	

Three special tests were conducted. The first has been described and was the helium mass spectrometer quantitative leak test performed before and after vibration on every system.

When pressure transducers failed several times during vibration, special vibration runs were made on the TA system to check transmissibility of the fixture and mounting of the transducers. Also, a bracket was fabricated to hold the cantilevered end of the transducer in close relation to the shear plate supporting this equipment. No significant reduction in transmissibility to the transducer was achieved and that approach was abandoned.

Finally, an additional set of three axes of TA level vibration tests was run with the fill manifold, a 1.35-lb, nearly solid, block of steel, replaced by its flight plug and only 200-psig pressure in the vessel. It was observed that the pressure vessel rotated approximately 15 deg in its mount during any axis of vibration. This resulted in a special adjustment of the Belleville springs holding it in place for any vibration test at pressures below 1500 psig.

The advantage of lightness (a complete half system less gas in the vessel weighs 12 lb) meant that the unit could not support itself. Construction on a weld-handling fixture provided a means to handle the unit and simple structure to put in a shipping container as shown in Fig. 59. This weld-handling fixture was also designed to adapt to the vibration test fixture (Fig. 54) with about 200 bolts providing a good measure of solidarity. Another fixture, the "transfer fixture," attached to the gas actuator outside of the weld-handling fixture, provided means of transferring the unit to the spacecraft bus without causing unwanted strains in the plumbing and cables. Figure 60 shows the system supported by this fixture.

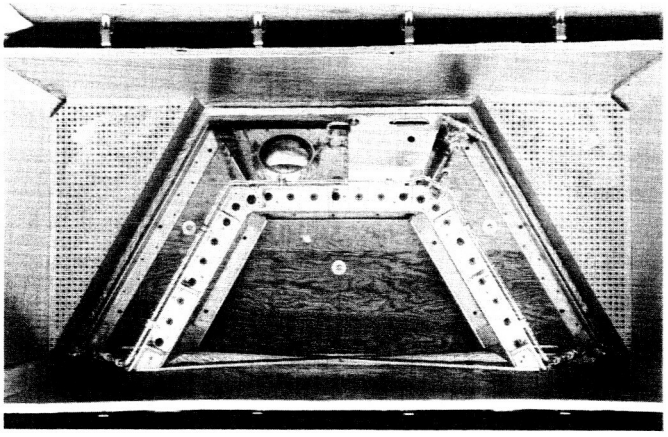

Fig. 59. Gas subsystem installed in carrying case

Transportation of the unit on the weld-handling fixture was limited to hand carrying or riding the padded bed of a pickup truck around the Laboratory at a 5-mph limit. All other transportation was accomplished with the unit in its shipping case. This is a large wooden crate with an inner plywood box lined with a water tight film and supported by 4 in. of rubberized hair padding on all sides (Fig. 59).

5. Hardware Limitations

In general, hardware limitations are not known because testing to destruction was not undertaken; however, limits in some areas were established. Some items received environmental loads far above specification input requirements without failure.

With respect to the vibration environment, there is considerable gain in the 385-lb fixture used to support a complete half system and also in the structure of the subsystem. The pressure transducer was instrumented to measure g loading along three mutually perpendicular axes and was found to be loaded to approximately 30 times the TA input level across the transducer axis and approximately 20 times the input level along the transducer. This means that the unit sustained successfully loads of 135 to 270 g for short time intervals in a direction across the cylindrical axis of the transducer and 90 to 180 g along the axis at certain frequencies.

A pitch valve manifold was instrumented with a single accelerometer and was found to be loaded to 150 g perpendicular to the cylindrical axis of the valve. This loading sometimes caused failure of an electrical lead at the soldered terminal until the length of the service loop was drastically shortened.

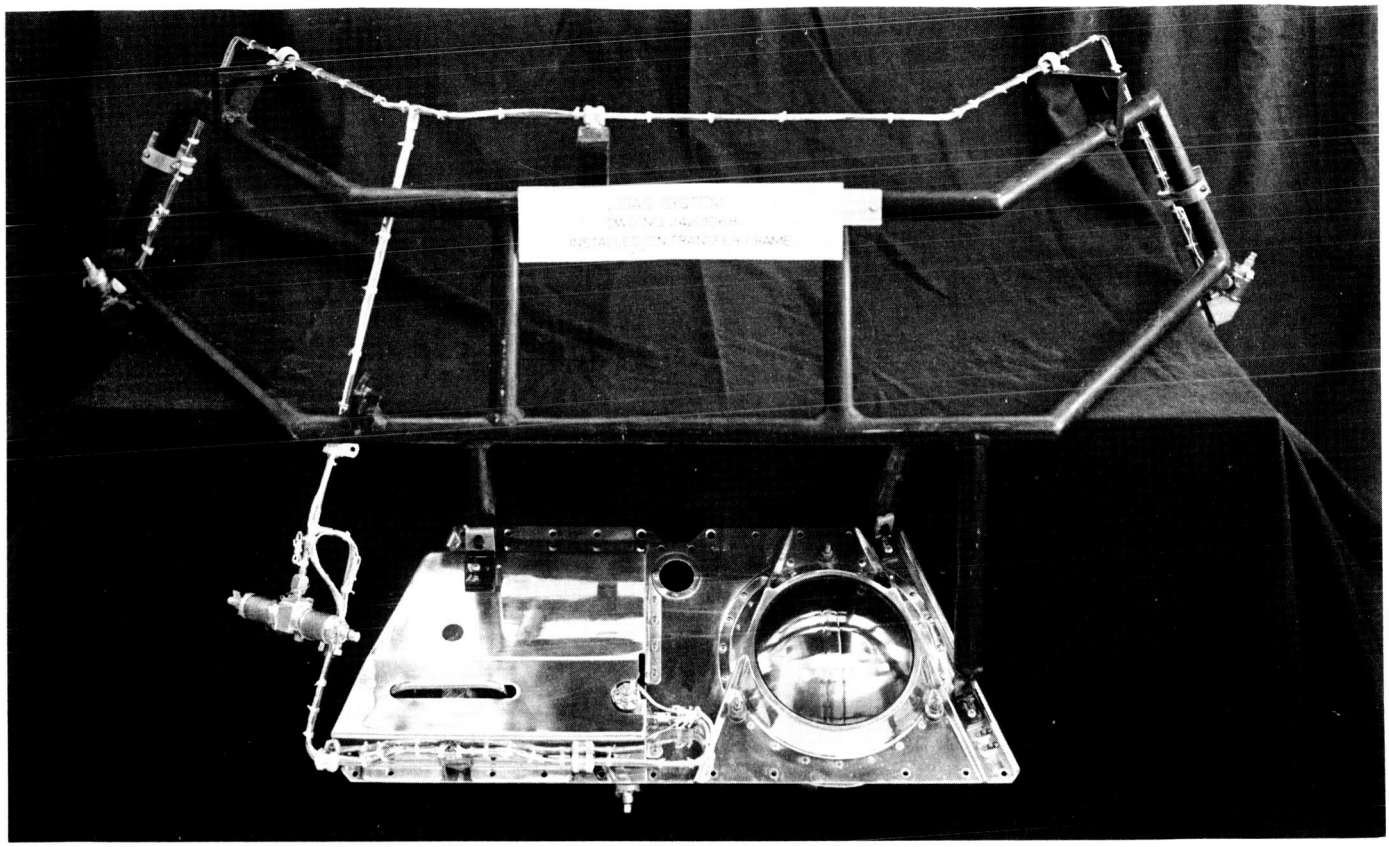

Fig. 60. Gas subsystem installed on transfer frame

The temperature limits of the unit were not reached in any testing; however, an upper limit of 135°F during flight was established from the standpoint of pressure vessel safety. A fully charged pressure vessel will reach 4000 psi at this temperature, which is the limit with a specified minimum burst of 8030 psi. Regulator icing could be produced if the changing gas was not dry enough.

In flight (as noted previously) pure couples are not provided about pitch and yaw axes; this fact results in a small velocity increment along each of these axes being generated each time a pair of valves fires. These changes are not significant to the accuracy of the *Ranger* trajectory because of small magnitudes and the very small amount of gas used.

It has been customary to require a 4 to 1 factor of safety on pressure vessels where personnel are concerned. In this case, this is observed during most testing by limiting pressures in the system to 1800 psi or less. It was felt that TA testing should be done at a pressure that would be expected during that environment and that valid FA vibration tests should be done at full flight pressure. In these cases, a protective barricade was used for personnel protection.

Definite limitations exist in the handling of this subsystem in two areas: those of cleanliness and the inability of the unit to support itself mechanically. Cleanliness is maintained by the careful assembly procedures already described and the careful control of the charging gas, including the very small pore filter in the fill manifold.

In the last stages of the program, several difficulties were traced to too liberal use of soap bubble leak detecting solutions which seemed to enter the jet valves by creeping around the ball poppet and then concentrating collections of fine particulate contamination in critical areas until failures occurred.

6. Operations Summary

Significant operating time of the major components of this subsystem can be measured only by a count of the

number of operating cycles of a valve or regulator. These operations can conveniently be divided into four areas:

(1) Predelivery and acceptance cycling.

(2) System checkout and FA testing.

(3) Spacecraft systems testing.

(4) Actual flight operations.

As mentioned previously, a signficant portion of the life of the regulator and valves was used prior to and during assembly into a system to avoid infant mortality failures. This amounted to 50,000 cycles for jet valves and 80,000 cycles for regulators. During the system checkout and FA tests, only a few cycles of operation occur except during the thermal vacuum testing where each jet valve is opened about every 20 min or about 126 cycles during the 42-hr test. The total for this period will probably average about 150 cycles. Here each jet valve operation is of considerable duration, permitting the assumption that the regulator operates each time a valve operates, or

$$150 \times 6 = 900 \text{ cycles}$$

The spacecraft systems tests nominally run to 1000 cycles per jet valve and consist of three space vacuum mission tests, six systems tests, one subsystems test, and one spares verification test. This totals some 11,000 cycles of a jet valve. For *Rangers VI* and *VII*, the on time of each operation was variable and, in general, long enough to cause the regulator to operate; on *Rangers VIII* and *IX*, with derived-rate control systems, each valve pulse was limited to an on time of 20 msec. Here approximately three operations would be required to cause the regulator to operate, so its usage would be only one-third the valve operations, or say 22,000 cycles rather than the 66,000 cycles expected.

Reduction of flight data in the *Rangers VIII* and *IX* mission report lists actuations of 978 and 768 in pitch, 265 and 222 in yaw, and 157 and 151 in roll. Again the regulator will operate about one-third of the time or 467 for *Ranger VIII* and 380 for *Ranger IX*.

On occasion, extra cycles were added to evaluate malfunctions. An example is cited for *Ranger VIII:* High leakage was discovered on one yaw valve and some 6035 cycles were added to clear it and establish confidence that its flightworthiness was intact.

The totals shown in Table 27, while large, do not approach the required 250,000-cycle life requirement of a jet valve or the 500,000-cycle life of a regulator. By actual test, these figures have been bettered. A 300,000-cycle value is quite reasonable for a valve as shown by seven

Table 27. Summary of estimated valve and regulator operations

Tests	*Ranger VII*		*Ranger VIII*		*Ranger IX*	
	Each jet valve	Regulator	Each jet valve	Regulator	Each jet valve	Regulator
Pre-delivery and acceptance cycling	50,000	80,000	50,000	80,000	50,000	80,000
System operation and FA	150	900	150	900	150	900
Spacecraft systems tests	11,000	66,000	11,000	22,000	11,000	22,000
Flight operations						
Pitch	764	—	978	—	768	—
Yaw	416	—	175	—	123	—
Roll	192	—	106	—	81	—
Regulator	—	2,392	—	467	—	380
Special test						
Yaw			6,035	6,035		
Totals						
Pitch	61,914		62,128	—	61,918	—
Yaw	61,566		61,325	—	61,273	—
Roll	61,342	—	61,256	—	61,231	—
Regulator	—	149,292	—	109,402	—	103,280
Life test	300,000	1,500,000	300,000	1,500,000	300,000	1,500,000
Life requirements	250,000	500,000	250,000	500,000	250,000	500,000

out of eight test units, and a regulator operated 1,500,000 after two TA vibration tests with no measurable degradation in performance.

7. Reliability

This discussion is concerned with the problem and failure reports generated between the time a gas actuator subsystem was completed and the time installation on the spacecraft was complete. Of a total of 25 reports, 15 are listed initially as problems and 10 as failures.

Eleven of these problems were a matter of minor assembly problems and mechanical interferences, which had little bearing on the function of the subsystem and were easily eliminated. The next large group of failures related to the pressure transducer where six failures occurred during this time. At least two other failures of this nature occurred before and after the period covered here. The final analysis seemed to indicate that lack of cleanliness and handling care by the manufacturer resulted in the later problems, but a completely conclusive answer was not found. Four of the eight remaining items were random single items such as a short, a failed temperature transducer, and a broken lead (which occurred twice on the same unit) before an adequate solution was determined. The other four failures occurred in jet valves and a regulator and were, in general, caused by contamination in the system. Many other failures by this cause occurred earlier in the manufacturing process and, when combined with the pressure transducer problems, made up the prime trouble source. The significance of cleanliness and problems involved in achieving and maintaining the proper degree cannot be over emphasized. This may be a function of the particular designs of moving parts used in this assembly, but all mechanical devices face this problem. The final cleanliness achieved through care is shown by the perfect flight record.

8. Engineering Change Requirements

The major engineering change to this subsystem occurred between *Rangers V* and *VI* when the flared tube fittings were replaced with welded joints at all possible points and the single system with ten valves was replaced by two identical interchangeable half systems using a total of 12 valves to provide redundancy. A brief description of other changes is given below.

(1) Updating of weight allocations for attitude control systems.

(2) Provision of mounting facilities for transfer fixture.

(3) Provision of clearance between plumbing and solar panel brackets by chamfering corner of tee.

(4) Provision for new nozzle design with greater thrust.

(5) Provision of holes to mount pressure vessel protective shrouds prior to launch.

(6) Piercing of pressure transducer case so possible internal leaks do not become a hazard.

(7) Rerouting of leads to pitch and jet valves to permit tie points close to solder terminals.

(8) Revision of pressure vessel shroud to allow use over thermal shields.

(9) Improved welding techniques to process specification.

(10) Increase of jet valve closing time from 5 to 7 msec.

(11) Increase of jet test nozzle orifice from 0.020- to 0.030-in. diameter for use with derived-rate systems.

(12) Increase of acceleration requirement from 0.60 ± 0.06 to $0.72 \pm 0.18 \times 10^{-3}$ rad/sec^2.

(13) Provision of lockwire hole in fill manifold replacement plug to anchor B nut safety wire.

(14) Revision of curing procedure for bonding temperature transducers to pressure vessel to obtain more reliable bonding.

(15) Two hardware changes.

G. Accelerometer

1. Description

The magnitude of the velocity increment, to be added during the corrective midcourse maneuver of Blocks II and III, was measured by means of a linear accelerometer and integrator combination. Since a digital computer was carried in the CC&S unit and the magnitude of the corrective velocity increment was transmitted digitally from Earth, a digital accelerometer subsystem was required. This subsystem was developed at JPL and was used in combination with the digital computer for midcourse motor shutoff.

This digital accelerometer subsystem (Fig. 61) consists of a force balance accelerometer with a pulse-torqued rebalance loop to provide capture current to the proof mass. In this method of operation, the pulsing rate is directly proportional to the applied acceleration; each pulse produced represents a constant value of velocity increase (or decrease, depending on the direction of the acceleration). In the *Ranger* application, this value, or scale factor, was 0.10 ft/sec per pulse.

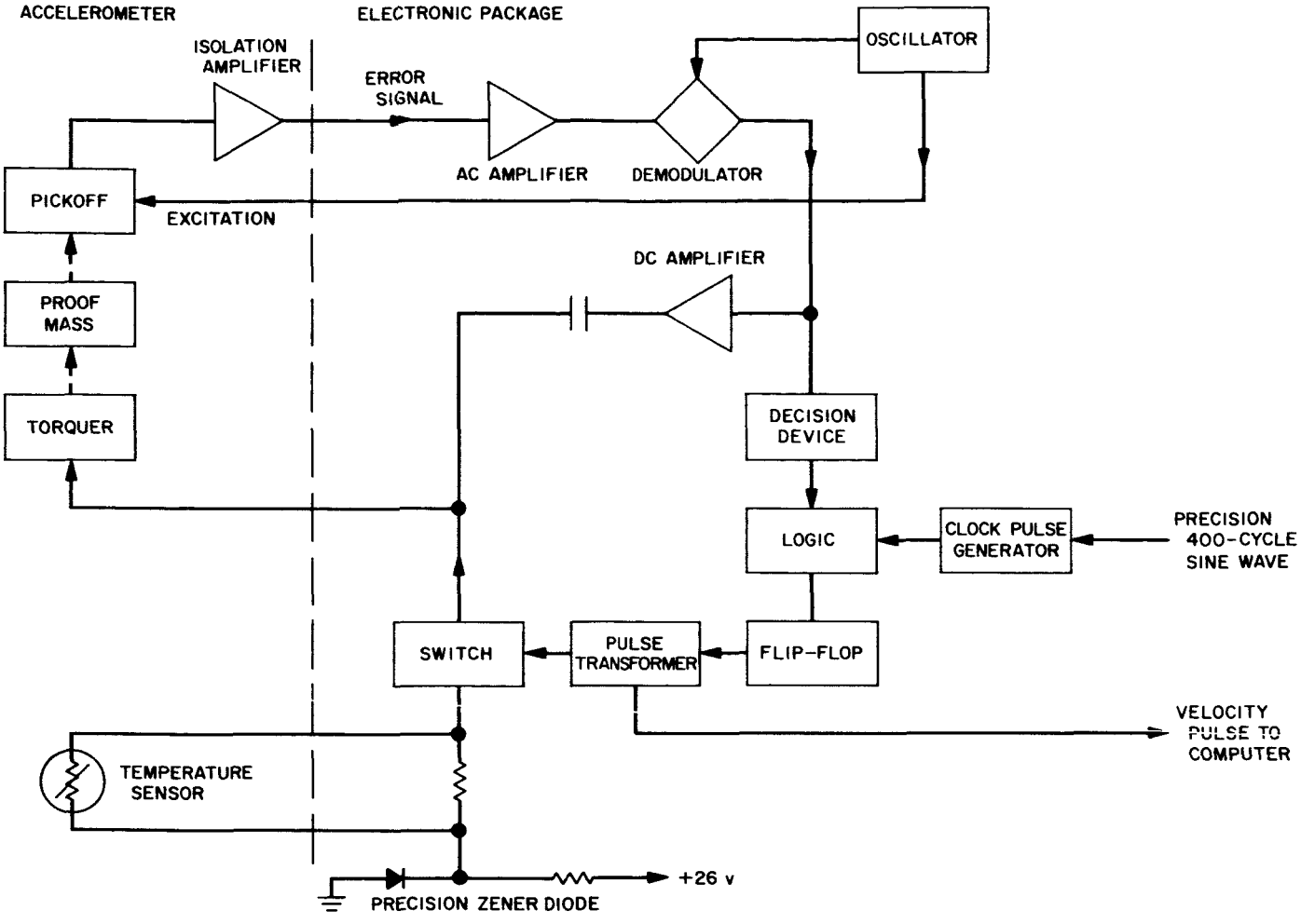

Fig. 61. Accelerometer subsystem

The accuracy is determined to a large extent by how precisely the current pulses to the torquer can be generated. The method for developing this pulse in the *Ranger* system is referred to as the "open-loop" system. Basically, this system uses an accurate frequency (from the computer clock) to control the pulse width and an accurate voltage, controlled from a precision Zener diode, to determine the pulse height.

The accelerometer pickoff is a capacitive type, which is excited with 200 kc from an oscillator in the electronic package. This pickoff produces an error signal to the AC amplifier, which has a gain of 200. The output of the AC amplifier is coupled through a one-to-one transformer to a double bridge demodulator. The demodulator reference signal is obtained from the same 200-kc oscillator as the accelerometer excitation.

The demodulator error signal is applied to a Schmitt trigger circuit, which is a decision device. This circuit will detect displacement of the proof mass, which for a predetermined amount of acceleration, will develop a rebalance pulse. When the Schmitt circuit changes state, the logic circuit will then allow the precision clock pulses to pass through to the flip-flop. (In this circuit, the flip-flop is actually a trigistor.) The first positive clock pulse will cause the trigistor to conduct. At 1250 μsec later, a negative clock pulse turns the trigistor back to the nonconducting state. This on–off action of the trigistor is transformer-coupled to a low-leakage, high-speed transistor switch. The switch is supplied with a +8.4 v from a precision Zener diode. This diode voltage is stable to $\pm 0.1\%$ over 100°F temperature range.

A current limiting resistor is placed in series with the switch and Zener diode. The value of this resistor is varied

as a function of the accelerometer temperature to compensate for the change in accelerometer permanent magnet torquer characteristic. This torquer has a gain function which changes rapidly with temperature.

It will be noted from this description that pulses of only one polarity can be generated. This provides capture in only one direction as the *Ranger* spacecraft can only accelerate in one direction.

The accelerometer has a built-in eddy current damper associated with the proof mass. This damping is not sufficient for restraining the pendulum against vibration, so an additional rate feedback loop is applied around the accelerometer. This loop uses the same demodulated signal as the decision device. This signal is amplified by a low-gain DC amplifier. The output is capacitor-coupled back to the torquer to produce a current proportional to the proof mass rate of motion. This circuit provides a damping increase of five.

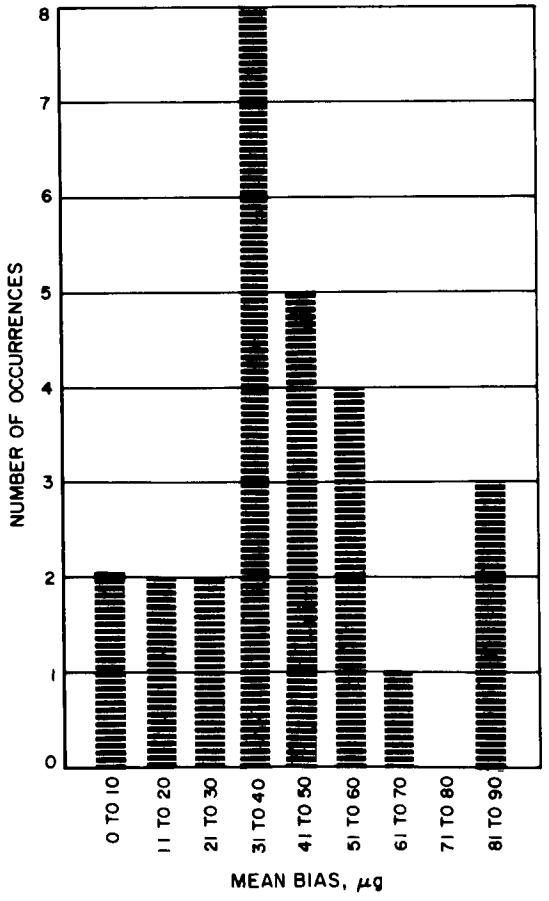

Fig. 62. Accelerometer mean bias (null offset)

a. Performance. Accuracy for the digital accelerometer scale factor was 0.25% of applied, 1 sigma. While no system requirement was placed on the accelerometer bias (null offset) error, a control value of 100 μg, 1 sigma, was used by the cognizant group.

The actual performance of the accelerometer subsystem is shown in Figs. 62–65, which were compiled from data taken during the entire *Ranger* Project.

2. Fabrication

The accelerometer module was fabricated in a single assembly containing the accelerometer transducer and all electronics. A modified version of the standard magnesium subchassis was used for the basic structure.

After the initial prototypes, all systems were fabricated, tested, and calibrated. No significant major problem areas have been associated with the accelerometer subsystem.

3. Testing and Calibrations

Test procedures on the accelerometer and the digital electronics module have been standardized since the

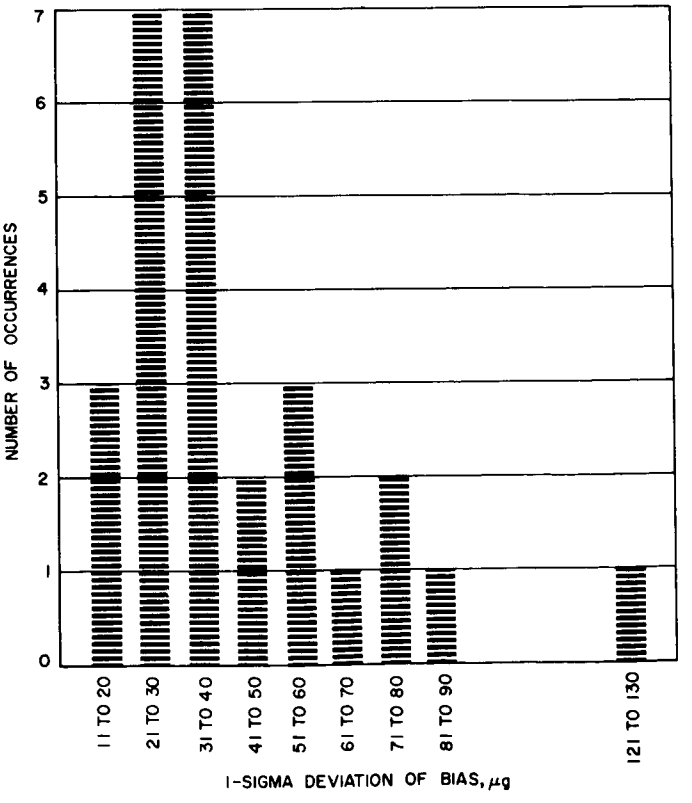

Fig. 63. Accelerometer standard deviation bias

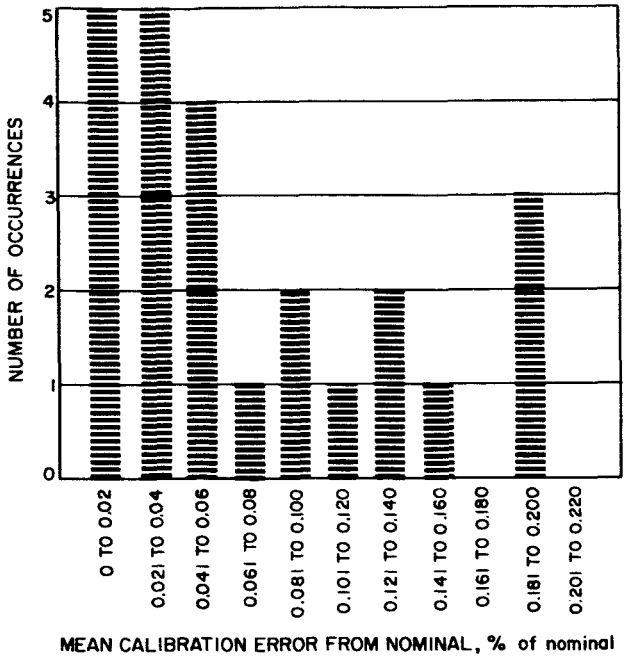

Fig. 64. Accelerometer mean digital calibration

inception of the *Ranger* Project. The only changes were in the instrumentation: The analog rebalance amplifier was changed in January 1962 to a design using newer planar transistors, and the Kin-Tel microvoltmeters were replaced with more stable instruments manufactured by Dynamics Instrumentation Corporation.

Because of the unidirectional rebalance nature of the digital module, it was not possible to obtain several important accelerometer parameters while in the digital mode. The principal missing parameters were the accelerometer bias error (null offset) and the sensitive axis alignment angle. It was therefore necessary to perform several operations on the unit using an external analog rebalance amplifier. Such measurements as bias, current scale factor, alignment angle, and frequency response are all obtained in the analog mode of operation.

Equipment used in the analog mode consists of the Lietz optical dividing head, the Dynamics microvoltmeter, and the Tinsley vernier potentiometer. All of the bias data was obtained from the microvoltmeter readings

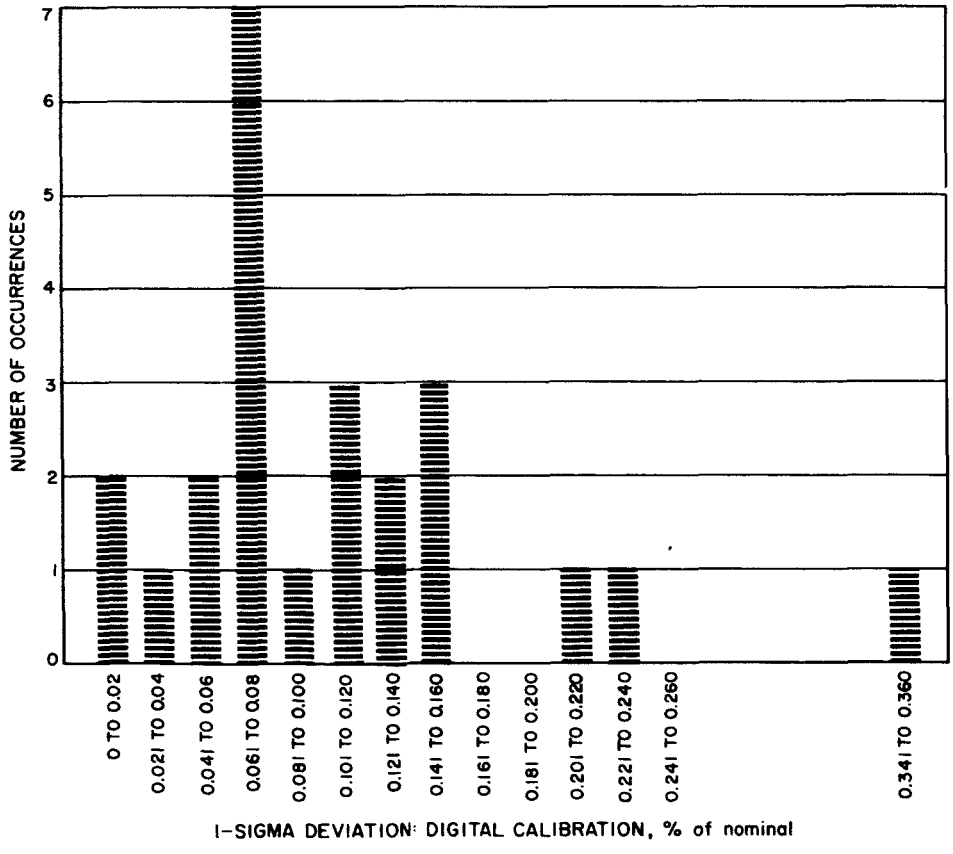

Fig. 65. Accelerometer standard deviation of calibration

rounded off to the nearest 10 μg point. Readings were not carried beyond this point because subsystem accuracies did not demand it and because 1-μg resolution is obtainable *reliably* only with the Tinsley potentiometer (and is a very time-consuming operation).

Measurement of digital parameters was confined to calibration (digital scale factor), threshold (finite amount of input acceleration required to obtain a rebalance pulse), and visual observation of the pendulum position signal. Numerous other functional electronic tests were made on the module, but never on a repetitive basis.

The calibration measurement was of major importance from the system standpoint as it directly affected the midcourse velocity increment. Digital calibration was an all-inclusive number as almost everything in the accelerometer had an effect on the number obtained. Principal contributors were accelerometer analog current scale factor, accelerometer bias, Zener reference diode voltage, and 400-cps clock frequency. Most of these error sources affected the calibration in a 1-for-1 ratio; however, the bias error caused a 0.14% shift in calibration for each 100 μg of bias shift. The system requirement for digital scale factor accuracy was 0.25% of applied, 1 sigma. The applied value was 0.07 g. The measurement was obtained by tilting the accelerometer module in a Lietz dividing head to an angle 4 deg from the known horizontal sensitive axis position. This produced a g input close to the expected spacecraft midcourse acceleration level. The rate of pulsing (approximately 22.4 pulses/sec) was then recorded on a special digital counter with a gate period of 1000 sec. This test method would yield a measurement accuracy of between 0.005 and 0.01% if performed carefully.

4. Qualification for Flight

Flight-acceptance testing was performed with the accelerometer module mounted in the same case (Case IV) as the gyros and attitude control system electronics. No power was applied to the module during vibration, as this is the normal boost phase operation. The comparison of dividing head data taken before and after vibration and vacuum–temperature environments was the primary means of telling whether the module had passed FA and TA testing.

One of the early type units was placed on an extended life test in March 1962 in such a manner that a pulse rate of 160 pulses/sec was developed in the digital mode. This unit remained in almost continuous operation until January 1965 with an accumulation of 24,332 hr of digital pulsing. A plot of performance during this time is shown in Fig. 66. This life test has supplied strong evidence that the flexure springs do not "wear out" because of the constant motion involved in digital rebalance systems. It will also be noted from Fig. 66 that a long-term trend is present in the bias error. This type of trend has been observed in other units not in constant operation. It is felt, therefore, that this trend is not caused by the pulsing in any way.

5. Limitations

Principal limitations on the use of the *Ranger* digital accelerometer were vibration during operation and shocks above 100 g peak.

Because of the low capture capability, which was +1 g maximum, with no capture in the negative direction, the proof mass could not be restrained during any (even moderate) vibration condition. Special tests were performed at the beginning of the *Ranger* Project to evaluate the accelerometer performance with the midcourse rocket motor vibration. The motor-induced vibration proved to be less than 0.1 g, and therefore caused no problem to the accelerometer. No capture was attempted during boost vibration environment.

Shocks cause the proof mass to slam against the stops within the instrument and have been known to cause significant null offsets when the peak shock level is above 100 g.

No severe handling problems were associated with the accelerometer, however, because the other half of the inertial sensor system was hand carried to ETR; the accelerometer was taken by the same method at the same time.

6. Operations Summary

A decision was made in the Block III program to provide a burn-in period for each flight module,during which the entire module was allowed to operate in the digital mode for 500 to 750 hr. Several data points were taken during this burn-in phase, thus providing information on long-term stability of the module. This burn-in period far exceeded the actual operating time accrued by the module during spacecraft system testing.

7. Reliability

During the Block III program, two accelerometer modules developed large null offset shifts; these were explained by mishandling at some point during the time they were away from the inertial sensor group. One instrument

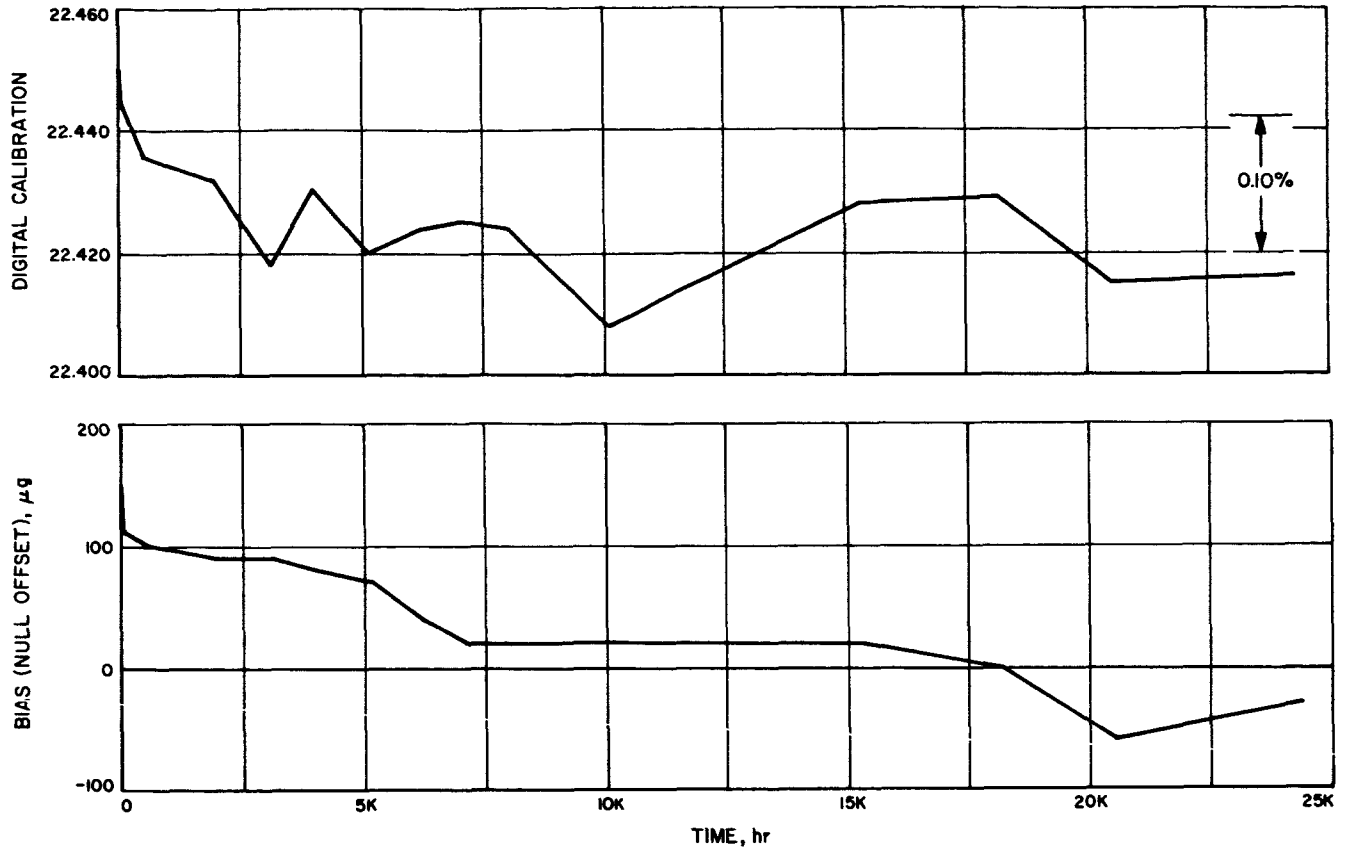

Fig. 66. Performance during life test

was returned to the manufacturer for internal examination, which disclosed damage to the suspension flexures. As no place could be located where such damage was allowed to happen, the condition remained an anomaly.

8. Engineering Change Requirements

During Block III, two Engineering Change Requirements were introduced to the accelerometer module: a dimensional change to the module mounting flange in order to make it compatible with the hold-down screw dimensions; and a general upgrading to the Block III design philosophy, e.g., addition of all Hi-Rel components and rearrangement of components on circuit boards for better vibration support.

H. Gyro

1. Description

The *Ranger* attitude control system requires angular rate and position information, used during the acquisition and cruise periods for stabilization of the system and during the maneuver period for midcourse correction, about each of the three major axes: pitch, yaw, and roll. This information is derived by a unique application of three single-degree-of-freedom, floated integrating gyros; these gyros are filled with a high-density, low-viscosity fluid, which permits operation of the gyros without heaters, and provides full flotation at 115°F. Both damping and precession axis restraint are accomplished by a torque feedback loop (Fig. 67). The restraint provided by this electronic loop remains relatively constant, independent of changes of fluid viscosity due to temperature.

Three modes of operation are possible within the gyro subsystem:

(1) A conventional rate mode in which the rebalance currents to the three gyro torques are used to develop voltages which are proportional to spacecraft turning rates. This rate mode is used to damp spacecraft turns during the acquisition of the Sun or Earth.

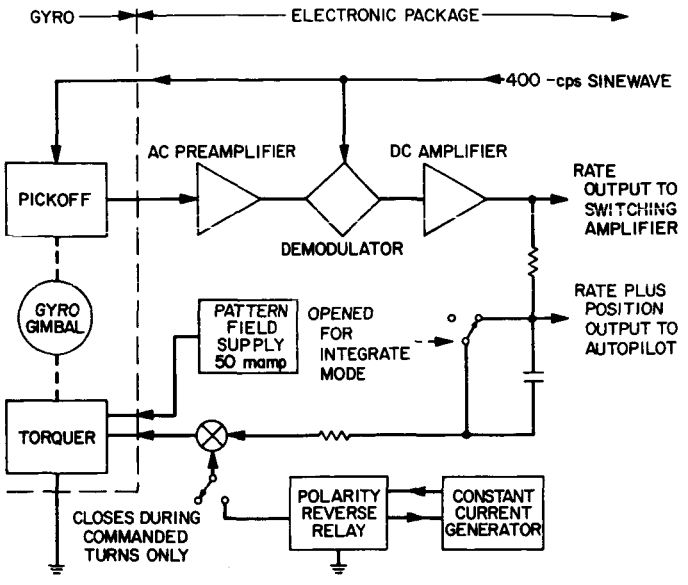

Fig. 67. Single gyro loop

(2) A mode in which the gyro gimbal is torqued by a precision current for a controlled length of time. Motion of the gyro gimbal produces an error signal to a switching amplifier in the attitude control system. Gas is then vented through the appropriate jets, thus causing the spacecraft to follow the gyro gimbal motion. In order to allow a wider range of motion for the gyro input axis, a large integrating capacitor is inserted into the rebalance loop during this mode. This capacitor stores a voltage proportional to the gimbal motion and allows greater gyro input range to be obtained.

(3) A mode used to steer the spacecraft during midcourse maneuver. The rebalance loop is the same as the second mode; however, the precision command current is removed. Gyro output signals are then sent to the autopilot and jet vane actuators in order to keep the spacecraft on the correct heading during the midcourse motor burn period.

a. Performance. Two parameters were dominant in establishing the performance of the gyro subsystem and its effect on the spacecraft: the gyro fixed drift rate, referred to as the fixed torque (F_t), and the commanded turn rate. Both were of primary importance in performing an accurate midcourse maneuver.

The GG49 gyro, as used in the *Ranger* system, has a relatively large fixed torque, due to reaction torques developed within the Dualsyn pickoff-torquer. Gyros were acceptable for use in the system at fixed torques as high as ± 12 deg/hr, although none were actually used higher than 8 deg/hr. This large fixed component was then bucked out by adding a small current to the torquer in the opposite direction. The current was adjusted to bring the apparent fixed torque to near zero; thus, it is obvious that what is important is not the magnitude of the fixed torque, but its long-term stability.

Tables 28 through 31 show the performance of the four systems flown on *Rangers VI* through *IX*. The RMS of all fixed torque 1-sigma deviations for the 12 gyros involved is 0.278 deg/hr, well within the allowable tolerance for the system.

Table 28. *Ranger VI* gyro package

Axis	Fixed torque, deg/hr			Commanded turn rate, deg/hr	
	Average	Deviations	Average compensated value	Average rates vs temperature	Deviations of all rates
Pitch	−1.15	1 sigma = 0.063 3 sigma = 0.189	−0.90	At 85 = 779.45 At 100 = 779.25 At 115 = 779.20 At 130 = 778.73	1 sigma = 0.154 3 sigma = 0.462
Yaw	+6.91	1 sigma = 0.403 3 sigma = 1.21	−0.002	At 85 = 794.03 At 100 = 794.56 At 115 = 794.60 At 130 = 794.30	1 sigma = 0.166 3 sigma = 0.498
Roll	−2.03	1 sigma = 0.364 3 sigma = 1.09	0.023	At 85 = 796.96 At 100 = 797.28 At 115 = 797.37 At 130 = 796.93	1 sigma = 0.193 3 sigma = 0.579

Table 29. *Ranger VII* gyro package

Axis	Fixed torque, deg/hr			Commanded turn rate, deg/hr	
	Average	Deviations	Average compensated value	Average rates vs temperature	Deviations of all rates
Pitch	−6.29	1 sigma = 0.190 3 sigma = 0.570	+0.143	At 85 = 796.59 At 100 = 796.78 At 115 = 796.95 At 130 = 796.59	1 sigma = 0.091 3 sigma = 0.273
Yaw	−5.96	1 sigma = 0.108 3 sigma = 0.324	+0.030	At 85 = 794.12 At 100 = 794.20 At 115 = 794.05 At 130 = 794.01	1 sigma = 0.113 3 sigma = 0.339
Roll	+4.75	1 sigma = 0.450 3 sigma = 1.350	+0.157	At 85 = 819.06 At 100 = 819.30 At 115 = 819.17 At 130 = 819.01	1 sigma = 0.071 3 sigma = 0.213

Table 30. *Ranger VIII* gyro package

Axis	Fixed torque, deg/hr			Commanded turn rate, deg/hr	
	Average	Deviations	Average compensated value	Average rates vs temperature	Deviations of all rates
Pitch	+6.09	1 sigma = 0.440 3 sigma = 1.320	+0.220	At 85 = 802.45 At 100 = 802.70 At 115 = 803.02 At 130 = 802.99	1 sigma = 0.209 3 sigma = 0.627
Yaw	+6.32	1 sigma = 0.185 3 sigma = 0.555	−0.042	At 85 = 791.50 At 100 = 791.80 At 115 = 791.80 At 130 = 791.94	1 sigma = 0.140 3 sigma = 0.420
Roll	+4.18	1 sigma = 0.280 3 sigma = 0.840	+0.180	At 85 = 794.15 At 100 = 794.30 At 115 = 794.24 At 130 = 794.15	1 sigma = 0.199 3 sigma = 0.597

Table 31. *Ranger IX* gyro package

Axis	Fixed torque, deg/hr			Commanded turn rate, deg/hr	
	Average	Deviations	Average compensated value	Average rates vs temperature	Deviations of all rates
Pitch	−6.81	1 sigma = 0.171 3 sigma = 0.513	−0.178	At 85 = 784.50 At 100 = 784.46 At 115 = 784.42 At 130 = 784.05	1 sigma = 0.138 3 sigma = 0.414
Yaw	−3.56	1 sigma = 0.192 3 sigma = 0.576	−0.370	At 85 = 780.48 At 100 = 780.48 At 115 = 780.47 At 130 = 780.03	1 sigma = 0.123 3 sigma = 0.369
Roll	+6.42	1 sigma = 0.074 3 sigma = 0.222	+0.061	At 85 = 782.85 At 100 = 782.92 At 115 = 782.63 At 130 = 782.21	1 sigma = 0.176 3 sigma = 0.528

Commanded turn rate is nominally 720 deg/hr; however, again, the stability, rather than the exact value, is what is important. This rate is expected to be very temperature sensitive; thus, a temperature compensation circuit is built into the command current regulator using the gyro temperature sensor. The actual rate is a product of the pattern field current (nominal: 50.0 mamp) and the command current (nominal: 7.2 mamp). The stability of the rate produced is therefore critically dependent on two current variables as well as the gyro torquer, which acts as the multiplying device; nevertheless, the RMS of all rate deviations for the four flight systems involved was 0.168 deg/hr out of a nominal 720 deg/hr. The variation of rate with temperature is also shown in Tables 28 through 31. A temperature transducer was attached to the gyro package and was used to telemeter the actual temperature in flight. The maneuver rate used was the one nearest to the actual temperature at the time.

In summarizing the performance, it can be said that all design goals were met or exceeded with a gyro subsystem of minimum complexity and requiring a minimum of power.

2. Fabrication

The gyro subsystem is fabricated in two parts: the gyro package, which contains the three Honeywell GG49-E19 floated rate integrating gyros; the 12 General Electric Bi-Polar Tantalum integrating capacitors; some relays; and the capacitor cycling circuitry, and the electronics module, which contains the three gyro rebalance amplifiers, the pattern field and command current regulators, and some associated relays.

The entire subsystem was fabricated and initially calibrated by the Nortronics Division of the Northrop Corporation. Flight-acceptance testing and final calibration was accomplished at JPL by Nortronics and JPL personnel.

The principal difficulties with the gyro were solved early in the Block II portion of the *Ranger* Project. These involved a change in the type of wire used in the Dualsyn (the combined torquer–pickoff used in the GG49 gyro) to permit sterilization at 125°C, and the reduction of the clearance between the gimbal pivot and jewel to decrease the gyro response time. No recurrence of these conditions was observed during Block III.

There was one minor problem, first noticed at ETR during prelaunch operations of *Ranger VI*, regarding the slow runup characteristic of the gyro at low ambient temperatures. The bearing preload within the gyro increased to such an extent at 50°F that no positive indication of motor sync was available to the blockhouse observer. In order to evaluate this condition, an intensive program, which confirmed this condition, was conducted at JPL. As a result, all remaining gyros in the Block III system were checked for runup capability at 50°F and low supply voltage. Ten gyros were returned to the vendor; five were confirmed as being out of sync at 50°F and 22-v-RMS supply. In addition, operational procedure changes were made at ETR; the problem did not recur.

Early in Block III, a number of the special 1020-μf tantalum integrating capacitors failed. The failure mode was a large increase in the capacitor leakage current. In an effort to obtain a true hermetic seal on the capacitor feedthrough terminals, a change was made from the former Block II capacitor design to a new type. After an aging period, this new design began to allow a small quantity of the electrolyte within the capacitor to leak up around the tantalum riser rod and cause an electrical leakage path to be formed from the rod to capacitor case to the other riser rod.

Because of the relatively large number of failures encountered in a short time, it was decided to abolish all capacitors and purchase a new design of the same capacitor, which was being qualified for use in the *Minuteman* Project and which was also being considered for *Mariner* Mars 1964. The capacitor subassembly was a part of the gyro package that could be detached as a unit. New capacitor banks were fabricated using the latest capacitor design; the failure rate for leakage dropped to zero through the remainder of the gyro program for Block III.

3. Testing and Calibrations

Testing of the gyro subsystem involved three major phases: acceptance testing of the gyros, servo calibration of the gyros and electronic modules together, and environmental testing of the entire assembly.

Acceptance testing of the gyros was performed at JPL and at Nortronics during the course of the Block III program. This test phase involved several days of repetitive "Heading" tests using a Leitz optical dividing head for positioning the gyro input axis and an integrating digital voltmeter to read out the gyro rebalance current obtained. The gyro was positioned so as to pick up different components of Earth rate with the output or precession axis both vertical and horizontal; a total of eight

sets of rebalance currents was obtained. These sets were fed into a small digital computer for reduction to obtain the important gyro parameters of torquer scale factor, fixed torque, mass unbalance spin axis component, and mass unbalance input axis components; they were then observed for absolute values and for any drift trends during the acceptance test phase.

The gyro was also subjected to a series of "Tumble" tests, in which the gyro was rotated slowly and accurately about its output axis (aligned to the Earth's polar axis) by a special machine. This test gave a dynamic indication of mass unbalance components and also indicated any small changes in stiction, flotation, or other similar irregularities in the gyro's behavior.

The electronic module received a number of functional electronic tests over a wide temperature range and was then mated to the gyro package. The entire subsystem was then placed in a temperature-controlled chamber mounted on a servo table. A rate and position loop was closed from the gyro output through the servo table and its electronics and back to the gyro. In this manner, it was then possible to test accurately the commanded turn rate of each of the three gyros at four different temperatures and two different gyro orientations. Rates obtained from this test were used in calculating the duration of the spacecraft commanded turn during the midcourse maneuver. This test was performed many times, typically before and after environmental testing and before shipment to ETR. A similar test was performed at ETR at a single temperature (115°F) prior to installation into the spacecraft.

4. Qualification for Flight

The gyro subsystem was qualified for flight by subjecting the entire subsystem to normal FA vibration testing, combined in the same spacecraft case with the modules of the attitude control system. During the FA shake test, the outputs from the three gyro rebalance amplifiers were monitored by a strip chart recorder for any sudden changes in output or discontinuities in the data.

The entire case was then subjected to the FA vacuum–temperature environment. During this prolonged test, the entire subsystem was carried through all of its operating functions; again, the output of the gyro rebalance amplifiers was recorded. None of these tests showed gyro performance degradation.

Special test equipment and procedures are required to produce the gyro performance data; therefore, the entire gyro subsystem is also run through a complete series of heading and servo calibration tests both before and after the environmental test sequence.

5. Hardware Limitations

The chief limitation which the gyro subsystem places on spacecraft operation is in regard to temperature. The normal spacecraft temperature range for electronic modules was 32 to 150°F. The gyro subsystem was calibrated and compensated only over the temperature range of 85 to 130°F. The decision to operate within this temperature range was due to the fact that no gyro heater power was available for use in an active temperature control loop. Only the passive temperature control provided to the case was available. During the flight phases of operation, this passive control was very predictable and allowed the gyros to operate very close to their design temperature.

The second point of limitation is concerned with handling of the gyro package. The very-low-viscosity flotation fluid within the gyro does not provide any damping to the gimbal. This means that when no capture power is applied, the gimbal is free to rotate back and forth against the internal stops in a random manner. If this condition were allowed to exist for a long time, it would be possible to damage the gyro by breaking the stops or pivot and jewel suspension system. To reduce this possibility to a minimum, it was decided at the start of the *Ranger* Project to hand carry the gyros during each long portion of their transportation as well as from the vendor to JPL. The gyros are not shipped with the spacecraft on the trip to ETR. No gyros have ever been damaged or undergone any significant shifts during these transportation periods.

I. Electronics Assembly IV

1. Description

The electronics assembly IV (Case IV) contains all of the inertial and electronic components of the attitude control system, with the exception of the Earth sensor electronics. It consists of the following subassemblies:

a. Switching amplifier. The switching amplifier utilizes rate and position signals to control the gas valve actuators; its input–output characteristics are such that a

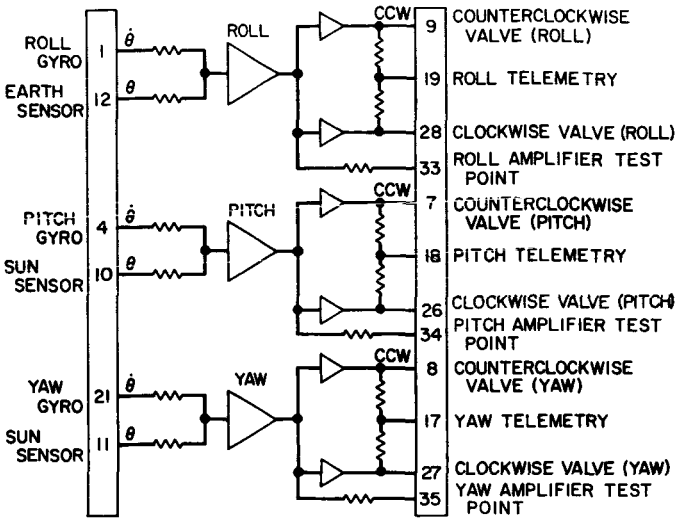

Fig. 68. Hysteresis switching amplifier

no-output region, or "dead zone," is provided so that the gas jets will not be on continuously. There were two types of switching amplifier used on Block III: the *hysteresis* (Fig. 68), which had a voltage deadband and a hysteresis (used on *Rangers VI* and *VII*) and the *derived-rate* type (used on *Rangers VIII* and *IX*). The derived-rate type (Fig. 69) differed from the hysteresis type in two significant areas:

(1) The amplifier was a "minimum-on-time" amplifier instead of a hysteresis amplifier, which resulted in all valve firings (with the exception of saturated conditions) having a predetermined on time.

(2) The amplifier has circuitry to transfer the rate inputs to the switching amplifiers from the gyros to the derived-rate networks. These networks provide rate feedback for the system by the integration of the valve actuations. As may be seen by comparing Figs. 68 and 69, the derived-rate switching amplifier is more complex, which necessitates an increase in the number of components used; however, the overall reliability of the system is enhanced by its ability to function in cruise without the gyros, the gyro power supply, or the synchronizer for three-gyro power unit.

During bench testing of the switching amplifiers, 61 measurements were made or observed on the derived-rate type switching amplifiers; 39 were made or observed on the hysteresis type. A review of all test data and applicable tolerances revealed that no out-of-tolerance conditions existed.

b. Autopilot. This subassembly (Figs. 3 and 6) is used for controlling the spacecraft attitude during motor burn. It uses four jet vanes located downstream of the midcourse motor nozzle. These jet vanes are continously adjusted during the motor burn period, and non-zero angles of the jet vanes produce controlling torques about the three respective axes. As seen from Figs. 3 and 6, four jet vanes are utilized: two ($+x$ and $-x$) are aligned along the pitch axis; two ($+y$ and $-y$) are aligned along the yaw axis. Control about these axes is obtained by deflection of the vanes along their respective axes. Roll control is obtained by controlling all four jet vanes. Each jet vane loop uses an actuator, a feedback potentiometer, and an amplifier.

The autopilot subassembly contains four DC power amplifiers for position control of the jet vane actuators and one DC inversion amplifier for roll signal inversion of the $-x$ and $-y$ actuator channels. The inputs to the amplifiers are rate and position signals from the gyros and position feedback signals from the jet vane actuators. The subassembly also provides the excitation for the potentiometers of the jet vane actuators.

c. Command switch and logic (CS&L). This subassembly (Fig. 70) was designed into the Block III attitude control system in order to provide an interface for the central computer and sequencer (CC&S) and to accommodate circuit additions for increasing the reliability of the commanded turns and for adapting to the derived-rate switching amplifier. It consists of the following:

(1) *Relay control of CC&S relay excitation.* The excitation to the CC&S relays is relay controlled so that commanded turns can be programmed by the CC&S, but inhibited by a real-time command (RTC 8). In the event that the CC&S relay excitation has been removed, it can be restored through the use of a real-time command and a subsequent CC&S "capacitor cycle" stored command. This capability was designed in order to safeguard against anomalies which result in commanded turns of undesirable magnitude or direction.

(2) *Relay control of gyro command current.* The gyro torquer inputs are switched through relays in order to safeguard against external anomalies that may result in a commanded turn being issued in more than one axis at a time. In the event that commanded turns are issued in two axes at once, the CS&L relay logic would transfer such that a single turn in the third axis would be the result.

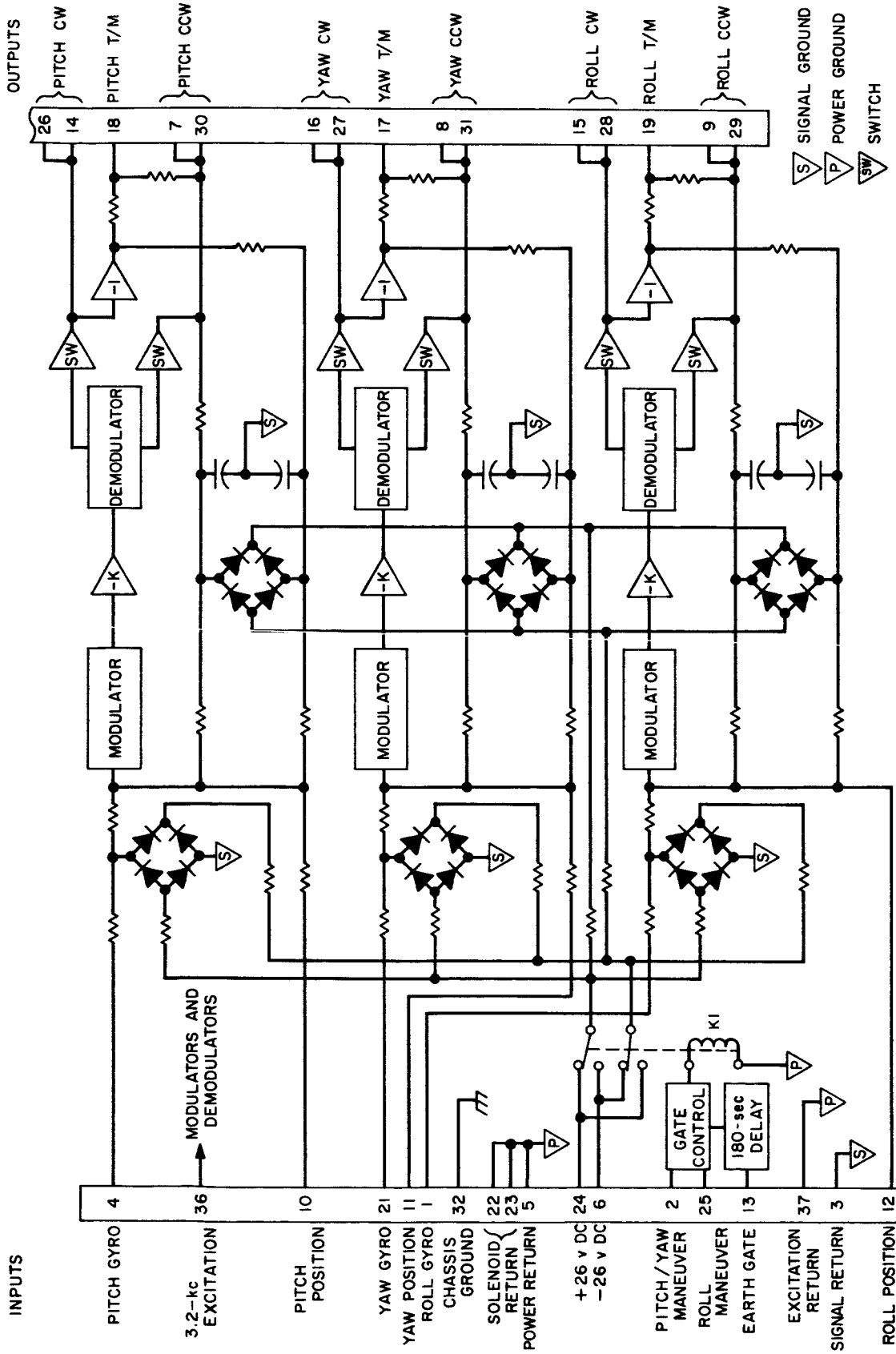

Fig. 69. Derived-rate switching amplifier

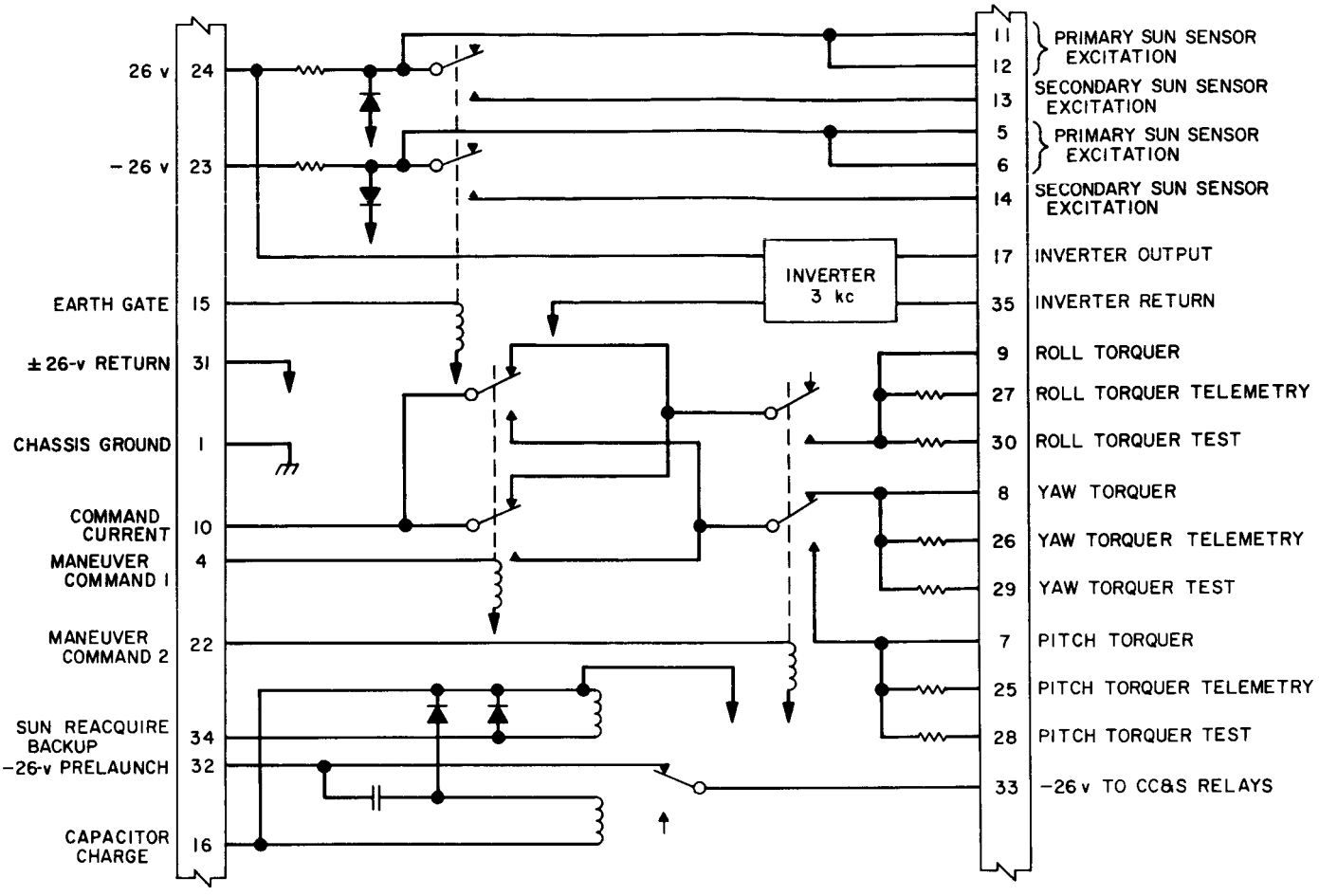

Fig. 70. Command switch and logic

(3) *Relay control of secondary Sun sensor excitation.* The switching of the secondary Sun sensor excitation was transferred from the antenna drive electronics subassembly in Block II to the CS&L in Block III.

(4) *Sun sensor power supply.* The precision Sun sensor power supply was relocated in the CS&L in Block III from the switching amplifier. The power supply in the hysteresis switching amplifier was retained because the power supply voltage was needed within the switching amplifier. The derived-rate switching amplifier did not require its continuation.

(5) *3.2-kc inverter.* A 3.2-kc inverter was used to supply the excitation for the modulators and demodulators of the derived-rate switching amplifiers. On *Rangers VI* and *VII*, which did not use the derived-rate system, the inverter was flown unloaded.

d. Antenna control electronics. The antenna control electronics subassembly contains electronic circuits, which operate in conjunction with the Earth sensor, the antenna actuator, and the roll attitude control. The antenna control electronics subassembly is shown in Fig. 71 and contains the following circuitry:

(1) *Roll and hinge demodulators.*

(2) *Roll-search generator.* This was changed during the Block III effort. The *Ranger VI* and *VII* roll-search generator was −11.4 v; the *Ranger VIII* and *IX* roll-search generator was −8.2 v. The change from the *Ranger VI* and *VII* value was required in order to accommodate the high input impedance of the derived-rate switching amplifier.

(3) *Preset angle circuit.* The angle selection circuit consists of an array of resistors connected to the

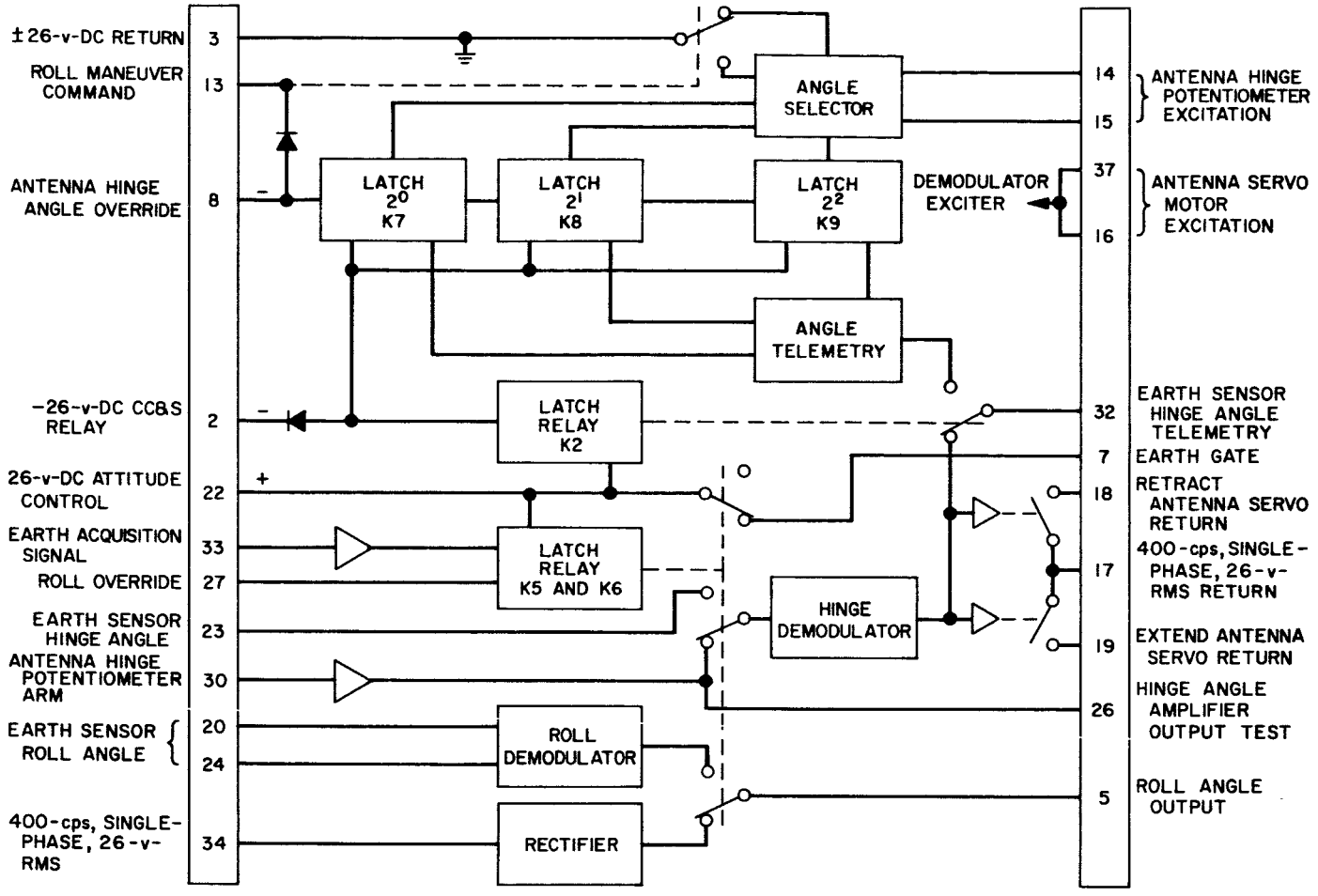

Fig. 71. Antenna control

contacts of a counter. The resistors are also connected across the antenna actuator hinge potentiometer excitation inputs and form half of a bridge circuit, the other half of which is the antenna hinge potentiometer wiper. As the counter switches through its eight positions, the resistors are switched through eight combinations. The ratio of the potentiometer wiper arm voltage required to null the hinge error amplifier to the excitation voltage determines the preset angles.

The counter advances one position each time that a −26-v pulse appears at the antenna hinge override input. At roll maneuver command, the counter advances one position and connects the exit angle resistors to the angle selection circuit. Regardless of the position of the counter at power shutdown, upon application of power the counter will always reset itself to the first position.

(4) *Antenna actuator amplifier.* In conjunction with the hinge error signal and the hinge demodulator, the antenna actuator is controlled by the antenna drive amplifier. A relay amplifier controls the actuator by opening and closing the returns of the extend and retract windings of the antenna actuator motor.

e. Three-phase inverter. The 400-cps, three-phase inverter is supplied to the electronics assembly IV by the secondary spacecraft power section and performs the function of supplying three-phase sine wave power to the gyros, modulators, and demodulators of the attitude control system. The inputs to the inverter are three square waves displaced 120 deg in phase with respect to each other. The input is then amplified through a driver stage and then amplified through a subsequent power amplifier. The power amplifier uses an output transformer which has four separate windings on the secondary. The outputs of the power transformer are combined (a stepped

square wave is obtained) and filtered to a sine wave. The inverter power is unswitched so that the gyros will run whenever spacecraft power is turned on.

f. Single-phase inverter. The single-phase inverter is supplied by the secondary spacecraft power section and is a DC-to-AC inverter. The AC output is obtained by converting the regulated DC source to AC by means of a flux oscillator and transforming the AC to the designed level. The inverter contains circuitry that permits synchronization to be established by means of an external synchronizer for frequency control. The inverter also has a free-running capability. In the event that the synchronizer signals fail, the inverter will continue to operate at a slightly lower frequency. The output of the inverter is switched through a latching relay to either the Earth sensor power supply or the Earth sensor heater. The power is transferred to the Earth sensor power supply by the Earth-acquire command, and as a backup command the roll override real-time command (RTC 1).

g. Attitude control converter. The attitude control converter is also supplied by the spacecraft power section and is a DC-to-DC converter which supplies seven DC outputs to the attitude control system. The DC outputs are obtained by converting the regulated DC source to AC by means of a flux oscillator, transforming the AC to the desired level, and then rectifying it back to DC. The converter is synchronized, and has free-running capability. The converter has two pairs of outputs which are switched: one pair to power the midcourse autopilot subassembly and the other to power the attitude control system (Fig. 72).

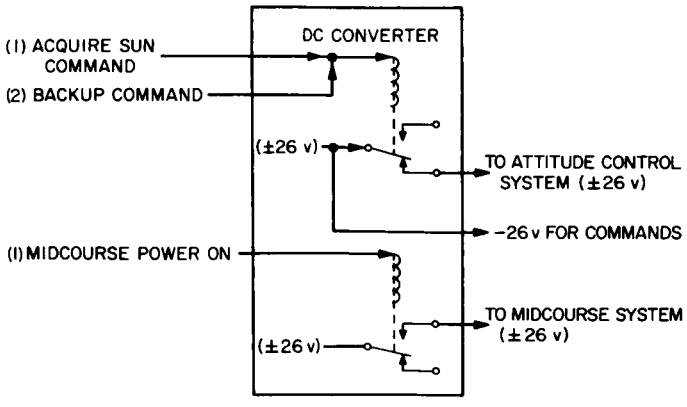

Fig. 72. DC converter power switching

2. Qualification for Flight

a. Type-approval testing. The electronics assembly IV unit used in TA testing was manufactured and tested under the same conditions and used the same procedures as all flight assemblies. As a result of several subassembly reassignments, the accelerometer was replaced with an accelerometer that had experienced a null offset after FA testing and that appeared to warrant observation over a long period of time. The power supplies were also replaced with updated Block II power modules.

The laboratory functional test set was used throughout the testing program and was comprised of the various switching and monitoring functions plus instrumented valves, Earth sensor, primary Sun sensors, jet vane actuator ring, and antenna actuator. The power subsystem was synchronized with a modified Block II synchronizer, modified to be representative of Block III. The plan for the TA testing is shown in Fig. 73. Individual tests are described below.

Transportation vibration. After completion of the incoming functional test, the unit was installed in the carrying and shipping container. The ring harness connectors on the case harness were placed in plastic bags and the harness tied back to simulate the "case closed" configuration on the spacecraft. The container was installed in a cardboard box, lined with a double layer of rubberized horsehair, and placed on the shake table. No special monitoring devices were used. Since this was a nonoperating test, no instrumentation was required.

The high-frequency portion of the test was performed without incident; however, the low-frequency portion was stopped after one plane of shake because the container appeared to be wobbling in its cardboard box. The box was opened and the rubberized horsehair was found to have packed so that the container was allowed to rock during the test. The unit was removed and returned to the lab for testing, which revealed that a yaw gyro had failed; the yaw spin motor would not start.

Humidity. After replacement of the gyro subassembly, and after obtaining a waiver to change the specified sequence, the TA program was resumed at the humidity test. Wet and dry bulb thermometer recordings were made during the test; the lab test rack and all associated test equipment required were used.

No anomalies were noted during the test. The unit performed normally after the case was dried and returned to ambient conditions.

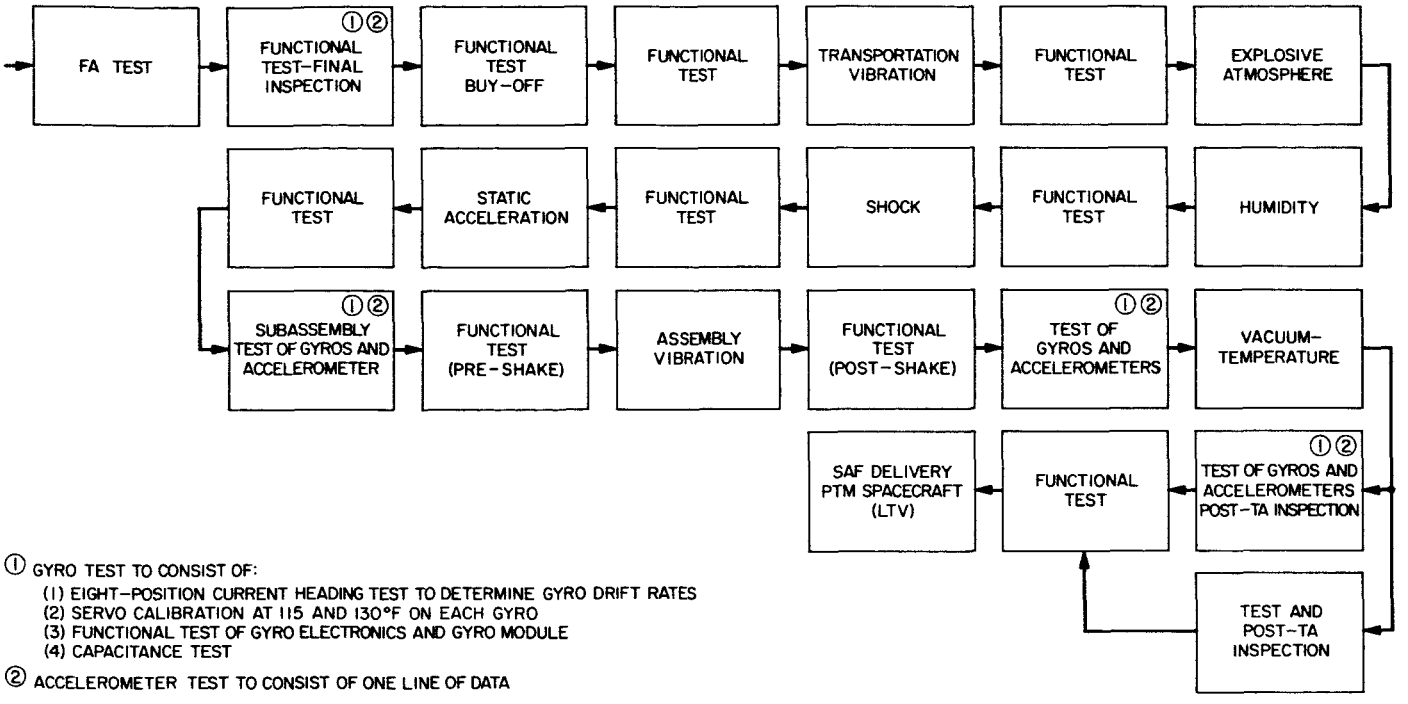

① GYRO TEST TO CONSIST OF:
(1) EIGHT–POSITION CURRENT HEADING TEST TO DETERMINE GYRO DRIFT RATES
(2) SERVO CALIBRATION AT 115 AND 130°F ON EACH GYRO
(3) FUNCTIONAL TEST OF GYRO ELECTRONICS AND GYRO MODULE
(4) CAPACITANCE TEST

② ACCELEROMETER TEST TO CONSIST OF ONE LINE OF DATA

Fig. 73. TA test plan

Shock. This test consisted of five shocks in each orthogonal direction. The test was performed in the launch mode of operation.

Prior to mounting Case IV on the shock tester, the system was calibrated to obtain the proper magnitude waveform with a dummy case. The subassembly was then mounted on the fixture and the system calibration decreased approximately 4% in order to provide for some margin from the dummy to the TA assembly. Aside from the control accelerometer, three accelerometers were added to the subassembly to record on magnetic tape the magnitude of the shock at several places. The lab test rack and a six-channel Sanborn recorder were used; gyro amplifier outputs and gyro torquers were recorded.

Figure 74 shows the typical results of a single shock. All data were as expected; the unit performed normally during and after the test.

Static acceleration. This test consisted of submitting the assembly to a static acceleration of 14 *g* for 5 min in three orthogonal directions. The unit was mounted on the static acceleration spin table, which was balanced with weights. No special instruments were installed. Since this was a nonoperative test for the assembly, no instrumentation was required.

The spin table was slowly started, and its angular velocity gradually increased to the specified level (2.5 rev/min to 117 rev/min in 7 min); the same procedure was used to stop the table. The unit performed normally after the test.

Vibration. In each plane, the assembly was first mounted on the shake fixture, torqued to flight values (45 in.-lb), equalized, and then shaken. The test was performed in the launch mode of operation.

Various accelerometers were attached to subassemblies and the fixture and recorded on magnetic tape. The accelerometer locations are varied from plane to plane. The lab test rack and all required associated test equipment were utilized. The gyro amplifier outputs and torquers were continuously recorded during the equalization and the actual test. A voltmeter was set to continuously monitor the antenna preset angle.

No abnormal indications were noted during this test; the assembly performed normally after vibration.

Vacuum–temperature. The unit was mounted in the heat exchanger and installed in the space chamber. Cables and unit were isolated from the walls. The chamber had cold walls; the heat exchanger fluid was ethylene glycol

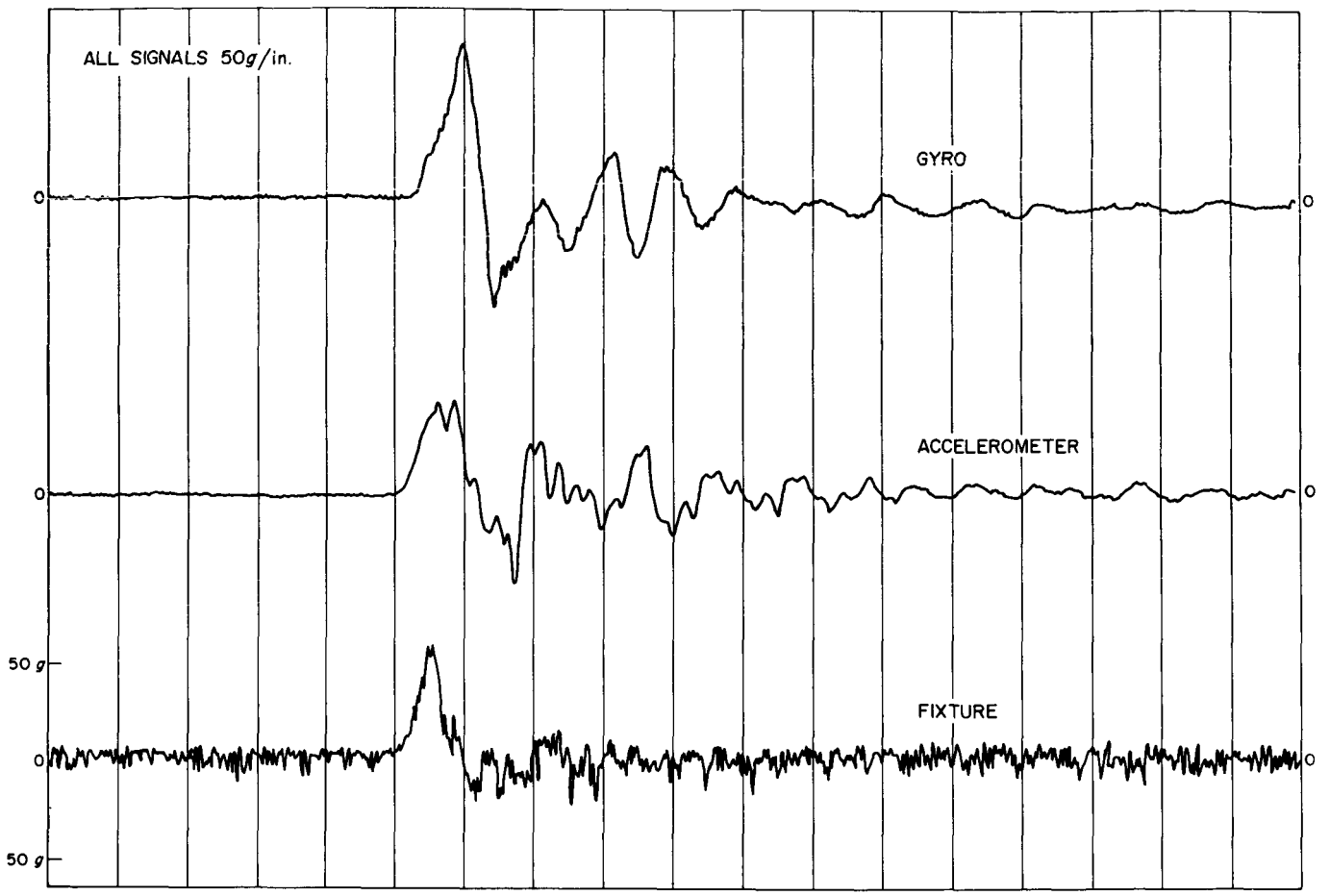

Fig. 74. Typical results of single shock

and water. An aluminum foil cover was used over the top of the heat exchanger.

Thermocouples were attached and recorded. The lab test rack, Sanborn recorder, and all required associated equipment were used. The unit was installed on a 4-deg angle plane in order to evaluate the accelerometer.

The assembly performed normally at the low ambient test; upon stabilization at the high ambient, a failure in the AC-to-DC converter required that the test be stopped and the chamber opened. Since it was not the intent of the test to evaluate the power supplies, the supply was replaced and the test resumed with stabilization at the high ambient; the unit performed normally throughout the test.

Post-TA tests. After the normal cycle of the program was completed, two tests were conducted:

(1) The complete assembly was subjected to the *explosive atmosphere* test. The assembly operated normally for the required turn-on and turn-off cycles at the various gaseous mixtures.

(2) The assembly without the gyros, gyro electronics, and accelerometer was subjected to the *transportation vibration* test. For this test, the unit was mounted in its handling fixture and installed in the carrying case. It was then placed on the shaker without the cardboard box or packing material. The unit performed normally after the test.

Derived-rate TA tests. In order to qualify the derived-rate switching amplifier for flight use, a flight-accepted switching amplifier was subjected to the following tests:

(1) *Humidity.* A temperature and humidity test was performed on the subassembly with the subassembly energized. The first test failed when a bench

test of the subassembly revealed that the roll clockwise channel was inoperative. Further examination revealed that a resistor had opened. The component was replaced and the humidity test successfully repeated. Because there had been a previous failure of a resistor during spacecraft operation, an extensive analysis program was undertaken to determine the cause of the failures. Final analysis indicated that small pin holes existed in the insulating material, thereby allowing moisture to penetrate and become absorbed by the body of the resistor and subsequently, through electrolysis (which dissolves the nichrome element), the resistor would fail. Other factors which apparently affected the resistors included the high body temperatures during burn-in, the adhesive used for putting on serial numbers, and the derated operating power level.

(2) *Shock.* The subassembly was shock tested successfully on the subassembly level.

(3) *Static acceleration.* The subassembly was subjected to this test in a nonenergized condition. The test was preceded and followed by a bench test.

(4) *Vibration.* The vibration test was performed in three phases: (a) The subassembly was tested at the subassembly level. This configuration was used because retrofitting of the hysteresis type required that some subassemblies be tested on a modular level. (b) The subassembly was tested in a Case IV assembly so that FA testing of derived-rate systems could be covered by a TA test. (c) The subassembly was installed on the STM spacecraft and subjected to the spacecraft TA vibration tests. In (a) and (b) the subassembly was energized and monitored; in (c) the subassembly was nonenergized and was evaluated with a bench test performed after the test. In all tests, the subassembly performed normally.

(5) *Vacuum–temperature.* The vacuum–temperature test was performed with the subassembly in a modular heat exchanger. The control method and the details are identical to the assembly level tests. The subassembly performed normally throughout the tests.

b. Flight-acceptance testing. The flight-acceptance program consisted of two tests: a *complex wave vibration* test, which was a sequence of band-limited Gaussian noise and combined noise and sinusoidal vibration with a test duration of 3 min and 32 sec in each orthogonal direction and a *vacuum–temperature* test, which used a vacuum chamber with cold walls, a circulating fluid heat exchanger, and a radiation shield to reduce the radiation exchange of the case with the chamber walls. In all cases, the FA configurations and control point locations were required to be identical to the TA tests. During the vibration testing, this requirement extended to the type and size of vibration exciter used. In addition, the cumulative testing time during vibration was limited to three complete cycles of the standard tape for any one axis. There was no limit on the vacuum–temperature test time. The cumulative test time limit for vibration testing required considerable planning and complete instrumentation recordings so that relatively detailed failure analyses could be conducted after a vibration failure or suspected failure without the necessity of repeating the plane of shake more than once. In general, low-level tests over limited frequency ranges were used to isolate and verify vibration anomalies.

The hardware configuration for FA testing was identical to the flight configuration with the exception of the power supplies. All subassemblies and the case harness were torqued down with the flight hardware (screws) to flight torque values. The lab test rack was used throughout the testing program to provide a more uniform basis for evaluation between the various systems tests performed and the FA tests. The lab test rack contains non-flight hardware that is identical to the flight subassembly inputs and loads of the Case IV. In general, the testing consisted of a complete system test before and after the environmental test with modified system testing performed during the environmental test. During high- and low-temperature tests, the Case IV assembly was tested at power supply voltage limits to verify stable operation within the power supply limits. Nine complete FA tests were performed. In addition, there were subassembly tests performed to qualify the derived-rate switching amplifiers.

Two failures were experienced during FA testing. The first occurred during the vibration testing. The anomaly, as observed during the test, occurred during the vibration frequency range of 480 to 500 cps and appeared as a constant torque equivalent to 480 deg/hr from the roll gyro when shaken in the pitch axis. The gyro was replaced; vendor examination indicated a higher than normal aniso-elasticity. The second failure occurred because, during vibration, all but two of the subassembly mounting screws had worked loose. Recalibration of the torque wrench indicated a change in calibration such that the screws had been torqued to 13.5 in.-lb instead of 16 in.-lb.

Post-FA tests. Post-FA testing of the gyro subsystem revealed that the mass unbalance along the spin axis of the yaw gyro had changed approximately 1.9 deg/hr/g from the pre-FA tests. Information indicated that 2 deg/hr/g was the allowable limit; the subassembly was returned to the system for additional testing.

c. Life testing. Upon completion of the post-TA evaluations, the inertial subassemblies were reassembled and the TA Case IV was started on a room ambient life test. The assembly used the lab functional test set which was used throughout the TA program. The test rack was modified to include voltage sensor circuits, which controlled the primary power to the test rack and turned it off in the event that any voltage changed value beyond predetermined limits. The system was put into a cruise mode of operation, with the Earth and Sun acquired and the system on derived-rate control. The deadbands and other cruise and acquisition parameters were periodically checked. The inertial subassemblies (gyro, gyro electronics, and accelerometer) were removed at 500, 1200, 3000, and 4000 hr for evaluation; 6500 hr have elapsed to date. The data are normal without significant trends.

d. Worst-case analysis. A DC worst-case analysis was conducted of all electronic circuits. It was conducted with a Recon II computer using a SPARC program. The program evaluated all circuit components under variations of temperature, power supply voltages, and component parameters. As a result of the investigation, two resistors were found to be operating at power levels greater than the recommended derated levels when subjected to worst-case conditions. These two resistors (one in antenna control electronics, six in switching amplifier) were replaced with resistors with higher power dissipation ratings.

e. Special tests. A series of special tests was performed with the derived-rate switching amplifier to experimentally verify the compatibility of the derived-rate switching amplifier parameters with the system. A TA flight system unit was used with a flight type Earth sensor and the single-axis table mechanization of Fig. 75.

As can be seen from Fig. 75, the gyro and Earth sensor packages were mounted on the single-axis table. The gyro was mounted so that it sensed the rate input of the table. The Earth simulator was mounted off of the table to provide an input to the Earth sensor. The Earth simulator was capable of simulating an Earth of various angle diameters, intensities, and phase angles.

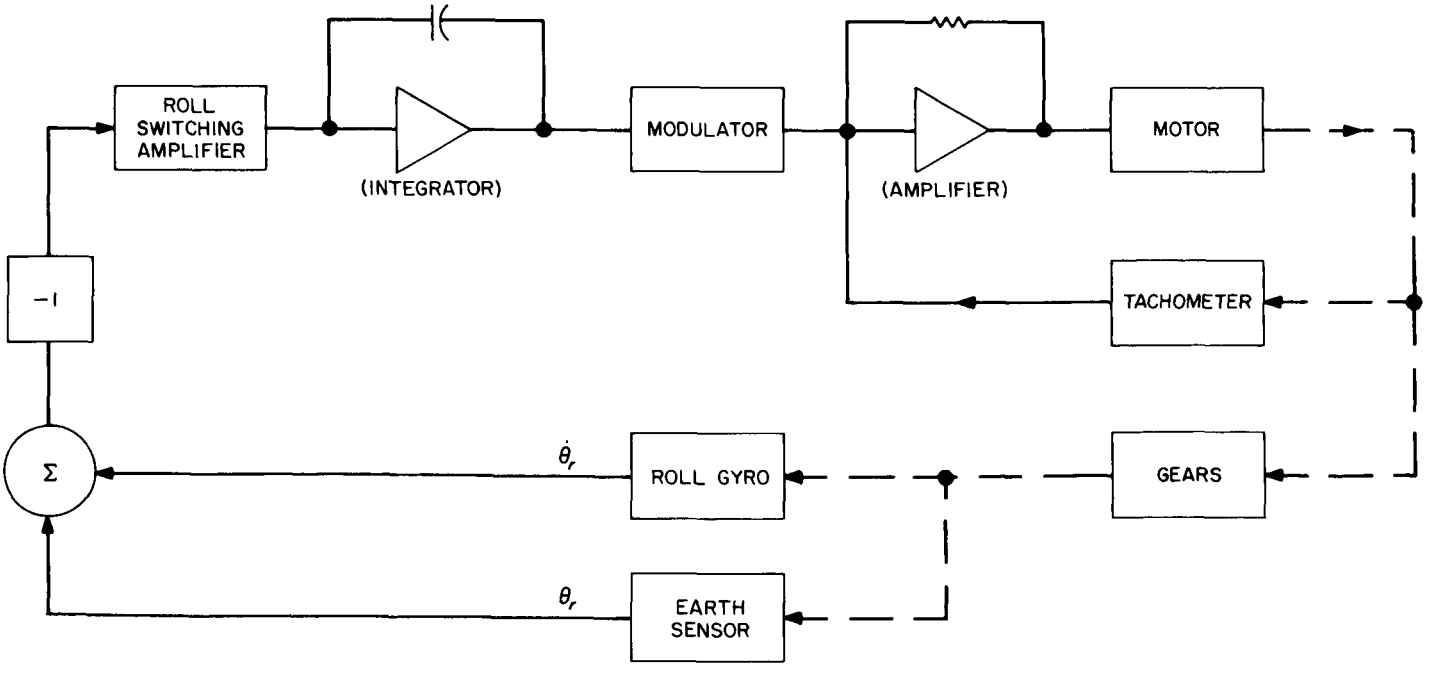

Fig. 75. Single-axis simulation

The testing was categorized in two sections: The first section verified and studied closed-loop system acquisitions for various possible conditions of the Earth. These conditions (angular diameter, phase, intensity) were evaluated at a normal gas subsystem acceleration constant and at a half (failure mode) gas subsystem acceleration constant. A typical acquisition is shown in Fig. 76. The second section was used to determine the capture threshold of the subsystem when it is in derived-rate limit cycle control and is subjected to acceleration disturbances. These thresholds were determined for various acceleration constants (α) and are listed below for an Earth of 1.9 deg (angular diameter), 90 deg (phase angle), and 0.2 ft-cd (intensity).

α, mrad/sec^2	Maintained control, deg/sec	Lost control, deg/sec
0.60	−0.29 +0.31	−0.30 +0.32
0.30	−0.19 +0.20	−0.20 +0.21
0.21	−0.14 +0.16	−0.15 +0.17

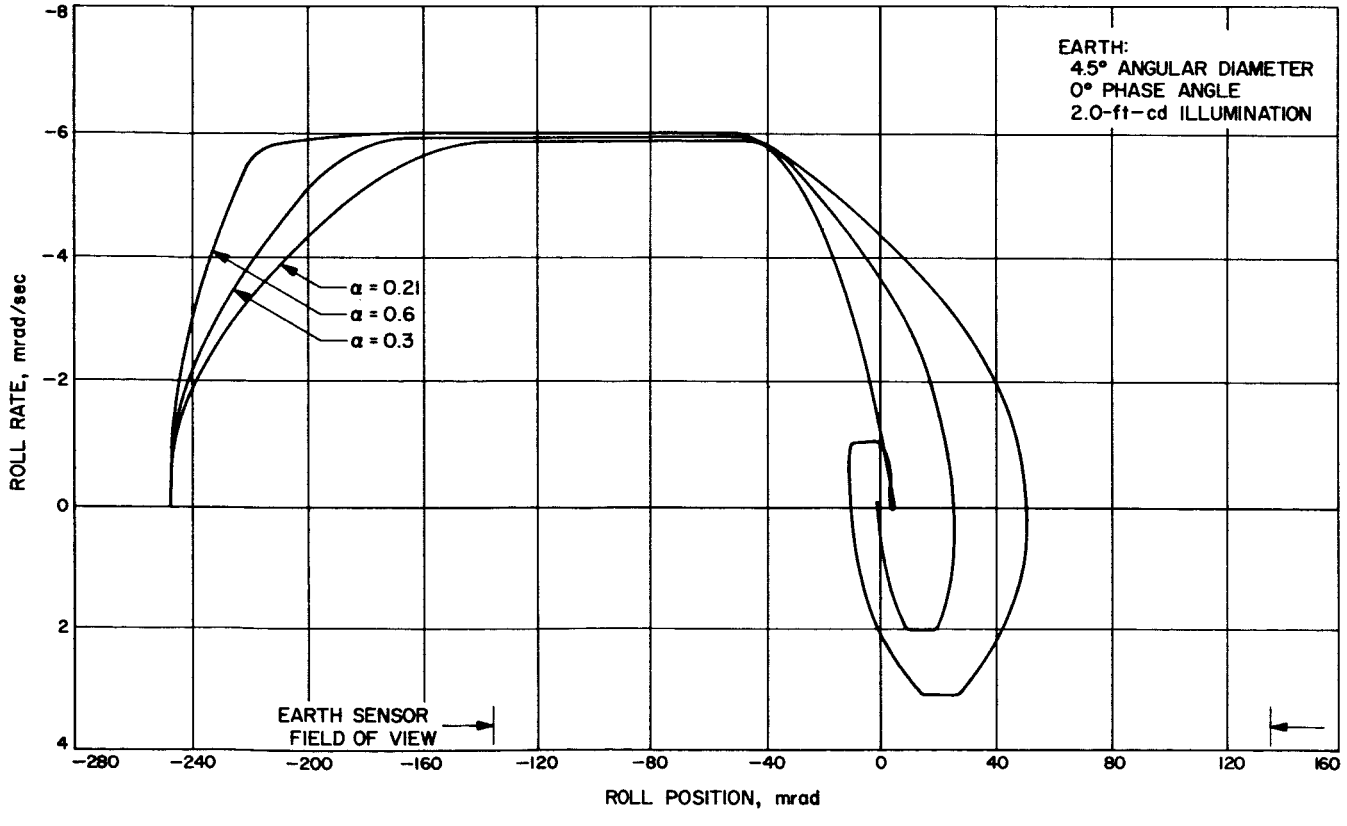

Fig. 76. Typical closed-loop system acquisition

As can be seen from the data listed, even the worst case examined (half gas system $\alpha = 0.27$ mrad/sec^2) was capable of maintaining acquisition with step inputs of acceleration equivalent to the roll-search rate.

During general operation of the system, the roll scale factor was found to be considerably lower than the design goal and resulted in a roll deadband at midcourse conditions of 8.8 mrad instead of 5 mrad. This condition was found to be caused by the harmonic distribution of the single-phase inverter. Since the single-phase inverter was well within its allowable limits, the calibration procedure for the Earth sensor was changed to allow for calibration with the flight inverter. During the two remaining missions (*Rangers VIII and IX*), the large roll deadband error was eliminated prior to midcourse maneuver by plotting in real time the roll position and transmitting the execute command when the roll position was near zero.

3. Hardware Limitations

Since Case IV was delivered to the Spacecraft Assembly Facility as a unit, all of the transportation, handling procedures, and restrictions which applied to the gyro and the accelerometer were applicable to the assembly. In general, these restrictions required that angular rates and shocks be minimized.

As a result of an unexplained failure of a flight accelerometer, an investigation was conducted of the shock characteristics of the torque wrenches that were used to assemble the case to the spacecraft. This investigation resulted in discontinuation of the use of Cal Roto torque wrenches in favor of the deflection gage type wrenches for the assembly of Case IV. Of concern was the magnitude of the shock (50 to 100 g) imparted to the assembly when the release mechanism of the torque wrench impacted.

4. Reliability

a. Subassembly running time. The accumulated running times of all the subassemblies are given in Table 32; the spare hardware running times are given in Table 33.

b. Component failures. A summary of all component failures from the time that the subassemblies are assembled to the time that they are committed to a flight assembly for flight acceptance is given below:

(1) *Hysteresis switching amplifier.*

(a) Five units: no defective components.

Table 32. Flight hardware running times at launch

Subassembly	Time, hr		
	Ranger VII	*Ranger VIII*	*Ranger IX*
Gyros	664.9	841.0	734.0
Gyro electronics	574.7	778.8	764.0
Accelerometer	825.0	1654.8	816.0
Antenna control	374.6	909.4	529.0
CS&L	376.6	875.3	527.0
Autopilot	931.3	950.7	527.0
Switching amplifier (hysteresis)	553.3	NA[a]	NA[a]
Switching amplifier (derived-rate)	NA[a]	416.3	715.7

[a]Not applicable.

Table 33. Spare hardware running times

Subassembly	Time, hr	
	Spare 1[a]	Spare 2[b]
Gyros	863.4	281.7
Gyro electronics	779.3	281.7
Accelerometer	635.1	863.7
Antenna control	552.2	257.6
CS&L	629.9	257.6
Autopilot	622.1	257.6
Switching amplifier (derived-rate)	631.4	257.6

[a]Running times on February 15, 1965.
[b]Running times on February 12, 1965.

(b) One unit: a Zener diode was replaced when inspection revealed a crack in the body.

(c) One unit: Two transistors were replaced. The voltage drop across the transistors increased at cold temperatures.

(2) *Antenna control electronics.*

(a) Nine units: no defective components.

(b) One unit: shorted diode.

(3) *Command switch and logic.*

(a) Eight units: no defective components.

(b) Two units: a transformer had an open winding.

(4) *Autopilot.*
- (a) Four units: no defective components.
- (b) One unit: diode had lead separation problem.
- (c) One unit: transistor had fracture in collector lead near transistor body.
- (d) One unit: transistor was replaced. However, since replacement of transistor cured decrease in actuator gain problem, and the transistor check was subsequently normal, an insulating washer or associated solder joint was suspected of causing the problem.

(5) *Derived-rate switching amplifier.*
- (a) One unit: no defective components.
- (b) One unit: transistor had open base-to-emitter junction; diode was shorted.
- (c) One unit: resistor had broken lead.
- (d) One unit: two transistors replaced. One had emitter-to-collector short; other inoperative at elevated temperatures.
- (e) One unit: transistor had open base-to-emitter junction; transformer was replaced.

(6) *Case harnesses.*
- (a) Eight units: no defective components; however initial connector inspection did reject connectors for do-nuts and incorrect insert material.

5. Engineering Change Requirements

A brief description of the ECR's generated during the Block III effort for electronics assembly IV is given below.

(1) *Case IV and system.*
- (a) Seven miscellaneous hardware changes.
- (b) Polarity of jet vane telemetry signals.
- (c) Weights of system, subassemblies.
- (d) Weight of jet vanes, antenna actuator, Earth sensor, gas subsystem.
- (e) System change from hysteresis to derived rate.
- (f) Midcourse motor alignment, antenna exit angle to 180 deg.
- (g) Increase of acceleration constant.

(2) *Command switch and logic.*
- (a) Authorizing of subassembly.
- (b) Change in isolation resistors (value).
- (c) Addition of diodes to remove RTC 8 transients on capacitor charge circuit.
- (d) Change in capacitor values for high-temperature operation of inverter.
- (e) Change of diode types to improve voltage regulation.
- (f) Change in resistors (power rating).

(3) *Antenna control electronics.*
- (a) Telemetry change.
- (b) Deletion of Sun sensor excitation switching, generation of Earth gate signal.
- (c) Count reversal of angle selection counter.
- (d) Modification of roll-search generator for derived-rate system.
- (e) Addition of filter to roll demodulator output.
- (f) Antenna exit angle to 180 deg.
- (g) Replacement of resistors.

(4) *Autopilot.*
- (a) Circuit repackaging.
- (b) Removal of path guidance integrator; installation of jet vane excitation supply.

(5) *Switching amplifier (hysteresis).*
- (a) Removal of Sun sensor power supply; increase of voltage.

(6) *Gyros.*
- (a) Subassembly repackaging (Hi-Rel parts).
- (b) Change in integrating cacapitor types.

(7) *Gyro electronics.*
- (a) Addition of telemetry isolation (resistors).
- (b) Change in gains of AC and DC amplifiers.
- (c) Subassembly repackaging.

(8) *Accelerometer.*
- (a) Subassembly repackaging.
- (b) Correction for tolerance buildup of machining tolerances.

V. TESTING

A. Lab System Testing

The testing scheme for the attitude control system requires that all major components (less gas subsystem and Sun sensors) be integrated and a system test be performed prior to delivery. The flight gas subsystem is duplicated in the lab test rack so that flight type loads are presented to the switching amplifier. Once the system is delivered to the spacecraft, a spacecraft attitude control system test is performed in which the spacecraft wiring, power, command, CC&S, and telemetry are integrated. This test enables one to verify the operation of the attitude control system in the spacecraft and its ability to accept spacecraft commands. After the completion of this test, a spacecraft test is performed to evaluate the operation of all subsystems in a mission oriented procedure. The measurement data obtained by the various tests are shown below:

(1) *Prelaunch.*
   (a) Gyro runup time.
   (b) All power supply voltages (AC and DC).
   (c) Gyro heading (fixed torques not compensated).
   (d) Preset angle counter (using RTC 2 and reading angle on telemetry and antenna actuator).

(2) *Sun acquire.*
   (a) Gyro heading (fixed torques compensated).
   (b) Switching amplifier deadbands, nulls, saturated input condition.

(3) *Earth acquire.*
   (a) Roll-search generator.
   (b) Earth-gate timer.
   (c) Hinger servo deadband and hysteresis.
   (d) Derived-rate gains.
   (e) Minimum on time (on time pulse width).

(4) *Midcourse maneuver.*
   (a) Capacitor charge, antenna to exit.
   (b) Accelerometer count.
   (c) Midcourse maneuver turns.
   (d) RTC 8.
   (e) Preset angle (second).
   (f) Autopilot.

(5) *Terminal maneuver.*
   (a) Terminal maneuver turns.

VI. FLIGHT PERFORMANCE FOR BLOCK III MISSIONS

A. Prelaunch

During prelaunch operations, the correct antenna preset angle is selected by ground command. This angle is predetermined and is selected to supplement the Earth–spacecraft–Sun angle at Earth acquisition. Since the orientation of the spacecraft axes on the launch complex is known, the outputs of the three gyros can be correlated to the known Earth rate. In general, correlation of the gyro data was within 1 deg/hr of the Earth rate. The total gas storage at launch is tabulated below; the nominal gas weight at launch is 4.18 lb.

Spacecraft	Preset hinge angle, deg	Gas storage at launch, lb
Ranger VI	135	4.18
Ranger VII	122	4.24
Ranger VIII	135	4.21
Ranger IX	122	4.20

B. Separation

The spacecraft separation rates observed were within the 48-mrad/sec specification limit and are tabulated below. While some of the rates exceeded the 9-mrad/sec limit of the telemetry measurement, they are known to be within the 48-mrad/sec specification.

Spacecraft	Separation rates, mrad/sec			After solar panel deployment, mrad/sec		
	Pitch	Yaw	Roll	Pitch	Yaw	Roll
Ranger VI	1.6	<-10	1.5	—[a]	—[a]	—[a]
Ranger VII	2.0	<-10	0.4	2.0	−7.0	+0.4
Ranger VIII	−1.5	−6.6	1.5	—[a]	—[a]	—[a]
Ranger IX	<-9	−4.5	−0.6	−0.6	−8.2	+1.2

[a]No noticeable change.

C. Sun Acquisition

In response to the Sun acquire command, power is applied to the attitude control system. Upon this application of power, the system is in a configuration such that the switching amplifier is receiving position error signals from the primary and secondary Sun sensors (pitch and yaw) and rate signals from all three gyros. The Sun sensors are positioned so that the primary sensor field of view is 40 deg off the negative roll axis, and the secondary sensor field of view is 4π sterad. The spacecraft rates are increased or reduced to the acquisition rates, until the pitch and yaw rate and position errors are reduced to the limit cycle values. The roll rates are at this time reduced to within its limits. Acquisition rates are listed below;

Spacecraft	Acquisition rates, mrad/sec	
	Pitch	Yaw
Ranger VI	3.7	−6.5
Ranger VII	2.0	5.0
Ranger VIII	4.2	−3.9
Ranger IX	4.2	−5.8

D. Earth Acquisition

At approximately 2.5 hr after Sun acquisition, the power to the Earth sensor is switched from Earth sensor heater to Earth sensor power supply. At this point, the roll position error has been replaced by a roll search generator, causing the spacecraft to search in a negative direction. When a body of sufficient brightness enters the Earth sensor field of view, the search generator is switched out and the roll hinge error signals are switched in; the roll position and roll rate error signals are reduced to limit cycle values. As can be seen in the following tabulation, the *Ranger VIII* and *IX* derived-rate system had a slower acquisition rate. The derived-rate system transfers to a derived-rate mode of operation after Earth acquisition.

Spacecraft	Roll acquisition rates, mrad/sec
Ranger VI	−3.8
Ranger VII	−4.0
Ranger VIII	−2.4
Ranger IX	−2.4

E. Cruise

The performance of the system in the cruise configuration is basically that of limit cycle operation. The deadbands of the limit cycle were within the nominal ± 2.8 mrad in pitch and yaw, and a variable scale in roll (variable as the spacecraft to Earth distance increases and the angular diameter of the Earth decreases). The external torques on the spacecraft were:

Spacecraft	Torque, dyne-cm		
	Pitch	Yaw	Roll
Ranger VI	−170	<4	$0<t<3.5$
Ranger VII	−370 to −160	—[a]	—[a]
Ranger VIII	−240 to −80	−28 to −8	<8
Ranger IX	−124 to −60	$-5<T<0$	$0<T<1.5$

[a]Below measurement thresholder.

Only the torques in pitch appear to be significant; these torques are caused by the high-gain antenna presenting an asymmetrical area to the solar radiation about the pitch axis.

The velocity increment was nominal; as seen in the following tabulation, the design goal of the derived-rate system was considerably lower than the *Ranger VI* and *VII* configuration.

Spacecraft	Velocity increment, μrad/sec		
	Pitch	Yaw	Roll
Ranger VI	≈0	≈90	≈90
Ranger VII	60	55	55
Ranger VIII	17	17	20
Ranger IX	18	18	19

F. Midcourse

During the midcourse maneuver, the position sensors are switched out and the gyros provide rates and position signals to the system. The various midcourse parameters were as listed below. Of significance is the low acceleration constant in roll during *Rangers VI* and *VII*. The low acceleration constant was found to have been caused by an error in the assumed roll moment of inertia. In between *Rangers VII* and *VIII*, the roll moment of inertia was measured and a new nozzle design was effected.

Spacecraft	Turns, deg		Acceleration constant, mrad/sec^2			
	Roll	Pitch	Roll:start	Roll:stop	Pitch:start	Pitch:stop
Ranger VI	−19.91	−111.34	−0.48	0.45	−0.57	0.59
Ranger VII	5.56	− 86.80	0.48	−0.48	−0.56	0.59
Ranger VIII	11.6	151.75	0.76	—[a]	—[a]	—[a]
Ranger IX	−27.41	127.96	−0.83	0.70	0.77	−0.78

[a]No date available.

G. Reacquisition

Reacquisitions are identical to the acquisitions. The acquisition rates were as given below.

Spacecraft	Sun acquisition, mrad/sec		Earth acquisition roll, mrad/sec
	Pitch	Yaw	
Ranger VI	4.9	0	—[a]
Ranger VII	4.0	0	—[a]
Ranger VIII	−4.5	0	−2.8
Ranger IX	−4.8	0	−2.7

[a]Acquisitions were instantaneous.

H. Terminal Maneuver

The terminal maneuver configuration is similar to the midcourse configuration except that Earth lock is maintained. For *Rangers VI, VII,* and *VIII,* the terminal maneuver was preceded by a command that left the attitude control system in the cruise configuration. Therefore, the attitude control system continued in a limit cycle of operation to impact. In *Ranger IX,* the terminal maneuver parameters were as follows:

Ranger IX turns, deg			*Ranger IX* acceleration constants, deg					
Pitch	Yaw	Pitch	Pitch		Yaw		Pitch	
			Start	Stop	Start	Stop	Start	Stop
+5.20	−16.30	−20.50	0.75	−0.70	−0.66	0.58	−0.70	0.84

The performance of the Block III attitude control system was generally nominal. No anomalies have been detected in the analyses of the flight data.

REFERENCE

1. Turk, W., *Ranger Block III Attitude Control System,* Technical Report No. 32-663, Jet Propulsion Laboratory, Pasadena, California, November 15, 1964.

ACKNOWLEDGMENT

Although there are many persons whose efforts on this project are sincerely appreciated, we wish particularly to acknowledge R. G. Forney, Manager of JPL's Spacecraft Control Section, and R. E. Hill, *Ranger* Project Engineer for *Rangers I* through *VII,* under whose direction the project was conducted.